DEVELOPMENT OF POLYMERIC FOAMS FOR MITIGATION OF BLAST EFFECTS

Thesis submitted to the Delhi Technological University

For the award of the Degree of

DOCTOR OF PHILOSOPHY

By

A.V. ULLAS
(2K13/PhD AC/07)

DEPARTMENT OF APPLIED CHEMISTRY

DELHI TECHNOLOGICAL UNIVERSITY

BAWANA ROAD, DELHI-110042

AUGUST 2018

Dedicated

To

My Family

DECLARATION

I hereby declare that this Ph.D thesis entitled "**Development of Polymeric Foams for Mitigation of Blast Effects**" was carried out by me for the degree of Doctor of Philosophy under the joint guidance and supervision of Dr. Devendra Kumar, Professor, Department of Applied Chemistry and Polymer Technology, Delhi Technological University (D.T.U) Delhi and Dr. Prasun Kumar Roy, Scientist 'F', Centre for Fire, Explosive and Environment Safety (CFEES), Defence Research and Development Organization (DRDO), Delhi, India.

This thesis is a presentation of my original research work. Wherever contributions of others are involved, every effort has been made to indicate this clearly.

For the present thesis, which I am submitting to the University, no degree or diploma has been conferred on me before, either in this or in any other University.

<div align="right">

A.V.Ullas

Delhi Technological University

</div>

DELHI TECHNOLOGICAL UNIVERSITY

(Formerly Delhi College of Engineering)
Shahbad Daulatpur, Bawana Road, Delhi-110042, India

CERTIFICATE

This is to certify that the thesis entitled "**Development of Polymeric Foams for Mitigation of Blast Effects**" submitted to the Delhi Technological University, Delhi-110042, in fulfilment of the requirement for the award of the degree of **Doctor of Philosophy** by the candidate **Mr. A.V.Ullas,** (Reg. No.: 2K13/Ph.D.AC/07) under the supervision of **Prof. D. Kumar** and **Dr. P.K.Roy**. It is further certified that the work embodied in this thesis has neither partially nor fully submitted to any other university or institution for the award of any degree or diploma.

Dr. P.K. Roy

Scientist 'F'
Centre for Fire, Explosive and
Environment Safety (CFEES)
Defence Research and Development
Organization (DRDO)
Delhi-110054

Dr. D. Kumar

Professor
Department of Applied Chemistry
Delhi Technological University (DTU)
Main Bawana Road
Delhi-110042

Head of Department
Department of Applied Chemistry and
Polymer Technology
Delhi Technological University (DTU)
Main Bawana Road
Delhi-110042

ACKNOWLEDGEMENT

ABSTRACT

Polymeric syntactic foams belong to a class of composite cellular materials, which are prepared by dispersing hollow microbubbles in a suitable polymeric matrix. These cellular materials possess exceptional ability to respond against dynamic loadings. The mechanical properties of the resultant foam are strongly dependent upon the type of the hollow bubbles being incorporated, and lately, hybrid foams have garnered a lot of attention, where another component, usually reinforcing, is included in the composition. This thesis is an attempt to fabricate polymeric syntactic foams containing hollow microbubbles at varying loadings and explore their potential towards blast mitigation. The primary benefit of these foams is their tunability that can produce foams with good specific mechanical properties.

Fabrication of syntactic foams requires addressing two issues related to the maximum permissible limit of microbubbles for easy fabrication of syntactic foams and the determination of optimal concentration of hollow microballoons that will favour the formation of strong yet lightweight syntactic foams. In view of this, an in-depth rheological study has been performed on epoxy–glass microbubbles foam formulations by varying the glass microbubbles loading from 10 to 70 % v/v. The studies indicate that although hexagonal close packing of microspheres allows 74 % v/v packing limit, in practice, such high loadings are not feasible, which restricts the upper limit of microbubble packing to 60 % v/v without the aid of solvents. Addition of glass microbubbles (10-60 % v/v) in epoxy resin brings about a sudden increase in the viscosity of the system, ranging from 10^3 m.Pa.s at 30 °C, for neat epoxy resin, to 10^5 m.Pa.s,(40 % v/v microbubble loading). At a microballoon loading greater than 60 % v/v, the viscosity becomes prohibitively high for the formulations to be processed by conventional stir casting techniques. Rheological studies also reveal that inclusion of glass microbubbles

does not alter the curing profile as evidenced by calorimetric studies; however, there is a slight delay in the curing phenomenon. The same is also evidenced by the appearance of longer gel times during isothermal (60-100 °C) rheological studies. Epoxy-amine reaction is a classical nucleophilic substitution reaction following second order kinetics. The reaction mechanism is not altered upon inclusion of glass microbubbles. In view of the lower density of the glass microbubbles compared to epoxy, it is highly probable that the hollow fillers drift towards the surface. In fact the digital photographs of epoxy-HGM formulations containing low loadings of glass microbubbles (10-30 % v/v) result in the formation of two separate layers: a microbubble rich phase at the top and epoxy rich phase at the bottom. However, this process require extended time periods: much longer than what is mandated by the epoxy-amine curing reaction. The mechanical properties of syntactic foams (10-70 % v/v glass microbubbles) in the quasi-static regime have also been investigated which suggests a simultaneous decrease in mechanical properties with increasing volume fraction of purposely placed voids. Our studies reveal that formulations with microbubble loading of 40-60 % v/v form stable syntactic foams with no visible evidence of layering and excellent mechanical properties. Specific compressive toughness is maximum for 40 % v/v glass microbubble formulation which indicates its better energy absorption capability compared to other formulations of syntactic foams. The strain rate sensitivity of syntactic foams is confirmed by high strain rate studies performed using Split Hopkinson pressure bar. In line with the quasi-static tests, the flow stress of these foams increases with decreasing microbubble loading. Moreover, the flow stress values increase with increasing strain rates. Shock tube testing of syntactic foams reveals that syntactic foam does not undergo any deformation even at a blast load of ~ 90 psi, unlike control aluminium sheets that underwent extensive deformation (~1700 $\mu\varepsilon$) at

significantly low blast loads (~ 36 psi). This clearly reveals the role of syntactic foams as core materials in sandwiched configuration for blast mitigation applications.

The role of different types of fillers towards improving the mechanical properties, particularly in terms of the energy absorbing ability of syntactic foams has been explored. The incorporation of two-dimensional layered fillers, i.e. molybdenum disulfide (0-0.04 % v/v), reduced graphene oxide (0-1 % v/v) and nanoclay (0-1 % v/v) on the mechanical, rheological and thermal properties of epoxy-hollow glass microbubble syntactic foams have been investigated. The dispersion of these fillers is an extremely important issue which needs to be addressed for obtaining syntactic foams with improved properties. This has been achieved by ultrasonication of these fillers in the epoxy resin for extended periods. However, due to the extremely low loadings of these fillers, their presence could not be discerned in the SEM imaging or PXRD pattern. Isothermal rheological studies were performed at 60 °C, which involved the determination of complex viscosity, storage and loss modulus with time. The studies reveal that the introduction of these layered fillers did not affect the processability of the formulations. The effect of introducing 2D fillers can be clearly seen in the quasi-static mechanical properties of the hybrid syntactic foams. There is a significant improvement in the quasi-static mechanical properties of all 2D filler-reinforced syntactic foams as compared to base foam, however, the extent of reinforcement is much more pronounced for molybdenum disulfide (0.02 % v/v) probably due to the lubricating action of the filler through a crack extension mechanism. High strain rate studies on two-dimensional fillers were also found to follow similar trend as observed during quasi-static tests.

The potential of preformed elastomers as a toughening agent has also been explored for epoxy-glass microballoons syntactic foams. Poly(dimethylsiloxane) microspheres have been prepared by suspension polymerization route. The microsphere

dimensions range from 58-255 µm by varying the stirring speeds (600-1000 rpm) and feed concentration (30-60 %). The replacement of glass microbubbles with PDMS microspheres (63 µm, 3-7 % v/v) in syntactic foams (total filler volume fraction of 0.4) did not lead to any significant increase in the viscosity which indicates that the formulations can be processed in the same manner as neat syntactic foams. The extent of improvement upon introduction of elastomeric microspheres (diameter ~ 63 µm, 5 % loading) are 40 % and 185 % respectively in flexural strength and flexural toughness without any undesirable increase in foam density.

In another attempt to strengthen epoxy-glass microbubbles syntactic foams, they have been reinforced with electrospun polyamide nanofibers. Nylon 6 nanofibers have been prepared by electrospinning and the operating parameters namely solution concentration and flow rate were varied to obtain fibers of requisite dimensions. These nanofibrous mats were employed for reinforcing glass microbubbles epoxy syntactic foams. The introduction of nanofibers (0.25 % v/v) brought about a marginal improvement (~ 7 %) in the compressive strength, when the direction of loading was perpendicular to the fiber axis. Nonetheless, flexural properties of the reinforced foam are significantly higher, with 75% and 62 % enhancement in flexural strength and elongation, respectively.

The mechanical properties of epoxy syntactic foams can also be increased by improving the interfacial adhesion between the matrix and the hollow fillers. We hypothesised that the extent of interfacial adhesion can be strengthened by replacing glass microbubbles with epoxy microbubbles. The improved compatibility between the hollow epoxy microbubbles and epoxy matrix can have a lasting influence on the mechanical properties. In this regard, hollow epoxy microbubbles have been prepared by interfacial engineering wherein the reaction takes place only at the interface of the epoxy

microcapsules. This has been made possible by varying the stoichiometric ratio of epoxy and amine hardener from 100:13 to 100:2. Monolithic epoxy microcapsules obtained using a epoxy: hardener ratio of 100:2 were found to possess a core content of 25 %. Effect of incorporation of 40-60 % v/v of epoxy microbubbles on the mechanical properties demonstrated a proportional decrease in the mechanical properties with increasing volume fraction of the microbubbles. At 40 % v/v loading, an improvement of ~ 127 % in the compressive toughness is obtained as compared to neat epoxy. However, due to the relatively higher density of epoxy microbubbles, there is an increase in density of the resultant syntactic foam.

This thesis also explores the findings of polybenzoxazines glass microbubble syntactic foams for high-end applications. Thermally stable bisphenol-F based polybenzoxazines syntactic foams have been prepared by the introducing 30-60 % v/v hollow glass microbubbles. The primary objective is to establish the quasi-static mechanical response of such foams. To identify suitable processing conditions, the effect of introducing glass microbubbles on the curing profile of benzoxazine resin has been evaluated by non-isothermal calorimetric studies and rheometry. The curing profiles of syntactic foam formulations remain unperturbed and similar to that of neat polybenzoxazine. The introduction of glass microbubbles leads to an increase in the viscosity of the formulations, and the gel time, as determined by rheology, increases from ~ 3690 to ~ 3800s due to the physical hindrance posed by glass microbubbles. Polybenzoxazines possess a high char yield (~ 48 %) at a temperature of 600 °C and it increases to 83 % (60 % v/v glass microbubble loading). Polybenzoxazines exhibit a quasi-static compressive strength of 171 MPa and the addition of glass microbubbles lead to a decrease in the compressive strength to ~ 60 MPa. Maximum compressive toughness was observed at 40 % v/v of glass microbubble loading which was ~ 200 % higher

compared to neat resin. The potential of polybenzoxazines as a matrix material for syntactic foams is thus evaluated.

CONTENTS

Chapter 3: Two-Dimensional (2D) Layered Filler Reinforced Epoxy Syntactic Foams

Chapter 4: Poly(dimethylsiloxane)Toughened Epoxy Syntactic Foams

LIST OF FIGURES

XVII

XX

LIST OF TABLES

LIST OF SCHEMES

ABBREVIATIONS

EPS	Expanded Polystyrene
HDPE	High Density Polyethylene
PET	Polyethylene Terephthalate
HGM	Hollow Glass Microbubble
DGEBA	Diglycidyl ether of bisphenol A
SHPB	Split Hopkinson Pressure Bar
DSC	Differential Scanning Calorimetry
TG	Thermogravimetric Analysis
DTG	Derivative Thermogravimetric
SEM	Scanning Electron Microscopy
XRD	X-Ray Diffraction
PDMS	Poly(dimethylsiloxane)
PMMA	Polymethylmethacrylate
TETA	Triethylenetetramine
HSP	Hansen Solubility Parameter

Chapter I

Introduction
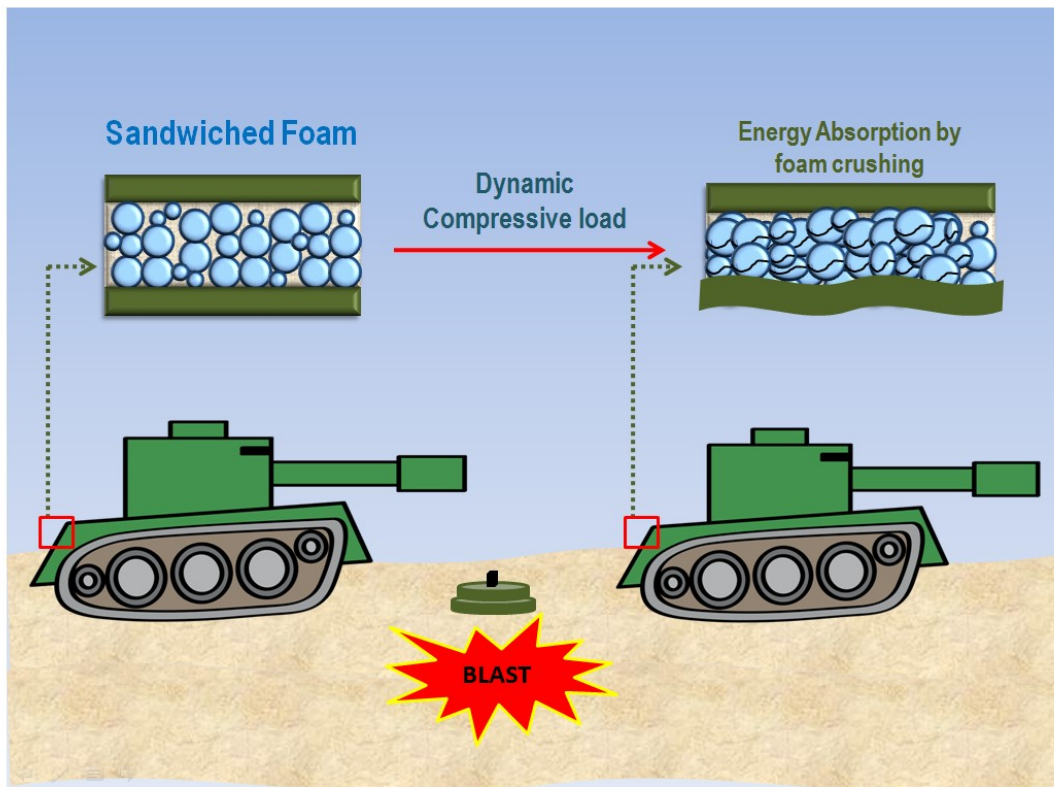
1.1. Introduction

In the wake of terrorist attacks, enormous attention is being directed towards the development of materials, capable of mitigating the primary and secondary effects of blast. Such incidents usually take the form of small bombings and result in damage to nearby structural elements leading to the generation of high-energy fragments, which are the real cause of injuries and fatalities. Suitable materials need to be developed which can prevent the loss of lives and minimize damage to nearby structures. In this context, polymeric materials are finding increasing usage because of their desirable properties, particularly an optimal balance of high mechanical strength and low weight.

Polymeric foams are being strongly advocated as energy absorbing materials for dynamic loading applications. The potential of polymeric foams in the context of mitigation of blast effects has been explored in the last few decades [1-5]. Foams in general, contain gases within its pores, which bestow them light-weight features and excellent specific mechanical properties, particularly in terms of energy absorption. Polymeric foams are especially useful as core materials in sandwiched structures. Both open and closed cell foams have been used to absorb the energy associated with blast/dynamic loads. However, closed cell foams are reportedly more effective against dynamic loads, owing to the presence of entrapped air. These foams find themselves suitable to a wide range of operations, even for framing temporary structures within explosive handling magazines for the purpose of storing explosives to prevent sympathetic detonation. The underbellies of tanks have been reportedly lined with closed cell foams to attenuate the effects of blast upon encounter with a buried land-mine [6]. Open celled foams have been used as sandwich cores in naval applications such as surface ship deck structures and in boat hulls [7, 8].

In general, foams are dispersion of spherical gaseous bubbles in a liquid or solid phase. The presence of large quantity of air renders these materials less dense in comparison to the liquid or solid phase. Since the surface energy is lowest for a spherical configuration, all the gas bubbles tend to assume a spherical configuration. Polymeric foams are dispersion of entrapped air bubbles in a solid polymer phase, which can stay either isolated from each other or may be interweaved through connecting tunnels. The physical properties of foams are strongly dependent on the volume fraction of the entrapped air bubbles. With increasing volume fraction of solid matrix, the property of the resultant foam is dictated primarily by the properties of matrix material and vice versa. Other factors, e.g. the nature and distribution of the cells are also strong determinant of the end property. The introduction of porosity, through air entrapment, can be accomplished through the use of blowing agents or by adding hollow fillers in the resin, and both these classes of foams exhibit widely varied properties.

1.2. Classification of Foams

Since, foams are numerous in number and can be designed to exhibit different kinds of properties; a proper classification is desirable, which is discussed in the following sub-sections.

1.2.1. Thermoplastic and Thermoset Foams

In general, thermoplastic polymers exhibit a unique viscoelastic behaviour, wherein the change of phase from solid to melt occurs within a narrow specified temperature window. Due to this thermo-reversible nature of thermoplastics, they are a rather preferred choice of materials for processing purposes. Thermosets, on the other hand, are crosslinked three-dimensional networks that are formed as a result of an irreversible curing process between 'resin' and the curing agent. Common examples of thermosetting resins include epoxy, vinyl esters, silicones, unsaturated polyesters.

The introduction of a gaseous phase in the matrix results in the formation of thermoplastic and thermoset foams. Thermoplastic foam formation is generally temperature and pressure dependent whereas formation of thermoset foams is precluded more often by participating materials chemistry and reaction kinetics. Thermoplastic foams are prepared by the incorporation of a blowing agent, and practically any gas with suitable transport parameters can serve this purpose provided it is soluble in the polymer. From this viewpoint, the foaming process encompass three major steps: first being the introduction of the blowing agent into the polymer matrix to form a polymer gas solution which is followed by formation of a fully differentiated cellular structure of polymer containing gas and finally the evacuation of the gas bubbles in the polymer foam to form an air filled foam. The blowing agents can be gases or they can be substances that lead to gas release, when triggered either by some chemical reaction or physical agents. Common examples of thermoplastic foams include polystyrene foams, polyvinyl chloride foams and polyethylene foams etc. Thermosetting foams include polyurethane foams, polyisocyanurate foams etc. For the sake of comparison, characteristics of thermoplastic and thermoset foams are tabulated in **Table 1.1**.

Table 1.1: Comparison of thermoplastic and thermoset foams [9]

	Thermoplastic foams	*Thermoset foams*
Raw material	Thermoplastic polymer pellets	Reactive chemicals (resin + curing agent)
Generation of porosity	Gas dissolution by pressure or gas generation by heating	Gas generation by chemical reaction
Growth of foam	Diffusion of dissolved gas	Diffusion of generated gas
Foaming time	Less than 3 seconds	2-5 seconds
Foam stabilization	Natural cooling	Polymerization, crosslinking
Expansion ratio	Upto 50 times	Upto 250 times

1.2.2. Rigid and Flexible Foams

Rigid foams, as the name suggest, are relatively stiffer and are characterized by the presence of closed spaces in a polymer matrix. They possess cell integrity and hence exhibit excellent mechanical properties. Rigid foams are finding applications in building, insulation, appliances, transportation and food and drink containers etc. Flexible foams, on the other hand, exhibit relatively inferior mechanical properties compared to rigid foams but are light weight and less dense. They are widely used in transportation, bedding, carpet overlay, sound attenuation etc.

1.2.3. Open and Closed Cell Foams

Open cell polymer foams are characterized by the presence of open spaces in the polymer network (**Figure 1.1 a**). The cells are well connected and they exhibit a soft and spongy appearance. The integrity of the cell wall is poor and hence it is not able to hold the gaseous phase together. When compressed, these tend to deform elastically and exhibit poor mechanical properties especially in terms of compressive strength and energy absorption ability. Nevertheless open-celled polymer foams perform well for moisture absorption and are extremely effective in sound deadening applications.

Closed cell polymer foams comprise of isolated cell walls (**Figure 1.1 b**). The cells retain their integrity and hence this class of foams possesses higher compressive strength and energy absorbing ability. They also have low permeability to water and have good insulation properties. Closed cell polymer foams are denser compared to open celled foams and are therefore more expensive. Based on the size of air pockets, foams can further be classified as macro-cellular(> 100 μm), micro-cellular (1-100 μm), ultra-microcellular (0.1-1 μm) and nanocellular (0.1-100 nm) [10].
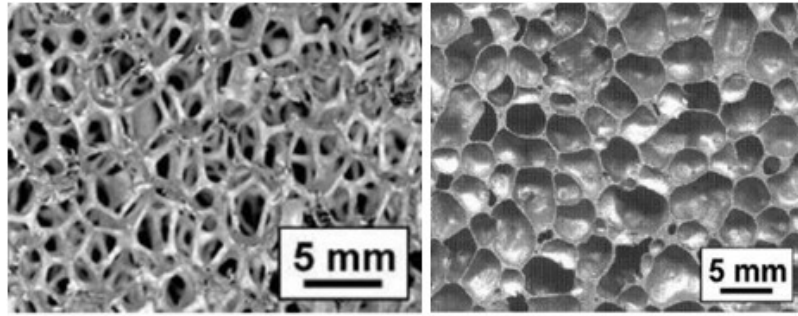
Fig.1.1 :(a) Open cell and (b) closed cell polymer foams

All categories of foams discussed above involve the use of either a chemical or a physical blowing agent. The application of foams is a function of their mechanical properties, which in turn is dependent upon their densities as is illustrated in **Figure 1.2**.
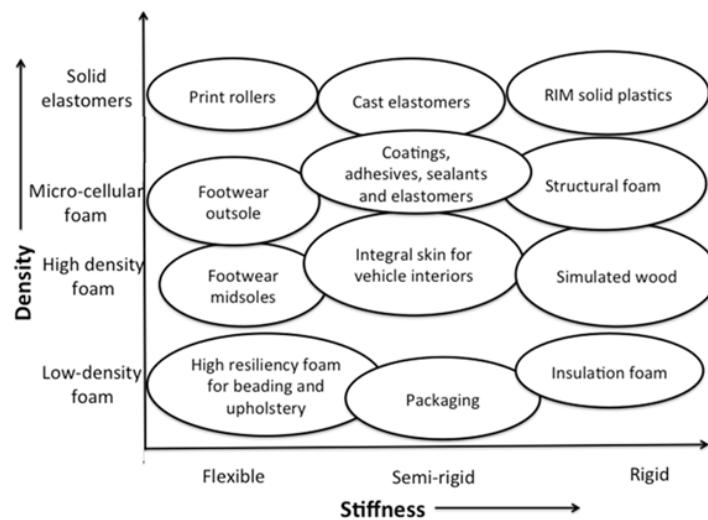
Fig.1.2: Varied applications of foam depending on density and stiffness

As per the foam definition, these materials can very well be obtained by introducing hollow fillers in the matrix, which gives rise to an altogether new category of thermoplastic or thermoset foams. These physical foams are called syntactic foams because the porosity in the foams is induced physically and is not a result of any chemical reaction. Keeping in view the formation process, these foams are generally considered to be a sub-class of composites.

1.3. Foaming Techniques

Thermoplastic foams are manufactured by foam extrusion and injection moulding processes. Structural foam moulding is also a widely used processing tool for the manufacture of thermoplastic foams. Thermoset foams production makes use of manual or mechanical stirring in the laboratory or by reaction injection moulding. However, these foaming techniques are broadly categorized into reactive foaming, soluble foaming and quenching technologies. Reactive foaming accounts for the production of cross-linked polyethylene and polyurethane foams via chemical blowing agents. Soluble foaming makes use of physical blowing agents, which is dissolved at high pressure in the polymer melt resulting in the formation of thermoplastic foams. This technique facilitates continuous processing such as used in extrusion process. Quenching involves the dissolution of polymer in a suitable solvent (the blowing agent) followed by the removal of the solvent post quenching resulting in a porous structure. The method is popular with water soluble or biodegradable polymers.

1.4. Syntactic Foams

Syntactic foams are closed cell foams, which fall under the broad umbrella of composite materials. Syntactic foams are fabricated by the incorporation of hollow microspheres in a suitable matrix. American Society of Testing and Materials (ASTM) defines syntactic foam as "a material consisting of hollow sphere fillers in a resin matrix" [1]. The primary purpose of introducing hollow microspheres is to emulate conventional foams with a higher reduction in the weight of syntactic foams with enhanced mechanical properties. Syntactic foams are thus, lightweight materials with low density but high specific strength, particularly designed for marine, aerospace and in all demanding areas, where weight is a restraint. The hollow microspheres can be regarded as reinforcements in polymer matrix hence they can be also termed as foamed composites.

1.4.1. Constituents of Syntactic Foams

Microbubbles and matrix form the basic component of syntactic foams, the mixing of which leads to a two phase structure. However, the presence of voids results in a three phase structure of syntactic foams. Syntactic foams can be fabricated with a vast variety of matrices that include polymers [11], metals [12] or ceramics. In the case of polymer syntactic foams, both thermoplastic and thermosetting polymers have been explored as matrix materials. The commonly used thermosetting resins include epoxies [13], phenolics [14], vinyl esters [15], bismaleimides [15], polyurethanes [16] etc. Examples of thermoplastic resin matrices used include polyethylene [17-22] and polypropylene [23]. Hollow microspheres lead to density reduction in addition to providing high specific strength and low moisture absorption properties to the syntactic foam. The choice of microbubble is varied ranging from glass [24-29], fly ash [15, 30], polymer [31], carbon [14], ceramic [12], or even metal [32, 33]. Bio based reinforcements e.g. silk cocoons have also been explored as natural microbubbles for polyurethane syntactic foam preparation [34].

From the processing viewpoint, thermosetting syntactic foams offer several advantages compared to their thermoplastic analogues, and therefore most of the research on syntactic foams focusses on thermoset matrix. The processing conditions are relatively favourable, particularly low viscosity which results in low microbubble breakage during processing operations. Thermosetting foams exhibit less solvent sensitivity, and can be conveniently processed at ambient temperatures, thus reducing the energy costs associated with processing.

Nevertheless, several attempts have been made to process syntactic foams with a thermoplastic matrix by using a solvent [35], or even by using an injection moulding machine [17, 36] or by use of compression moulding technique [18]. Thermoplastic

7

foams can be used to produce intricate parts using 3D printing, which are not possible using the analogous thermosetting resins.

1.4.2. Microstructure of Syntactic Foams

The structure of syntactic foams consists of hollow microbubbles as reinforcement surrounded by a matrix phase. During the processing of syntactic foams, certain amount of air also gets entrapped in the area between the microbubbles and the matrix. This gives rise to a three phase structure consisting of matrix, reinforcements and voids. Uniformly dispersed fillers can also be added to the resin to obtain better end properties compared to neat syntactic foams. Representative SEM micrograph of neat epoxy- hollow glass microbubble syntactic foam is presented in **Figure 1.3**.
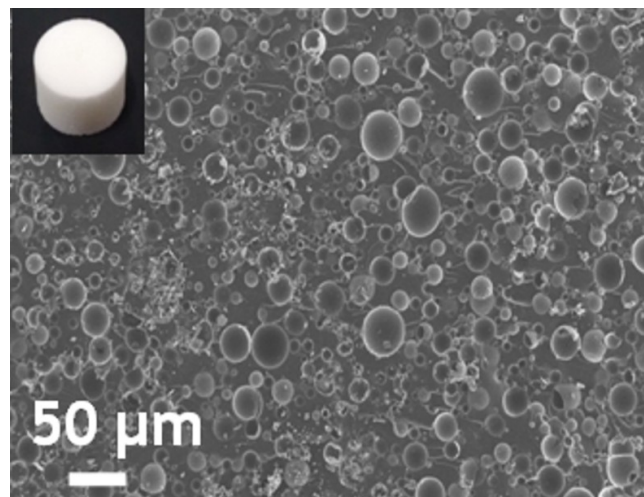
Fig.1.3: *SEM image of syntactic foam. Inset shows the optical image of the specimen*

1.4.3. Ternary Phase Diagram

In general, syntactic foams are three phase systems which can be best understood through a phase diagram. A representative phase diagram is presented in **Figure 1.4**. The components forming the system can be represented by three apexes of the triangle in the ternary phase diagram. The points A, B and C located on this ternary phase diagram represent three demonstrative syntactic foam formulations. Point A refers to a formulation containing 15 % (v/v) polymer resin, 60 % (v/v) microbubbles and 25 % (v/v) voids.

Similarly points B and C lying entirely on one of the vertices of the equilateral triangle corresponds to two phase syntactic foams constituting of only the polymer and microbubble. Point B depicts a formulation consisting of 40 % (v/v) of polymer and 60 % (v/v) microbubbles and point C represents a formulation of syntactic foam having 60 % (v/v) and 40 % (v/v) of polymer and microbubbles respectively.

The shaded region in the ternary phase diagram corresponds to a region where existence of syntactic foam is practically not possible. This is because the upper limit of packing of microbubbles for hexagonal close packing is restricted to 74 % (v/v). Similarly, the lower limit for cubic packing of spheres is maintained around 52 % (v/v). **Table 1.2** corresponding to the packing density of microbubbles is presented below.

Table 1.2: Characteristic parameters associated with microsphere packing

	Co-ordination number	*Packing*	*Occupancy (%v/v)*
Uniform size spheres	6	Cubic	52
	8	Body-centred cubic	62
	12	Face-centred cubic	74
	12	Hexagonal	74
Non-uniform spheres	-	Random	90
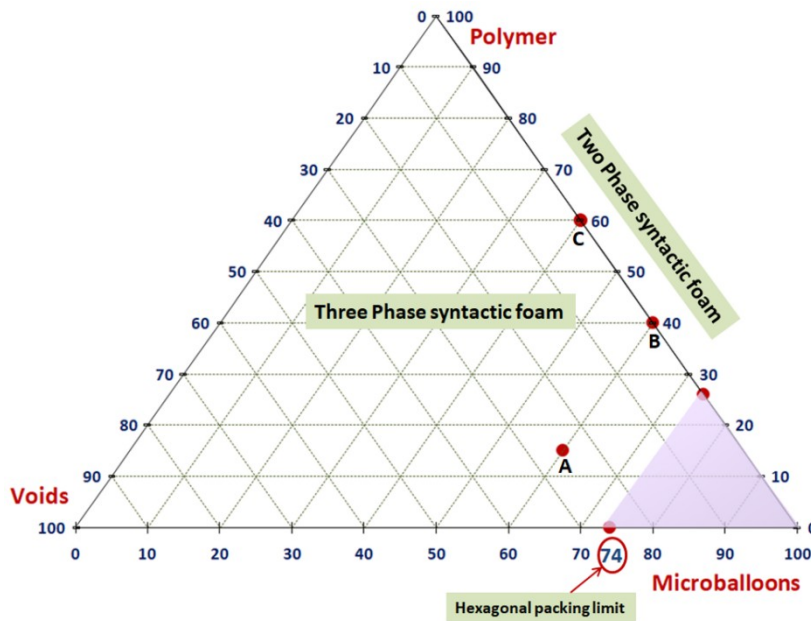
Fig.1.4: *Ternary phase diagram for syntactic foams*

1.4.4. General Methods of Preparation of Syntactic Foams

The methods of preparing conventional foams include incorporation of chemical blowing agents into a suitable matrix. Syntactic foams, on the other hand, make use of preformed microbubbles that are mechanically mixed with a polymer, be it thermoset or thermoplastic to form a composite material. The exact method of producing a syntactic foam varies with the type of matrix engaged i.e., thermoplastic or thermoset and on the amount of microbubbles employed for its processing. The manufacturing of syntactic foams is done via moulding, casting, extrusion, rotational moulding or buoyancy methods depending upon the filler and resin volume fraction. Volume percentage of microbubbles in excess of 40 indicates a moulding composition while that below 40 denotes a casting composition. Moulding compositions, thus being difficult to process, requires the use of a solvent to facilitate processing, however, this could lead to increased cost of production and may pose environmental hazards.

1.4.5. Comparison with Conventional Foams

Blown or self-expanding foams possess a fairly random distribution of open pores of varying sizes and shapes. In contrast, cellular pockets in syntactic foams are controlled by the judicious choice of microbubble size and wall thicknesses. The open cell structure of traditional foams is interconnected as opposed to an isolated closed porosity in syntactic foams. Syntactic foams are relatively denser, more rigid and less sensitive to moisture as compared to conventional foams. The compressive properties of syntactic foams are an order of magnitude higher than that of self expanding foams. Syntactic foams are therefore suited for structural applications that demand good mechanical properties and less weight that cannot be met by conventional foams.

1.4.6. Syntactic Foams: Challenges

The major challenge associated with polymer syntactic foam is the viscosity of the molten formulation (for thermoplastic) that restricts its processing. Introduction of hollow microbubbles appreciably alters the rheological profile of the thermoplastic melt; thereby affecting the extrusion processability of the polymer. It is extremely important to optimize conditions, especially shear stresses to avoid microbubble crushing during extrusion. Rupture of glass microbubbles during extrusion result in an undesirable increase in the density of the composite [21]. These challenges have held back the popularity of thermoplastic matrix syntactic foams. As far as the thermoset resins are concerned, it is essential to ascertain the volume fraction of microbubbles to obtain a homogeneous distribution of microbubbles to produce parts with isotropic properties and reduced weight. Too high volume fraction can lead to an abrupt increase in the viscosity of the formulations. On the contrary, low volume fractions can result in density gradation in the foam formulation resulting in uneven part properties. These challenges can be overcome by judicious choice of microbubbles and matrix and the determination of optimal

concentrations of microbubbles that can be dispersed uniformly.

1.4.7. Property Tailoring

The end-properties of syntactic foams depend upon the constituent properties, i.e. matrix as well as microbubbles. One of the principal advantages offered by syntactic foams is the ability to tune the properties of syntactic foams according to the type of application. Both the type of matrix and microbubbles can be varied to obtain a wide range of syntactic foams. Thermoplastic syntactic foams can be fabricated not only by common processing techniques, ofcourse taking due care of the fracture of microbubbles, for commodity applications but also by rapid prototyping and 3D printing techniques to produce parts with specialised geometry where cost is not a concern. Similarly, thermoset precursors can be utilized in syntactic foam fabrication for advanced, scientific and research oriented applications. Induction of closed cell porosity in syntactic foams can lead to varied properties of the syntactic foams. Microbubbles are available in wide range of densities (0.1-0.6 g cm^{-3}). Preparation of syntactic foams with these hollow microbubbles can alter the mechanical properties of the composite materials radically. In addition to the choice of microbubbles based on density, the volume fractions of the microbubbles can also be tailored to obtain syntactic foams with widely varying densities and properties. Polymer microbubbles are also being preferred nowadays compared to inert glass or fly ash microbubbles. These can be synthesized to obtain better interfacial adhesion with the matrix and consequently improved end properties. Thermoplastic microbubbles in this context have shown to improve the upper limit of microbubble loading and thus create syntactic foams with very low densities [31]. Functional gradation in syntactic foams can be created either by varying the volume fraction or the wall thickness of the microbubbles along one dimension of the material. Such kinds of foams have the ability to undergo progressive failure and possess large energy absorption under

compression [37-39].

Syntactic foams possess high strength, modulus and good dimensional stability attributed to the presence of microbubbles. Due to the presence of closed microbubbles, syntactic foams are found to exhibit low moisture absorption [40, 41]. Syntactic foams are isotropic in nature [42, 43]. The hollow fillers are dispersed uniformly in the resin to attain isotropic properties. Syntactic foams are characterised by low dielectric constants due to the presence of closed pores in its microstructure [44, 45]. These pores contain air that has a low dielectric constant of 1. As a result, syntactic foams are finding applications in various electronics applications too. The coefficient of thermal expansion of syntactic foams is remarkably low as compared to neat polymers and decreases with increasing concentration of deliberately placed voids in the system [46, 47].

1.4.8. Applications of Syntactic Foams

Syntactic foams are used in a variety of applications due to the presence of both microbubbles and matrix. The combined capabilities account for the development of strong yet lightweight materials. They are preferred as core materials in sandwich structures in the areas of blast mitigation [33, 48]. Syntactic foams present an excellent candidature for the development of buoyancy modules for submarines and undersea structures due to its lightweight and low moisture absorption coupled with good hydrostatic compressive strength [49-51]. The rudders and flaps of submarines are manufactured from syntactic foams. Remotely Operated Vehicles (ROVs) and Human Operated Vehicles (HOVs) which are extensively used in deep-sea exploration are fabricated using syntactic foams [47]. They are also used in the construction of radomes for aircraft, spacecraft and automobiles etc. [52-54]. Use of lightweight materials can permit weight savings and can lead to fuel economy in automobiles and aircraft. Space shuttle vehicles make use of thermal insulation properties of syntactic foams to retain

their dimensional stability over wide temperature regimes [55]. Syntactic foams have also been successfully utilised in electrical and electronics applications [44, 56]. Thermal insulation properties of syntactic foams make its way in the oil and gas industry. The presence of entrapped air helps to maintain the thermal insulation characteristics of syntactic foams. The miscellaneous applications of syntactic foams include them being used in the manufacture of sports equipments, furniture, radio equipment, fire protection, etc [47]. However, the applications of these foams are not restricted to the above mentioned areas, and will further widen as more research is undertaken in these areas.

1.5. Deformation in Cellular Materials

The density and volume fraction of the matrix and microbubbles are principle factors influencing the mechanical properties of the composite material. The failure mechanism is strongly dependent on the mode of testing of syntactic foams. Tensile failure is brought about by the failure of the matrix whereas, under compression, the microbubbles undergo extensive crushing and the failure of the foam is initiated by shear cracking and/or axial splitting. Flexural testing is basically a combination of tensile and compressive forces and results in microbubbles debonding as well as matrix failure.

Uni-axial compression testing is the primary test, which is performed on polymeric foams. It is to be noted that the mechanical behaviour of foams in compression is different from that in tension. Polymer foams are usually ductile in compression but they are brittle in tension [57]. The compressive stress-strain curve of syntactic foams, in general, reveals three sections. An initial linear elastic (Hookean) region characterized by a proportional increase in strain at increased stress is observed. This is followed by a long plateau region of constant stress at increasing strains. The final regime in the compressive stress-strain plot of polymer foams is represented by densification in which the stresses rise exponentially at low strains [58, 59].

The mechanism of deformation of the polymer foams in each of the three regions is different. As discussed above, the initial linear region in compressive stress-strain plot is governed by elastic bending of cell walls in the case of open cell foams unlike cell wall stretching observed for closed cell foams [60-62]. The Young's modulus can be calculated from this elastic (Hookean) region by computing the slope of this initial region.

The plateau region is associated with the collapse of cells (elastic buckling) and in the case of syntactic foams, by an irreversible shear cracking mechanism [54]. When all the microbubbles have collapsed and the cell walls touch each other, the foams can no longer withhold this plateau. As a result, a steep increase in stress is observed at low strains. This is called densification and signals the complete failure of the foams. Increasing the density of foams leads to the generation of higher plateau stress but may also lead to less strain as opposed to low density foams.

The area under compression stress-strain curve till the plateau region is therefore quantified as an index of the amount of energy absorbed by the foams, hence the toughness [63]. As a measure of this, polymer foams must possess a good combination of high plateau stress also called compressive stress and long plateau region or large strain in order to absorb a significant amount of energy. A representative stress-strain curve of syntactic foam is presented in **Figure 1.5**. The shaded region is used for the quantification of energy absorbed.
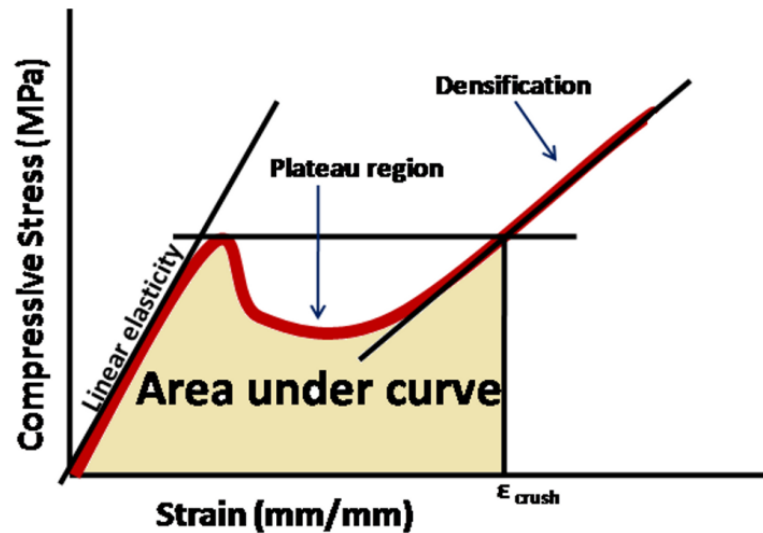
Fig.1.5: *Compressive stress-strain curve of syntactic foams*

In view of the large area under the stress-strain curve, syntactic foams are finding increasing use in blast mitigating applications, such as core material in sandwich structures. The following section deals briefly with this phenomenon of blast, and the damage resulting from the blast on the structures.

1.6. Blast loading

"Blast" is a term used for a destructive wave of highly compressed gases spreading outwards from an explosion. A fraction of the explosive energy is released as thermal radiation and the gases expand radially as blast waves or shock waves. As the shock wave expands, the pressure decays rapidly with time (i.e. exponentially) and have a very brief lifespan, measured in thousandths of second or milliseconds (**Figure 1.6**). Explosive detonations lead to an incident shock wave that is characterized by a rise in atmospheric pressure to peak overpressure. **Table 1.3** gives an indication of the probable damage that can result due to incident overpressure.
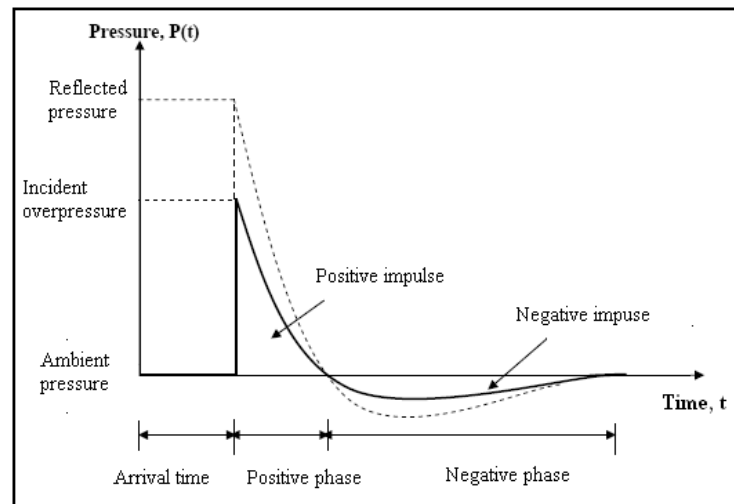
Fig.1.6: *Qualitative pressure-time history due to blast loading* [64]

In general, the following features are associated with the phenomenon of explosion

❖ The intensity of pressure is usually of several orders of magnitude greater than earthquakes, winds or floods, etc.

❖ Explosive pressures decay rapidly with distance from the source

❖ The duration of the event is very small, measured in thousandths of a second or milliseconds. This differs from an earthquake or winds which are measured in seconds

Table 1.3: *Qualitative estimates of damage resulting from increasing overpressure* [64]

Damage	Incident Overpressure (psi)
Typical window glass breakage	0.15-0.22
Minor damage to some buildings	0.5-1.1
Panels of sheet metal buckled	1.1-1.8
Failure of concrete block walls	1.8-2.9
Collapse of wood framed buildings	Over 5.0
Serious damage to steel framed buildings	4-7
Severe damage to reinforced concrete structures	6-9
Probable total destruction of most building	10-12

17

1.7. Literature Survey

It has been mentioned that the properties of syntactic foams are strongly dependent on its constituents, i.e. matrix, the type of hollow filler and its density (**Table 1.4**). In general, the compressive strength decreases with increasing microbubble loading. For a representative bisphenol-A based epoxy resin, the compressive strength has been reported to be ~ 105 MPa [25]. With the introduction of hollow glass bubbles, the compressive strength decreases, the extent of which is proportional to the extent of loading. For the bisphenol-A based epoxy resin, the compressive strength decreases from 105 MPa to ~ 25 MPa at 60 % loading of hollow microbubble (K15, density = 0.15g/cc) [25].

The strength of the constituent microbubble also plays an extremely important role in defining the mechanical strength. With increasing radius ratio of the microbubble, the mechanical strength decreases proportionally. For similar microbubble loading, the formulations containing microbubbles with higher crush strength, relatively higher mechanical properties are observed. The failure of syntactic foams is similar to cellular solids and occurs primarily by shear cracking as well as axial splitting. The modulus has also been reported to decrease with increasing microbubble loading. For the epoxy- glass bubble system, the energy absorption ability of foams is optimum at 40-50 % (v/v) of hollow glass microbubbles. Tensile properties are also dependent on the type of microbubble employed for its preparation. For S22 microbubble (density = 0.22 g/cc), the tensile strength has been reported to increase from ~ 17 MPa (30 % microbubble loading) to ~ 25 MPa for K46 (density = 0.46 g/cc) system. Interestingly the effect of introducing microbubbles with higher density and strength does not affect the tensile properties substantially, with the increase in tensile strength being ~ 56 % for similar microbubble loading with K46 microbubble [51]. The matrix also defines the compressive properties appreciably. For a vinyl ester system, the compressive strength decreases from ~ 52 MPa

to ~ 22 MPa with a concomitant increase in the volume percentage (30-60 % v/v) of glass

microbubbles (density = 0.22 g/cc) [52].

A variety of fillers [65-68] have also been explored for syntactic foams with an aim

to improve the mechanical properties without a further increase in weight. The volume

fraction, geometry and dispersion of fillers are vital parameters while preparing syntactic

foam formulations. A range of filler with dimensions ranging from nano to micro has

been explored to formulate syntactic foams with damage tolerant properties. In this

context, the potential of nanoclay (0-2 % w/w) and short carbon fibres (10 mm length) in

1-3 % by weight for epoxy resin based syntactic foam was explored. The volume

percentage of phenolic microbubbles (BJO-093) was kept constant at 30 % (v/v).The

tensile strength of neat syntactic foam was ~ 27 MPa. The inclusion of nanoclay (2 %

w/w) reduced the tensile strength to ~ 24 MPa whereas short carbon fibres (2 % w/w)

enhanced the tensile strength to ~ 32 MPa. However, fracture toughness values reported

an enhancement of ~ 42 % for either type of filler (1 % w/w) increasing from 1.15 MPa

$m^{0.5}$ to 1.63 MPa $m^{0.5}$ for neat and filler reinforced systems respectively [69]. The effect

of introducing different kinds of fillers on the properties is briefly tabulated in **Table 1.4**.

Table 1.4: Improvement in mechanical properties due to reinforcement

Ref.	Matrix	Hollow filler		Reinforcement	Properties
		Type	Volume percent		
[8]	Epoxy	Glass microbubbles (S22 and K46)	35 and 65 % (v/v)	-	Compressive modulus of S22 and K46 syntactic foams, in their dry state, decreased from initial values of ~ 1500 and ~ 2500 MPa respectively by 49 % and 48 % respectively for wet samples (exposed to de-ionized water at low temperature). Compressive strength remained unaltered for samples containing S22 and K46.

[70]	Epoxy	Glass microbubble Particle size range (µm) 149-175 125-149 100-125 44-100 < 44	67.8 %	-	Increasing the specimen aspect ratio from 0.4-0.9 did not alter the compressive yield strength substantially (19.7-22.4 MPa) but the mechanical response of the specimen to compression changes.
[25]	Epoxy	Glass microbubbles (K15, S22, K46)	0-60 % (v/v)	-	The compressivestrength of neat epoxy being ~ 105 MPa decreased to ~ 25 MPa for 60 % (v/v) microbubble loading. The failure of syntactic foams was similar to cellular solids and failure occurs by shear as well as axial splitting.
[71]	Epoxy	Epoxy hollow spheres	Complete filling of the mould.	-	Compressive strength ~ 19 MPa, compressive modulus 187 ± 0.7 MPa.
[51]	Epoxy	Glass microbubbles (S22, S32, K37, K46)	30-50 %(v/v)	Carbon Nanofibers (0.25 %v/v)	Tensile properties increase from ~ 15 MPa to ~ 20 MPa for formulation containing K46 (40 % v/v) upon adding carbon nanofibers.
[72]	Epoxy	Glass microbubbles (K25)	15 %(w/w)	Fiberglass mesh, short fiber	Flexural strength (~ 31 MPa) and modulus (~ 2 GPa) of unreinforced foam increased by 28% and 19 % respectively upon addition of 1.5 % w/w fiber.
[73]	Epoxy	Glass microbubbles (S22, K46)	30 and 50 % (v/v)	Carbon nanofibers (0.30 % v/v)	Tensile modulus of neat syntactic foams was 1910 ± 145 MPa (SF22, 50% loading) and 3615 ± 190 MPa (SF46, 50% loading). Improvements by 9.8% and 12.5% respectively for carbon nanofiber reinforced syntactic foams were observed. Tensile strength of neat foams was 12.4 ± 2 MPa (SF22, 50% loading) and 22.87 ± 4.02 (SF46, 50% loading) and it increased by 29% and 46.6% respectively upon addition of carbon nanofibers (0.3% loading)|.
[74]	Epoxy	Glass microbubbles	35-40 % (w/w)	Nanoclay (Cloisite	Compressive strength and modulus of neat foam was 48

Ref	Matrix	Filler	Content	Reinforcement	Observations
		(K37)	30 B) (1,3,5 %w/w)		± 5 MPa and 1.08 ± 0.05 GPa respectively. It increased to 71 ± 2 MPa and 1.19 ± 0.02 GPa respectively, an increase of 48 % and 10 % in compressive strength and modulus respectively with 5 %(w/w) nanoclay. Flexural strength and modulus increased by 16 % and 21 % respectively for 5 wt % clay.
[68]	Epoxy	Glass microbubbles (S22, S32, S38, K46)	60 % and 63 % (v/v)	Nanoclay (Nanomer I.30E) (2 and 5 % v/v)	Reinforcing with 5 % (v/v) nanoclay enhanced the tensile strength by 6-22 % and toughness by 33-58 %.
[75]	Epoxy	Glass microbubbles (K15)	60 % (v/v)	Inorganic nanoclay (K-10) (1-3 wt %)	Incorporation of 2 wt% nanoclay improved the flexural strength, flexural strain and modulus by ~ 42 %, ~ 38 % and ~ 18 % respectively. Toughness increased by ~ 89 % at 2 %w/w nanoclay. Storage modulus and loss modulus improved by 30 % and 28 % respectively at 2 %w/w loading of nanoclay.
[76]	Epoxy	Glass microbubbles (S38)	30 % (v/v)	Graphene platelets (0.1, 0.3, 0.5 % v/v)	Compressive strength increased by 3.6 % and 2.4 % upon adding 0.1 % (v/v) and 0.3 % (v/v) graphene platelets. Tensile strength increased by 15.9 % and 14.7 % at 0.1 and 0.3 % (v/v) respectively.
[77]	Epoxy	Glass microbubbles (S22, S32, S38, K46)	(60 and 63) % (v/v)	Crumb rubber (2 % v/v), nanoclay (2 and 5 % v/v)	Flexural strength of neat syntactic foams increased proportionally with increased densities of hollow glass microbubbles and K46 containing system exhibited a flexural strength of ~ 23 MPa. Incorporation of 2 % (v/v) of 40 μ crumb rubber led to a reported increase in the flexural strength of 29 MPa. Nanoclay addition (5 % v/v) decreased the flexural strength by 7 %.
[78]	Epoxy	Glass	63 % (v/v)	Crumb	The compressive properties

		microbubbles (S22, S32, S38, K46)		rubber 2 % v/v (40 μm and 75 μm)	were found to be inversely proportional to the radius ratios of glass microbubbles. The extent of improvement was higher for smaller rubber particles. The compressive strength of neat foams reduced upon rubber addition. Epoxy/K46 glass microbubbles displayed compressive yield strength of ~ 70 MPa that reduced to ~ 62 MPa upon addition of rubber (40 μm).
[79]	Phenolic resin	Hollow amino resin microspheres	77 %(w/w)	Aramid fiber (K-49), carbon fiber (C-30)	Shear compression and tensile properties increased by 30-40% in one orientation; while in other orientation, tensile strength, compressive strength and elastic modulus increased by a factor of 7, 2, and 8 respectively.
[80]	Polybenzoxazine (bisphenol A)	Glass Microbubbles	10-50 % w/w	Silica fibers (38.5 % v/v)	Tensile, flexural and compressive strengths of benzoxazines/silica fiber composite (BSM0) were 36 ± 4.3, 75.7 ± 6.4, 116.8 ± 17.5 respectively. Increasing weight percent of microbubbles led to a concomitant decrease in the mechanical properties of the composite compared to BSM0.
[52]	Vinyl ester	Glass microbubbles (S22 and K46)	30-60 % (v/v)	-	Quasi-static compressive strength of vinylester/glass microbubbles (S22) (30-60 % v/v) syntactic foams lies in between ~ (56-24) MPa. At high strain rates, compressive strength increases. This strain rate sensitivity is attributed to the properties of the matrix material.
[66]	Phenolic resin	Hollow carbon microspheres	28 % (v/v)	Carbon nanofibers (0.5-2 % v/v)	No significant increase in compressive strength was observed. Flexural strength increased by 196 % at carbon nanofibers loading upto 1.5 % (v/v)

| [53] | Polybenzoxazine (bisphenol A) | Glass microbubbles (K25) | (~ 61 to ~ 78 % v/v) | - | The tensile, flexural and compressive strength of benzoxazines syntactic foams for 29.9 % v/v resin and 61.4 % v/v microbubble were 1 ± 0.4, 3.8 ± 0.4 and 4.8 ± 0.6 MPa respectively. Optimum results for tensile, flexural and compressive strengths were 2.7 ± 0.2, 3.2 ± 0.5 and 7.2 ± 1.1 MPa respectively for the formulation containing 68.1 %v/v and 22 % v/v of glass microbubbles and resin respectively. Further microbubbles loading led to deterioration in the mechanical properties. |

In comparison, polyurethane foams of density 128 kg/m^3 and 192 kg/m^3 exhibit quasi-static compressive strength of ~ 2MPa and ~ 4 MPa respectively. Similarly, EPS foam of density 61 and 112 kg/m^3 exhibit quasi-static compressive strengths of ~ 0.5 and ~ 1 MPa respectively and HDPE foam of densities 80 and 110 kg/m^3 has compressive strengths of 0.4 and 0.7 MPa respectively, as studied by Ouellet et.al. [81].

Polyurethane foams derived from tertiary recycling of PET waste using microwave assisted process recorded compressive strengths of the order of 200 ~kPa [82]. Roy et.al studied the compressive strength of polyisocyanurate foams at 10 % strain and found the compressive strength to be ~ 158 kPa for a foam of density 376 kgm^{-3} [83]. Luong et.al studied the compressive properties, especially the energy absorption of polyurethane resin and polyurethane syntactic foams containing alumina hollow spheres, and found that both polyurethane resin and polyurethane syntactic foam displayed strain rate sensitivity wherein compressive strength increased with strain rate. However, it was observed that energy absorption was much higher for

polyurethane syntactic foams (400 %) compared to polyurethane resin at 10 % strain in the quasi-static regime [84]. A comparison of the compressive stress-strain curves of different types of foams mentioned in the literature has been placed in **Figure 1.7**.
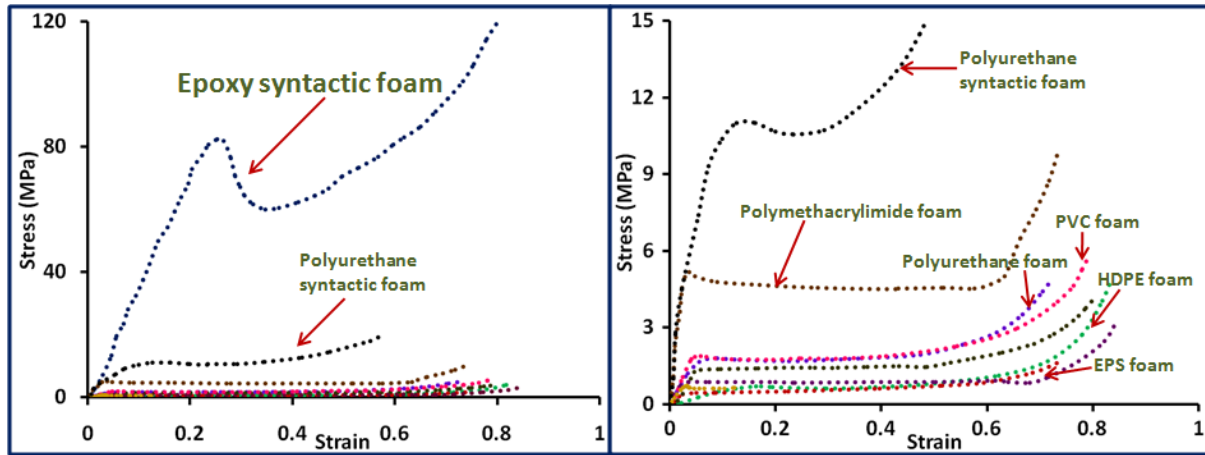
Fig.1.7: Comparison of compressive stress-strain curves of different foams. Data obtained from the literature

In the last two decades, the activity of terrorist groups against military assets has grown significantly. A small boat filled with explosives attacked the USS Cole on 12th October, 2000, while it was refuelling in Aden Harbor in Yemen. The attack resulted in the formation of a wide hole (40ft x 60ft) on one of the sides of the ship (**Figure 1.8 a**), leading to immediate crippling of the ship and 17 fatalities.

The threat due to improvised explosive devices (IED) against land vehicles, especially in the Middle East regions has been even more devastating. About 1400 fatalities due to IEFs have been reported during the Operation Enduring Freedom (OEF) alone. Therefore, innovation in the design of blast protection vehicles has been underway in the last decade to deliver safe transportation of both equipment as well as personnel. The best of designs are still vulnerable to IED attacks, e.g. Cougar Mine-Resistant Ambush Protected (MRAP) vehicle, as shown in **Figure 1.8 b**. Therefore, there is a

pertinent interest in blast armour technologies to this day, and hence development of high strength foams with enhanced energy absorption characteristics are the need of today.
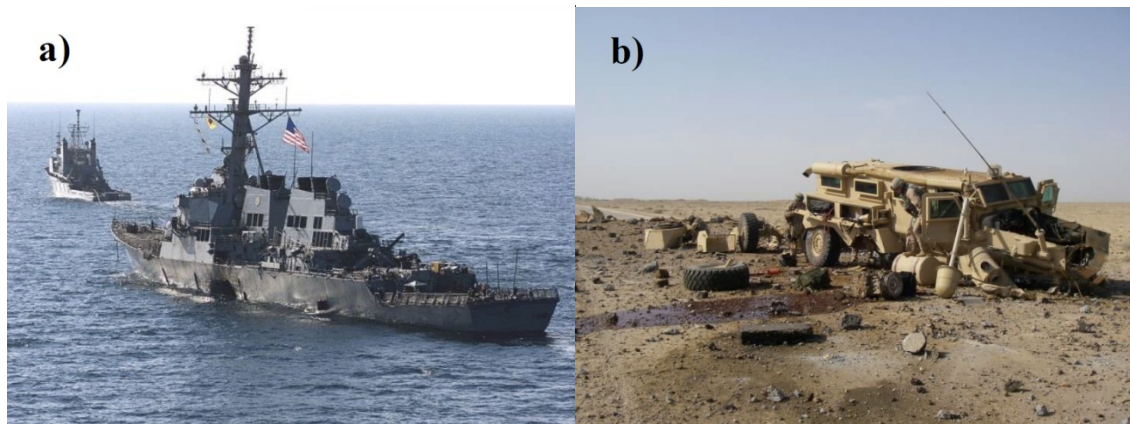
Fig.1.8: Targeted damage to sea and land vehicles by terrorists a) the USS Cole and b) the Cougar MRAP vehicle [85, 86]

1.8. Objective of the Work

The main goal of this research project is to prepare polymeric syntactic foams and quantify the extent of energy absorption upon being subjected to static and dynamic loads. Another objective is to study the effect of the introduction of different types of fillers on the energy absorption characteristics. More specifically, the objectives include:

❖ Preparation and characterization of different types of syntactic foams, while varying the type of polymeric matrix and microbubble. In the present work, the following formulations have been studied.
   o Epoxy- hollow glass microbubble syntactic foams
   o Epoxy- hollow epoxy microbubble syntactic foams
   o Benzoxazine-hollow glass microbubble syntactic foams

❖ To study the rheology of syntactic foam formulations with an aim to establish the optimal concentration of microbubbles that can be processed without the aid of solvents

❖ To study the effect of the introduction of additives in the polymeric matrix during processing.

    o 2-Dimensional fillers

        ➢ Molybdenum disulfide

        ➢ Reduced graphene oxide platelets

        ➢ Nanoclay (Cloisite 30 B)

    o Electrospun nanofibers

        ➢ Nylon 6

    o Elastomers

        ➢ Poly (dimethylsiloxane) microspheres

❖ To study the mechanical behaviour of syntactic foams under dynamic loads

❖ To study the effect of strain rate on mechanical properties of syntactic foams

1.9. Plan of Work

A systematic methodology highlighting the work involves the following steps:

❖ Preparation of polymer syntactic foams containing appropriate fillers

❖ Mechanical characterization including quasi-static testing and high strain rate testing of the developed polymer foams

❖ Quantification of energy absorption characteristics of polymer composites based on quasi-static tests

❖ Determination of mechanical properties of the polymeric foams under dynamic loads

1.10. Thesis Organization

The thesis is organized into eight chapters. Most of the studies compiled in this thesis have either been published in peer-reviewed journals or have been communicated. The thesis deals with studies on the preparation, characterization and evaluation of syntactic

foams based on epoxy and polybenzoxazine. The effect of incorporation of two kinds of microbubbles i.e. glass and epoxy on the rheological and mechanical properties of syntactic foams have also been studied. The chapters are briefly discussed below:

Chapter 1: Introduction

This chapter "Introduction" lays special emphasis on the properties and applications of polymer syntactic foams, and the techniques used for their preparation. The results of the literature survey on the mechanical properties of resin-hollow filler system and the effect of introducing different types of fillers have also been compiled.

Chapter 2: Chemorheology and Mechanical Properties of Epoxy Syntactic Foams

This chapter deals with the preparation of epoxy based syntactic foams containing hollow glass microbubbles in varying volume percentage ranging from 10-70 % (v/v).The optimal concentration of glass microbubbles has been determined through detailed rheological studies. The mechanical properties of the resultant syntactic foams have also been evaluated.

Chapter 3: Two-Dimensional (2D) Layered Filler Reinforced Epoxy Syntactic Foams

This chapter deals with the reinforcing effect of three different 2D fillers, namely molybdenum disulfide (MoS_2), reduced graphene oxide and nanoclay, on the mechanical properties of epoxy syntactic foams. Introduction of fillers, especially MoS_2, led to significant improvements in the quasi-static mechanical properties.

Chapter 4: Poly(dimethylsiloxane) Toughened Epoxy Syntactic Foams

The aim of this chapter is to study the role of preformed spherical rubber particles as toughening agents for epoxy based syntactic foams. Poly (dimethylsiloxane) microspheres have been prepared by suspension curing route, and the effect of

introducing these microspheres on the compressive, tensile and flexural properties of epoxy-HGM is discussed in detail.

Chapter 5: Electrospun Nanofiber Reinforced Epoxy Syntactic Foams

The potential of nanofibers towards improving the properties of syntactic foam has been studied. Processing conditions like feed concentration, flow rate, operating potential and nozzle-collector distance have been optimized for obtaining smooth electrospun nylon 6 nanofibers. The effect of introducing these nanofibers (0.25-4 % v/v), in epoxy-hollow glass bubble syntactic foam formulation is studied. The results of the studies have been discussed in this chapter.

Chapter 6: Epoxy- Epoxy Microbubble Syntactic Foams

Hollow epoxy microbubbles have been prepared by interfacial engineering approach. The core content has been determined and the mechanical properties of the syntactic foams containing epoxy with the developed epoxy hollow microbubbles have been discussed in detail.

Chapter 7: Polybenzoxazine-Glass Microbubble Syntactic Foams

The preparation of bisphenol F aniline based polybenzoxazines syntactic foams with varying content (30-60 % v/v) of hollow glass microbubbles (K46) is discussed. The rheological properties of the foamed composite have also been evaluated.

Chapter 8: Summary and Conclusions

This chapter summarizes and concludes the work and outlines suggestions for future exploration.

Chapter II

Chemorheology and Mechanical Properties of Epoxy Syntactic Foams

Parallel plate rheometer

Glass microballoons embedded in epoxy network

Glass microballoon

Epoxy

Hollow glass microballoons

Mixing

Epoxy Syntactic foam formulation

Quasi-static testing
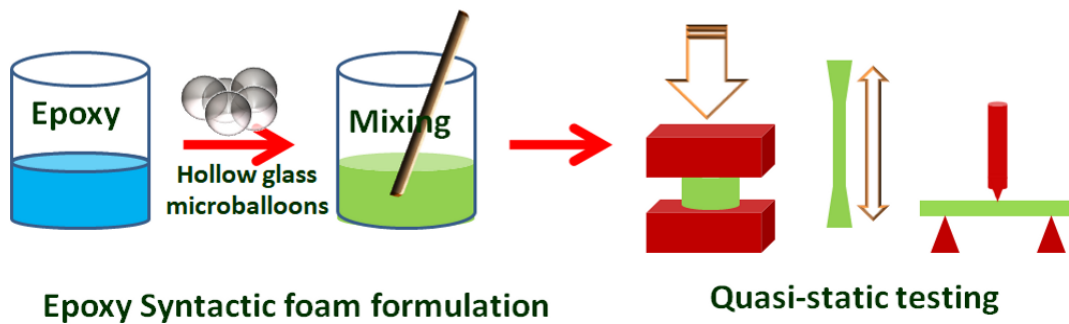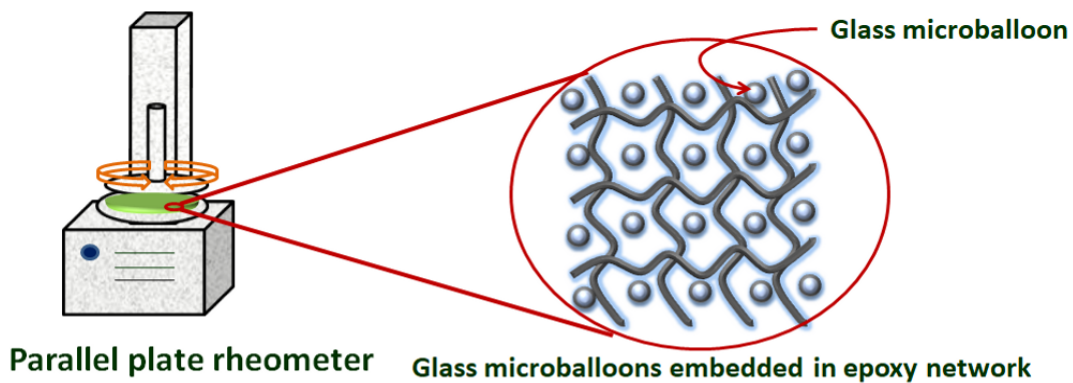
2.1. Introduction

Syntactic foams are light weight composite materials prepared by incorporating hollow microbubbles of glass [87], polymer [23, 88] or metal [89] in a suitable matrix. The inclusion of these hollow counterparts allows for significant weight savings, which is crucial for certain applications, especially marine [90, 91], aerospace [70, 73] and blast mitigation [92]. The presence of soft condensed matter helps reduce the damage arising from impact and other transient loads [93]. Although, both open and closed cell foams have been effectively utilized in their ability to resist blast/dynamic loads [78, 94], the latter owing to the presence of entrapped air, forbears additional deformation at high strain rates and increase the compressive strength and energy absorbing ability of the foams [4].

Polymeric syntactic foams refer to a sub-class of cellular materials, where hollow fillers are dispersed within a mechanically robust polymeric matrix. Apart from the nature of the matrix, concentration and type of microbubble are critical parameters, which decide its final properties [95]. Amongst all hollow fillers, glass microbubbles (HGM) are most extensively used [16, 96-98], due to their low coefficient of thermal expansion, chemical inertness, high strength and low density [97]. Additionally, these microspheres act as independent energy absorbing loci on being subjected to compressive loads. Potential applications of syntactic foams as core materials, utilizing their ability to act as energy absorbers, include them being used in the underbelly of tanks to attenuate the blast effects arising out from anti tank mines or other such applications where the ability to mitigate the effects of explosion are vital. The use of sandwich cores have been reported in the literature [4, 99], most important being balsa and foam cores in various naval applications such as surface ship deck structures and in boat hulls [2, 100]. Amongst all polymeric matrices, epoxy has been extensively studied [29, 72, 101-104], in view of its excellent

mechanical properties and low shrinkage [105, 106]. Rigid polymeric foams, usually prepared by the chemical reaction of isocyanates with polyols, are not strong enough to withstand blast loads and therefore mandate reinforcement [107]. Also, the processing of polymer-based foams is an involved process with interfacial phenomena and fluid dynamics being very critical [108, 109]. In the field of defence technologies, in view of their excellent mechanical properties syntactic foams have been reported to withstand dynamic loads [110].

The density of syntactic foam decreases with increasing concentration of purposely-placed voids and for maximal weight savings, high loadings of microbubble is desirable. The density of the syntactic foam can further be tuned by astute choice of microbubbles, which are available in a variety of sizes and grades. Hexagonal close packing of rigid spheres is expected to restrict the upper limit of microbubble loading to 74% v/v [31]. However, it is very unlikely to achieve hexagonal close packing under conventional conditions employed for processing. Interestingly, assuming random packing, the upper limit of microbubble loading is restricted to ~ 64 % v/v [111-113]. It is perhaps for this reason that very few studies deal with syntactic foams with very high microbubble loading ($\phi > 60$ %) [8, 53, 68, 70, 114].

Syntactic foams are conventionally processed using moulding, casting, extrusion, rotational moulding or buoyancy methods, with the choice of technique depending upon the microbubble loading and the type of product being manufactured [46, 115, 116]. Processing using conventional techniques mandate fluidity of formulation for subsequent casting into moulds. Increasing the microbubble loading beyond a critical value may render its processing impracticable by stir-casting techniques, which is perhaps most common. It is very important to establish the relationship of viscosity with curing time to ascertain optimal conditions required for processing. Surprisingly, rheological studies on

syntactic foam formulations are rather scarce, with most of the studies dealing with thermoplastic matrix [117-119]. In general, processing of compositions containing high microbubble loading is possible through moulding [46], and casting mandates the use of solvent [120]. Unfortunately, there are issues associated with the subsequent solvent removal step, which in turn leads to void formation and a concomitant decrease in mechanical properties and increased production costs.

Chemo-rheology of curing thermosets has been widely studied and extensive reviews are available [121, 122]. Here, in this chapter, we attempt to establish the role played by HGMs towards the curing of epoxy with an aim to determine the maximum amount of microbubbles that can be dispersed properly within the resin in the absence of diluent. It has been brought out in the literature that the presence of glass fibers does not affect the curing mechanism, but notable difference in the reaction rates has been observed [123, 124]. We hypothesize that in view of the physical restraint posed by the glass bubbles, the curing process will be adversely affected, especially at high microbubble loadings.

In this chapter, the rheological profile of glass microbubble filled polymeric syntactic foams using a cycloaliphatic epoxy resin in the presence of two different types of hollow glass microbubbles of varying crushing strength and density is discussed, to establish the optimal processing conditions. The effect of inclusion of hollow glass microbubbles on the quasi-static and high strain rate regimes has also been evaluated. Their response on being subjected to controlled transient loading has been studied on a shock tube facility. The aim is to explore the potential of these syntactic foams as core materials for energy absorbing applications.

2.2. Experimental

2.2.1. Materials

Low viscosity cycloaliphatic epoxy resin (Ciba Geigy, Araldite CY 230; epoxy equivalent 200 eq g^{-1}, η ~ 1000 mPa.s at 30 °C ($\dot{\gamma}$=0.1s^{-1}), hardener (HY 951; amine content 24 eq kg^{-1}) and Hollow Glass Microbubbles (Grade K46 and K15, 3M®) were used without any further treatment.

2.2.2. Epoxy Resin

Epoxies are one of the most important classes of thermosetting polymers. They are widely employed as matrix materials for preparation of composites [125, 126]. They possess good chemical and corrosion resistance, good dimensional stability and high tensile strength and are used for adhesive applications [127, 128]. Epoxies are two component system formed by a chemical reaction of epoxy resin with stoichiometric amounts of hardener. Epoxy resins are characterized by presence of at least two 1, 2 oxirane groups per molecule. Epoxy resins are prepared either by the reaction of epichlorohydrin with a phenol or by direct epoxidation of olefins with per-acids. The non-epoxy part in epoxy resins may be aliphatic, cyclo-aliphatic or aromatic hydrocarbon. Using proper choice of curing agents and their chemical reaction with epoxy resins, crosslinking occurs that transform epoxies into a solid that is insoluble and infusible. The only drawback associated with epoxies is their inherent brittleness which can be improved upon by incorporation of suitable modifiers [129, 130].

Commercially, the most important class of epoxy resins is manufactured by reaction of bisphenol A with epichlorohydrin in the presence of sodium hydroxide [131, 132]. It is commonly referred to as the diglycidyl ether of bis-phenol A (DGEBA); the schematic for its preparation is presented in **Scheme 2.1**.
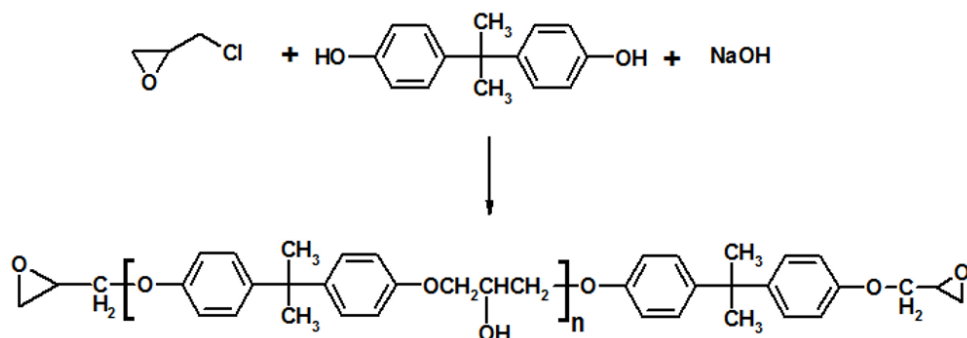
Scheme 2.1: *Synthesis of diglycidyl ether of bisphenol A (DGEBA)*

Yet another class of epoxy consists of cycloaliphatic rings in the molecules to which the oxirane ring is fused. They are prepared from Tischenko condensation of tetrahydrobenzaldehyde followed by epoxydation of resulting olefin with peracids [133]. The general scheme for the synthesis of cycloaliphatic resin is shown in **Scheme 2.2**.
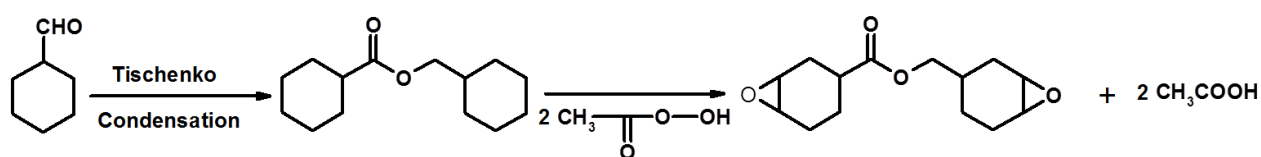
Scheme 2.2: *Synthesis of cycloaliphatic epoxy*

Cycloaliphatic epoxies are commonly used for structural applications that require improved resistance to elevated temperatures, uv radiation and moisture compared to bisphenol A and bisphenol F epoxies. This class of epoxides display low viscosity, higher temperature resistance and better electrical properties at higher temperatures. Another advantage of this class of resin is the complete absence of chlorine since no epichlorohydrin is used in the manufacturing process.

2.2.3. Curing Agents for Epoxy

The epoxide ring can react with chemicals that have activated hydrogen atoms such as amines, alcohols and carboxylic acids. The choice of curing agents depends on the physical and chemical properties, processing methods and curing conditions which are

desired. Epoxy resins can be cured with either catalytic or co-reactive curing agents that function as initiators for epoxy ring- opening homopolymerization.

2.2.3.1. Amine Curing Agents

Primary and secondary amines are most commonly employed chemicals that have the potential to act as epoxy curing agents. The active hydrogen of the primary amine reacts with the epoxy group to form secondary amine, which further reacts with the other epoxy group and undergo curing. The resultant tertiary amine polymerizes epoxy group and the so obtained polymer is heavily cross linked, rigid and mechanically strong. A reaction scheme representing the reaction between the primary amine functionality of TETA with epoxy group is shown in **Scheme 2.3**.
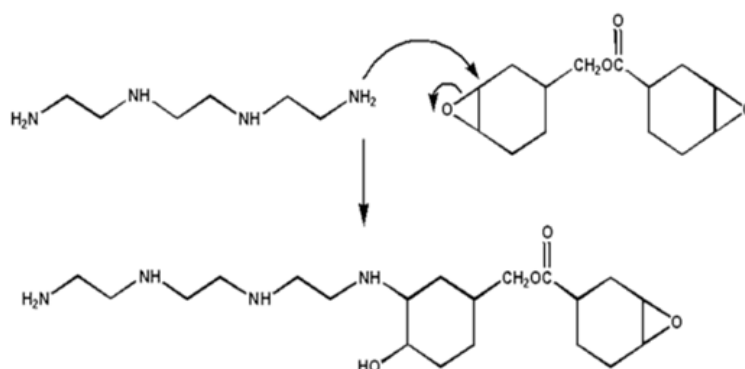
Scheme 2.3: *Reaction scheme of primary amine of TETA with epoxy group*

This process is also referred to as "curing", and can be controlled through proper choice of temperature, type of resin and hardener, and the ratio of said compounds. The curing process is exothermic, that can take several minutes to hours for completion. Some formulations benefit from heating during the cure period, whereas others require time and ambient temperatures. Conventionally, the reaction between epoxy and amine curing agent is a classical nucleophilic substitution reaction, reportedly following second order kinetics [134] (**Scheme 2.4**).
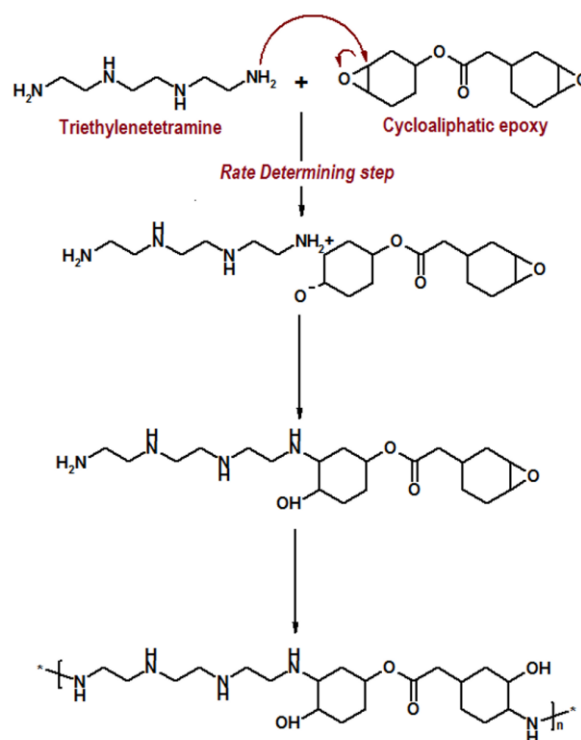
Scheme 2.4: *Cycloaliphatic epoxy-amine curing reaction mechanism*

2.2.4. Microspheres in Syntactic Foams

It is mandatory for the formation of syntactic foams that the microspheres must be hollow mainly for two reasons, one of which is to imitate foams which also possess hollow spaces inside and second, hollow microspheres provide low density, high specific strength, and low moisture absorption to the syntactic foam. It is evident from the literature that different varieties of microspheres have been used e.g. glass [24], polymer [31], carbon [14], ceramic [12], or even metal. Microspheres must be properly embedded in the matrix. These hollow microspheres, when acted upon by stress, they tend to break or get crushed and absorb energy and therefore, improve the mechanical properties of syntactic foams. Several terminologies are used in the literature to describe microspheres (e.g., microbubbles, cenospheres, microbubble etc). The microspheres have a burst pressure sufficient to withstand the forces imposed upon them during the formulation, mixing and dispensing processes. Properties such as high temperature resistance, good

strength-to-weight ratios, low thermal conductivity and low dissipation factor make microbubbles an important reinforcing material in these composites.

Microspheres are characterised by their particle size, wall thickness and density. In general, microspheres used in syntactic foams have a diameter of 1–50 μm, wall thickness of 1–4 μm, bulk density of 70–500 kg/m^3, and apparent density of 50–500 kg/m^3. Hollow macrospheres (diameter, 1–100 mm) are also used as fillers in syntactic foams. The wall thickness of a microbubble is related to a parameter termed the 'radius ratio', η which is defined as the ratio of the inner radius, r_i, to the outer radius, r_o, of the microbubbles (**Equation 2.1**):

$$\eta = \frac{r_i}{r_o} \ldots\ldots\ldots\ldots\ldots 2.1$$

Increase in the radius ratio corresponds to a decrease in wall thickness, which leads to a decrease in true particle density of the microbubble. Therefore, microbubbles having a higher radius ratio give rise to lower-density syntactic foams and vice versa. The parameter η is related to the microbubble density (ρ_{mb}) and the material of the microbubble and is given by **Equation 2.2**:

$$\eta = \left(1 - \frac{\rho_{mb}}{\rho_g}\right)^{\frac{1}{3}} \ldots\ldots\ldots\ldots\ldots\ldots 2.2$$

Where, ρ_g is the density of the microbubble material.

The microbubbles selected for the study have different wall thicknesses which are calculated using **Equation 2.3** [29]

$$w = \left(\frac{d_0}{2}\right)\left[1 - \left(1 - \frac{\rho_{mb}}{\rho_g}\right)^{1/3}\right] \ldots\ldots\ldots\ldots 2.3$$

Where ρ_{mb}, ρ_g and d_0 refer to true particle density of microbubbles, density of glass material used in fabricating glass microbubbles and average particle diameter respectively.

Polymeric microbubbles are commonly prepared from epoxy resin, unsaturated polyester resin, silicone resin, phenolics, melamine formaldehyde, polyvinyl chloride, polypropylene, or polystyrene. As a general rule, these microspheres are produced by spraying low-viscosity solutions and melts. Among the various polymeric microbubbles, phenolic microbubbles have been widely used for processing syntactic foams. The main advantage of phenolic microspheres over those of glass is their lower density. Organic microspheres are also used in syntactic foams. However, these suffer from several limitations and their use is rather limited. Some organic microspheres are further converted into carbon microspheres. Usually, these spheres are derived from phenolic microspheres or carbon pitch spheres. Conversion of the organic spheres to carbon microspheres is usually accomplished by heating in an inert atmosphere at 800–1000 °C. A temperature of ~ 2000 °C is sufficient to convert most of the organic materials to carbon and to achieve graphitization. Carbon microspheres obtained from phenolic resins exhibit densities of about 0.15 g/cm^3, whereas, those obtained from pitch sources have densities of 0.05–0.25 g/cm^3. Materials made from carbon microspheres of low apparent density have a substantially lower thermal conductivity (0.049–0.064 W/ m.K).

Another type of microbubble are the fly-ash microspheres which are the by product of thermal power plants. Fly ash in the form of hollow particles is also used in syntactic foams. They possess an irregular structure due to surface defects. The concern for effective waste utilization has led to their widespread applicability in the areas of syntactic foams and other composites. Metal and metal oxide microspheres have also been used in syntactic foams.

2.2.4.1. Glass Microbubbles in Syntactic Foams

3M™ Glass Bubbles are engineered hollow glass microspheres that are alternatives to conventional fillers and additives such as silica, calcium carbonate, talc,

clay, etc., for many demanding applications. The most commonly used microspheres in syntactic foam are glass microspheres. They possess high specific strength, smooth surface, good wetting characteristics, low viscosity of the resin–microbbubble mixture, energy absorption properties, low cost and ease of fabrication. Also, hollow glass particles have very low densities as compared with corresponding hollow metallic and ceramic particles. These low-density particles are used in a wide range of industries to reduce part weight, lower costs and enhance product properties. The unique spherical shape of glass-bubbles offers a number of important benefits, including: higher filler loading lower viscosity/improved flow and reduced shrinkage and warpage. Glass microbubbles blend readily into compounds and make them compliant to a variety of production processes including spraying, casting and moulding. The chemically stable soda-lime-borosilicate glass composition of glass bubbles provides excellent water resistance to create more stable emulsions. They are also non-combustible and nonporous so they do not absorb resin. 3M Glass Bubble K Series and S Series are specially designed to provide high strength-to-weight ratios suited for demanding conditions. They also produce stable voids, which results in low thermal conductivity and a low dielectric constant. 3M glass microbubbles cater to a wide range of products and processing conditions. The physical properties of glass microbubbles used in the thesis are presented in **Table 2.1**. Their size varies from 10-300 microns.

Table 2.1: *Properties of glass microbubbles*

HGM	Density (kgm^{-3})	Wall thickness (μm)	Radius ratio (η)	Microbubblesize (μm) (mean diameter)	Isostatic crush strength (psi)	Thermal Conductivity (Wm^{-1}K^{-1}) at 21° C
K15	150	0.70	0.98	43.6	300	0.055
K46	460	1.29	0.93	40	6000	0.153

2.2.5. Rheological Studies

Rheological studies were carried out for HGM-epoxy formulations using an Anton Paar Rheometer (MCR 102) using 25 mm disposable aluminium parallel plates. During the experiments, the shear stress was maintained at 1000 Pa to produce reliable and reproducible results. Shear rate sensitivity studies were performed, while varying the shear rate over the range of 0.1 to 1 s^{-1} under isothermal conditions (30 °C).The oscillatory shear flow studies were conducted under both isothermal as well as dynamic conditions. The test fixture was initially preheated to the desired temperature. The plates were subsequently separated and the HGM-resin formulation was rapidly inserted. The plates were then brought back to a gap of approximately 1.0 mm and excess sample was trimmed. The experiment was finally initiated when the desired set temperature was achieved. The viscoelastic properties of the sample during cure, including the complex dynamic viscosity (η^*), shear storage modulus (G'), and shear loss modulus (G'') were monitored. Experiments were performed over temperatures ranging from 60 °C to 100 °C in increments of 20 °C and temperature sweep from 30 °C to 150 °C at a heating rate of 5 °C/min were performed using a constant frequency of 1Hz for all experiments.

2.2.6. Processing of Syntactic Foams

Epoxy based syntactic foams were prepared as per the procedure reported in the literature [95]. The processing steps are as follows: firstly, pre-calculated amount of epoxy and hardener (mix-ratio of 100:13 by weight) are weighed and mixed together in a suitable beaker for about 5 min. Then, pre-calculated amount of microbubble (0–70 vol %) is added while mixing the constituents together by stirring, using a wooden spatula (**Equation 2.3**, **Table 2.2**). To prevent breakage of hollow microbubbles, slow stirring was performed for the uniform dispersion of microbubbles. In view of the low density of microbubbles of the epoxy resin, the HGMs have a tendency to drift towards the surface

of the mould while curing at room temperature. To circumvent the same, the stirring time was adjusted depending upon the amount of microbubble added, to achieve an optimal increase in the viscosity of the mixture. The formulation was degassed and was transferred into silicone moulds and placed at 65 °C inside an oven for 24 h. Finally, test samples are machined from the cured panel for mechanical and thermal characterization. The nomenclature for sample is SFxx-yy, where SF refers to syntactic foams, xx denotes the type of glass microbubble employed for processing, i.e. 15 for K15 and 46 for K46 and yy corresponds to the volume percentage of glass microbubbles.

$$\frac{Mass\ of\ HGM}{Mass\ of\ Syntactic\ foam} = \frac{\rho_{HGM} \times \phi_{HGM}}{\rho_{HGM} \times \phi_{HGM} + \rho_m \times \phi_m} \dots\dots\dots\dots2.4$$

where, ρ and ϕ refer to the density and volume fraction of the constituent respectively, and the subscripts, 'HGM', and 'm' refer to microbubbles and epoxy respectively. For the purpose of calculation, density of epoxy has been assumed to be 1.17 g cc^{-1} [63] respectively.

Table 2.2: Compositional details of syntactic foam

Sample designation	Epoxy* (g)	Microbubble (K 46) (g)	Sample designation	Epoxy* (g)	Microbubble(K 15) loading (g)
SF46-10	1.69	0.08	SF15-10	1.74	0.02
SF46-20	1.61	0.17	SF15-20	1.71	0.06
SF46-30	1.51	0.28	SF15-30	1.67	0.10
SF46-40	1.39	0.42	SF15-40	1.63	0.15
SF46-50	1.27	0.56	SF15-50	1.56	0.22
SF46-60	1.13	0.74	SF15-60	1.48	0.32
SF46-70	0.92	0.95	SF15-70	1.36	0.46

*Epoxy:hardener ratio = 100:13w/w

2.2.7. Quasi-static Testing

Mechanical testing was performed using Universal Testing Machine (International Equipments). For compression, standard specimens of 12 mm diameter and 6 mm thickness were compressed at a cross head speed of 1.3 mm min^{-1}. Five specimens of each composition were tested and compressive strength was determined from the load-displacement data obtained from the tests. The area under the compressive stress-strain curve till the end of plateau region was quantified to determine the amount of energy absorbed by the foams (**Equation 2.5**) [63].

$$E_a = \frac{1}{2}(\rho_c \times \varepsilon_{crush}) + (\rho_c \times \varepsilon_{crush})\ldots\ldots\ldots.2.5$$

Where E$_a$, ρ_c and ε_{crush} refer to the energy absorbed, compressive yield strength and crushing strain of the foam respectively.

Flexural testing of syntactic foam specimens of standard dimensions (127 mm length $\times$ 12.5 mm width $\times$ 3.5 mm thickness) was performed by subjecting them to a deformation rate of 2 mm min^{-1} and span length of 60 mm under three point bending mode as per ASTM D790. The tensile properties were determined as per ASTM D638 using a Universal Testing System (International Equipments) at ambient temperature. The dog bone shaped specimens used for tensile testing were 165 mm long, 3 mm thick, and 13 mm wide along the centre of the casting for syntactic foams. The samples were subjected to a cross-head speed of 10 mm min^{-1}.

2.2.8. High strain-rate Testing

The mechanical response of the samples under high strain rates was investigated using a Split Hopkinson Pressure bar. The basic principle of SHPB is based on one-dimensional wave propagation in elastic bars, and since it is not possible in practice, the theory is adopted with certain approximations. The setup at Terminal Ballistic Research Laboratory (TBRL), Chandigarh comprises of two high strength maraging steel with yield

strength 1750 MPa, diameter 20 mm and length 2000 mm. A projectile (300 mm length, 20 mm diameter) is made to hit the cylindrical foam sample sandwiched between the two bars to produce different strain rates varying between 1376-2574 s^{-1}. Strain gauges of 120 Ω, 90 ° tee rosette precision strain gauges designated as EA-06-125TM-120 were used. For wave shaping a 1.5 mm OFHC copper wave shaper was used.

In all the experiments, cylindrical specimens with length to diameter (L/D) ratio of 0.5 were used, with the diameter of the specimen being 12 mm. This ensures the impact on full cross-section of the specimen and also permits the specimen to expand along radial direction within the cross-sectional area of the bars after the compressive load is applied.

2.2.9. Shock tube Test

The dynamic response of the syntactic foams was evaluated by subjecting disc shaped specimens to controlled blast loadings on a shock tube. A shock tube assembly essentially comprises of a long rigid cylinder, sub-divided into a high-pressure driver section and a low pressure driven section, which are separated by a mylar diaphragm. The shock tube, used for the present study has an overall length of 8.7 m, which is divided into a 1.7 m driver section and a 7 m driven section. A cylindrical disc of syntactic foam specimen (12 cm diameter, thickness 1 cm) was sandwiched between two aluminium sheets (0.25 mm thickness), held under simply supported boundary conditions in front of the driven section. Pressurised air is used as the driver gas, the driven gas being ambient air. The rapid release of gas due to diaphragm rupture results in the creation of a shock wave, which travels down the driven tube to impart dynamic blast loadings. A circular region of 10 cm diameter was effectively subjected to blast loading, as pictorially shown in **Figure 2.1**. Pressure sensor (113B21, PCB make), placed at a distance of 11.3 cm from the sample was used to monitor the pressure profile during the testing. Strain gauge

(HBM:K-LY4-1-11-120-3-2) was affixed on the blast–opposing face of syntactic foam specimen to measure sample deflections.

The signal recorded on the strain gauge installed on the opposite face of the blast is indicative of the extent of deformation in the syntactic foam sample due to blast loading. A control set of experiments was also performed, which comprised of two aluminium sheets with no foam between.
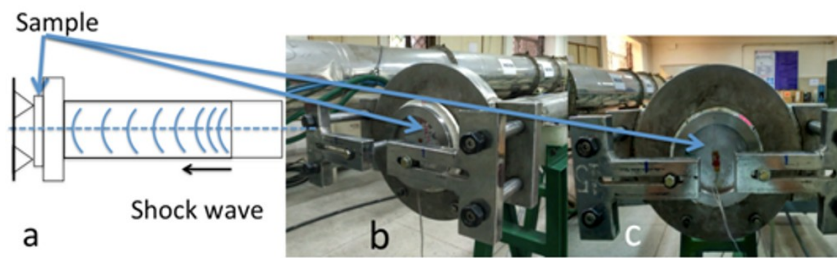
Fig. 2.1: a) Representation of the specimen loading on shock tube (b) Specimen placement
c) Front view

2.2.10. Density Determination

Syntactic foams are usually three phase systems consisting of voids, microbubbles and resin. The presence of voids accounts for a reduction in the experimental density of the syntactic foams [135]. Theoretical density of syntactic foam (ρ_{th}) was estimated as per the standard rule of mixtures (**Equation 2.6**)

$$\rho_{th} = \rho_{HGM} * \Phi_{HGM} + \rho_{matrix} * \Phi_{matrix} \ldots\ldots\ldots\ldots.2.6$$

Experimental density was determined by averaging the mass: volume ratio of five specimens as per ASTM D1622–98. The ratio of the difference between theoretical and experimental densities to the theoretical density was used to quantify the air void porosity trapped in the matrix during fabrication according to the following **Equation 2.7**:

$$Void\ volume\ \% = \frac{\rho_{th} - \rho_{ex}}{\rho_{th}} \times 100 \ldots\ldots\ldots\ldots\ldots\ldots....2.7$$

The thermal degradation behaviour was investigated using Perkin Elmer Diamond STG-DTA under N_2 atmosphere in the temperature range 50-600 °C. A heating rate of 15

°C/min and sample mass of 5.0 ± 0.5 mg was used for each experiment. Calorimetric studies were performed on a differential scanning calorimeter (DSC) (TA instruments Q 20). For dynamic DSC scans, samples (10 ± 2 mg) were sealed in aluminium pans and heated from 0 to 200 °C at 5 °C/min. The experiments were performed under flowing N_2 (50 mL/min) to minimize oxidative degradation of the sample during the curing process. The morphology of fractured surface was studied using a scanning electron microscope (Zeiss EVO MA15) under an acceleration voltage of 1 kV. Samples were mounted on aluminium stubs and sputter-coated with gold and palladium (10 nm) using a sputter coater (Quorum SC7620) operating at 10-12 mA for 120 s. Visual inspection of the hollow glass microbubbles was performed using an optical microscope (OLYMPUS) at 40 X magnification.

2.3. Results and Discussion

The chemo-rheological behaviour of cycloaliphatic epoxy containing different types of hollow glass microbubbles is studied to arrive at the optimal conditions required for processing of syntactic foam formulations.

2.3.1. Effect of Microbubble Loading on Viscosity

The effect of increasing microbubble loading (K46) on theviscosity of the composition in terms of viscosity-shear rate dependence is presented in **Figure 2.2**. Compositions prepared using lighter microbubbles (K15) also exhibit a similar profile. It can be seen that the cycloaliphatic epoxy resin exhibits a viscosity of ~ 1000 mPa.s at 30 °C ($\dot{\gamma}$=0.1s^{-1}) and the inclusion of microbubbles lead to a considerable increase in its viscosity, the extent of which is proportional to the microbubble loading. It is to be noted that at microbubble loadings ~ 60 %, the viscosity of the formulation is too high to permit solvent-less processing. For the sake of visualization, photographs of representative formulation (ϕ=40-60 %) are also included as an inset in **Figure 2.2**. It is clear that for

the present system, a microbubble loading of 60 % v/v is the upper limit of fluidity and formulations with higher loading are too viscous to be processed in the absence of a diluent.
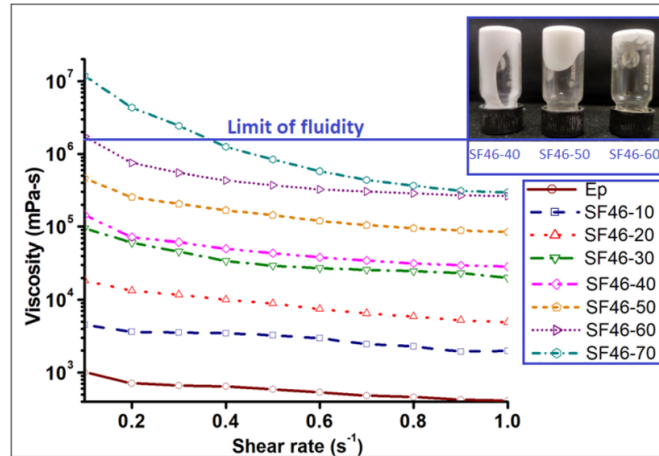
Fig.2.2: *Dependence of increasing shear rate and microbubble loading (ϕ) on viscosity. Inset shows flowability of formulations at 40-60 % (v/v) loadings of glass microbubbles*

The data associated with an increase in viscosity as a function of microbubble loading and shear rate is presented in **Figure 2.3**. Our studies indicate that although, a theoretical packing efficiency of 74 % is achievable for hexagonal close packing, it is only practical to process foam formulations with HGM loadings 40-60 % v/v, where the packing of microbubbles is random (Upper limit = 64 % v/v).
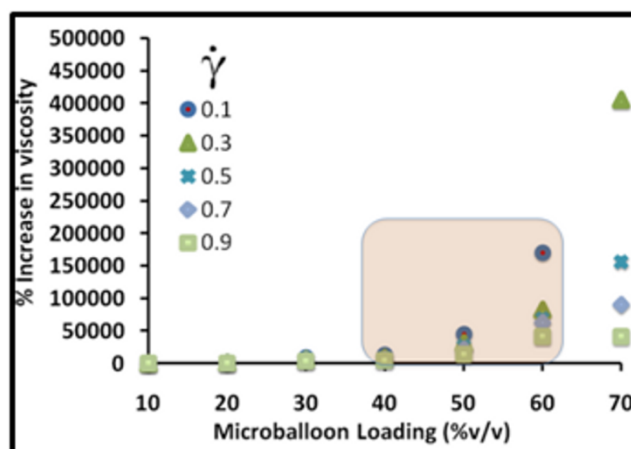
Fig.2.3: *Increase in viscosity as a function of microbubble loading and shear rate (γ̇)*

It is to be noted that in view of the substantial difference in the density of HGM and epoxy, the lighter microbubbles tend to drift to the surface of the resin, the time for drifting depending on the density difference. Digital photographs of representative formulations containing varying microbubble (K46) loading are presented in **Figure 2.4**. At loadings less than or equal to 30 % v/v, separation of the components into distinct layers is evident, with the formation of an upper layer of light, hollow microbubbles and clear layer of epoxy at the bottom. However, this drifting mandates a finite amount of time, depending on the viscosity of the medium (~10 h in the present case).
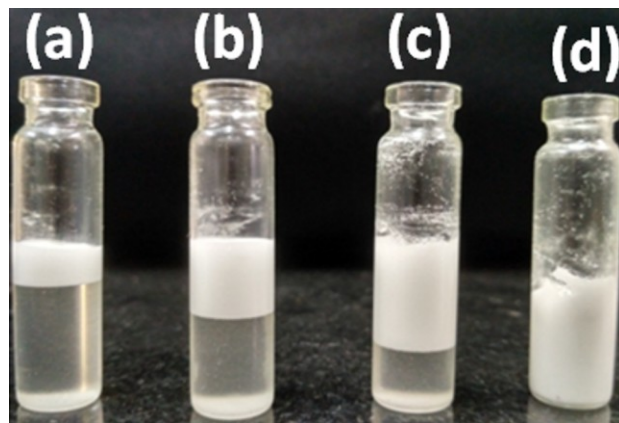
Fig.2.4: Drifting of microbubbles to the surface of epoxy-HGM formulations with varying glass microbubble loading (a) 10, (b) 20, (c) 30 and (d) 40 % (v/v)

Our study clearly highlights that the curing temperature of epoxy-HGM formulations should be astutely chosen such that the rate of network formation is rapid enough to prevent microbubble agglomeration at the surface. The DSC traces associated with the curing of epoxy at different isothermal temperatures is presented in **Figure 2.5**. The time associated with the curing process decreases from 200 min to 20 min as the temperature is raised from 40 to 70 °C. For the present scenario, a temperature of 65 °C appears to be appropriate.
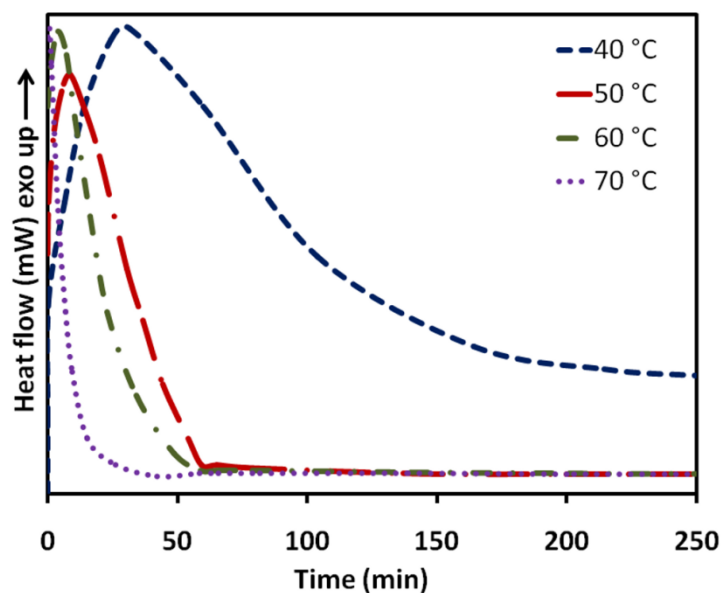
Fig.2.5: *Calorimetric traces associated with curing of epoxy at different isothermal*

temperatures

Rheological studies can generate valuable inputs with regard to the viscoelastic nature of the material. The rheological profile associated with the curing of microbubble filled compositions was studied under oscillatory mode using a parallel plate geometry which is routinely used for studying epoxy based systems [136]. The variation in the viscosity for both unfilled and glass microbubble filled compositions (40-60 % microbubble loading) is presented in **Figure 2.6**. Three distinct regions are clearly evidenced. Initially, a slight decrease in viscosity is observed as the temperature was increased to ~ 90 °C, which could be attributed to the overcoming of intermolecular interactions with increasing temperature. Further increase in temperature (90-120 °C) leads to a sudden and exponential increase in viscosity: a feature attributable to the autocatalytic nature of curing. As the temperature approaches 120 °C, the viscosity levels off indicating complete curing of the system.
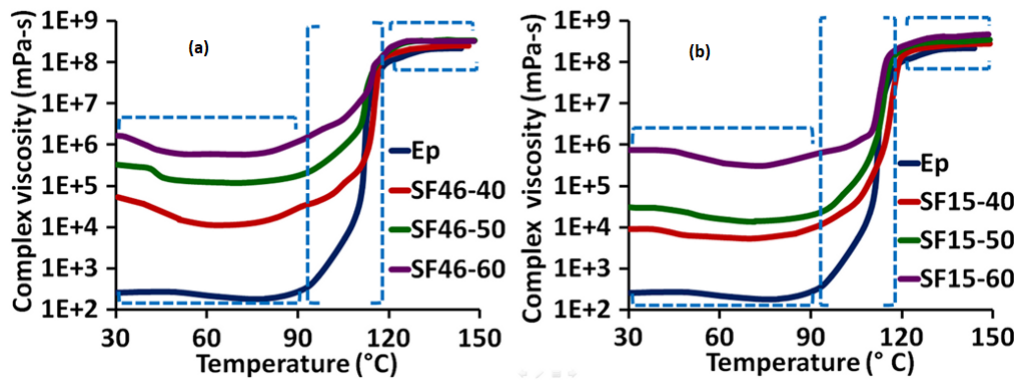
Fig.2.6: *The effect of increasing microbubble loading on complex viscosity (a) K46-epoxy formulations (b) K15- epoxy formulations*

The evolution of storage and loss modulus due to curing of representative formulations ($\phi = 40\%$) was studied under isothermal temperatures (60-100 °C) to arrive at the optimal temperature required for processing, and the results are presented in **Figure 2.7**. Initially, in view of the liquid nature of the reactants, the loss modulus of the formulation is substantially higher than the storage modulus. Due to the reaction of the epoxy with amine, both G' and G" increase rather rapidly and a crossover gelation region is evidenced; where the storage modulus increases to the level of loss modulus. This region marks a sudden transition of the viscous liquid to elastic solid, where the material can store and dissipate equal amount of energy and the time required for this is referred to as gelation time (t_{gel}).

Interestingly, when the curing was performed at T= 60 °C; after the initial increase in storage modulus, a slight decrease (in the form of a kink) was observed in the microbubble filled formulations (**Figure 2.7 a**), irrespective of the type of microbubble employed. At lower temperatures, the curing process requires much longer time periods, which reflects in terms of longer 't_{gel}'. Spherical microbubbles tend to roll due to shearing action offered by the plates, and the polymeric network formed is not strong enough to withstand the shearing force offered by the oscillating plates, thereby resulting in its

disruption. The network subsequently evolves with time, and the complete curing mandates ~ 1h. When the curing is performed at higher temperatures (Isothermal temperature = 80-100 °C), the rate of emergence of the crosslinked structure is much rapid, therefore the shear force offered by the plates is insufficient to result in any disruption of the network. Although storage and loss modulus are not design parameters, these data can be used to accurately predict the elastic modulus of syntactic foams which will be helpful in engineering applications of such foams [137, 138].
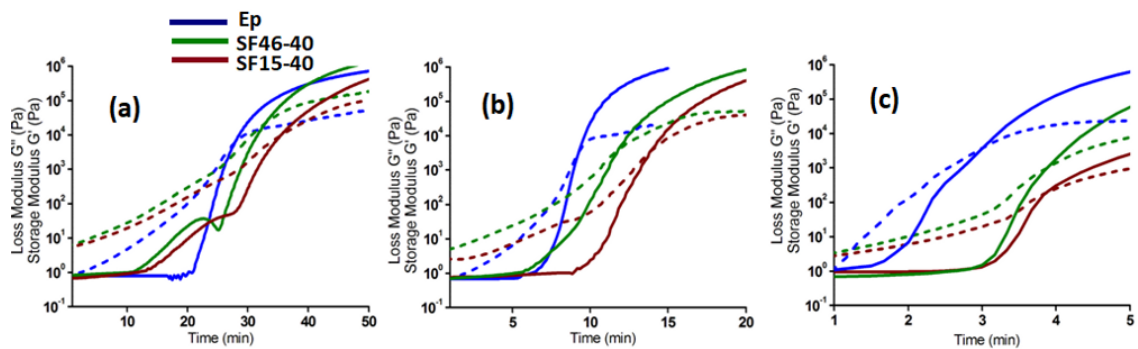
Fig.2.7: Isothermal gelation profiles of resin and syntactic-foam formulations at different temperature a) 60 °C b) 80 °C and c) 100 °C. (Dotted lines G'', Solid lines G')

The delay in the curing phenomenon due to inclusion of microbubbles in the resin is also evident from the calorimetric studies performed on formulations. Representative non-isothermal DSC traces (heating rate= 10 °C min^{-1}) are presented in **Figure 2.8**. It can be seen that neat epoxy cures at 89 °C (T$_{peak}$), which is relatively lesser that the T$_{peak}$ associated with formulations containing microbubbles.
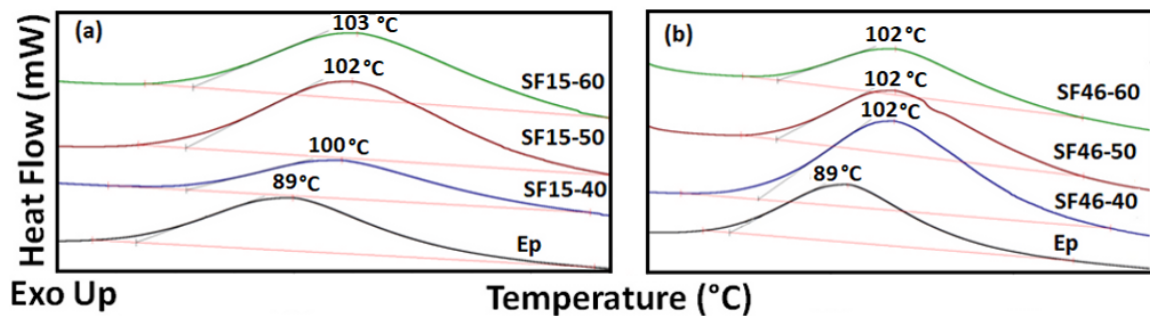
Fig.2.8: Non-isothermal DSC traces for epoxy-HGM formulations with increasing glass microbubbles loadings a) SF15 b) SF46

49

Gelation time-temperature dependence was used to arrive at the activation energy (E_a) associated with the curing process of epoxy. The detailed procedure is presented in Section 2.3.2., and the results are presented in **Figure 2.9**. A substantial delay in curing (as evidenced in terms of longer gelation time) is clear in formulations containing microbubbles, a phenomenon attributable to the physical hindrance posed by the microbubbles.

2.3.2. Activation Energy Calculations

The activation energy for polymerization was calculated from the gelation time (T_{gel}) assuming that curing reaction can be expressed by differential equations containing unique apparent activation energy, as follows:

$$\frac{dx}{dt} = Ae^{\left(-\frac{E_a}{RT}\right)}f(x)\ldots\ldots\ldots\ldots.2.8$$

Where A is a constant factor, E_a is apparent activation energy for the reaction, R is gas constant, T is the absolute isothermal cure temperature and $f(x)$ is a function of the reaction mechanism and the extent of reaction and is assumed to be independent of the cure temperature.

Integrating equation 1 from $x = 0 \ to \ x = x_{gel}$ by taking natural logarithm:

$$ln \int_0^{x_{gel}} \frac{dx}{f(x)} = \ln A + \ln\left(t_{gel}\right) - \left(\frac{E_a}{RT}\right)\ldots\ldots\ldots.2.9$$

The extent of reaction at gelation point is constant, so the above equation can be expressed as:

$$ln\left(t_{gel}\right) = constant + \frac{E_a}{RT}\ldots\ldots\ldots\ldots.2.10$$

Thus, from the slope of the plot of $ln(t_{gel})$ and the inverse of temperature, the activation energy can be calculated.

The presence of K15 results in a larger delay, which in turn can be attributed to the larger dimensions of the constituent filler (K15: Diameter 43 μm) as compared to K46 (Diameter: 40 μm). Further, in view of the low thermal conductivity (0.05 Wm^{-1}K^{-1}, K15 and 0.15 Wm^{-1}K^{-1}, K46) of microbubbles, the heat flow into the epoxy resin is also inhibited due to the presence of hollow glass microbubbles [139].
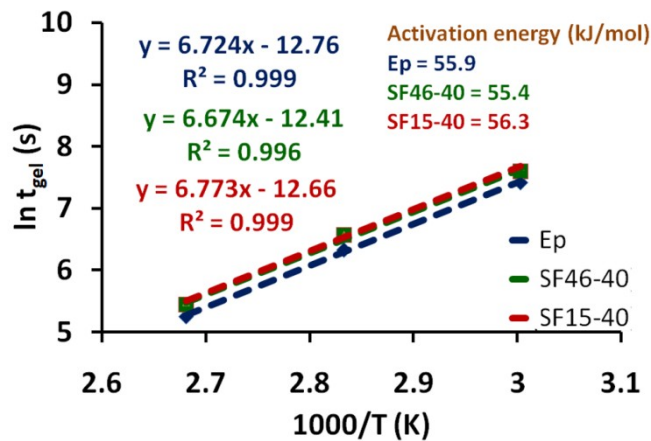
Fig.2.9: Arrhenius plot of ln(t$_{gel}$) versus 1/Temperature

Interestingly, the activation energy was found to be of the same order in all the formulations, which indicate that the presence of microbubbles do not alter the epoxy-amine curing mechanism. Our studies are in line with previous studies on glass fiber-epoxy compositions, which revealed that the glass fibers decreases the reaction rate associated with the curing process, without altering the mechanism [123].

2.3.3. Voidage in Syntactic Foam

The theoretical and experimental densities associated with syntactic foams (ϕ =10-70 %) are presented in **Figure 2.10**. As expected, cellular samples containing K46 (ρ= 460 kg/m^3) exhibit relatively higher densities than samples containing K15 (ρ= 150

51

kg/m³), under similar loadings. However, the experimental density was much lower than the theoretically predicted values. The difference in the densities was used to estimate the voidage, which too are included in the Figure. It is particularly interesting to notice the large voidage in samples containing high microbubble loading (ϕ= 70 %).
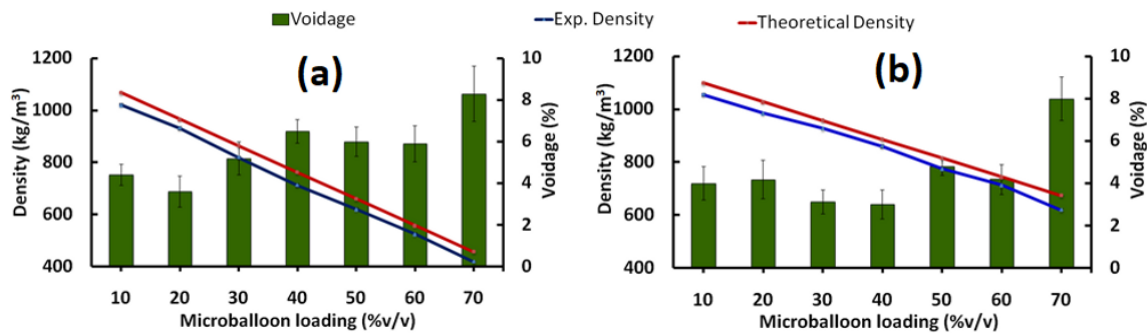
Fig.2.10: *Theoretical and experimental densities of syntactic foam specimens (a) SF15*

(b) SF46. The voidage is presented in the secondary axis.

2.3.4. Mechanical properties: Quasi-static

Since the low density of syntactic foam is the most favourable feature of cellular materials, the trends in mechanical properties need to be analyzed with respect to their density, which is best described in terms of specific mechanical properties. All, quasi-static mechanical properties irrespective of the testing mode (compressive, tensile and flexure), were found to decrease with increasing microbubble loading.

The compressive stress-strain curves of epoxy-microbubble syntactic foams at different microbubble volume fractions are presented in **Figure 2.11**. The stress-strain profiles reveal an initial linear elastic (Hookean) region, followed by an energy absorbing plateau region. The peak stress value is the compressive strength of the sample and the plateau region is visualized by an increase in strain without an appreciable increase in stress. In this plateau region, the microbubbles are subjected to extensive compressive loads, which results in their crushing. Beyond this, there is an exponential increase in stress without any appreciable increase in strain: a region signalling the onset of

densification [70].
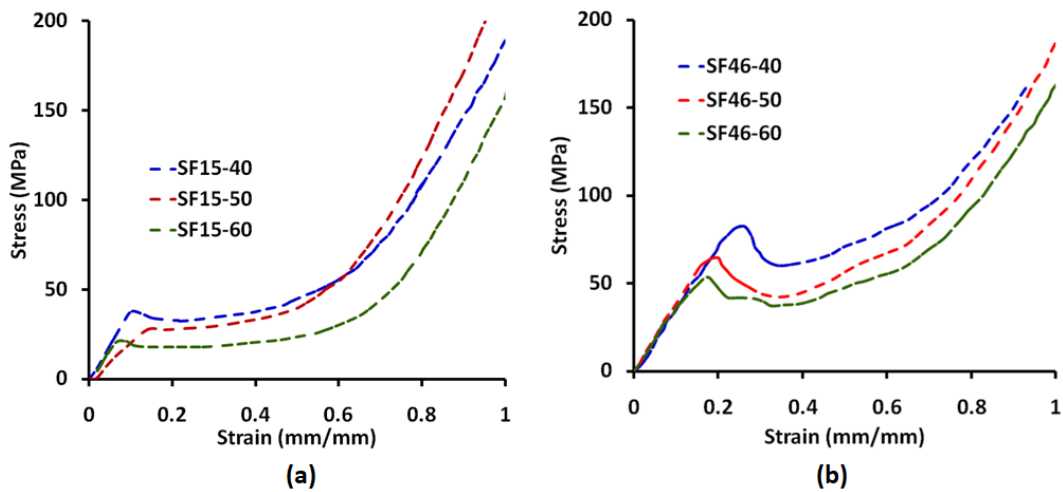
Fig.2.11: *Representative compressive stress-strain curves of (a) SF15 and (b) SF46*

syntactic foams

The quasi-static compressive properties of the syntactic foams containing varying loading (10-70 % v/v) and different types of microbubbles (K15 and K46) are presented in **Figure 2.12**. In general, the lower compressive strength of microbubbles (2 MPa and 41 MPa) in comparison to neat epoxy (138 MPa) [140] is expected to result in a reduction of compressive strength, which is very well evidenced from our studies. It is to be noted that under low microbubble loading, the hollow constituents are well embedded within the resin. During compression, substantial energy is absorbed by the matrix as well as the microbubble-epoxy interface prior to the fracture of microspheres [51]. With increasing microbubble loading, the contact between the microbubbles increases due to the reduction of resin content, leading to localised aggregation which leads to further reduction in the compressive properties.
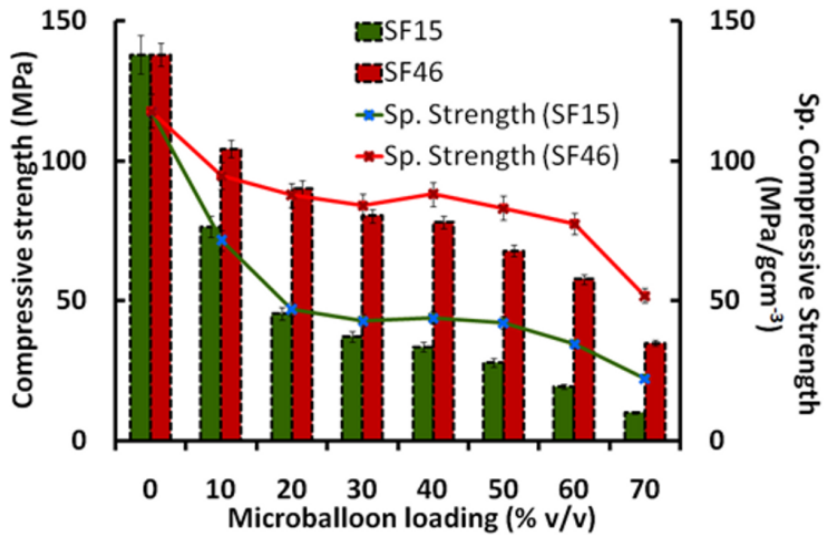
Fig.2.12: Compressive properties of epoxy syntactic foams

Microbubble crushing is the primary mechanism responsible for the energy absorption of the foams in compressive mode [51], which is usually quantified in terms of the area under the stress-strain curve till the end of plateau region (**Figure 2.13**).
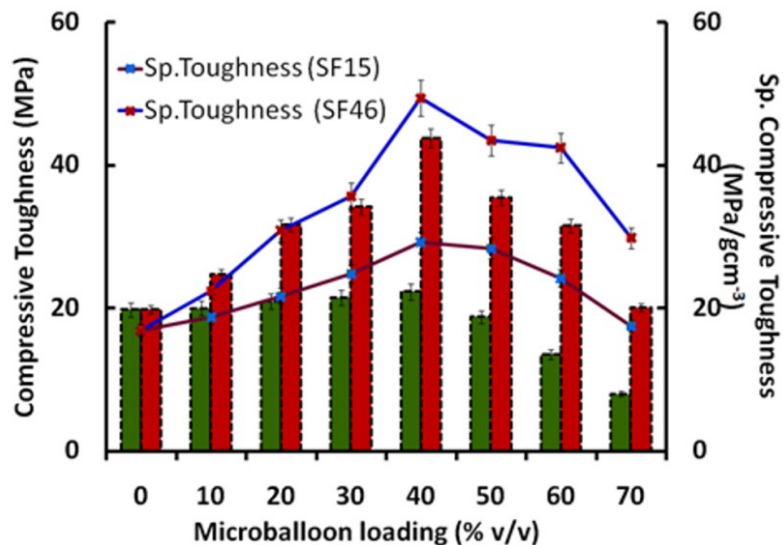
Fig.2.13: Compressive toughness and specific compressive toughness of epoxy syntactic

foams

Under flexural (**Figure 2.14**) loadings, the difference between the strengths of two types of syntactic foam specimen discernibly reduces. The precipitous drop in stress after the end of elastic region is indicative of the brittle failure in the sample in flexural mode. Flexural strength is also found to be inversely proportional to the microbubble

loading. However, it is to be noted that under flexure, failure occurs primarily due to matrix fracture and is less dependent on failure of microbubbles [66].
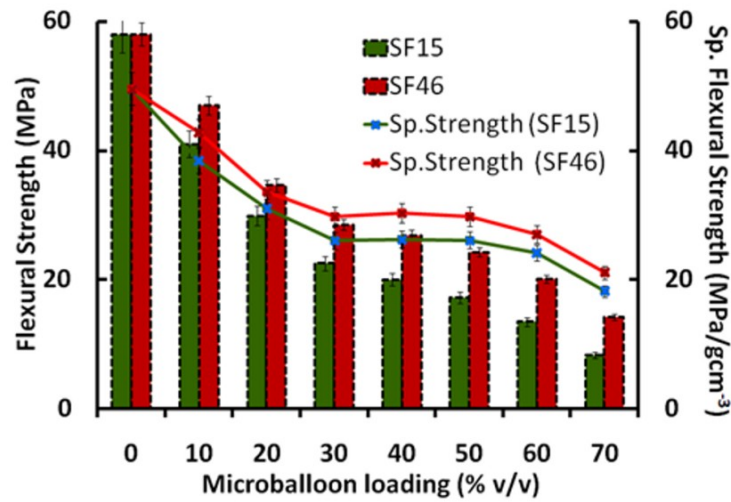
Fig.2.14: Flexural properties of epoxy syntactic foams

The tensile properties, which depend primarily on the response of the matrix rather than on the filler i.e. glass microbubbles [141], are presented in (**Figure 2.15**). It can be seen that the tensile properties are also inversely proportional to the microbubble loading [27]. It is to be noted that under flexure and tensile mode, the microbubbles are not the primary load bearing phase and failure depends to a large extent upon the matrix failure [27, 72]. The better specific properties at 40 % loadings of glass microbubbles have resulted in the choosing of this volume fraction as the optimal. What is particularly interesting to note is that the mechanical properties of the cellular materials drop significantly as the microbubble loading is increased to 70 % v/v.
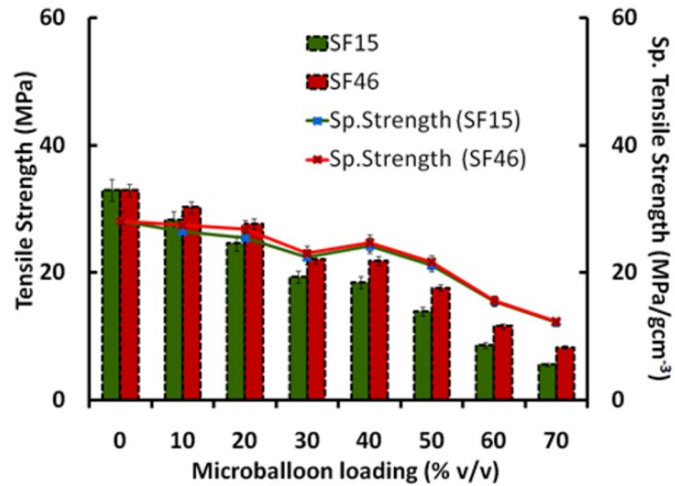
Fig.2.15: *Tensile properties of epoxy syntactic foams containing different microbubbles*

at varying loadings

It is to be noted that the properties of any reinforced material are decided by the extent of interfacial adhesion between the filler and the matrix. A condensation reaction between the surface hydroxyl groups of silica and oxirane rings of epoxy resin is responsible for the excellent adhesion between the glass and epoxy (**Scheme 2.5**).The inferior mechanical properties can be attributed to the fact that in such specimens (microbubble loading ~70%) the resin is unable to penetrate into the interstitial regions. This, in turn, is expected to lead to high voidage, which has also been observed experimentally (**Figure 2.10**). The decrease in mechanical properties exceeds the lowering in density; therefore the specific properties are also substantially reduced.
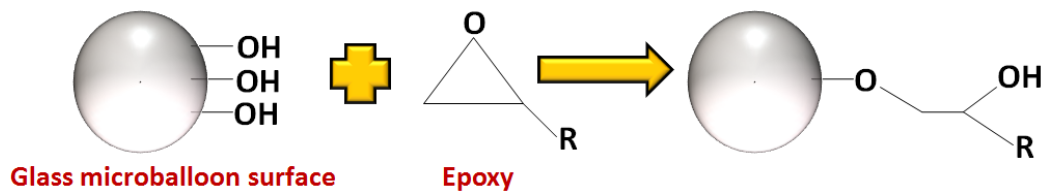
Scheme 2.5:*Representative reaction of hydroxyl groups (in glass) with epoxy* [142]

It appears that it is impossible to obtain a hexagonal close-packed structure in syntactic foams using common stir-casting techniques. In common words', packing is defined as a collection of non-overlapping solid objects in *n*-dimensional space. An

important attribute of packing is its packing densityϕ, which is defined as the fraction of space covered by the particles. Previously, computer algorithms have been used to study idealized random packing associated with monodisperse spheres. A rate-dependent densification algorithm[111] has indicated that a packing fraction between 0.642 and 0.649 is common. A Monte Carlo scheme yields a ϕ= 0.68, while a "drop and roll" algorithm yields a maximal packing efficiency (ϕ) of 0.60 [112]. Subsequently, a concept of "Maximally Random Jammed" (MRJ) state was developed, which can be viewed as prototypical glasses in that they are maximally disordered while simultaneously being mechanically rigid. This is associated with a maximum limit of ϕ= 0.64 [113]. A pictorial representation of hexagonal packing and random packing is presented in **Figure 2.16**. Our studies indicate that under the ordinary processing conditions; the "jammed" state appears to be the upper limit of packing with a packing efficiency of 64 %.
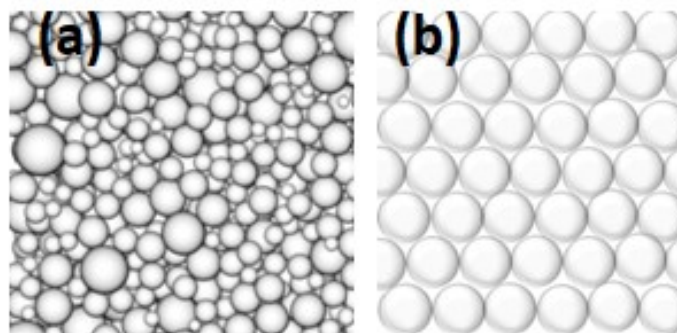
Fig.2.16: Close packing in syntactic foams (a) random packing (packing efficiency ~ 64%) (b) hexagonal close packing (packing efficiency ~ 74%)

2.3.5. High Strain-rate Studies

The effect of increasing strain rates on the compressive behaviour of syntactic foam was quantified using Split Hopkinson Pressure bar setup, which consists of input and output bar sandwiching a short specimen [143, 144]. The details of the setup are presented in our previous paper [140]. Pressurised air propels a projectile, which strikes at one end of the input bar. A compressive stress wave is generated, which upon hitting the

specimen, is partially transmitted and reaches the output bar while a part of it is reflected back to the input bar. In the present case, this propagation of the compressive wave leads to an irreversible plastic deformation in the specimen. The reflected pulse propagates as a tension wave, while the transmitted pulse remains in compression. The wave signal responses are quantified using strain gauges attached on the input and output bars. The stress – strain profile obtained for different samples are presented in **Figure 2.17**. Representative curve for each loading is presented for the sake of comparison of the results. It is to be noted that under high strain compressive testing, the strain rate rapidly increases during the initial stages of loading; therefore it was not attempted to estimate the Young's modulus from the strain gauge data. As in the case of quasi-static testing, the flow stress (maxima) decreased with increasing microbubble loading (38MPa SF46-60 (ε =2080 s^{-1}), 71 MPa, SF46-50 (ε =2580s^{-1}) and 151 MPa, SF46-40, (ε =1810s^{-1}).
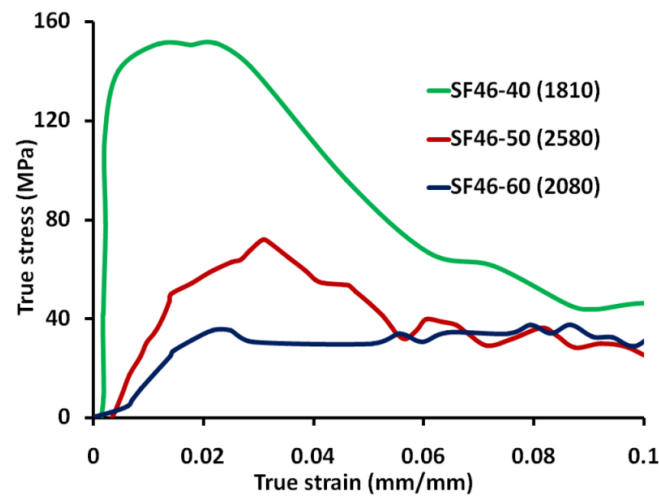
Fig.2.17: *Stress-strain profile of syntactic foams under high strain rates (~1810-2580 s^{-1})*

The mechanical response of the specimens under high strain rate was found to follow the same order as under quasi-static testing, however a distinct difference in terms of the absence of a stress plateau was clearly evidenced. In line with the quasi-static tests, decrease in microcapsule loading leads to a proportional increase in the maximum flow stress. The strain rate sensitivity of a representative formulation (SF46-40) is presented in

Figure 2.18. In line with previous studies [52], the flow stress was found to increase proportionally with increasing strain rates. The fracture mechanics of syntactic foams has been extensively studied, wherein significant dependence of the compressive failure upon the strain rate has been reported [52]. The failure has been reported to occur via varied mechanisms. At low strain rates, the foams have been reported to undergo shear cracking due to crushing of the microbubbles whereas at higher strain rates, the failure occurs primarily due to crack propagation in the direction of compression.
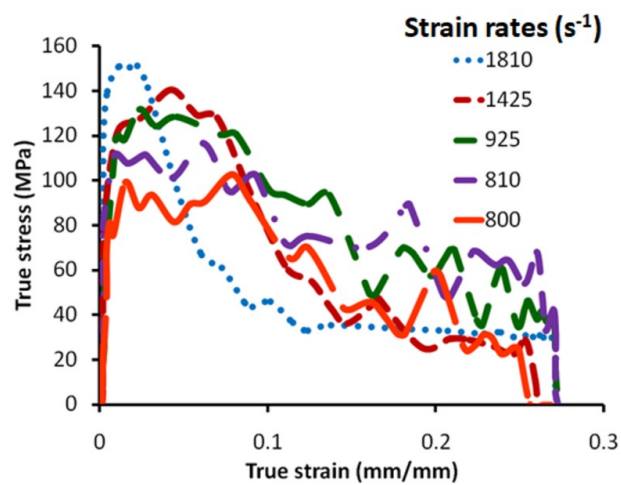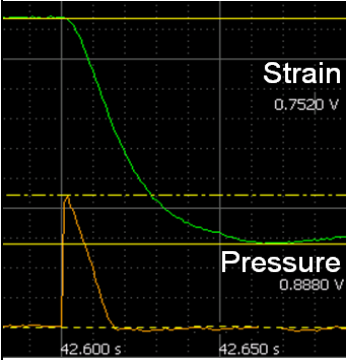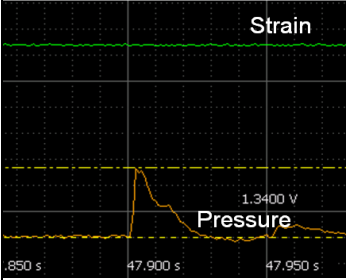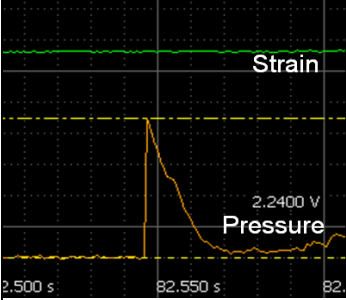
Fig.2.18: Effect of increasing strain rate on a representative syntactic formulation (SF46-40)

2.3.6. Shock tube Studies

The dynamic response of the syntactic foams was evaluated by subjecting circular disc shaped specimens to controlled transient loadings on a shock tube. The pressure profile along with the peak pressure, impulse as well as the response of the syntactic foam in terms of strain deformation is presented in **Table 2.3**.

Table 2.3: *Response of syntactic foam under blast loading conditions*

Sample	ΔP (Driver pressure-driven pressure)	Pressure/ strain profile	Peak pressure (psi)	Sample response
Control *Neat Aluminium sheets (2 Nos)*	2		35.5	Extensive deformation observed. Strain: 1701με
S40 (1cm) sandwiched between 2 Aluminium sheets	5		53.6	No strain observed. Sample intact post-blast
S40 (1cm) sandwiched between 2 Aluminium sheets	15		89.6	No strain observed. Sample intact post-blast

It can be seen that the control set (aluminium sheets, 2 Nos) undergo extensive deformation due to blast loadings (Overpressure: 35.5 psi). In comparison, the syntactic foam specimens do not undergo any deformation even when subjected to larger overpressures. A photograph of the SF46-40 specimen post-blast loading (Overpressure: ~ 89.6 MPa) is presented in **Figure 2.19**. It can be seen that the sample is intact, which

clearly highlights the potential of syntactic foams, as core material in sandwich configuration for blast mitigating applications.
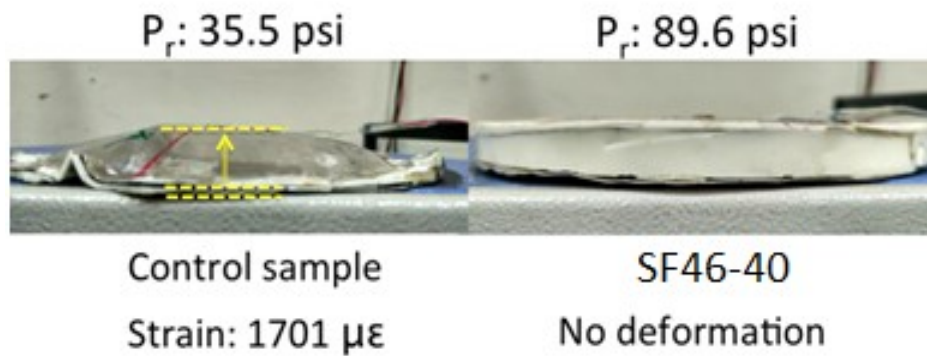
Fig. 2.19: Post-blast visuals of control and SF46-40 syntactic foam

SF46-40 syntactic foams were repeatedly subjected to blast pressures of ~ 90 psi. The post-blast visual of the sample exposed to 5 repetitive shock loadings is presented in **Figure 2.20**. It can be seen that the sample underwent chipping, with no visual evidence of microbubble crushing.

Fig.2.20: Post-blast visuals of SF46-40 syntactic foam after 5 repeated blast loadings (P_r ~ 90 psi)

2.3.7. Thermal Degradation

TG- DTG traces of syntactic foams containing K46 microbubbles are presented in **Figure 2.21**. The profile associated with the degradation of epoxy was found to remain unaltered, except for the substantial increase in the char content, from 15.7 % to 53 % (at 600 °C) as the microbubble loading increased from 10% to 70% (SF46), a major fraction being the incombustible glass microbubbles.
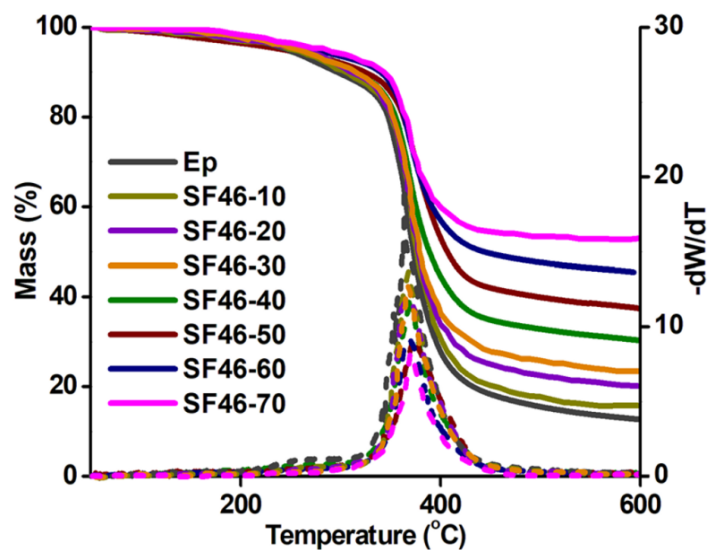
Fig. 2.21: *TG-DTG traces of epoxy syntactic foams SF46 (dotted lines represent DTG)*

The thermal properties of foams containing K15 present the same trendbarring the difference in the char content from 13.8 % to 34.8 % (at 600 °C) and are also included in the figure (**Figure 2.22**).
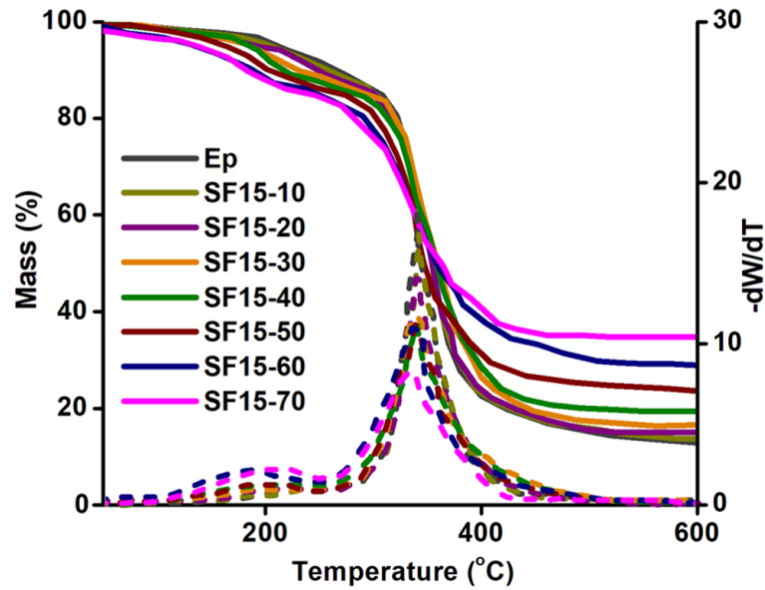
Fig. 2.22: *TG-DTG traces of epoxy syntactic foams SF15 (dotted lines represent DTG)*

The microstructure of syntactic foams was studied using a scanning electron microscope.The SEM image of syntactic foam specimen (SF46-40) post quasi-static testing (both compressive and tensile) is presented in **Figure 2.23**. Embedded hollow glass microbubbles are observed in the image. During compression, glass microbubbles undergo extensive crushing which results in the failure of the foams (**Figure 2.23 a**). On the other hand, tensile failure is brought about by the failure of matrix (**Figure 2.23 b**). Flexural failure occurs due to a combination of tensile and compressive forces and results in microbubbles debonding as well as matrix failure.
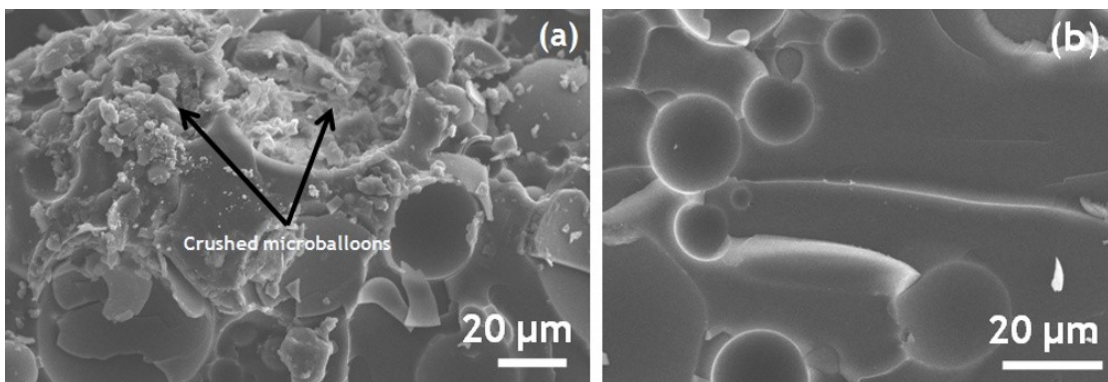
Fig.2.23: *(a) Compressive and (b) tensile fracture features of epoxy syntactic foam*

Processing of epoxy-glass bubble formulations (40-60 % microbubble loading) did not lead to any rupture of glass microbubbles under the experimental conditions employed. This was determined by performing oxidative degradation of epoxy syntactic foam specimens in a muffle furnace (at 600 ° C), and the leftover char was observed under an optical microscope. Representative images of the char obtained from SF46-60 and SF15-60 are presented in **Figure 2.24**. It is clear that all the microbubbles retained their physical appearance with no evidence of glass rupture.
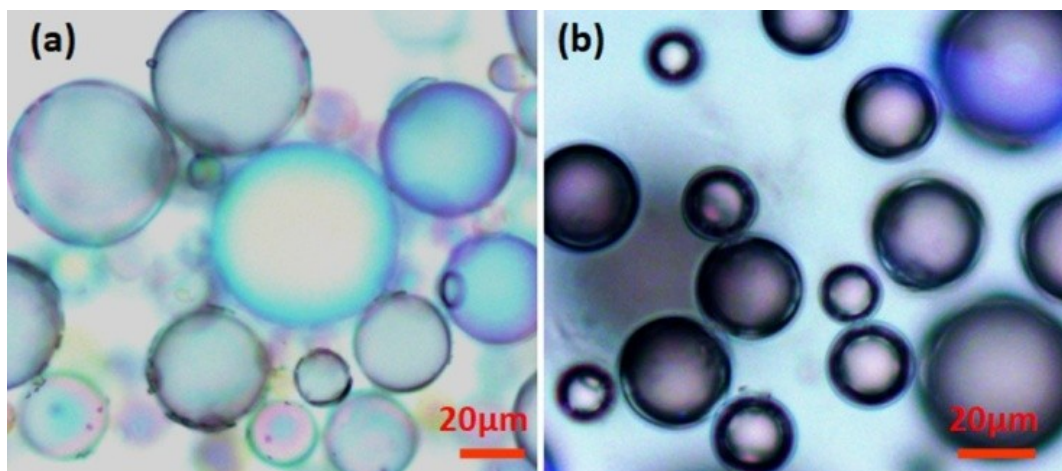
Fig. 2.24: *Optical images of the char obtained post-oxidative degradation of (a) SF15-60*

(b) SF46-60

Chapter III

Two-dimensional (2D) Layered Filler Reinforced Epoxy Syntactic Foams
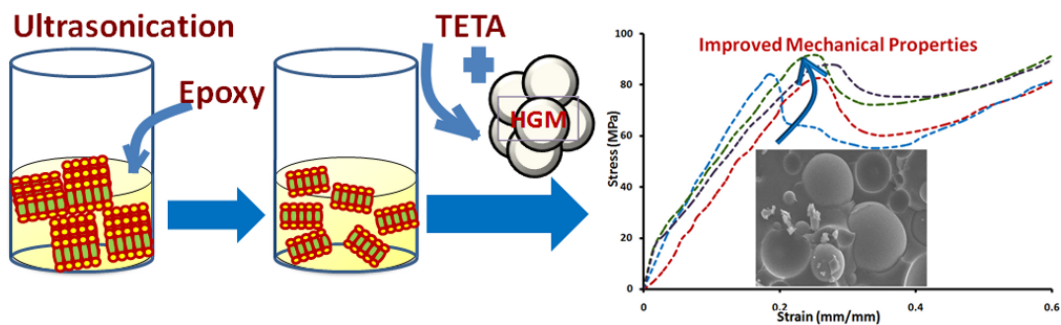
3.1. Introduction

Oriented two-dimensional (2D) materials have elicited enormous interest in the research community, for a plethora of reasons. These materials, exhibit an enormous degree of mechanical anisotropy, a property that can be judiciously exploited to disperse and dissipate energy controllably in specific directions, which can prove extremely effective in mitigating damage propagation. Since the foams under investigation are expected to be subjected to extreme compressive loadings, the presence of homogeneously dispersed high strength layered fillers can result in significant improvements. In this chapter, three different two-dimensional fillers have been explored for their ability to reinforce epoxy syntactic foams, namely molybdenum disulfide (MoS_2), reduced graphene oxide and organically modified nanoclay (Cloisite 30 B).

3.2. Two-Dimensional Fillers

3.2.1. Molybdenum disulfide (MoS_2)

Molybdenum disulfide, a silvery black inorganic solid reportedly occurs in two crystalline states hexagonal and rhombohedral. The hexagonal state, found commercially, consists of MoS_2 layers in which the molybdenum atoms have trigonal prismatic coordination of six sulphur atoms, with two molecules per unit cell [145]. In the layered structure of MoS_2, its constituent layers are held together by weak Van der Waals forces forming a sandwich structure. The layers or plates of MoS_2 are composed of one molybdenum sheet between two sheets of sulphur. The distance between the Mo and S sheets is of the order of 1.59 A° and the distance between the molybdenum layers of adjacent sheets is 6.15 A° (**Figure 3.1)** [145]. In view of its layered geometry, MoS_2 is often referred to as the inorganic analogue of graphene. Monolayers of MoS_2 have been reported to exhibit high tensile strength of the order of ~ 23 GPa, Young's modulus (~ 270 GPa) and tensile strain (6-11 %) [146] which is higher than most other engineering

materials such as stainless steel, polyimide, PDMS, Kevlar 49, WS_2 nanotubes etc., with the only exceptions being carbon nanotubes and graphene [147]. The application of MoS_2 as a reinforcing filler for epoxy resin has been reported by Eksik et.al [148]. In addition to increasing the tensile strength and elastic modulus of the base resin, introduction of as low as 0.2 % w/w MoS_2 has been reported to increase the fracture toughness and fracture energy of the resin by 60 and 160 % respectively [148].
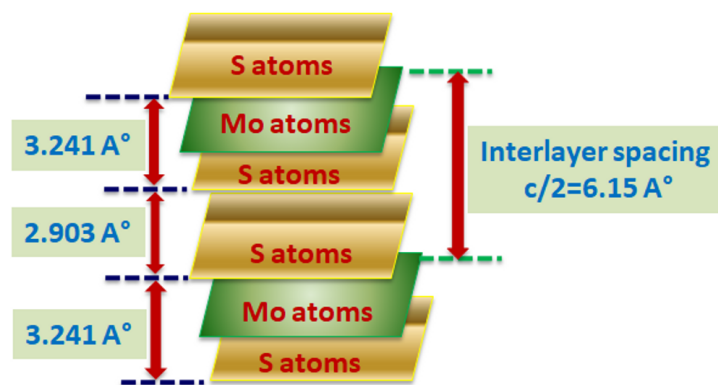
Fig.3.1: Representative structure of molybdenum disulfide

3.2.2. Graphene Platelets

Graphene, a basic building block for all graphite materials, exhibits a flat monolayer arrangement of carbon atoms, packed tightly in a two dimensional lattice. It can be converted into 0 D fullerenes, rolled up in to 1 D nanotubes and stacked into 3 D graphite [149]. Graphene platelets are two dimensional graphene thin plates having a few layers of graphene sheets (**Figure 3.2**). Their surface area (2360 m^2g^{-1}) [150] is higher than most of the other carbon nano structures that provide strong interfacial adhesion between the filler and the matrix. Moreover, it possesses good electrical and thermal conductivity (5000 $Wm^{-1} K^{-1}$) [150]. Graphene nanoplatelets can be economically produced in bulk quantities and can be easily dispersed in a variety of solvents due to the presence of various polar functional groups on its surface. It is thus used as high performance nanofiller to enhance the mechanical and electrical properties of the matrix.

Zegeye et.al. studied the effect of introducing graphene platelets (0.1-0.5 % v/v) on the mechanical properties of epoxy syntactic foams [76]. Introduction of 0.3 % graphene platelets led to 26 %, 14.7 % and 15.9 % improvement in compressive modulus, tensile modulus and tensile strength respectively.

Fig.3.2: *Structure of graphene*

3.2.2.1. Graphene Oxide

Pristine graphene exhibits excellent mechanical properties but the absence of functionalities renders its dispersion difficult in most organic polymers with the consequence that optimal enhancement in mechanical properties are not perceived in the resulting composites. Graphene oxide and reduced graphene oxide are thus used to offer better interfacial adhesion with the matrix resulting in improved properties. Primarily, graphene oxide possesses hydroxyl, carboxylic and epoxy groups, which are responsible for its improved compatibility with the matrix, which reflect in terms of the improved mechanical properties of the composites. The transformation of graphene to graphene oxide is usually effected using a well known Hummer's process (Hummer's and Offeman 1958) [151, 152].

3.2.2.2. Reduced Graphene Oxide

Reduced graphene oxide is obtained as a by-product of reduction process of graphene oxide in which some of the functionalities available with the graphene oxide are

removed. The presence of oxygen atoms in graphene oxide disrupts its sp^2 backbone which results in a decrease in the electrical conductivity. To overcome this, the graphene oxide is partially reduced by treating with hydrazine derivates to form reduced graphene oxide [153].
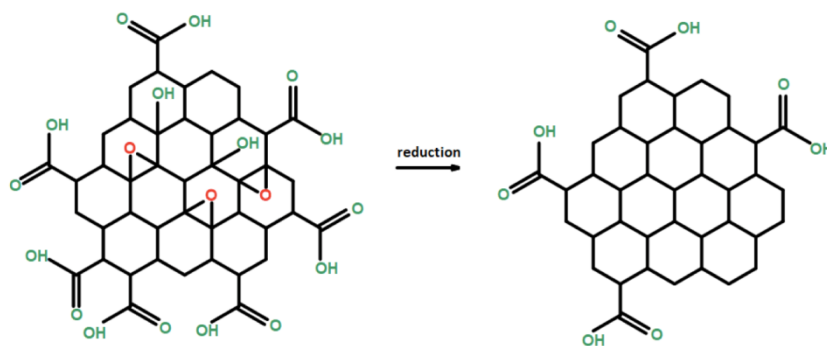
Fig.3.3: *Structure of graphene oxide and chemically reduced graphene oxide*

3.2.3. Organically Modified Nanoclay (Cloisite 30 B)

Nanoclays are two dimensional nanofillers, which belong to a wider group of clay mineral. They are basically silicates having a sheet like structure. Nanoclays are abundantly available, eco-friendly and low cost materials that are conventionally used as fillers in various mechanical applications. Cloisite is an organically modified montmorillonite with quaternary ammonium salt **(Figure 3.4)** [154]. There are different types of cloisite such as Cloisite 10A, Cloisite 20A, Cloisite 30B and Cloisite Na$^+$. The large library of published studies on nanoclay reinforced polymers have reported substantial improvement in mechanical, thermal and barrier properties [154-158], which is attributed to the high aspect ratio of the nanoclays. The optimum nanoclay content is generally ca. 2-3 percent by weight.

Introduction of nanoclay (5 wt %) was found to enhance the compressive modulus and compressive strength of epoxy based syntactic foams by 10 and 48 % respectively. Flexural properties, i.e. flexural strength and modulus, in nanoclay (5 wt %) reinforced

epoxy syntactic foams increased by 16 and 21 % respectively which was attributed to the increased interfacial interaction between the nanofiller and polymer matrix [74]. Improvement in the tensile strength in epoxy syntactic foam containing different grades of glass microbubbles is of the order of 22 % upon addition of 5 % nanoclay [68]. Saha et.al. reported improvements of ~ 42, 18 and 34 % in flexural strength, modulus and strain respectively at 2 % nanoclay. The storage and loss modulus also reportedly improved by 30 and 18 % respectively at same loading of nanoclay in epoxy syntactic foam [75].
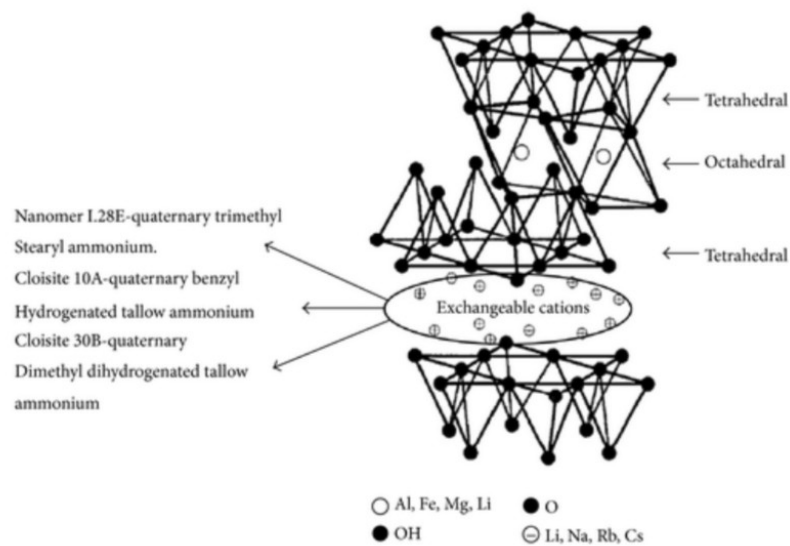
Fig.3.4: *Crystal lattice structure of Cloisite 30 B*

In the two-dimensional fillers, such as those discussed above, the individual layers are held together by weak Van der Waals forces. During conventional processing of thermosets by stir casting technique for the formation of nanocomposites, it is rather essential to disturb this structure to result in strong and stiff nanocomposites. Ultrasonication has been reported to be effective in resulting in intercalation and/or exfoliation of these nanofillers. Intercalation results in the introduction of polymer chains in between the layers of nanofillers thereby improving the mechanical properties, nevertheless the layered structure retains. For optimum improvements in mechanical

properties of nanocomposites, ultrasonication has to be performed for extended periods to result in exfoliation. Exfoliation is described as a stage wherein there is a disruption in the layered structure of the platelets and the polymer chains surround the individual layers. The different stages of dispersion of the layered fillers in polymeric matrix are presented in **Figure 3.5**.
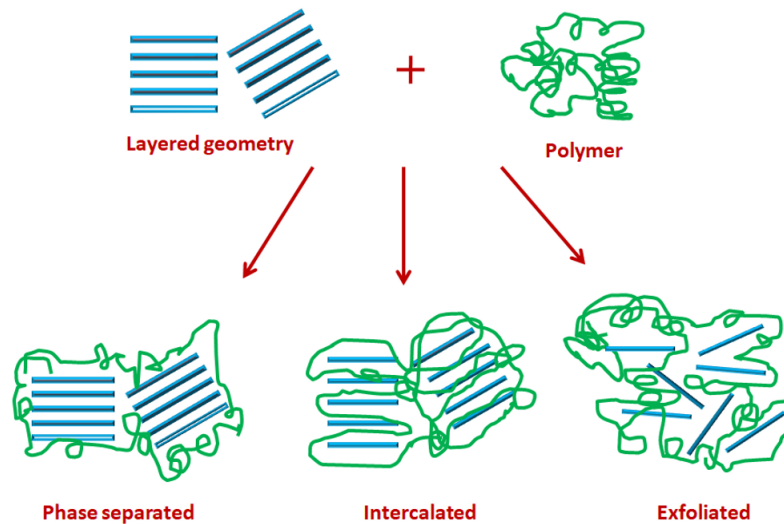
Fig.3.5: *Stages of dispersion of two-dimensional fillers in polymeric matrix*

3.3. Experimental

3.3.1. Materials

Cycloaliphatic epoxy resin (Ciba Geigy, Araldite CY 230; epoxy equivalent 200 eq g^{-1}), hardener (HY 951; amine content 24 eq kg^{-1}), Hollow Glass Microbubbles (K46, 3M), molybdenum disulfide (Loba Chemie), reduced graphene oxide and organically modified nanoclay (Cloisite 30 B) were used for the preparation of syntactic foam. Detailed characterization of reduced graphene oxide is presented elsewhere [152]. The physical properties of the HGMs are presented in Chapter 2. Ultrasonication was performed using a "Sonics Vibra-cell VC 505 tip sonicator, power ~ 500 W, frequency ~ 20 ± 0.05 kHz". Double distilled water was used throughout the course of study.

3.3.2. Preparation of syntactic foams

Epoxy syntactic foams containing increasing loadings of hollow glassbubbles (40, 50 and 60 % v/v) were prepared as per the procedure reported in Section 2.2.6. Requisite amounts of two-dimensional fillers were initially dispersed in epoxy resin through ultrasonication. For this purpose, the ultrasonic tip was immersed in epoxy-filler mixture and sonicated at a frequency of ~ 20 kHz (amplitude 40 %). The process was continued for extended time periods (12 h), to ensure uniform distribution of the fillers within the epoxy resin. Subsequently, HGM and hardener were mixed mechanically to prepare reinforced syntactic foams. The mass of HGM, Cloisite 30B, reduced graphene oxide platelets and MoS_2 to be added was calculated as follows (**Equation 3.1**):

$$\frac{Mass\ of\ nanofiller}{Mass\ of\ Syntactic\ foam} = \frac{\rho_{nanofiller} \times \Phi_{nanofiller}}{\rho_{2D-filler} \times \Phi_{2D-filler} + \rho_{HGM} \times \Phi_{HGM} + \rho_m \times \Phi_m} \ldots\ldots\ldots 3.1$$

where, ρ and Φ refer to the density and volume fraction of the constituent respectively, and the subscripts '2-D filler', 'HGM', and 'm' refers to the 2D fillers, i.e. molybdenum disulfide, organically modified nanoclay, graphene and epoxy respectively. For the purpose of calculation, density of MoS_2, nanoclay, reduced graphene oxide, HGM and epoxy have been assumed to be 5.06 g cc^{-1}, 1.98 g cc^{-1}, 1.8 g cc^{-1}, 0.46 g cc^{-1} and 1.17 g cc^{-1}[67] respectively. In view of the high density of MoS_2, its amount was restricted to a maximum of 0.04% (v/v), as further increase in the microbubble loading substantially increased the density of the composite.

The details of syntactic foam formulations and their respective designations are listed in **Table 3.1**. The numerical digits following S refer to the volume percent of microbubbles. For reinforced syntactic foams, M refers to molybdenum disulfide and the subsequent digits represent the volume percent of nanofiller (×100), similarly x refers to organically modified nanoclay (C) and reduced graphene oxide platelets (G) and the

subsequent digits represent the volume percent of 2D-filler (×10). S40 was chosen as a representative system on which effect of adding 2D-filler was studied in detail i.e. S40M1 refers to a formulation containing 40 % HGM and 0.01 % MoS_2 and S40G5 refers to a formulation containing 40 % HGM and 0.5 % reduced graphene oxide.

Table 3.1: *Sample designations and constituent composition of neat and reinforced foams*

Sample Code	Amount (% v/v)		
	Epoxy	Microbubbles	Filler
S40	60	40	-
S50	50	50	-
S60	40	60	-
S40M1	59.99	40	0.01
S40M2	59.98	40	0.02
S40M4	59.96	40	0.04
S40x1	59.90	40	0.10
S40x5	59.50	40	0.50
S40x10	59	40	1

The air-void porosity trapped within the matrix was determined as the ratio of the difference of theoretical and experimental density to theoretical density as per the procedure discussed in Chapter 2. The actual density (ρ_{ex}) was determined experimentally by averaging the mass : volume ratio of five specimens per sample as per the standard method ASTM D1622–98.

3.3.3. Characterization

The techniques used for the structural, rheological, mechanical, thermal and morphological characterisation of samples have been discussed in Chapter 2. The identification of crystalline phases in the sample was performed by powder XRD analysis on a Philips PANalytical 1730 (Netherlands) diffractometer using Cu K_α ($\lambda=1.54$ A°) where the diffractograms were recorded over a range of $2\theta = 2$ to $80°$.

3.4. Results and Discussion

3.4.1. Effect of introducing 2D fillers on Voidage

The ratio of experimental and theoretical densities was used to quantify the voidage in each sample, and the results are presented in **Table 3.2**. As expected, an increase in the microbubble loading lead to a decrease in the density of the foams. Interestingly, the voidage (%) in the samples containing 2D-fillers is relatively lower, which can be attributed to the preceeding ultrasonication step in the reinforced samples. It is to be noted that the presence of fractured microbubbles (present initially or ruptured during processing) is expected to lead to an increase in the density of the specimen [159, 160]. However, in view of the high crushing strength of the microbubbles used in the present study, a density of 0.46 g/cc has been used for all practical calculations.

Table 3.2: Experimental and theoretical densities of neat and reinforced syntactic foams

Sample Designation	Density(kg/m^3)		Voids
	Experimental	*Theoretical*	*(% v/v)*
S40	859.3 ± 4	886.0	3.0
S50	775.3 ± 4	815.0	4.8
S60	712.7 ± 4	744.0	4.2
S40M1	876.7 ± 2	886.4	1.1
S40M2	870.7 ± 3	886.8	1.8

S40M4	874.6 ± 2	887.5	1.4
S40C1	874.2 ± 3	887.3	1.4
S40C5	879 ± 2	890	1.2
S40C10	881.2 ± 4	894.1	1.4
S40G1	874.9 ± 4	886.6	1.3
S40G5	878 ± 2	887.8	1.1
S40G10	880.5 ± 3	892.3	1.3

3.4.2. Rheological studies

It is extremely important to be cognizant about the effect of introducing fillers on the processability of epoxy-glass microbubble formulations. The variation of complex viscosity as a function of curing time during time sweep experiments were performed isothermally at 60 °C and the results are presented in **Figure 3.6 a**. The resin was found to exhibit a complex viscosity of 1006 mPa.s. The effect of introducing glass microbubbles on the viscosity has already been discussed in **Section 2.3.1**.

In the presence of hardener, epoxy curing takes place, which leads to a concomitant increase in both the storage modulus and loss modulus. The variation of complex viscosity storage (G') and loss modulus (G") as a function of curing time, under isothermal conditions (60 °C) is also presented in **Figure 3.6 b**. In the initial period, the storage modulus remains constant over extended periods, where the formulation was practically liquid. With time, both G' and G" increase as the cross-linking reaction proceeds and subsequently a crossover region is observed, where the storage modulus becomes comparable to the loss modulus (Gelation region). Here, the system exhibit both elastic as well as viscous behaviour, where the amount of energy stored by the material is almost equal to the amount dissipated.

The gelation transformation induces various chemical and physical phenomena. The resin viscosity increases and the cross-linking densification advances. The curing proceeds till complete vitrification of the sample which essentially means the transformation of the rubbery network into a glassy solid.
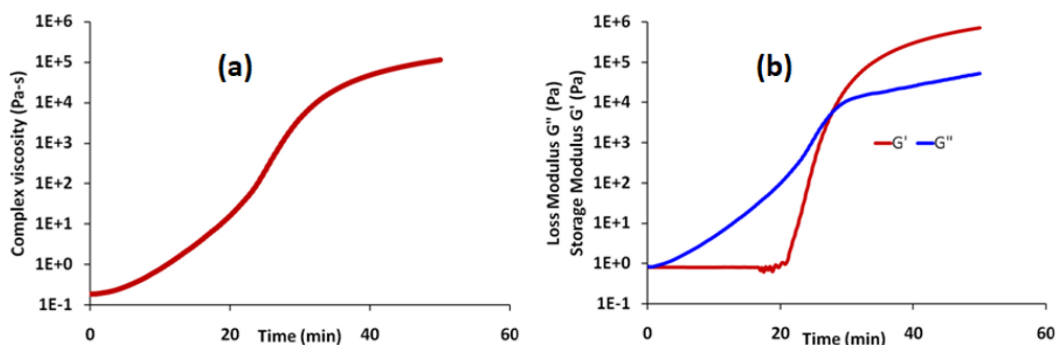
Fig.3.6 :(a) Complex viscosity and (b) storage modulus and loss modulus of neat epoxy (T =60 °C)

It is interesting to note that in the presence of glassbubbles, there is an increase in the complex viscosity of the formulations (**Figure 3.7 a**); however the final complex viscosity is the same when compared to that of neat epoxy without microbubbles. In the glass microbubbles filled formulation, the build-up in the storage modulus starts relatively early. In unfilled epoxy, this is evidenced at ~ 21min, and reaches crossover point at 27 min, while in the formulation containing glass bubble, the storage modulus starts increasing at 12 min. Another interesting phenomenon is the appearance of a kink at ~ 26 min in the filled system (**Figure 3.7 b**). This is due to the lubricating action of the glass bubbles. With curing, a three dimensional network formation takes place. However, during the initial period, the network is not strong enough to withstand the shearing force offered by the plates. Due to the spherical shape of the glass bubbles, the lubricating action leads to slippage of the polymeric chains formed. However, with time the crosslinking process continues and a strong network forms eventually.
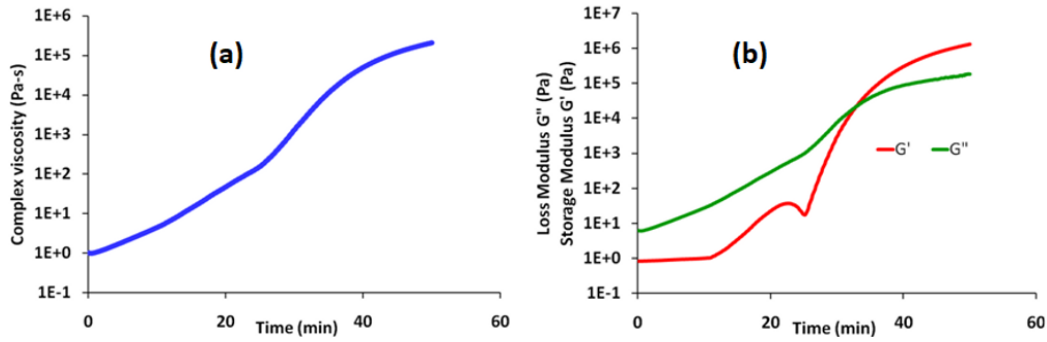
Fig.3.7 :_(a) Complex viscosity and (b) storage modulus and loss modulus of S40 (T =60_
_°C)_

The layered structure of MoS$_2$ is expected to result in a decrease in the viscosity of the formulation; however the extent of decrease was practically insignificant, probably due to its low loadings. Representative complex viscosity vs time curve of molybdenum disulfide reinforced epoxy syntactic foams is presented in **Figure 3.8 a**. The initial complex viscosities of both S40 and S40M4 are higher than neat epoxy. A drop in storage modulus is observed similar to S40. This drop corresponds to a disruption in the network due to the spherical shape of the glass microbubbles which act as tiny ball bearings and tend to roll due the shearing action of the parallel plates of rheometer (**Figure 3.8 b**). Due to the lesser loadings of the different 2D-fillers used for reinforcing epoxy glass microbubble syntactic foams; the change in rheology was insignificant.
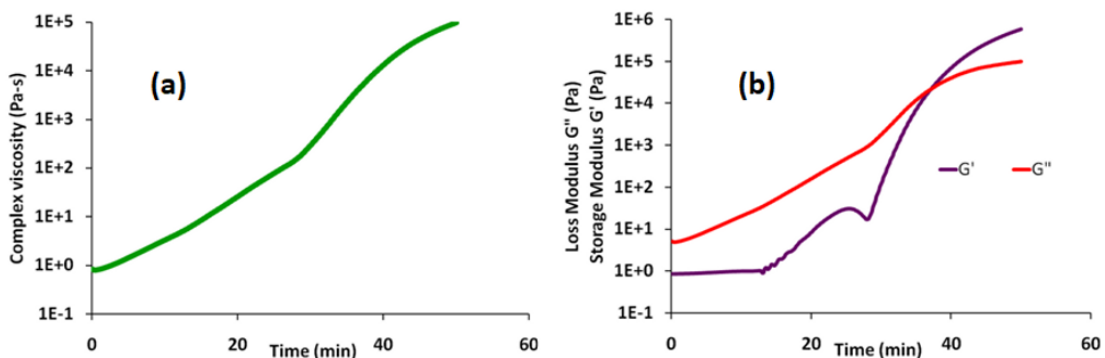
Fig.3.8 :_(a) Complex viscosity and (b) storage modulus and loss modulus of S40M4 (T_
_=60 °C)_

The variation of complex viscosity and storage-loss modulus as a function of time at a temperature of 60 °C for reduced graphene oxide and nanoclay reinforced epoxy syntactic foams is presented in **Figure 3.9** and **Figure 3.10** respectively. In can be observed that there is negligible change in the rheological parameters i.e. complex viscosity and storage-loss modulus compared to S40M4 due to the low loadings of the respective 2-D fillers in the epoxy matrix.
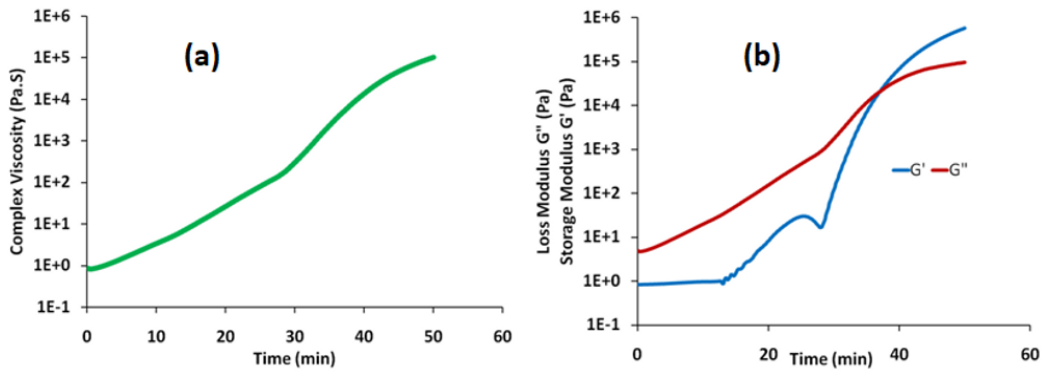
Fig.3.9:(a) Complex viscosity and (b) storage modulus and loss modulus of reduced graphene oxide reinforced epoxy syntactic foam (S40G10)
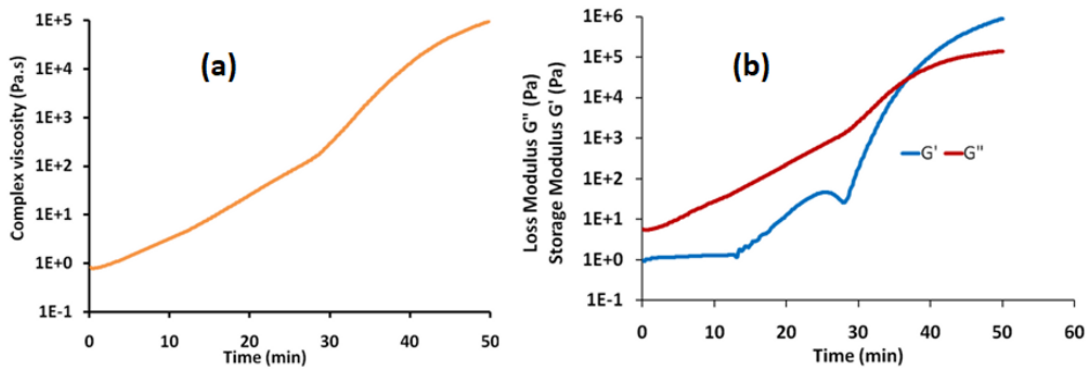
Fig.3.10:(a) Complex viscosity and (b) storage modulus and loss modulus of nanoclay reinforced epoxy syntactic foam (S40C10)

3.4.3. Mechanical properties

3.4.3.1. Effect of introducing 2D Fillers on Compressive Properties

The effect of increasing MoS_2 volume percent (0-0.04) on the stress-strain profile for a representative volume fraction of 40 % filler under compressive loading is presented

in **Figure 3.11**. The profile is clearly indicative of the sequence of events occuring during the compression process. The initial region of linear elasticity at low stresses is associated with the elastic bending of the spherical glass shells. The subsequent extended plateau region, in which the stresses remain practically constant, occurs due to the collapse of the closed cells and it is this region, which is responsible for the energy absorption of the foam. The toughness of foam is quantified in terms of the area under the compressive stress-strain curve till the plateau region. The final regime of densification leads to a steep rise in the stress values, and the point where the densification starts is considered to be the point of failure of syntactic foams. The stress-strain curves of neat syntactic foams present the same trend and hence are not expatiated here.
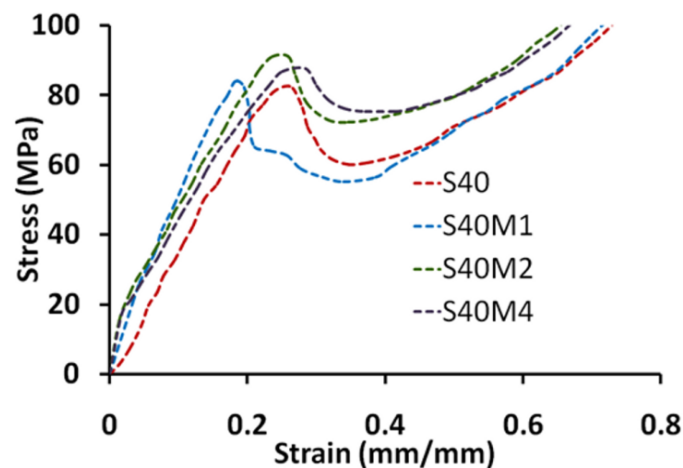
Fig.3.11: *Effect of loading on the stress-strain curve (under compression)*

The variation in characteristic compressive properties, namely compressive strength and toughness as a function of molybdenum disulfide loading is presented in **Figure 3.12**. Interestingly, the introductions of MoS_2 platelets lead to a substantial improvement in the compressive properties of syntactic foam i.e.16 % and 21 % improvement in compressive strength and toughness under optimal loadings.
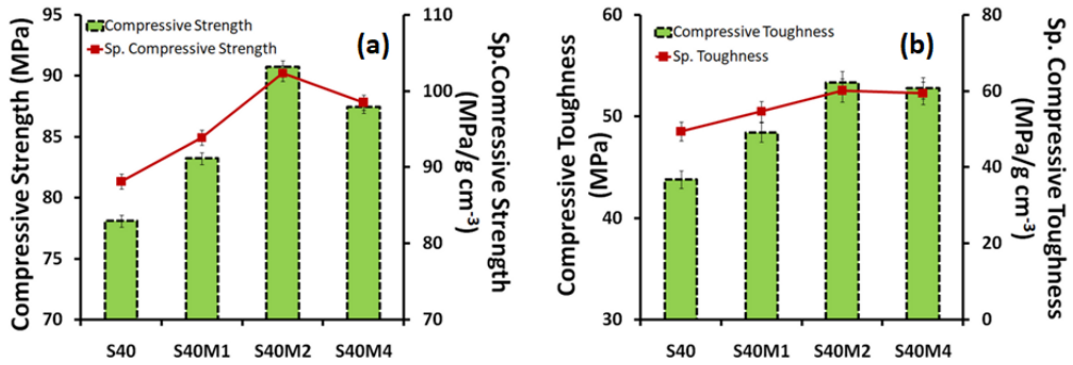
Fig.3.12: *Effect of MoS₂ loading on the compressive response of syntactic foam a)*

compressive and specific compressive strength b) compressive and specific compressive

toughness

MoS₂ possess a layered structure in which the individual layers are held together by weak Van der Waals forces forming a sandwiched structure (**Figure 3.13**). MoS₂ layers are composed of a single molybdenum sheet sandwiched between two sheets of sulphur. The distance between the molybdenum and sulphur sheets is 1.59 Å and the distance between the molybdenum layers of adjacent sheets are 6.15 Å [145].
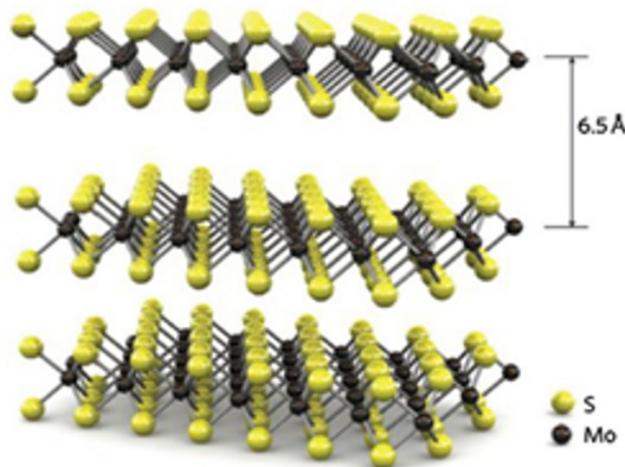
Fig.3.13: *Layered structure of molybdenum disulfide* [161]

We hypothesise that during the loading process, the molybdenum and sulphur layers slide past each other (**Figure 3.14**), which deflect the path of the advancing crack, leading to observed increase in the energy absorption. As an experimental evidence of the above phenomenon, studies on the mechanical properties of ternary artificial nacre were

carried out by Wan et.al. This showed that the crack front is bridged by the lubricating effect of MoS_2 through a crack extension mechanism [146].
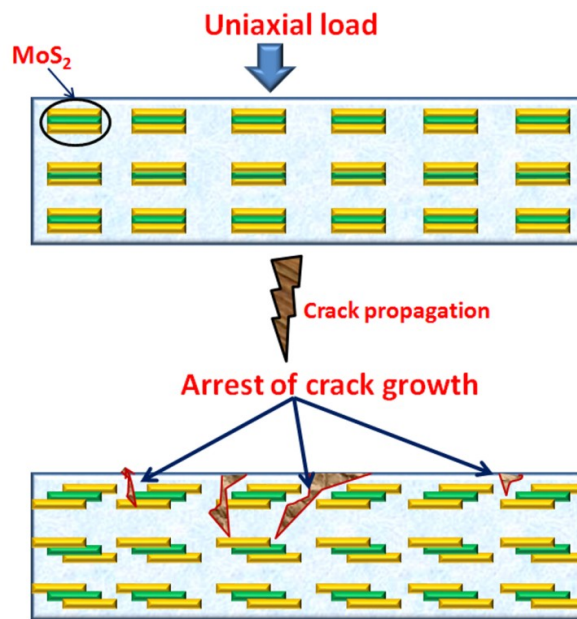
Fig.3.14: Probable mechanism of crack arrest in epoxy-MoS₂ composite

It is to be noted that inhomogeneous dispersion of MoS_2 in the polymeric matrix does not lead to any improvement in the properties of syntactic foams. As an evidence of this, a parallel set of experiments was performed where MoS_2 was introduced in the syntactic foam without the preceeding ultrasonication step, and the results are also included in **Figure 3.15**. It can be seen that the properties are almost similar to that of the neat foam.
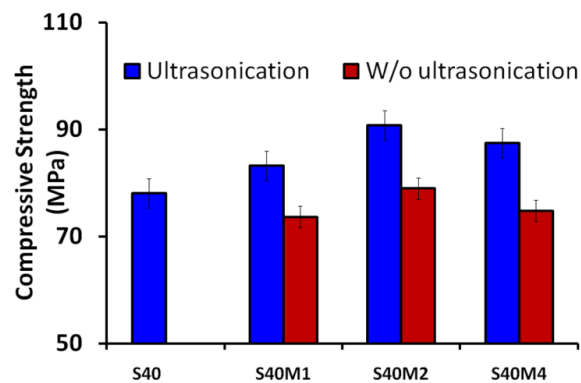
Fig.3.15: Effect of ultrasonication on the compressive strength of epoxy-MoS₂-HGM

hybrid syntactic foams

Ultrasonication reportedly brings down the average thickness of bulk MoS_2 platelets to ~ 5-10 nm [162].The effect of ultrasonication on the stability of MoS_2 – epoxy dispersion is presented in **Figure 3.16**. It can be seen that in the absence of ultrasonication, the flakes of MoS_2 settle down within 2 h, when undisturbed. Under similar conditions, the homogenously dispersed MoS_2 in ultrasonicated sample do not settle even after 24 h.

Ultrasonicated sample
Does not settle after 24h

Without ultrasonication
Settles within 2h
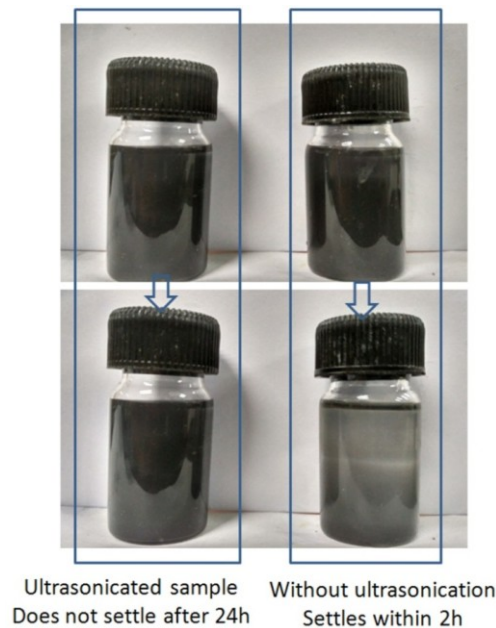
Fig.3.16: *Effect of ultrasonication on stability of epoxy- MoS$_2$ dispersion (0.04 % v/v)*
(Digital photograph)

Quasi-static compressive stress-strain curves of reduced graphene oxide platelets (0 - 1 % v/v) reinforced epoxy syntactic foams are presented in **Figure 3.17**. Representative compressive properties are presented in **Figure 3.18**.
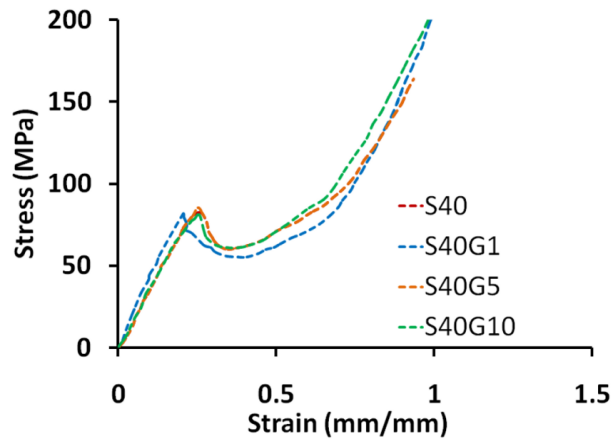
Fig.3.17: *Compressive stress-strain curves of reduced graphene oxide platelets*

reinforced foams

In view of the higher density of reduced graphene oxide compared to neat epoxy, the distribution of the former was restricted to a maximum value of 1 % (v/v). Introduction of reduced graphene oxide platelets (0.5 % v/v) in epoxy matrix led to marginal improvements of ~ 9 % and ~ 20 % in compressive strength and compressive toughness respectively. The unique properties of graphene i.e. its high specific surface area and good mechanical properties serves to enhance the interfacial interaction between the polymer and filler and deflects the path of the growing crack which resulted in improved compressive properties.
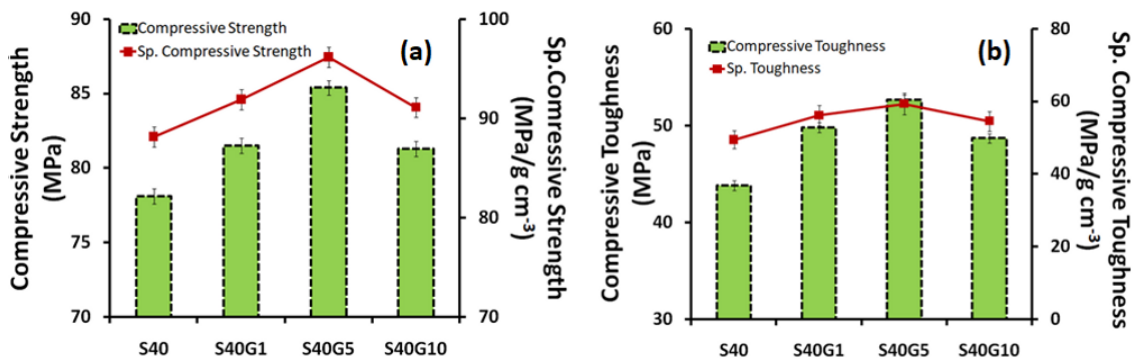
Fig.3.18: *Compressive properties (a & b) of reduced graphene oxide platelets reinforced*

epoxy syntactic foam

The effect of nanoclay incorporation on the quasi-static compressive properties of epoxy hybrid syntactic foam was also studied. Compressive stress-strain curves are presented in **Figure 3.19**. The curves depict the ductile behaviour of syntactic foams under compression. Compressive properties of nanoclay reinforced syntactic foam are presented in **Figure 3.20.**
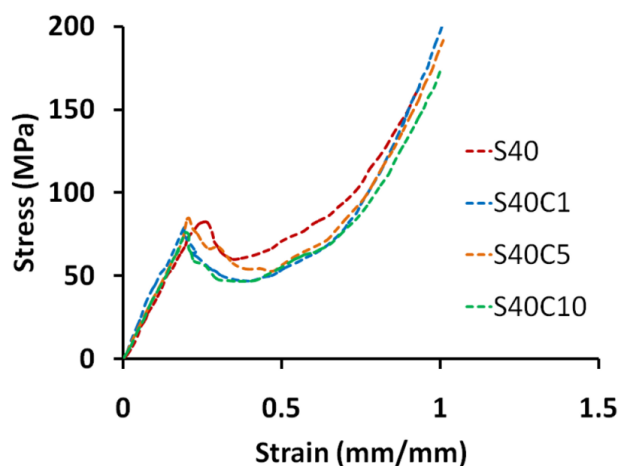
Fig.3.19: *Compressive stress-strain curves of nanoclay reinforced epoxy syntactic foams*

Minor improvement (~ 3 %) in the compressive strength was evidenced at 0.5 % (v/v) of nanoclay loading in epoxy resin. Intercalation/exfoliation of nanoclay brought about by ultrasonication resulted in enhanced interfacial interaction between nanoclay and epoxy matrix. The presence of intercalated nanoclay within the matrix was able to absorb the compressive load that resulted in improved toughness (~ 13 %) of the hybrid foam compared to neat syntactic foam. Specific compressive strength and specific toughness followed the trend observed in the case of compressive properties. Interestingly, the values deteriorated beyond 0.5 % of volume fraction due to the inhomogeneous dispersion of nanoclay and formation of nanoclay clusters in the matrix.
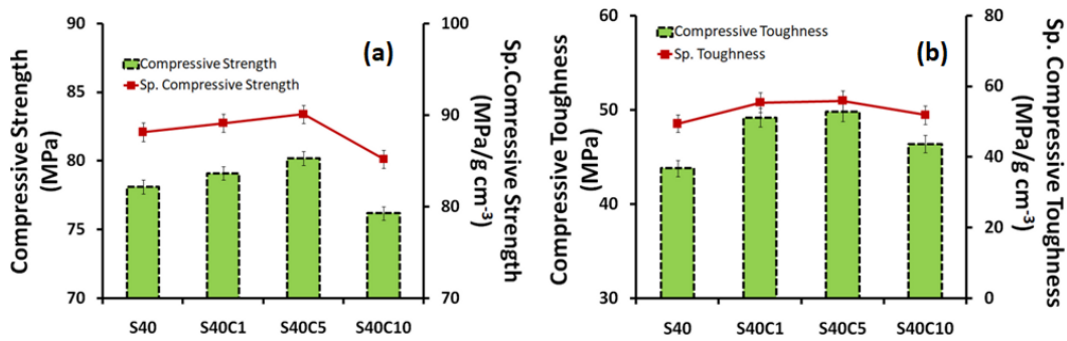
Fig.3.20: Compressive properties (a & b) of nanoclay reinforced epoxy syntactic foam

The PXRD pattern of neat epoxy and the resulting composites are presented in **Figure 3.21**. The pattern was characteristically reflective of amorphous epoxy, and no perceptible changes were observed. Under the concentration range of the fillers employed, it was not possible to evidence the exfoliation of the fillers through the technique: in fact the peaks associated with 2D-fillers were practically absent.

Consistent with the experimental results, similar improvement in compressive properties of epoxy syntactic foam has been observed with other 2D fillers. In a recent study, in foams containing reduced graphene oxide platelets, an increment of 3.6 % in compressive strength upon addition of 0.1 and 0.3 % (v/v) of reduced graphene oxide platelets respectively at 30 % v/v HGM was reported [76]. Improvement of the same order in the compressive properties of epoxy syntactic foam has also been observed with nanoclay filler [74].
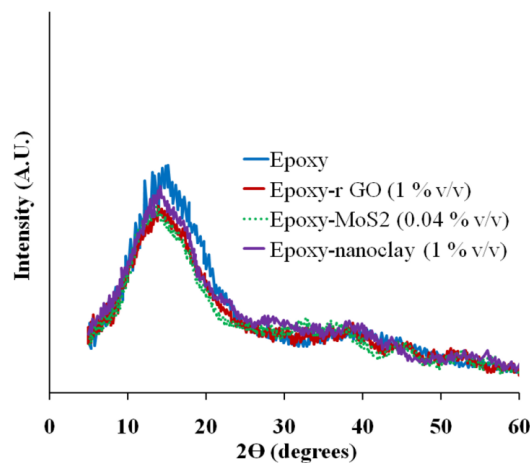
Fig.3.21: PXRD pattern of epoxy and 2D filler-epoxy composites

3.4.3.2. High strain-rate behaviour

The effect of increasing strain rate on the compressive behaviour of syntactic foam was quantified using Split Hopkinson Pressure bar setup: which consists of two long bars namely, input bar and output bar sandwiching a short specimen [143, 144]. Pressurised air propels a projectile, which strikes one end of the input bar. A compressive stress wave is generated, which upon hitting the specimen, is partially transmitted and reaches the output bar and a part of it is reflected back to the input bar. The reflected pulse propagates as a tension wave, while the transmitted pulse remains in compression. The wave signal responses are quantified using strain gauges attached on the input and output bars. Representative micro-deformations obtained during testing of a representative syntactic foam (S40M2) is presented in **Figure 3.22**.
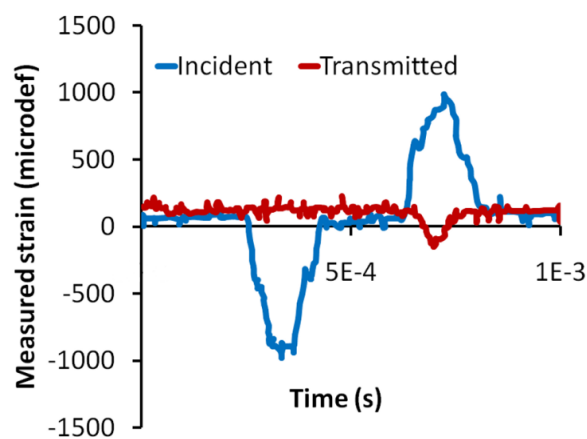
Fig.3.22: *Strain sensor micro-deformations as a function of time (S40M2)*

The micro-deformations were used to arrive at the stress-strain profiles. The values of flow stress (maximum) associated with the samples containing different fillers are presented in **Table 3.3**.

Table 3.3: *Flow stress for different syntactic foam specimens*

Sample designation	Strain rate (s^{-1})	Flow stress (MPa)
S40	1810	151
S40M2	1800	176
S40G5	1780	163
S40C5	1820	156

For unreinforced syntactic foams containing 40 percent microbubbles, an increase in strain rate leads to proportional increase in flow stress value (151 MPa, strain rate 1810 s^{-1}).The strain rate sensitivity of neat syntactic foams can be accounted on the basis of the reduction in the molecular mobility of the polymer chains leading to enhanced stiffness [163]. Introduction of MoS_2 leads to an increase in the flow stress values, highlighting the potential of MoS_2 as energy absorbing filler under high strain rates. It is to be noted that the crack propagation route through the specimen varies with varying strain rates. At low strain rates, the crack propagates mainly through the matrix whereas at high strain rate, the cracks propagation does not follow any fixed route. When the propagating crack encounters an inhomogenity (e.g. filler) at high strain rate, the growth of crack front is arrested and this leads to an increase in flow stress [164]. However, this effect is observable only at low volume fractions because at high volume fractions of the filler they tend to form clusters and thus reduce the flow stress. A representative high strain rate stress-strain profile is presented in **Figure 3.23**.
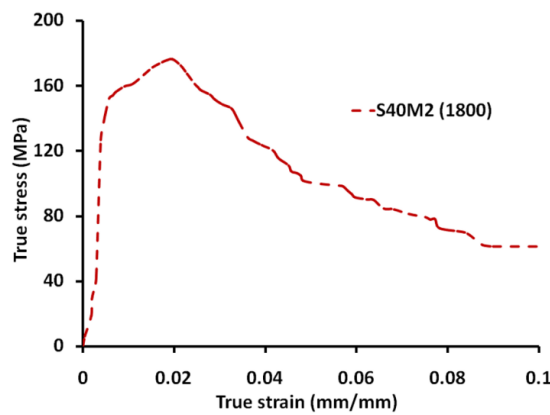
Fig.3.23: Stress-strain profile of S40M2 at high strain rate (~ 1800 s^{-1})

Introduction of reduced graphene oxide (0.5 % v/v) also lead to an increase in the flow stress values (163 MPa, 1780 s^{-1}) (**Figure 3.24**). At quasi-static strain rates when reduced graphene oxide are added, they tend to fit in between the polymer chains leading to a more stiff structure thus improved mechanical properties. However at higher strain

rates, the improvement in flow stress seems to be reduced due to the presence of already stiffened epoxy chains. This behaviour leads to minor improvement in flow stress values at high strain rates.
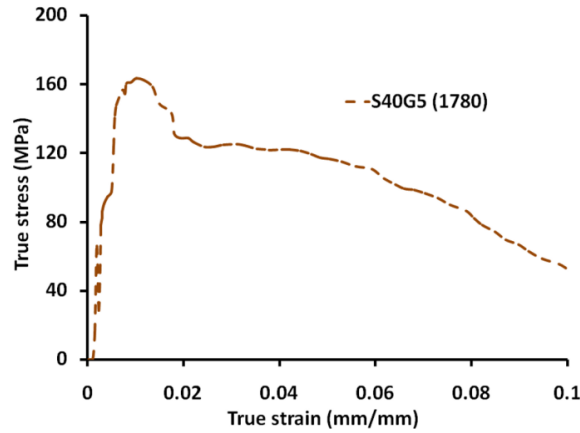
Fig.3.24: *Stress-strain profile of S40G5 at high strain rate (~1780 s^{-1})*

The high strain rate behaviour of nanoclay reinforced epoxy syntactic foams is presented in **Figure 3.25**. Inclusion of nanoclay in epoxy syntactic foams results in a marginal increase in the flow stress value of 151 MPa (unreinforced, 1810 s^{-1}) to 156 MPa (S40 C5, 1820 s^{-1}).
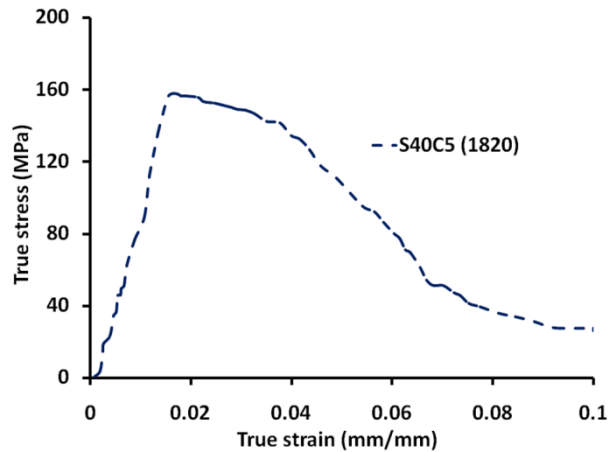
Fig.3.25: *Stress-strain profile of S40C5 at high strain rate (~1820 s^{-1})*

3.4.3.3. Effect of introducing 2D Fillers on Tensile Properties

The effect of increasing microbubble and MoS_2 loading on the tensile properties of syntactic foams is presented in **Figure 3.26**. As is apparent, a maxima (27 % increase) is

evident at 0.02 % (v/v) loading of MoS_2. At higher loadings, the tensile strength decreases but nonetheless the exhibited properties are higher than that of neat foam.
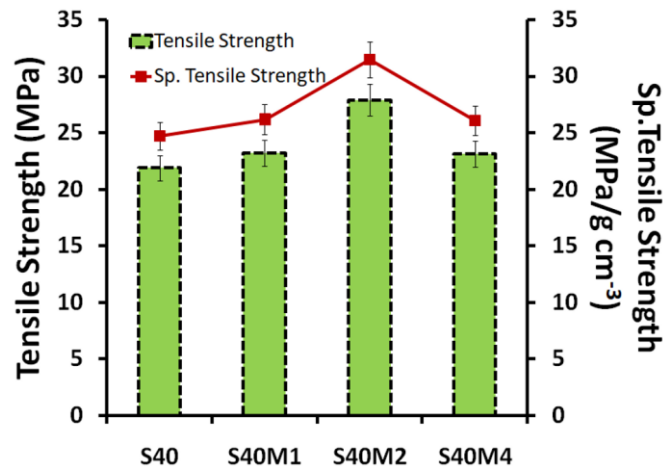
Fig.3.26: *Effect of increasing MoS_2 loading on the tensile properties of syntactic foams*

Effect of incorporation of reduced graphene oxide (0-1 % v/v) on the tensile properties of epoxy syntactic foams is presented in **Figure 3.27**. Addition of reduced graphene oxide in 40 volume percent filler loaded syntactic foams enhances the tensile strength by ~ 15 percent. Syntactic foam specimens observe much less ductility in tension unlike compression. In addition, the strength of the specimen reduces discernibly compared to compression. With the introduction of reduced graphene oxide, the chain stiffness increases resulting in the observed phenomenon.
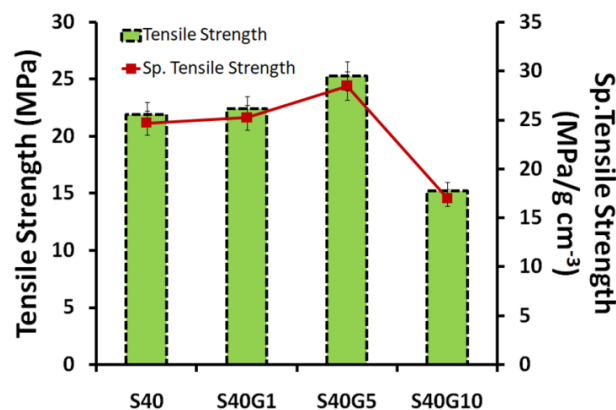
Fig.3.27: *Effect of increasing reduced graphene oxide loading on the tensile properties of syntactic foams*

Introduction of nanoclay (0.5 % v/v) to epoxy syntactic foams prevents the propagation of crack and increase the tensile strength by ~ 11 %. Nevertheless, at higher loadings, a reduction in properties is observed due to the agglomeration of the nanofiller. Effect of nanoclay incorporation on the tensile properties of epoxy hybrid syntactic foams is presented in **Figure 3.28**.
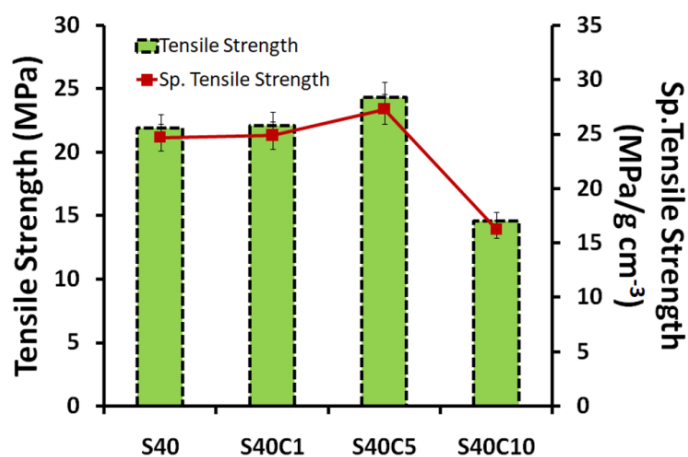
Fig.3.28: Effect of increasing nanoclay loading on the tensile properties of syntactic foams

Previous studies on clay and graphene (both with 2D structures) revealed similar results. Incorporation of reduced graphene-oxide nanoplatelets (0.1 and 0.3 % v/v) increased the tensile strength by 15.9 % and 14.7 % respectively compared to neat foam containing 30 % (v/v) loading of microbubbles [76].

It is to be noted that the tensile properties of syntactic foams depend primarily on the response of the matrix rather than on the filler i.e. glass microbubbles [141]. It appears that the interfacial adhesion between the epoxy and the filler increases significantly upon introduction of exfoliated/intercalated platelets, which in turn result in improved properties. The subsequent reduction in the tensile properties upon increased loadings can be attributed to the agglomeration of the fillers, which tend to behave as stress concentration loci.

3.4.3.4. Effect of introducing 2D Fillers on Flexural Properties

The effect of introducing 2D-fillers on the flexural properties of syntactic foams is presented in **Figure 3.29**. Due to its tri-layer structure (Mo layer sandwiched between two S layers), the bending modulus of single layered MoS_2 is significantly higher than that of graphene (by as much as seven times) [165]. It can be seen that under optimal conditions (0.01-0.02 % v/v), the flexural strength was found to increase by 33 %.
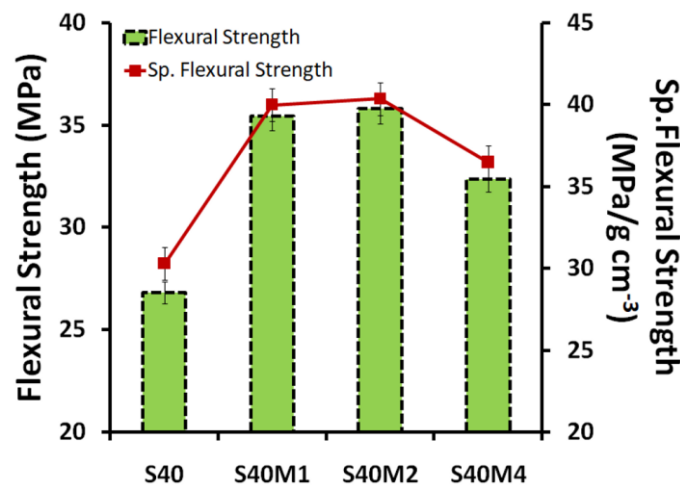
Fig.3.29: *Effect of increasing MoS_2 loading on flexural properties of syntactic foam*

The effect of reduced graphene oxide on the flexural properties is represented in **Figure 3.30**. The additive effect of reduced graphene oxide platelets on the tensile and compressive properties makes way for the increase in flexural properties also. An increase in flexural strength ca. 28 % was observed at 0.5 % (v/v) loading of reduced graphene oxide in epoxy syntactic foam.
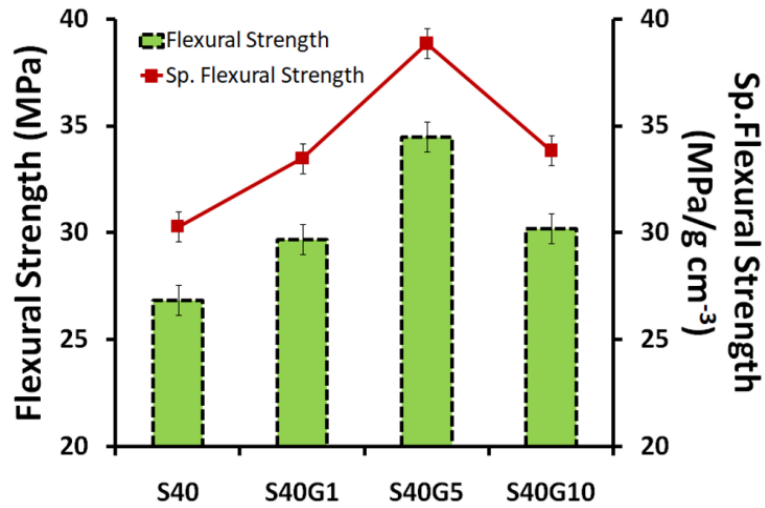
Fig 3.30: *Effect of increasing reduced graphene oxide loading on flexural properties of syntactic foam*

Effect of incorporating nanoclay on the flexural properties of epoxy syntactic foams is presented in **Figure 3.31**. An enhancement of ~ 17 % in flexural strength was evidenced on adding nanoclay to epoxy syntactic foam. This was attributed to the better interfacial interaction between nanoclay and epoxy matrix. Increase in specific flexural strength till 0.5 % (v/v) of nanoclay was ascribed to the increase in strength of syntactic foam compared to the increase in density of the foams.
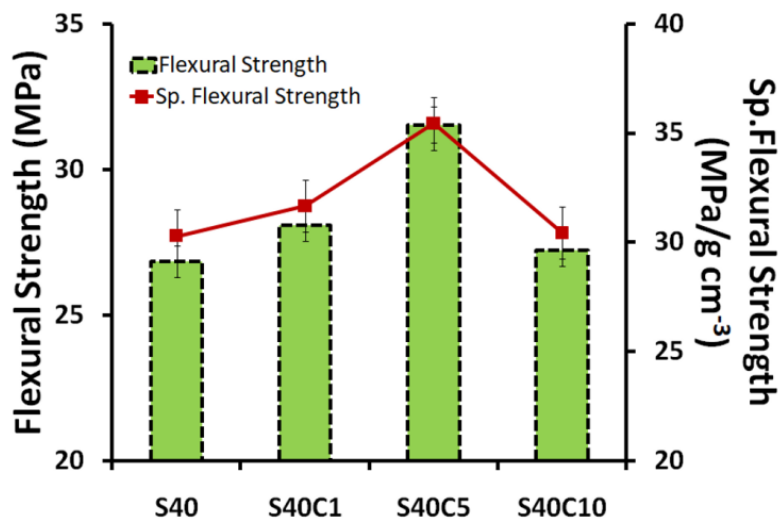
Fig.3.31: *Effect of increasing nanoclay loading on flexural properties of syntactic foam*

In a previous study, addition of 2 % nanoclay was found to increase the flexural strength of the foam by ~ 42 % [75]. SEM image of the fractured specimen is presented in the **Figure 3.32**. Flexural failure is a result of both compressive as well as tensile forces, which act on the specimen simultaneously. In view of the high strength microbubbles, which are used for the present study, the failure seems to result primarily in the epoxy matrix, with most of the glass bubbles remaining intact. A very few fractured glass microbubbles were observed on the fracture surface, however in view of the low loadings of the nanofillers, their presence could not be verified, even under high magnifications.
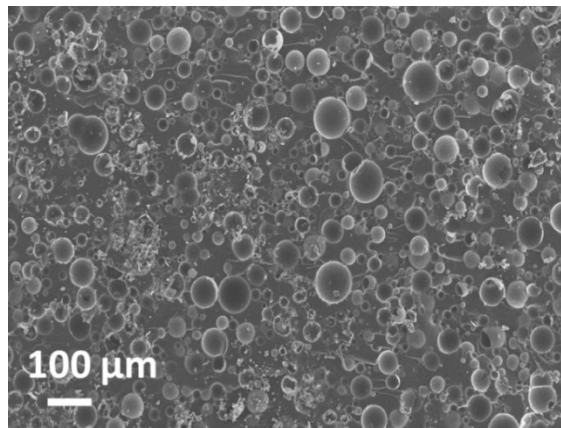
Fig.3.32: Fracture surface of hybrid glass-microbubble epoxy

3.4.4. Thermal Degradation Behaviour

TG-DTG trace (under inert atmosphere) of a representative 2D filler reinforced syntactic foam specimen (S40M4) is presented in **Figure 3.33**. It can be seen that microbubbles do not affect the degradation temperature of epoxy, and the introduction of MoS_2 did not lead to any appreciable change in the thermal degradation profile of the sample.
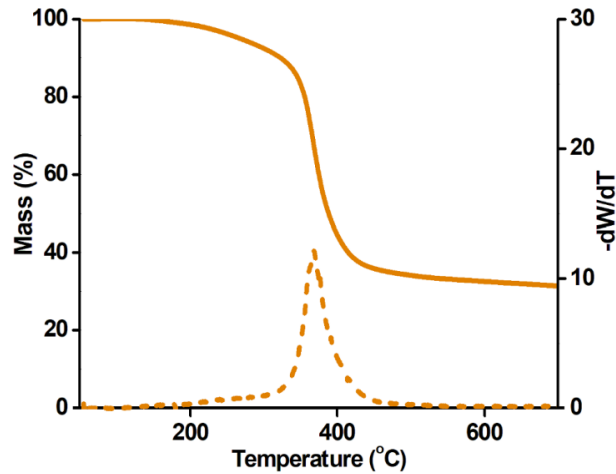
Fig. 3.33: TG-DTG traces of S40M4 syntactic foam under inert atmosphere

TG-DTG trace of hybrid syntactic foams remains unaffected upon addition of small volume percentage (1 % v/v) of reduced graphene oxide platelets. As in the case of neat foam, single step degradation profile was observed under nitrogen atmosphere (**Figure 3.34**).
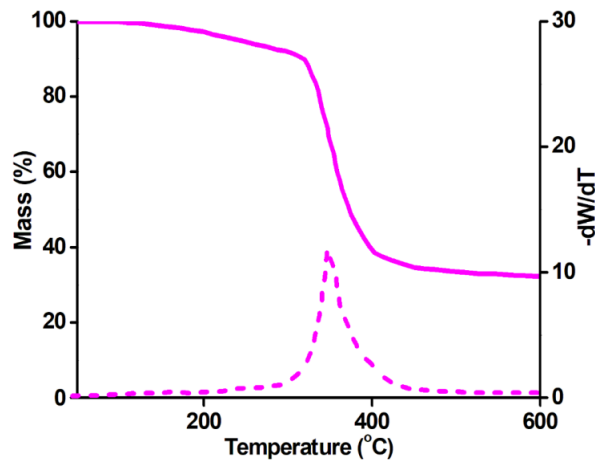
Fig. 3.34: TG-DTG traces of S40G10 syntactic foam (dotted lines represent DTG)

TG-DTG traces of epoxy glass microbubbles hybrid syntactic foams containing nanoclay (1 % v/v) is presented in **Figure 3.35**. The profile resembles that of neat epoxy containing glass microbubbles (40 % v/v), due to low loading of nanoclay.
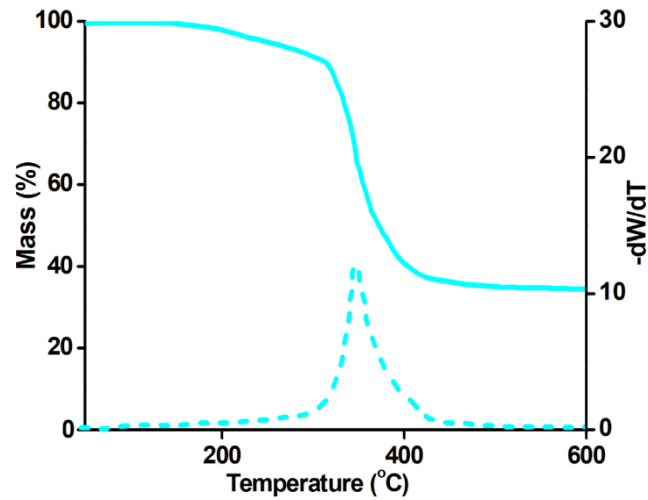
Fig. 3.35: *TG-DTG traces of S40C10 syntactic foam (dotted lines represent DTG)*

A comparison of the mechanical properties (quasi-static mode) of reinforced specimens is presented in **Figure 3.36**. Among all the fillers, it is evident that inclusion of MoS_2 led to highest improvements at very low loadings. MoS_2 therefore, offers an enormous potential in the field of syntactic foams to be used as reinforcing filler.
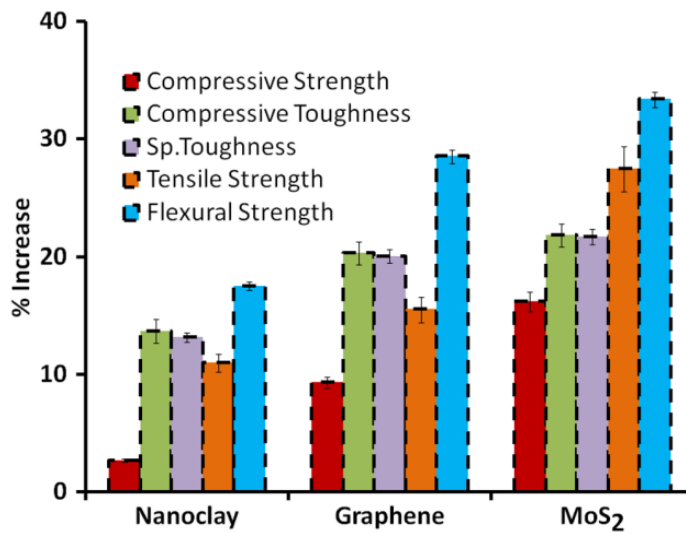
Fig.3.36: *Comparison of quasi-static mechanical properties of 2D fillers*

Chapter IV

Poly(dimethylsiloxane) Toughened Epoxy Syntactic Foams

Rubber microspheres

Epoxy

ultrasonicated

Hollow glass microballoons

PDMS toughened syntactic foams
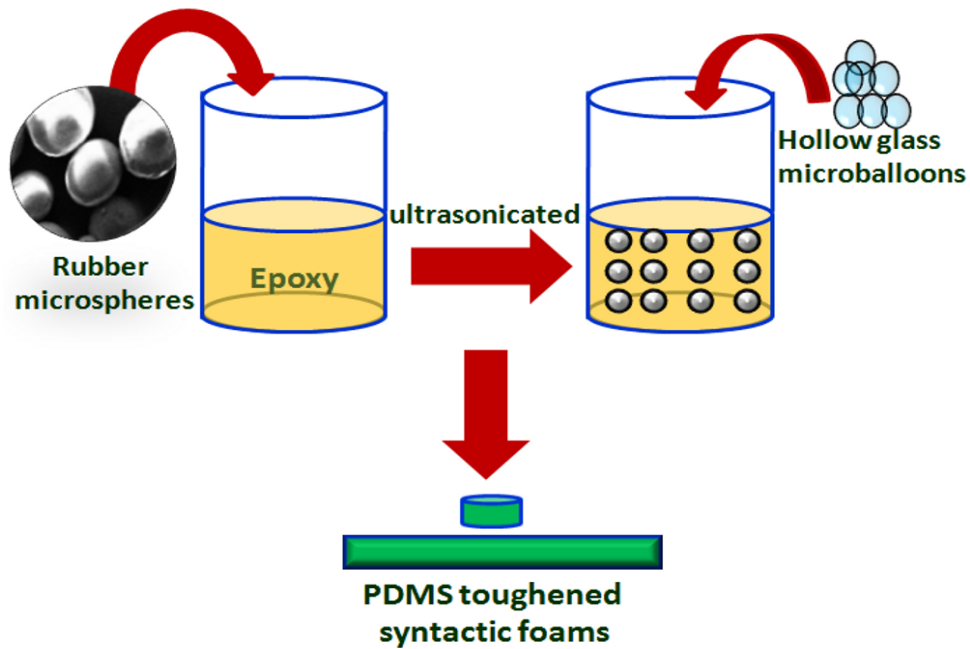
4.1. Introduction

Researchers worldwide are exploring various methodologies towards improvement of mechanical properties of syntactic foams, most common being the introduction of additives. Polymeric syntactic foams have been reinforced with different types of additives e.g. 1D dimensional carbon nanotubes [166], nanofibres [51, 66, 141, 167], 2-D dimensional graphene [76, 163], nanoclay [77, 168], etc. It is to be noted that the geometry, particle dimensions and the degree of loading plays a pronounced effect on determining the properties of resultant foams. The role of three different layered 2-D fillers on the energy absorption characteristic of epoxy-hollow glass bubbles has been reported in Chapter 3. It is to be noted that elastomers have been routinely employed to improve the toughness or the energy absorption capability of epoxy resin [169]. For this purpose, liquid rubber, usually functionalized e.g. amine terminated butadiene (ATBN), carboxy terminated butadiene (CTBN), phenol terminated butadiene (PTBN) [170-172] is first dispersed in the resin followed by addition of the hardener. As the crosslinking reaction progresses, the rubbery phase tend to separate out, resulting in the formation of a phase segregated structure. The rubber particles tend to blunt the crack tip and sometimes deflect the path of propagating crack, which leads to the significant increase in the energy absorption characteristics of the composite [173]. Cavitation and shear band formation are additional micro-mechanisms which contribute positively towards energy absorption [172]. It is to be noted that the mechanical properties of the toughened composite are strongly dependant on the extent of phase separation between the rubber and the plastic, which is, in many cases, rather difficult to control. Lately, preformed rubbers are being explored as tougheners for thermosetting resin, where it is relatively easy to gain control over the internal morphology. The feasibility of elastomeric poly (dimethylsiloxane) microspheres towards improving the energy absorption characteristic of epoxy resin has

been reported previously. Introduction of 5 % microspheres reportedly led to ~ 37 % increase in fracture energy and ~ 11 % increase in impact strength [174].

Although, the potential of elastomers has been extensively explored for neat resins, there seem to be limited attempts towards the usage of elastomers in toughening of syntactic foams. Introduction of small amounts (2 % v/v) of crumb rubber in epoxy based syntactic foams has been reported to increase the flexural properties of the foams substantially. Interestingly, the improvement was more pronounced, when the particle size of the rubber was smaller [77]. Crumb rubber, however, possesses an irregular morphology, which is expected to lead to higher voidage when mixed with glass bubbles of spherical shape.

The role of preformed spherical rubber particles as toughening agents for epoxy based syntactic foams has been explored. Poly(dimethylsiloxane) microspheres were prepared by suspension curing route. The dimensions of the elastomeric microspheres were tuned by altering the reaction parameters. The effect of rubber dimensions on the mechanical properties of syntactic foams was studied.

4.2. Experimental

4.2.1. Materials

Cycloaliphatic epoxy resin (Ciba Geigy, Araldite CY 230; epoxy equivalent 200 eq g^{-1}), hardener (HY 951; amine content 24 eq kg^{-1}) and Hollow glass microbubbles (HGM K15 and K46, 3M®) were used for the preparation of syntactic foams. Silicone resin (Elastosil M4644) along with the platinum based hardener was obtained from Wacker, Germany. PVA (mol. wt. 14000, CDH) and chloroform (CDH) were used without any further purification. Double distilled water was used throughout the course of study.

4.2.2. Characterization

The techniques used for characterisation of the foams have been discussed in Chapter 2. Shear rate sensitivity studies were performed for PDMS toughened syntactic foam formulations using an Anton Paar Rheometer (MCR 102) using 25 mm disposable aluminium parallel plates, while varying the shear rate over 0.1 to 1 s^{-1} under isothermal conditions (30°C).

4.2.3. Preparation of PDMS Microspheres

PDMS microspheres were prepared using a suspension polymerization technique as per the procedure discussed previously [174]. In brief, a feed solution was prepared by diluting vinyl terminated siloxane macromonomer with chloroform (30-60 % w/v). Thereafter, stoichiometric amounts of platinum based hardener (10:1:: siloxane: hardener) was added. A hypodermic syringe was used to introduce the feed into the aqueous PVA solution (1.5 % w/v) in a reaction vessel under inert atmosphere which in turn was maintained at 45 °C under continuous stirring. The reaction mixture was maintained for 8 h under varying stirring speeds (600-1000 rpm), after which the reaction mixture was cooled. The microspheres obtained were filtered and washed repeatedly with water. The extent of conversion was measured gravimetrically as the ratio of the solid microspheres obtained to the amount of macromonomer used for its preparation. The obtained PDMS microspheres were sieved to obtain three different particle size ranges for inclusion in the epoxy-HGM formulation (125-198 μm), (125-63 μm) and < 63 μm.

4.2.4. Preparation of Syntactic Foams

Epoxy based syntactic foams were prepared as per the procedure reported in the literature [67]. For this purpose, requisite amount of HGM was added in the epoxy matrix and the contents were manually mixed and degassed followed by introduction of calculated amounts of amine based hardener. The slurry hence obtained was transferred to

silicone moulds and cured for 48 hours at room temperature to prepare specimens for compressive and flexural testing.

For the preparation of analogous rubber toughened foams, weighed amounts of PDMS microspheres were initially dispersed in epoxy resin using an ultrasonic probe "Sonics Vibracell" operating at a power of 500 W. The probe was tuned to produce acoustic waves that resonate at a frequency of 20 kHz ± 50 Hz (amplitude of 40 %). The process was continued for 30 min to ensure a uniform distribution of the elastomeric microspheres into the epoxy resin. Subsequently HGM and hardener, in stoichiometric amounts, were added to prepare reinforced syntactic foams. The amount of filler, i.e. HGM and PDMS microspheres were calculated as per the formula (**Equation 4.1**):

$$\frac{Mass\,of\,PDMS}{Mass\,of\,composite} = \frac{\rho_{PDMS} \times \Phi_{PDMS}}{\rho_{PDMS} \times \Phi_{PDMS} + \rho_{HGM} \times \Phi_{HGM} + \rho_{matrix} \times \Phi_{matrix}} \dots\dots\dots\dots\dots 4.1$$

Where, ρ_{PDMS}, ρ_{HGM}, ρ_{matrix} refer to the density of PDMS microspheres (965 kg m^{-3}), HGM (460 and 150 kg m^{-3}) and epoxy resin (1170 kg m^{-3}) respectively and Φ_{PDMS}, Φ_{HGM} and Φ_{matrix} refer to the desired volume fraction of elastomeric microspheres, HGM and epoxy resin. The details of formulations and sample designations are listed in **Table 4.1**.

Table 4.1: Different compositions and designations of neat and reinforced foams

Sample Code	Matrix (% v/v)	Microbubbles(% v/v)	PDMS(% v/v)
SFx-40	60	40	-
SFx-50	50	50	-
SFx-60	40	60	-
SFx-40S3	60	37	3
SFx-40S5	60	35	5
SFx-40S7	60	33	7

x refers to the type of glass bubble x = 15 for K15 and 46 for K46

4.2.5. Density Determination

Theoretical density of syntactic foam (ρ_{th}) was calculated according to the standard rule of mixtures (**Equation 4.2**):

$$\rho_{th} = \rho_{PDMS} * \Phi_{PDMS} + \rho_{HGM} * \Phi_{HGM} + \rho_{matrix} * \Phi_{matrix} \ldots\ldots\ldots\ldots 4.2$$

The density of the foam was experimentally determined by averaging the mass: volume ratio of five specimens as per ASTM D1622–98. The ratio of theoretical and experimental densities was used to quantify the air void porosity trapped in the matrix during fabrication according to the following **Equation 4.3**:

$$Void\ \ volume\ \% = \frac{\rho_{th} - \rho_{ex}}{\rho_{th}} \times 100 \ldots\ldots\ldots\ldots 4.3$$

4.3. Results and Discussion

4.3.1. Silicone Microspheres

Poly(dimethylsiloxane) (PDMS) microspheres were prepared by suspension polymerization route, which permit tuning of the dimensions by varying the reaction parameters; especially macromonomer feed concentration and stirring speed. In the present study, vinyl terminated methyl hydrosiloxane dimethylsiloxane copolymer was cured at 45 °C in the presence of a hydrosilylation catalyst (**Scheme 4.1**).
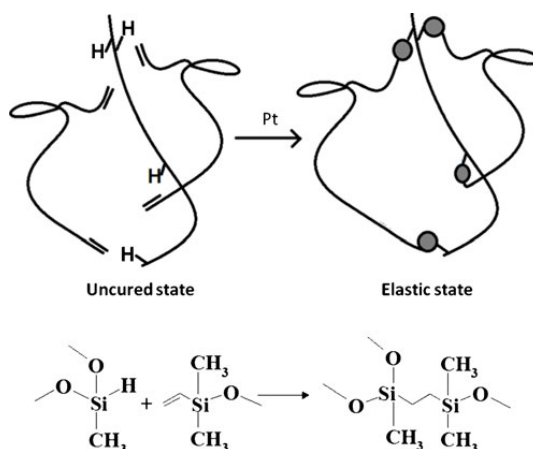
Scheme 4.1: *Reaction schematic for preparation of poly(dimethylsiloxane)*

The effect of increasing stirring speed on the particle size distribution of microspheres is presented in **Figure 4.1**. The SEM image of the microspheres is also presented in the inset. The smooth surface and spherical shape of the microspheres is clearly evident from the SEM images. As expected, higher stirring speed results in microspheres with relatively lower dimensions, which could be attributed to the increased shearing of the hydrophobic droplets at higher stirring speed.
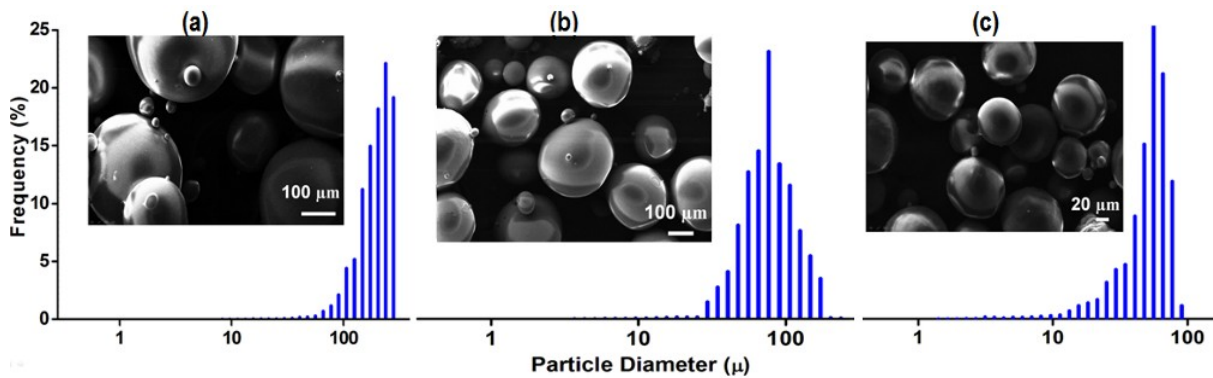
Fig. 4.1: Effect of stirring speed (a) 600 rpm (b) 800 rpm (c) 1000 rpm on dimensions of

PDMS microspheres (feed concentration = 60 %)

The effect of increasing feed concentration on the particle size distribution is presented in **Figure 4.2**. By altering the operating parameters, the microsphere dimensions could be varied from 58 to 255 µm.In all cases, > 98 % conversion could be achieved as evidenced by gravimetric analysis.
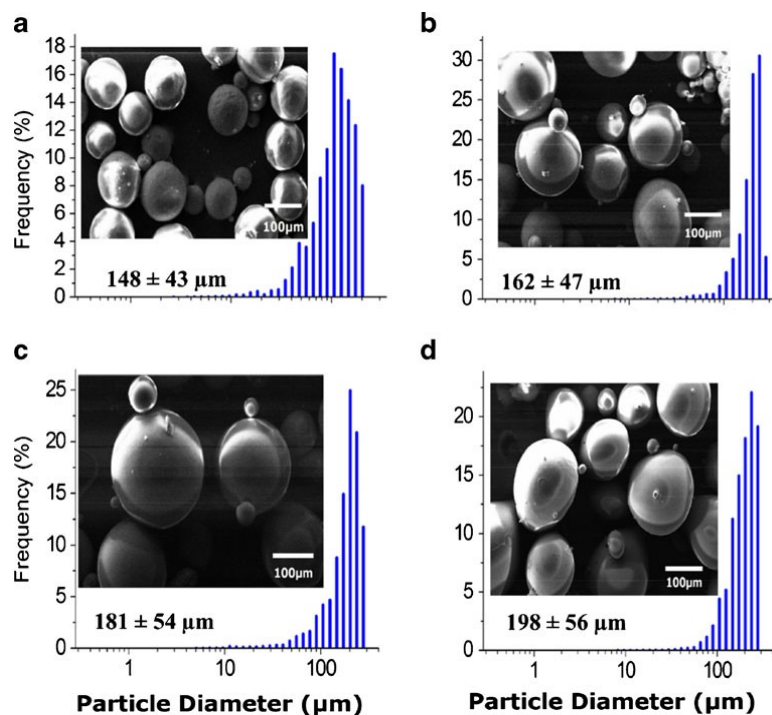
Fig.4.2: *Effect of increasing feed concentration on the particle size distribution (stirring speed 600 rpm) a 30 %, b) 40 %, c) 50 % and d) 60 %*

The TG-DTG traces associated with the poly(dimethylsiloxane) microspheres is presented in the **Figure 4.3**. As expected, in view of its non-carbonaceous chain, PDMS exhibit exceptional thermal stability, which is evident from the high $T_{5\%}$ (Temperature associated with 5% mass loss) of > 400 °C and char content (68 % at 600 °C).
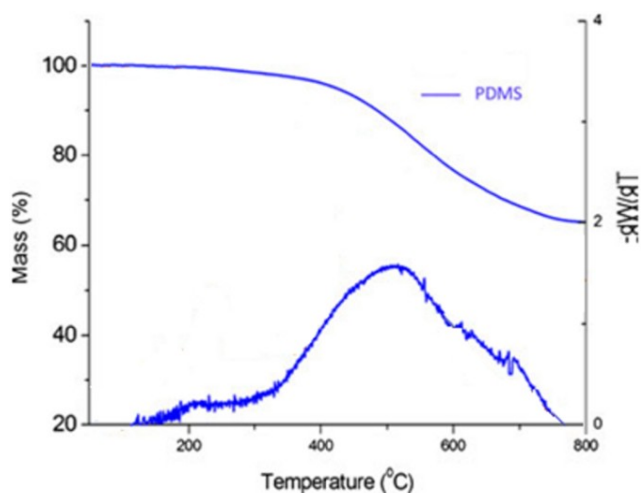
Fig.4.3: *TG-DTG traces of PDMS microspheres*

The FTIR of PDMS is presented in **Figure 4.4**. Characteristic absorption peaks at 802 and 1258 cm^{-1} due to the (CH$_3$)$_2$SiO group vibration and broad absorption at ~ 1000-1130 cm^{-1}, due to Si-O-Si stretching can be observed.
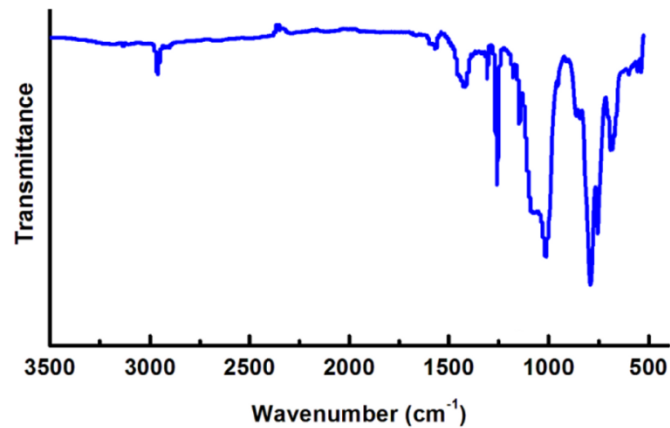
Fig. 4.4: *FTIR spectra of poly(dimethylsiloxane)*

The PXRD pattern of the siloxane (**Figure 4.5**) clearly reveals the amorphous nature of the elastomer.
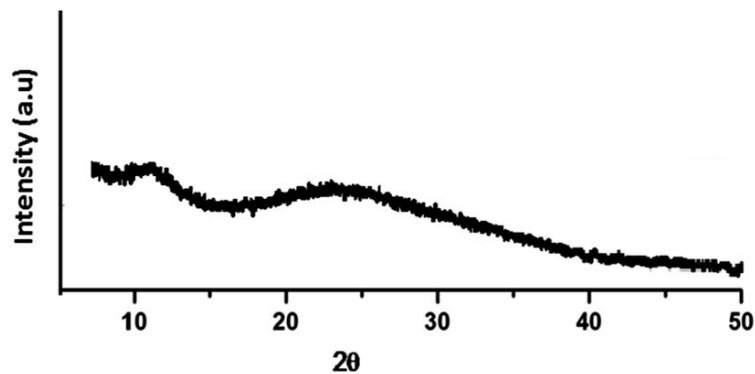
Fig. 4.5: *PXRD pattern of poly(dimethylsiloxane)*

4.3.2. Effect of Introducing PDMS into Epoxy: Rheological Behaviour

The effect of introducing glass micro bubbles and elastomeric microspheres on the rheological behaviour of the resin is of particular interest for processing of the foams. The shear rate dependence of the formulation is presented in **Figure 4.6**. Unfilled epoxy resin exhibits a viscosity of ~ 1000 mPa.s at 30 °C ($\dot{\gamma}=0.1s^{-1}$) and inclusion of microbubbles lead to a considerable increase in its viscosity, the extent of which is proportional to

microbubble loading. The variation in viscosity due to introduction of rubber microspheres (particle size < 63 μ) is also included in the inset. Interestingly, introduction of elastomeric microspheres (constant volume fraction ~ 0.4) did not significantly affect the rheological profile, which indicates that these formulations could be processed in the same manner as neat unreinforced foams. The viscosity-shear rate profiles of all the formulations are clearly indicative of the shear thinning nature of the composition.
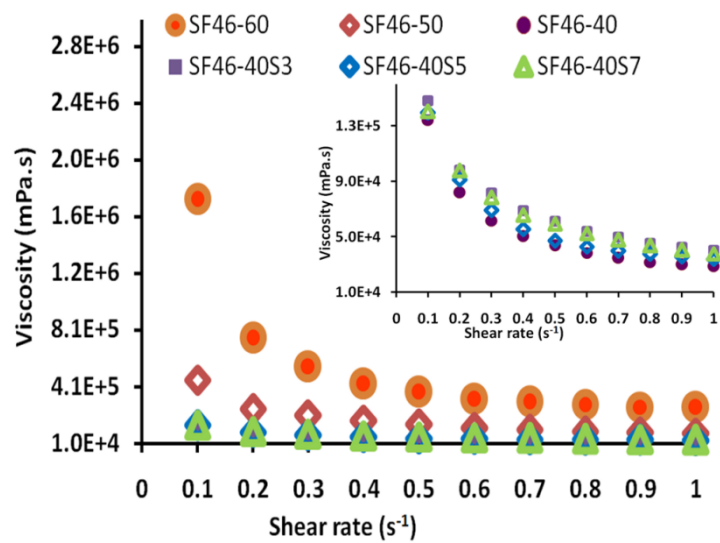
Fig.4.6: *Effect of increasing shear rate on viscosity of hybrid syntactic foam formulations*

4.3.3. Syntactic Foams

Theoretical and experimental densities, along with the voidage associated with each of the sample configuration are presented in **Figure 4.7**. As expected, increasing microbubble loading led to a substantial decrease in the densities, the extent of which was much higher for the lighter microbubbles (K 15, ρ= 150 *kg m^{-3}*) as compared to the denser counterparts (K 46, ρ= 460 *kg m^{-3}*).

In line with the previous studies [8, 28, 58, 76] which use the conventional methods of preparation, involving manual mixing of resin and microbubbles followed by degassing, syntactic foams with voidage ranging from 3.0 ± 0.69 to 6.5 ± 0.56 % were

obtained. Under similar microbubble loading, voidages ranging from 3.9-12.8 % have been reported previously [56]. It can be seen that introduction of poly(dimethylsiloxane) microspheres led to significant decrease in the voidage, which was found to decrease from 6.5 ± 0.5 % (SF15-40) to 1.9 ± 0.43 % (SF15-40S5) and from 3 ± 0.69 % (SF46-40) to 1.5 ± 0.49 % (SF46-40S5) respectively. This can be attributed to the combined effect of the spherical geometry of the PDMS microspheres as well as the preceding ultrasonication step, which reportedly play a major role in removal of air bubbles from the viscous formulations [175, 176]. However, in view of the comparatively higher densities of the siloxane microspheres, the densities of the rubber toughened compositions are relatively higher.
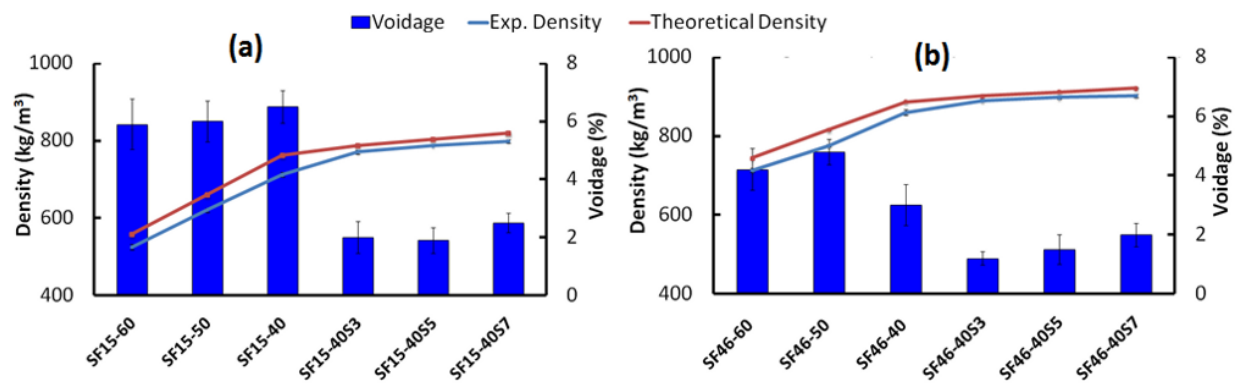
Fig.4.7: *Theoretical and experimental densities and void content (% v/v) of different syntactic foams (a) SF15 (b) SF46*

4.3.3.1. Mechanical Properties of Syntactic Foams

The effect of increasing microbubble content (40-60 % v/v) on the mechanical properties of syntactic foams, both in compressive as well as flexural mode, is presented in **Figure 4.8**. Specific characteristics, in terms of strength per unit weight, are also included for ready reference. The compressive strength of DGEBA epoxy-based syntactic foam, with microbubble loadings 40-60% has been reported to be in the range of 70-100

MPa [56]. In line with previous studies, both the compressive and flexural properties decrease with increasing loading of HGM.

In general, the lower compressive strength of microbubbles (41 MPa, K46 and 2 MPa, K15) in comparison to neat epoxy (138 MPa) is expected to result in a reduction of compressive strength, which is very well evidenced from our studies. For foams prepared at low microbubble loading, the hollow constituents are well embedded within the epoxy resin. During compression, substantial energy is absorbed by the matrix as well as the microbubble-epoxy interface prior to the fracture of microspheres. With increasing microbubble loading, they come in direct contact with each other due to the reduction of resin content, and aggregate at the local scale. This leads to further reduction in the compressive strength. The significant difference in the crushing strength of the microbubbles which in turn results from the difference in the wall thickness, lead to higher compressive strength of syntactic foams containing K46 as compared to K15. The precipitous drop in stress after the end of elastic region indicates that the neat foams fail in a brittle manner. The load–displacement data is used to calculate the flexural strength, strain and flexural toughness, measured by quantifying the area under the curve. As observed in the case of compressive properties, the flexural strength was also found to be inversely proportional to the microbubble loading. It is to be noted that under flexure, failure occurs primarily due to matrix fracture and is less dependent on failure of microbubbles.
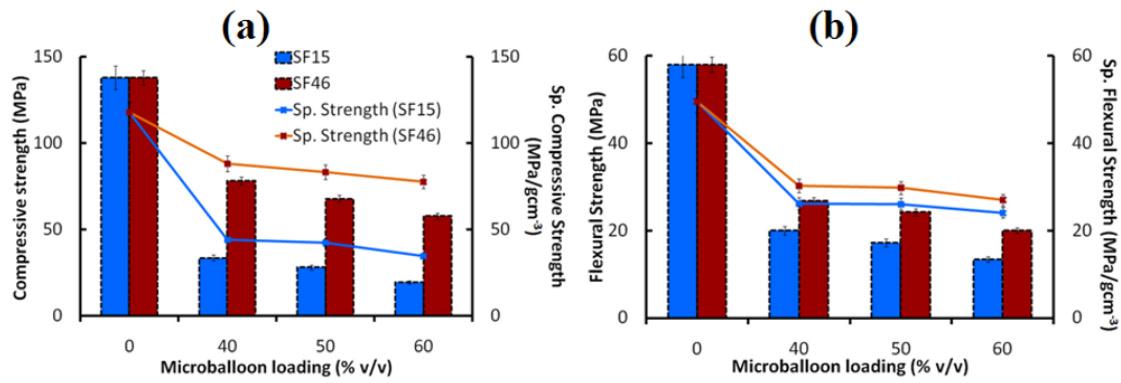
Fig.4.8: *Effect of increasing microbubble content on a) compressive and b) flexural*

properties of neat syntactic foams

4.3.3.2. Polysiloxane Toughened Syntactic Foams: Mechanical Properties

The effect of inclusion of elastomeric microsphere on the mechanical properties of representative epoxy-HGM syntactic formulation (SF 40) for both types of glass microbubbles (K15 and K 46) is presented in (**Figure 4.9 a** and **b**). Of particular interest was to study the effect of particle size of the rubber. It is clear that introduction of microspheres led to a considerable increase in both characteristic flexural properties i.e. flexural strength and strain. The improvement in flexural strength and strain was more pronounced in syntactic foams containing K15 microbubbles, and the extent of improvement was much higher for lower particle sized microspheres. The dimensions of elastomeric preformed fillers are one of the most important parameters, which affect its toughening ability. It has been reported that the preformed rubber particles should be large enough to allow their deformation energy to be higher than their interfacial bonding to the matrix to prevent cavitation. In our previous papers, we have observed that rubbers possessing ~ 100-200 μm are the most efficient impact modifiers, however, in the present case; it was observed that lowering of the dimensions (< 63 μ) led to further improvement. An improvement of 40 % and 78 % in flexural strength and strain

respectively was observed in the case of syntactic foams containing smallest particle size range rubber microspheres (< 63 μ). For the analogous foams containing K46, the observed improvement was ~ 18 % and 25 % in flexural strength and strain respectively. In comparison, the improvement in flexural strength and flexural strain has been reported to be 26 % and 25 % when crumb rubber was added as the toughening agent (40 μ) [77].
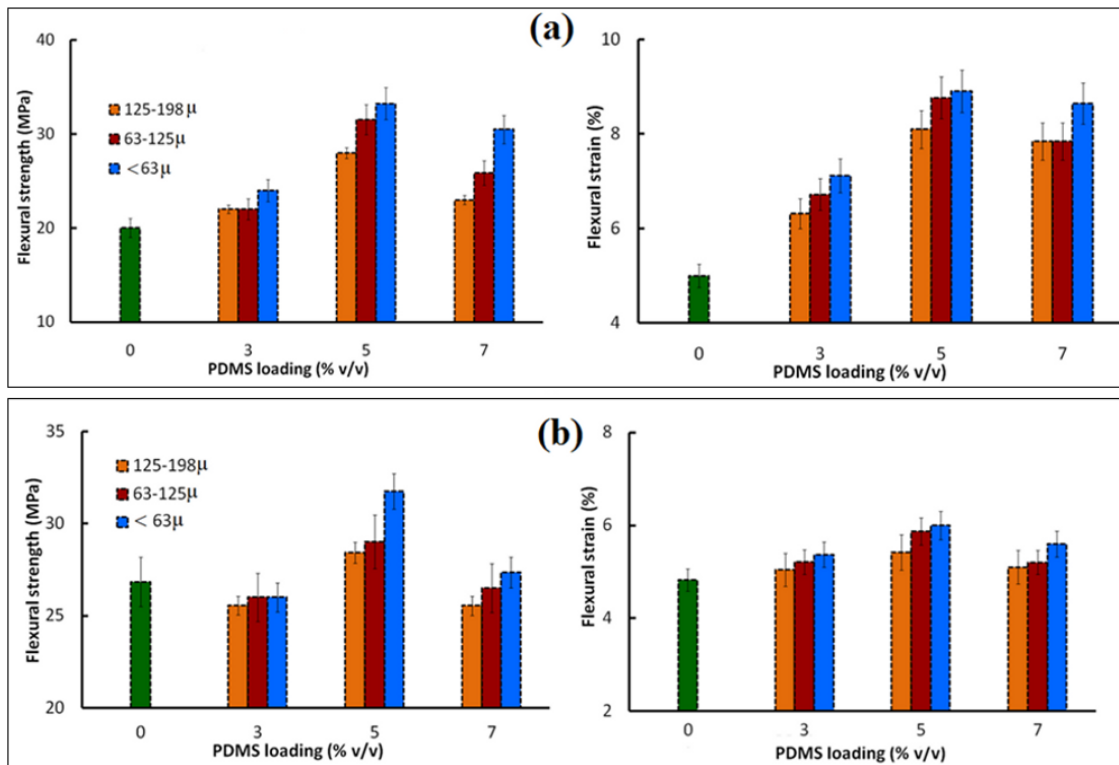
Fig.4.9: Effect of PDMS loading on the flexural properties of (a) SF15-40 (b) SF46-40 foams

The area under the stress-strain curve is indicative of the toughness of the syntactic foam formulation. The same was quantified and the results are presented in **Figure 4.10**. For compositions containing 5 % elastomeric microspheres, ~ 185 % increase in the flexural toughness was evidenced (SF15-40S5). The extent of improvement observed in case of smallest size rubber particle (63 μ) could be attributed to the increased number of rubber particles bridging the crack at the same loading. Our

results indicate that replacement of ~ 5 % microbubbles with equivalent volume of rubber microspheres lead to maximum improvements. Our work is in correlation with the studies carried out by Maharsia et.al. where addition of small sized rubber particles led to improvements in the flexural toughness of the syntactic foams [77].
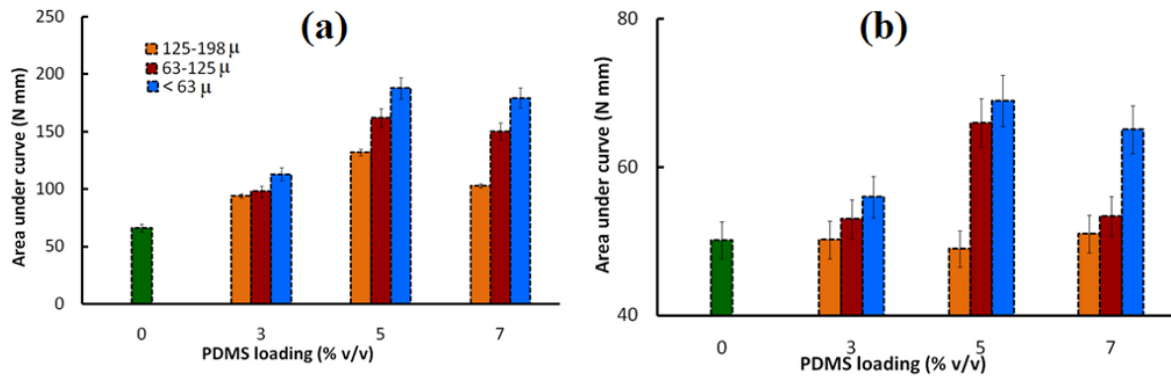
Fig.4.10: *Area under the load displacement curves in flexural mode for PDMS loaded syntactic foams (a) SF15-40 (b) SF46-40*

Mechanical response of syntactic foams under compressive mode has been discussed extensively in the literature. In general, the compression of syntactic foam leads to appearance of three distinct regions in the stress–stain curve. Initially, upon application of load, stress increases linearly with strain: which is indicative of the elastic behaviour of the foam and at the end of this stage, the foam reaches its compressive yield strength. Upon further loading, yielding and a slight decrease in strength can be observed in the second stage, which corresponds to the implosion of the hollow glass microbubbles. Finally, the microbubbles are crushed and compacted, and further application of load only results in the densification of the foam. In the present case, the inclusion of microspheres leads to a slight decrease in the compressive properties (**Figure 4.11-4.12**). This can be explained considering the fact that the compressive properties of the elastomer are relatively inferior as compared to the microbubbles or epoxy. However, the extent of deterioration was less pronounced when microspheres of lower dimensions are present.
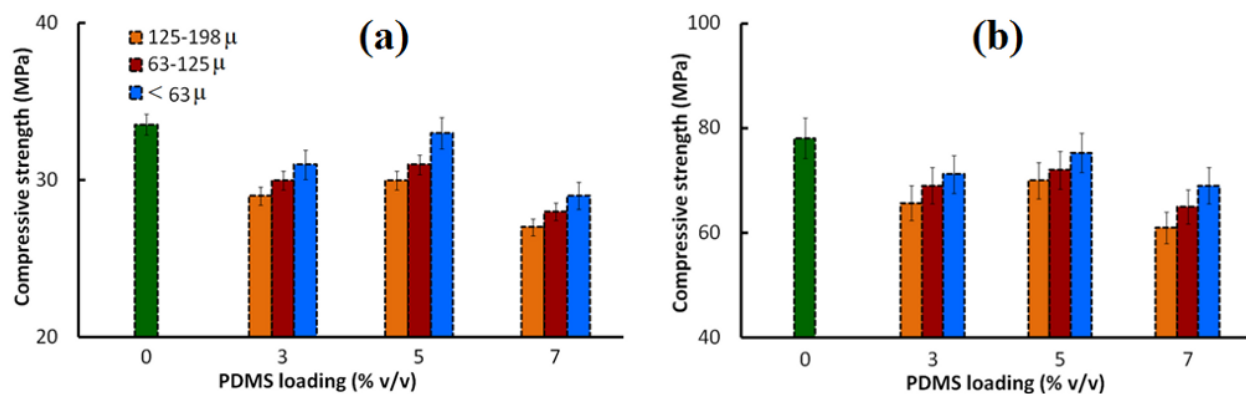
Fig.4.11: Effect of PDMS loading on the compressive strength of hybrid syntactic foam

(a) SF15-40 (b) SF46-40
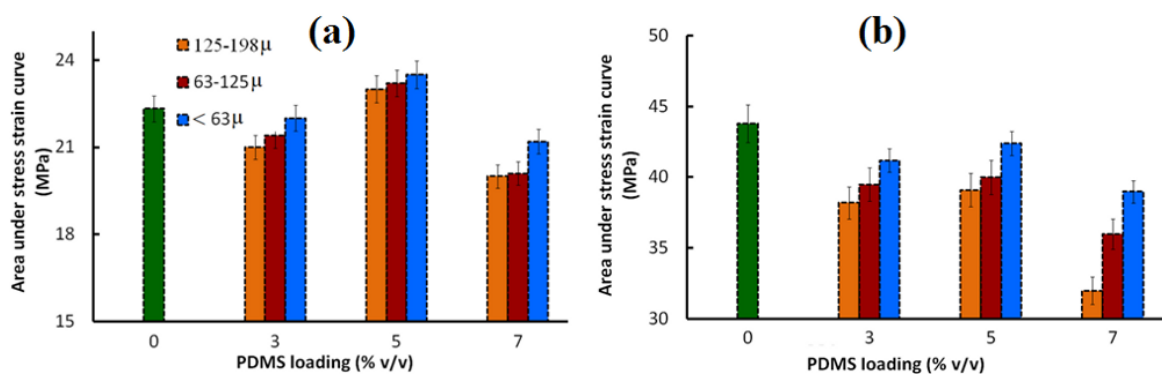
Fig.4.12: Influence of PDMS loading on the compressive toughness of hybrid foam (a)

SF15-40 (b) SF46-40

4.3.4. Thermal Characterization

TG- DTG traces of representative syntactic foam containing K46 and the rubber-toughened hybrids are presented in **Figure 4.13**. The profile associated with the degradation of epoxy was found to remain unaltered, except for the substantial increase in the char content, due to the presence of hollow microbubbles. For syntactic foams with 40 % microbubble loading, a char content of 29 % was observed (at 600 °C), a major fraction (~ 21 %), being the incombustible glass microbubbles.
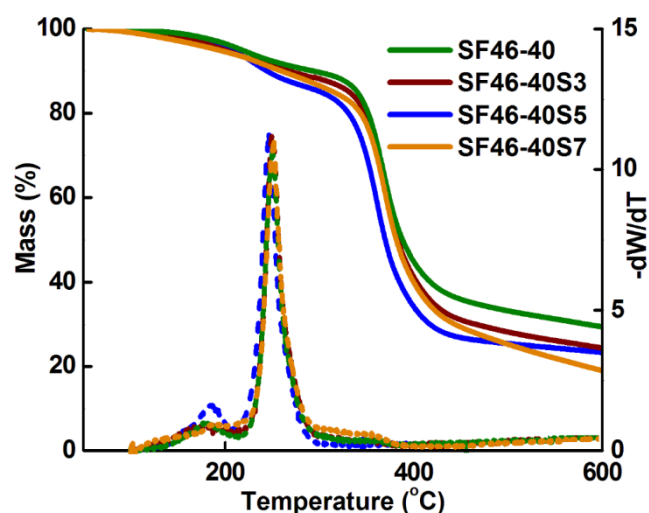
Fig.4.13: *TG/DTG traces of neat syntactic foam and toughened hybrids. Solid lines and dotted lines represent mass % and –dW/dT respectively.*

It is further observed that introduction of elastomeric fillers does not affect the thermal degradation behaviour of the base foam, and all the compositions can be used in service till 100 °C, irrespective of the type of microbubble used. The thermal properties of foams containing K15 present the same trend and are hence not expatiated here.

It is to be noted that durability of syntactic foams is of paramount interest, as these materials are intended for long-term usage. The major components of syntactic foam i.e. cured epoxy and glass, are reportedly inert and are not expected to cause any ecological damage, atleast over short time periods [177, 178]. However, long-term effects of polymers and especially their degradation products has always been a topic of much debate. Cured silicone rubbers are reportedly inert [179] and exhibit low sensitivity to ageing effects. In view of the same, the presence of PDMS microspheres in the toughened syntactic foam compositions is not expected to adversely affect the long-term stability of the syntactic foam or their environmental fate.

Chapter V

Electrospun Nanofiber Reinforced Epoxy Syntactic Foams

Electrospinning

Polyamide nanofibers

Glass Hollow Microballoons

Epoxy

Reinforced syntactic foam

Improved flexural properties
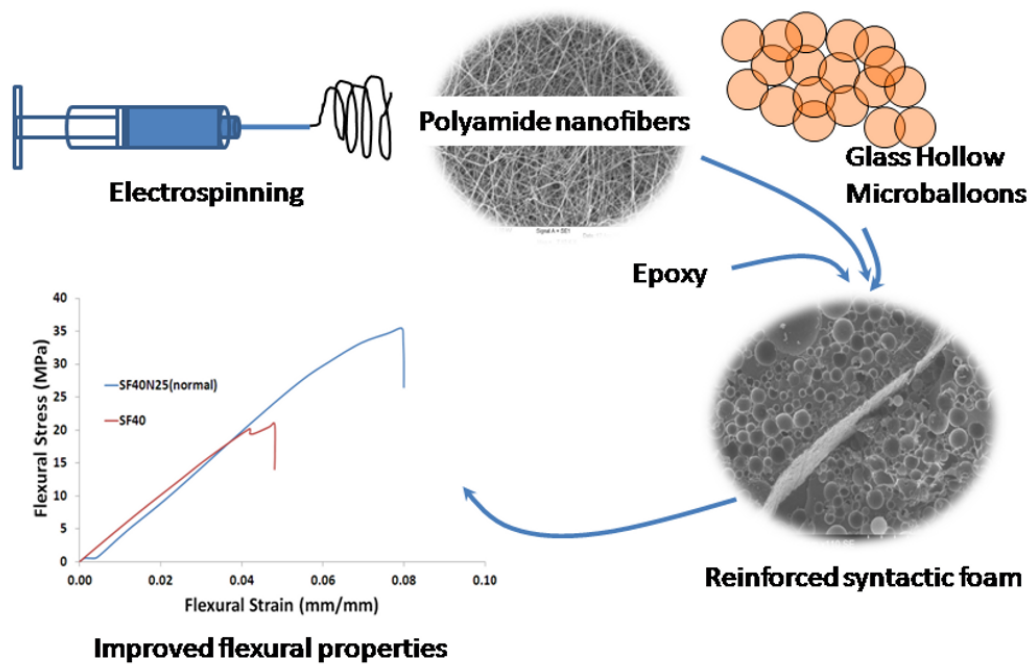
5.1. Introduction

The mechanical properties of syntactic foams are primarily dependent on the type of matrix resin and nature and amount of microbubbles [8]. It is of interest to improve the properties of syntactic foams without adding to their weight. Conventional methods include usage of high strength microbubbles [58]with reduced microbubble loadings [101] however, these lead to an undesirable increase in the density of the resulting foam.

Recent studies have revealed that reinforcing the matrix can lead to significant improvement in mechanical properties of the foamed composite [141], as the presence of an additional phase leads to auxiliary routes of energy absorption. In this context, reinforcing with conventional glass fibers has been attempted. However, this results in considerable microbubble damage while processing, particularly in formulations containing higher loadings. In addition, increasing the amount of fiber leads to agglomeration, which in turn leads to uneven transfer of stress resulting in structural failure of the foams. Alternately, polymeric fibers, particularly aramides have also been explored for their reinforcing ability. Studies suggest an improvement in the compressive strength ranging from 27 % to 34 % on adding Nomex® fibers to epoxy foams. This is associated with a modulus improvement of ~ 45 % under optimal loadings [104].

Nanomaterials are an interesting category of fillers that are employed as reinforcement in syntactic foams. The primary advantage of nanofillers, being there nanoscale dimensions which allow them to exist in the spaces between microbubbles, thereby unaffecting the packing limit. Nanoparticulates like graphene [76, 163], carbon nanotubes [166], nanoclay [77, 168] and carbon nanofibers [51, 66, 141, 167] have been extensively studied as reinforcing fillers for syntactic foams. Moreover, in view of their high surface to volume ratio, they are expected to exhibit good interfacial adhesion with the matrix. Surprisingly, the potential of electrospun nanofibers have not been explored as

reinforcement in syntactic foams till date. Electrospun polymeric nanofibers possess extremely high surface area due to which they are expected to exhibit high interfacial adhesion with the matrix. Intermolecular hydrogen bonding between the amide groups bestow excellent strength to polyamide fibers, which in turn can result in improved mechanical properties of the resulting composites [180, 181]. The present chapter deals with exploring the potential of electrospun nylon 6 nanofiber as reinforcement in syntactic foams. The primary objective of inclusion of nanofiber is to enhance the mechanical properties of epoxy syntactic foams without adding to its weight. The details regarding the preparation and characterization of the nanofiller and its effect on epoxy syntactic foam is presented in the following sections.

5.2. Experimental

5.2.1. Materials

Cycloaliphatic epoxy resin (Ciba Geigy, Araldite CY 230; epoxy equivalent 200 eq g^{-1}), hardener (HY 951; amine content 24 eq kg^{-1}) and Hollow glass microbubbles (HGM, K15, 3M) were used as materials for preparation of syntactic foam. Nylon 6 (Sigma Aldrich) and formic acid (CDH) were used without any further purification. Double distilled water was used throughout the course of study.

5.2.2. Polyamide Electrospinning

Nylon 6 was dissolved in formic acid by stirring, to prepare homogeneous solution of varying concentrations (5–20 % w/v). The solution was loaded into hypodermic syringe, fitted with 20G needle and fed through a pump at varying flow rates (0.1-1 ml h^{-1}) to obtain electrospun fibers. A constant voltage of 2 kV and a collecting distance of 14 cm between the needle tip and the grounded collector platform were maintained throughout the course of electrospinning.

5.2.3. Syntactic Foam Preparation

Hybrid epoxy syntactic foams containing different amounts of glass microbubbles (40, 50 and 60 % v/v) were prepared as per the procedure reported in the literature [141]. In brief, the procedure involved manual mixing of accurately weighed amount of constituents, namely HGM, nanofibers and epoxy followed by curing at room temperature in silicone moulds. The mass of HGM required for the preparation of each formulation was determined as per **Equation 5.1**.

$$\frac{Mass\,of\,HGM}{Mass\,of\,composite} = \frac{\rho_{HGM} \times \Phi_{HGM}}{\rho_{fiber} \times \Phi_{fibre} + \rho_{HGM} \times \Phi_{HGM} + \rho_{matrix} \times \Phi_{matrix}} \dots\dots\dots\dots\dots 5.1$$

Where, ρ_{HGM}, ρ_{fibre} and ρ_{matrix} refer to the density of HGM (0.15 g cc^{-1}), fiber (1.14 g cc^{-1}) and epoxy resin (1.17 g cc^{-1}) respectively and Φ_{HGM}, Φ_{fibre} and Φ_{matrix} refer to the desired volume fraction of HGM , fiber and epoxy resin. Weighed amount of HGM was added to the epoxy resin and the contents were manually mixed and degassed, followed by introduction of stoichiometric amounts of triethylene tetramine hardener (epoxy: hardener :: 100:13). The paste hence obtained was poured in silicone moulds and cured for 48 h at room temperature to prepare specimens for compressive and flexural tests.

For preparation of fiber reinforced foams, the requisite amount of nanofiber was first added to the epoxy resin, ultrasonicated for 30 min, followed by addition of HGM and hardener. The details of the formulations along with the sample designations are listed in **Table 6.1**. In the nomenclature, SF refers to syntactic foams, and the digits represent the volume percent of HGM. For the analogous nanofiber reinforced foams, N refers to Nylon and the subsequent digits represent the volume percent of nanofibers × 100. For e.g. SF40N100 refers to a formulation containing 40 % HGM and 1 % nylon 6 nanofiber.

Table 5.1: Syntactic foam formulations and sample designations

Sample Code	Epoxy (% v/v)	Microbubbles (% v/v)	Fibre (% v/v)
SF40	60	40	-
SF50	50	50	-
SF60	40	60	-
SF40N25	59.75	40	0.25
SF40N100	59	40	1
SF40N200	58	40	2
SF40N400	56	40	4

Fiber arrangement is expected to play an important role in modulating the mechanical properties of foams [79] and hence specimens with sandwich geometry were also prepared. For this purpose, nylon 6 nanofibrous web (0.25 % v/v) was introduced along the horizontal axis as sandwiched layers to result in a layered structure.

5.2.4. Characterization

Thermal characterisation was performed as per the procedure reported in Chapter 2. The degree of crystallinity (χ_c) of the samples was calculated according to **Equation 5.2**, where ΔH_f is the heat of fusion of the sample, and $\Delta H_{f,\,(100\%crystalline)}$ is the heat of fusion for 100 % crystalline nylon 6, which has been reported to be 239 J/g for nylon 6 [182].

$$\%Crystallinity = \frac{\Delta H_{(f,\,observed)}}{\Delta H_{f,\,(100\%crystalline)}} \times 100 \dots\dots\dots\dots\dots5.2$$

The surface morphology of samples was studied using a scanning electron microscope (Zeiss EVO MA15) under an acceleration voltage of 1 kV. Average fiber dimensions and standard deviations were determined by measuring the diameters of about 100 fibers using Image J software.

Theoretical density of syntactic foam (ρ_{th}) was calculated using the standard rule of mixtures (**Equation 5.3**).

$$\rho_{th} = \rho_{fiber} * \Phi_{fibre} + \rho_{HGM} * \Phi_{HGM} + \rho_{matrix} * \Phi_{matrix}...........5.3$$

Where, ρ_i and Φ_i represent density and volume fraction of the ith component, respectively. For calculation purposes, density of Nylon, HGM and matrix has been assumed to be 1.14 g/cc [183], 0.15 g/cc and 1.17 g/cc [184] respectively.

The actual density (ρ_{ex}) of the foam was determined experimentally by averaging the mass: volume ratio of five specimens per sample following ASTM D1622–98 standard. The theoretical and experimental density was used to arrive at the air void porosity trapped in the matrix during fabrication according to **Equation 5.4**:

$$Voidage\ \% = \frac{\rho_{th} - \rho_{ex}}{\rho_{th}} \times 100 ....5.4$$

Mechanical testing under compression mode was carried out in accordance with ASTM C365-94 standard using Universal Testing Machine (International Equipments) at ambient temperature. Standard specimens (25 mm length × 25 mm width × 12.5 mm thickness) were compressed at a rate of 1.3 mm min^{-1}. Five specimens of each configuration were tested and load-displacement data obtained from the tests used to obtain stress-strain curves for calculation of compressive strength and modulus. The area under compression stress-strain curve was determined to quantify the amount of energy absorbed by the foams (**Equation 5.5**) [63].

$$Energy\ absorption = \frac{1}{2}\frac{(\rho_{c} \times \varepsilon_c)}{} + (\rho_{c} \times \varepsilon_{crush})\ ....5.5$$

where ρ_c and ε_{crush} refer to the compression yield strength and crushing strain of the foam respectively.

Flexural testing of the samples was performed under three point bending mode using the same instrument. The sample dimensions and the procedure employed for testing have been detailed in Chapter 2.

5.3. Results and Discussion

5.3.1. Nanofiber Morphology: Effect of Solution Concentration

The SEM images of fibrous mats obtained by electrospinning nylon 6 solutions of varying concentrations (5-20 % w/v) are presented in **Figure 5.1**. The degree of entanglement between the macromolecular chains affect its fiber-forming ability, which in turn influence the morphology of the resulting fibrous mats [185, 186]. Increasing the polymer concentration increases the degree of entanglement between the macromolecules.
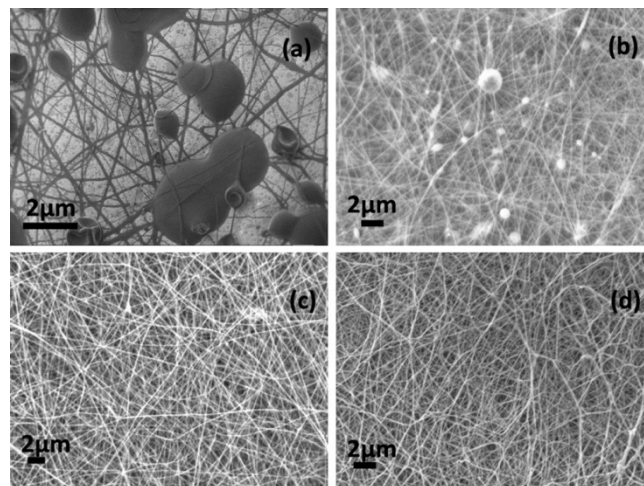
Fig.5.1: *SEM images of electrospun fibers prepared using different concentrations of nylon a) 5 %, b) 10 %, c) 15 % and d) 20 % w/v*

The variation of relative viscosity with increasing concentration is presented in **Figure 5.2**. As can be seen, a noticeable increase in viscosity was evident, when the concentration increases above 15 % w/v. This particular concentration is also referred to as the critical chain overlap concentration, c*, which is the crossover point between the dilute and the semi dilute concentration regimes [186, 187]. At concentrations lower than

c*, smooth nanofibers could not be electrospun, and the SEM images reveal a "beads on string" morphology.
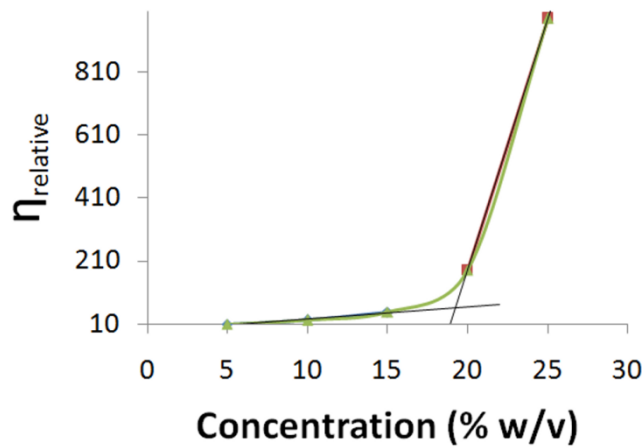
Fig.5.2: Variation of relative viscosity with nylon 6 concentration

At concentration further lower, the applied potential difference during electrospinning process converts the exit stream into droplets, leading to a process commonly known as electrospraying. The same is evidenced through SEM imaging (**Figure 5.3**), where fiber formation is absent.
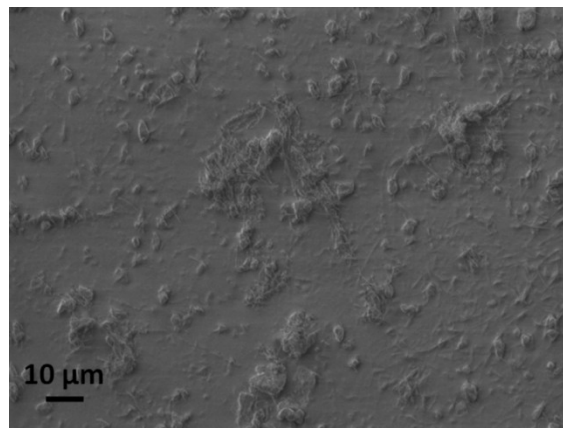
Fig.5.3: SEM image of electrosprayed Nylon 6 (2.5 % w/v, 20 kV, 0.1ml/h)

The effect of flow rate on the fiber size distribution, while maintaining a constant feed concentration of 15 % w/v is presented in **Figure 5.4**. As expected, the average fiber diameter was found to be directly proportional to the flow rate of the solution used for

electrospinning. Nanofibers obtained by nylon 6 electrospinning (15 % w/v, flow rate of 0.1 ml h^{-1}) were used for reinforcing syntactic foams.
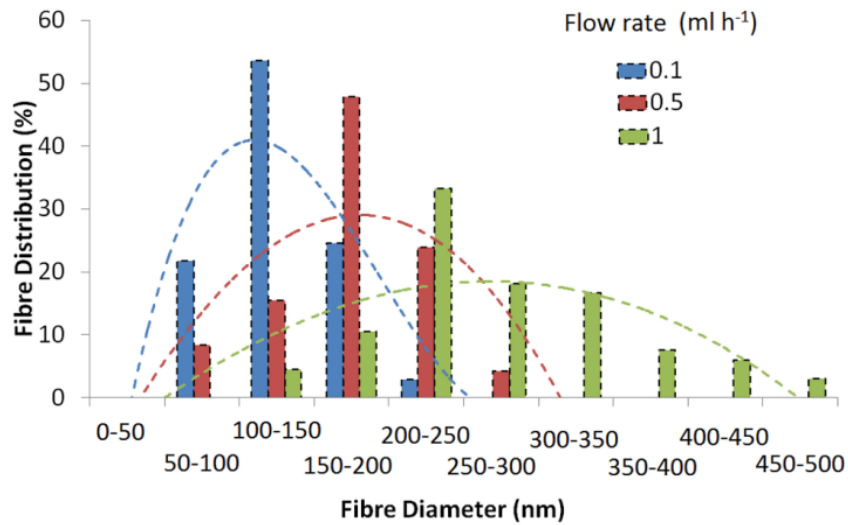
Fig.5.4: *Dependence of fiber size distribution on flow rates*

SEM image of a representative electrospun nanofibrous mat employed for reinforcing syntactic foam is presented in **Figure 5.5**.
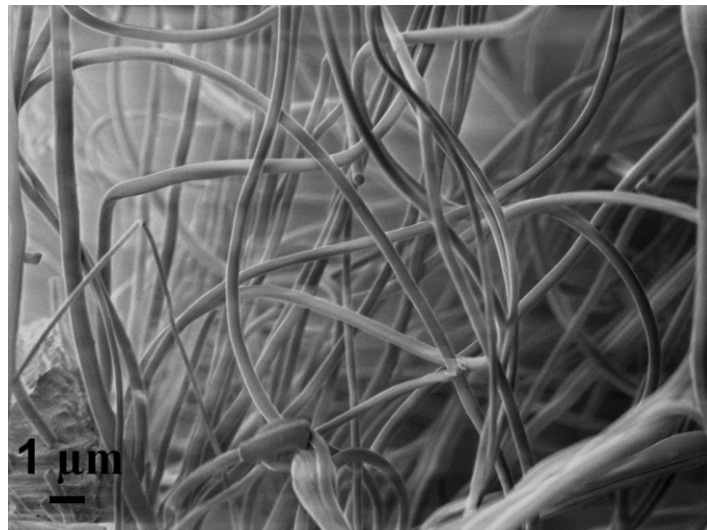
Fig.5.5: *SEM image of nylon 6 nanofiber prepared by electrospinning (15 % w/v, flow rate 0.1ml h^{-1}) used for preparing syntactic foams*

Representative TG-DTG and DSC traces of electrospun nylon 6 nanofibers (concentration 15% w/v, feed rate= 0.1 ml h^{-1}) are presented in **Figure 5.6**. Notably, varying the feed rate and solution concentration did not affect the thermal behaviour appreciably, with the samples exhibiting a melting point of 226 °C and an average crystallinity of ~ 29 %. Single step degradation was observed in the TG trace of nylon 6, with the maximum degradation temperature of ~ 429 °C. and a char content of 10 % at 650 °C.

(a)   **(b)**
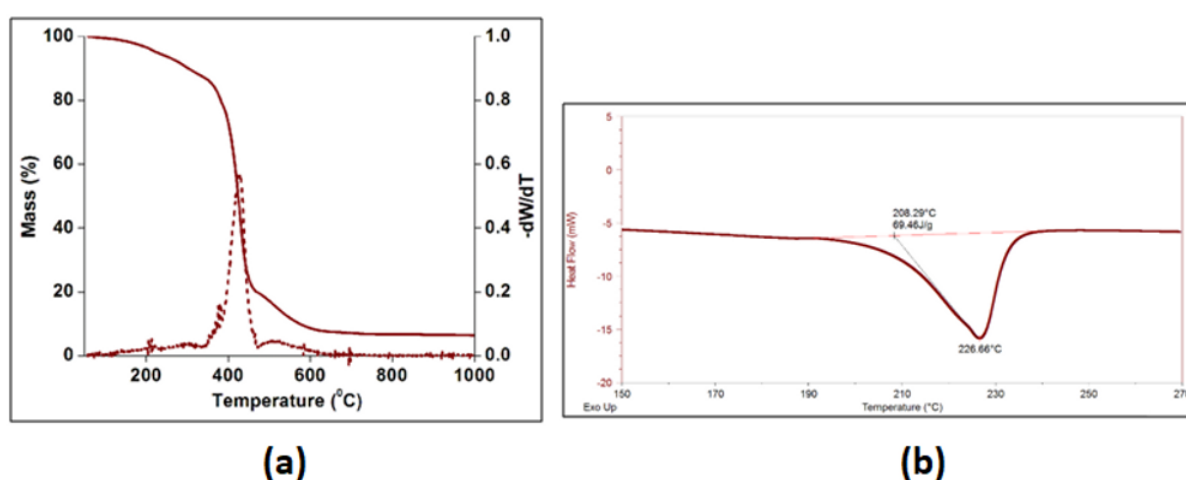
Fig.5.6: (a) TG-DTG (dashed lines represent DTG) (b) DSC traces of nylon 6 fibres

5.3.2. Syntactic Foams

Experimental and theoretical density of the syntactic foams along with the voidage associated with the different compositions prepared is presented in **Table 5.2**. As expected, increase in micro-bubble loading led to a decrease in the density of the samples, however the voidage was rather high (> 4 %). Interestingly, introduction of nanofibers led to a slight decrease in the voidage, which could be attributed to the ability of these nanofibers to exist in the air-gaps formed during processing.

Table 5.2: *Experimental and theoretical density of neat and fiber reinforced syntactic*

foam

Sample Code	Experimental Density (kg/m³)	Theoretical Density (kg/m³)	Voids (Vol %)
SF40	722	762	5.2
SF50	619 ± 7	660	6.2
SF60	534 ± 5	558	4.3
SF40N25	743 ±4	761.9	2.4
SF40N100	740 ±6	761.7	2.8
SF40N200	739 ±6	761.4	2.9
SF40N400	741 ±3	760.8	2.6

5.3.2.1. Mechanical Properties of Syntactic Foams

The effect of increasing microbubble content (40-60 % v/v) on characteristic compressive mechanical properties of syntactic foams is presented in **Figure 5.7 a**. Representative stress-strain curves obtained during testing are also included (**Figure 5.7 b**). The crushing strength of K15 is reportedly 300 psi, which is much lower than the compressive strength of cycloaliphatic epoxy used for the present investigation [126, 188]. As expected, the compressive yield strength and modulus followed a decreasing trend with increasing volume percent of HGM, a feature which can be attributed to the increasing unavailability of the matrix to bind the cenospheres, especially at high loadings. At high microbubble loading, the failure results from the structural collapse whereas at lower microbubble loading, the polymer properties become more important and larger number of spheres rupture before the entire structure collapses [189].
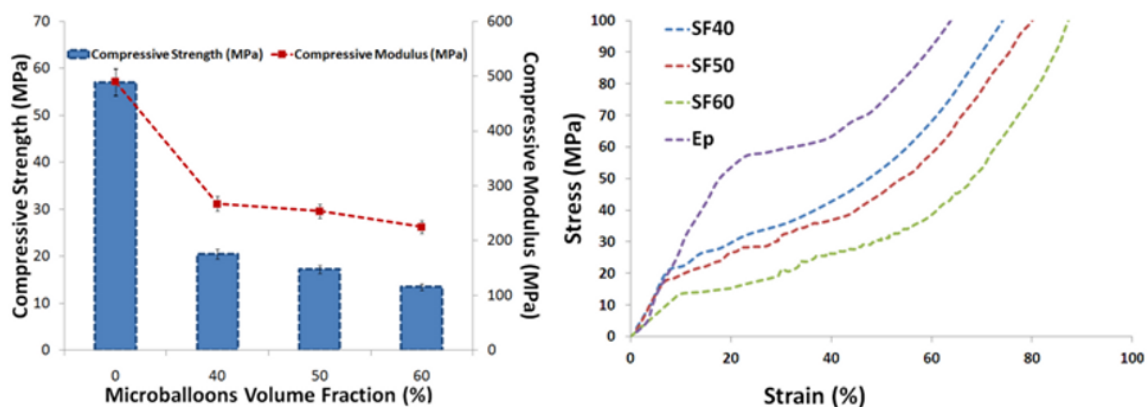
Fig.5.7: Effect of increasing microbubble content on the mechanical properties of syntactic foams a) compressive strength and modulus. b) Representative stress-strain curves

It is to be noted that the decrease in compressive strength was accompanied by a concomitant decrease in the density of the foam (**Table 5.2**), which in turn resulted in similar specific compressive strength (27.1 ± 1.3 MPa cm^3 g^{-1}) and modulus (415 ± 20 MPa cm^3 g^{-1}) (**Figure 5.8**). SF40 was chosen as a representative system on which the effect of nanofiber addition was studied in detail.
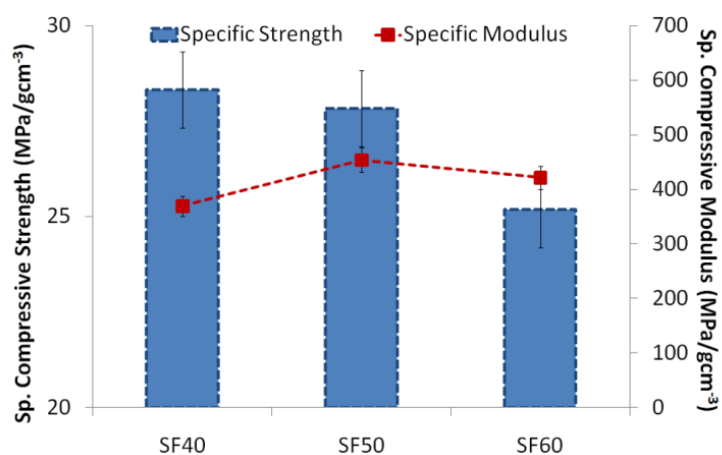
Fig.5.8: Comparison of specific compressive strengths and modulus of neat syntactic foams

121

5.3.2.2. Nanofiber reinforced Syntactic Foams

The microstructure of representative syntactic foams, prepared both in the absence as well as presence of nanofibers is presented in **Figure 5.9**. Glass microbubbles can be clearly seen as spherical particles embedded in the polymer matrix, and the existence of air gaps is also evident. Reinforcement with nanofibrous mat is evident in the form of a layer in the sandwiched samples.
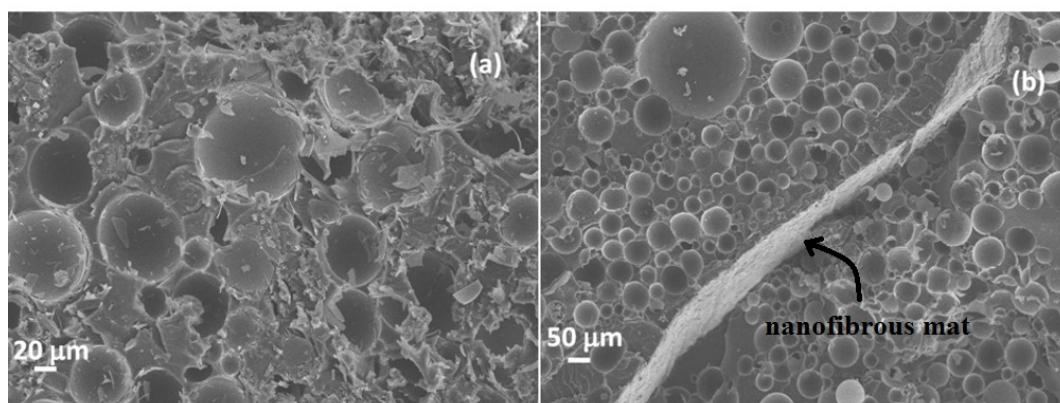
Fig.5.9: *SEM images of (a) neat and (b) nanofiber reinforced foam*

TG-DTG traces of syntactic foams are presented in **Figure 5.10**. As expected, increasing the glass bubble content led to an increase in the char content of neat epoxy (EP), however the characteristic decomposition temperature remained largely unaffected. For the sake of brevity, the traces of nanofiber reinforced foams have not been included, as their degradation behaviour is similar to that of unreinforced foams, an observation attributable to the small amount of fiber added.
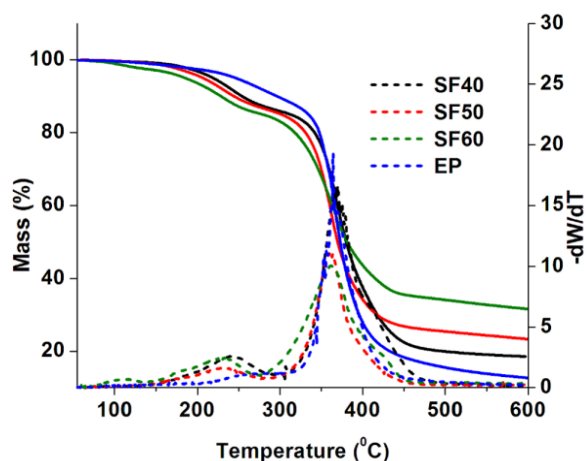
Fig.5.10: *TG-DTG traces of neat syntactic foams (dotted lines represent DTG)*

5.3.2.2.1. Random Dispersion

The effect of increasing fiber content on the compressive properties of SF40 foam is presented in **Figure 5.11**. It can be seen that except for marginal improvement at low loadings (< 1 %), the reinforcing effect is rather negligible, and the mechanical properties decreased upon further loading. Our results are in correlation with previous studies, where addition of fibers has been reported to lead to negligible enhancement in the compressive properties of syntactic foams [51, 66, 76]. Dimchev et al. reported that introduction of carbon nanofibers (0.25 % v/v) led to a reduction in the compressive modulus of the syntactic foam, however the compressive strength remained largely unaffected [51]. In another study, the flexural strength was found to increase by ~196 % upon addition of carbon nanofibers (1.5 % v/v) to phenolic matrix containing hollow carbon microspheres [66]. In syntactic foams containing thicker walled cenospheres, introduction of CNFs (1% w/w) has been reported to lead to ~ 7.3 % in compression strength [90]. Analogously , introduction of inorganic nanoclay (2 % w/w) to epoxy/K15 syntactic foam was found to enhance the flexural properties substantially (42%) [75]. In a separate study, addition of cloisite 30 B (5 % w/w) reportedly increased the flexural strength by ~16% [74] in epoxy K37 syntactic foam.

It has been reported that stress is concentrated on the wall of the microbubbles, when the shell thickness is less, whereas increasing the wall thickness results in shifting the location of maximum stress to the fiber [65]. Under compressive loadings, the failure of the syntactic foam occurs as a result of crushing of the microbubbles [66] where the role played by the matrix and fibers is rather secondary. The subsequent decrease in the properties at higher fiber loadings is attributed to agglomeration of the nanofibers which tend to act as stress concentrating loci.
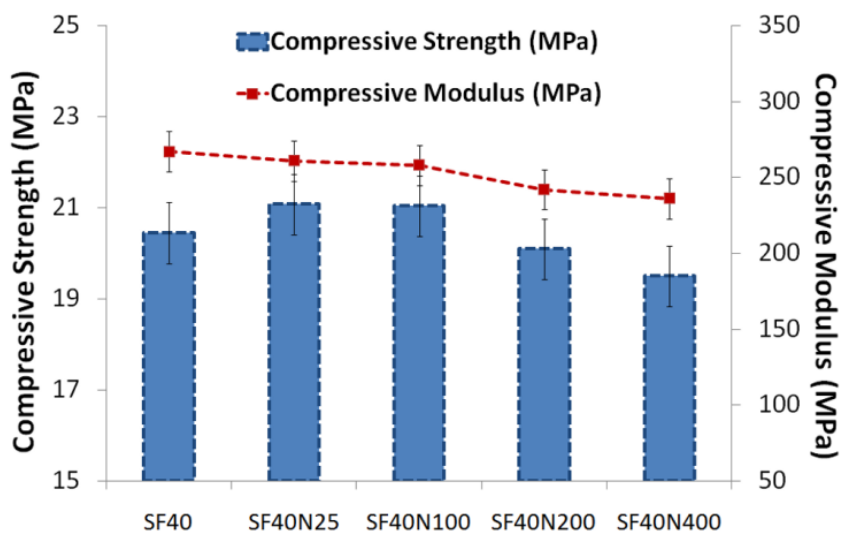
Fig.5.11: Comparison of neat and nanofiber foams under compression

5.3.2.2.2. Oriented Dispersion

To understand the effect of fiber arrangement on the mechanical properties of reinforced syntactic foams, nanofibers were placed layer by layer to arrive at a sandwich geometry, which were subsequently subjected to compressive loadings, both perpendicular and parallel to the direction of fiber axis, as shown in **Figure 5.12**.
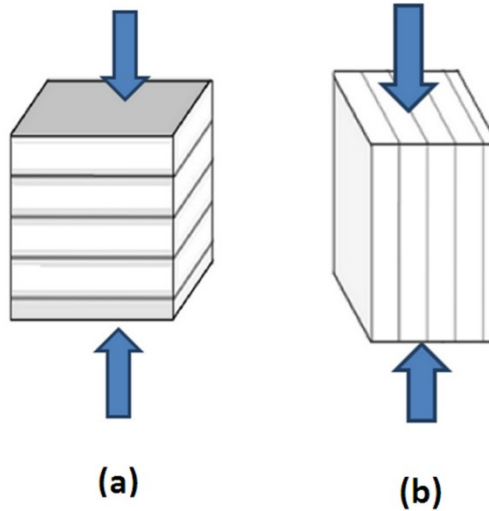
Fig.5.12: *Pictorial representation of layered nanofiber reinforced syntactic foam specimens. Arrows indicate the loading direction and lines indicate the fiber orientation.*

Representative stress strain curves of nanofiber reinforced foams and the characteristic properties are presented in **Figure 5.13 (a-b)**. Our studies reveal that the reinforced syntactic foams exhibited enhanced properties, as quantified in terms of the yield strength and modulus, when the loading direction was perpendicular to the fiber axis. This can be ascribed to the ability of nanofibrous film to distribute the stress homogenously. Interestingly, the samples failed catastrophically when tested in parallel mode, an observation attributable to the delamination of the plie.
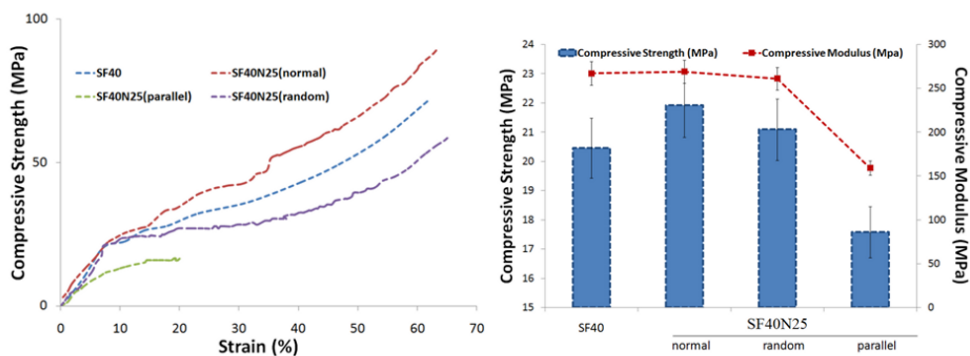
Fig.5.13: (a): *Compressive properties of SF40N25 at different orientations of nylon 6 a) representative stress strain plots (b) Compressive yield strength and modulus.*

Digital images showing the appearance of the samples post compressive testing are presented in **Figure 5.14.** Our results are in non-compliance with the results reported previously [79], where the compressive strength have been reported to improve by a factor of 2 when load was applied parallel to the chopped fiber orientation. This is ascribable to the difference in dimensions of the fibers, which were comparatively much larger and of much smaller aspect ratio than used in the present investigation. Here, the nanofibers existed in the form of mats, where the possibility of debonding is increased.
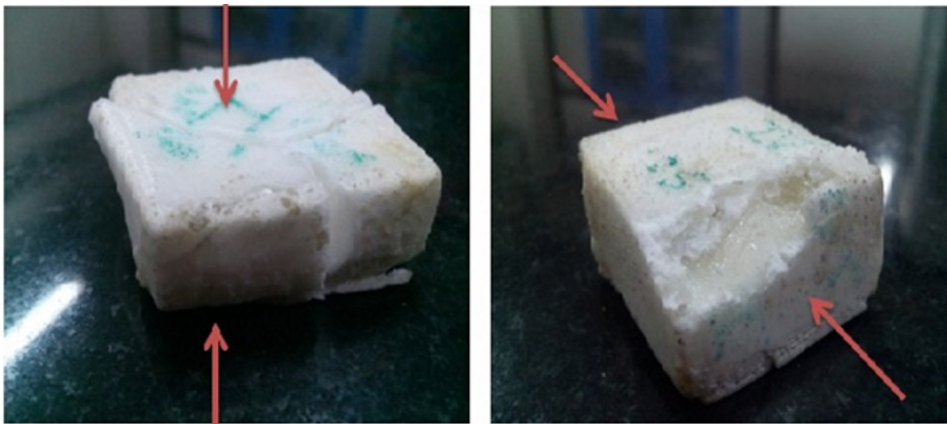
Fig.5.14: *Digital photographs of compression tested sandwich specimens (a) perpendicular, (b) parallel (arrows indicate direction of loading)*

5.3.2.3. Energy Absorption

Area under the stress-strain curve, which is indicative of the inherent energy absorption ability of the foams, was quantified, and the results are presented in **Figure 5.15**. It is clear from **Equation 5.5** that the toughness of these systems depends primarily on the crushing strain (ε_c) of the microbubbles and enhances with increasing length of the plateau region associated with HGM crushing. It is interesting to note the effect of fiber orientation on the energy absorption capability of the samples. It can be seen that on application of load perpendicular to the plane of fiber, the plies were capable of absorbing larger amount of energy. However, the toughness decreased, when the fibers were dispersed randomly. When the loading direction was parallel to the plane of the fibers,

debonding occurred at the fiber-foam interface, thereby leading to specimen failure at relatively low strains, in turn leading to reduced toughness.
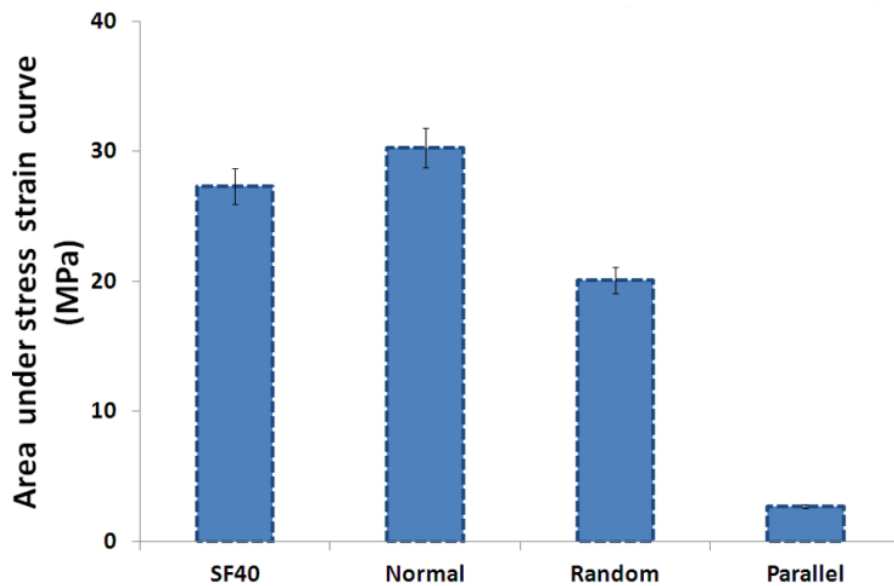
Fig.5.15: Influence of fiber arrangement on the toughness of SF40N25

5.3.2.4. Flexural Testing

The effect of adding nanofibers on the flexural properties of syntactic foams was studied, and the improvement in terms of flexural strength and strain was quantified. Representative stress strain curves are presented in **Figure 5.16**, where the behaviour of neat syntactic foam has been compared with reinforced foams, where the load was applied normal to the fiber axis. The brittle behaviour of syntactic foams is evident under flexural loadings. Unlike compressive properties, there is a significant enhancement in the flexural strength and strain of SF40N25 by 75 % and 62 % respectively in comparison to neat foam, when the load is applied perpendicular to the fiber axis. It appears that the presence of electrospun nanofibrous mats forces the crack front to bow out and arrest the growth of the propagating crack thereby leading to the observed improvement in the flexural properties. There was no improvement, when the fibers were randomly dispersed or placed parallel to the loading direction. It is worth mentioning that microspheres are not

127

the primary load bearing phase under flexural loading, and the failure is dominated by matrix fracture, an observation dissimilar to the conditions under compressive loading.
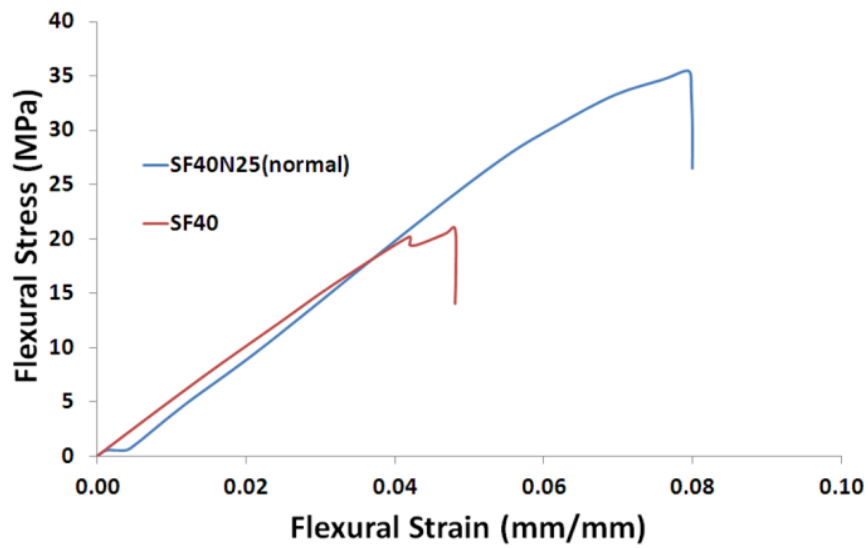
Fig.5.16: Flexural stress-strain plots of neat and fiber reinforced foam

The difference in the failure mechanism is also evident from the SEM images of the samples captured post testing (**Figure 5.17**). Microbubble debonding is evident in the images captured under flexural mode, a feature which could not be observed in compression tested sample. Similar improvement in flexural properties upon introduction of nanofillers have also been reported previously [75].
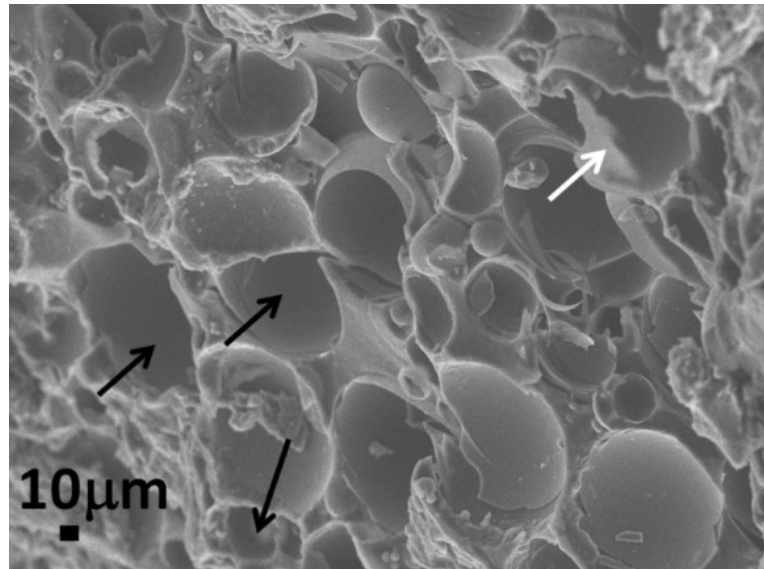
Fig.5.17: SEM micrographs of fracture surface of neat syntactic foam after flexural test (black and white arrows depict microsphere debonding and broken microbubbles respectively)

It is to be noted that in view of the difference in the dimensions of nanofibers and glass microbubbles, it is practically impossible to view them under similar magnifications. SEM imaging was performed on flexure failed specimen and a representative image is presented in **Figure 5.18**. As expected, the extent of damage/crushing to the microbubbles in flexural mode is relatively lesser than what was observed in compression tested samples. The nanofibrous film remained largely undamaged with the individual fibers being observed only under higher magnification (**Figure 5.18, inset**).
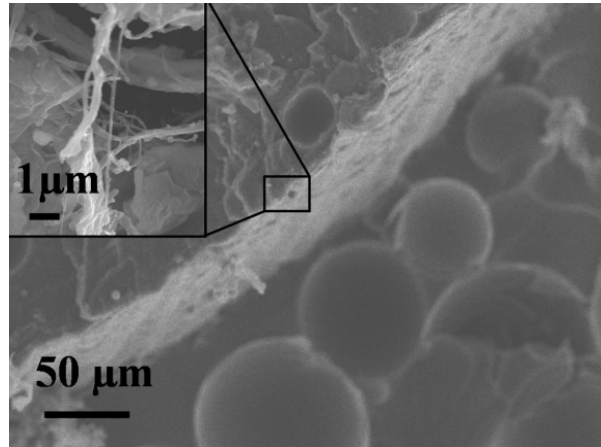
Fig.5.18: Flexural failed nanofiber reinforced syntactic foams. Inset shows nylon 6 nanofibers at high magnification

Syntactic foams are gaining considerable importance as core materials in sandwich composites with potential applications in the field of transportation and packaging, where flexural properties play a decisive role. The polyamide nanofiber reinforced syntactic foams developed in the present work appear to be a better candidate than most other conventionally used core materials in view of their enhanced specific flexural properties. It is to be noted that depending upon the nature and type of nanomaterial, the extent of reinforcement on the mechanical properties of the foam can vary. In addition, the mechanical properties of syntactic foams prepared using thicker walled glass microbubbles may vary substantially as the same do not scale proportionately with particle wall thickness [190].

Chapter VI

Epoxy-Epoxy Microbubble Syntactic Foams
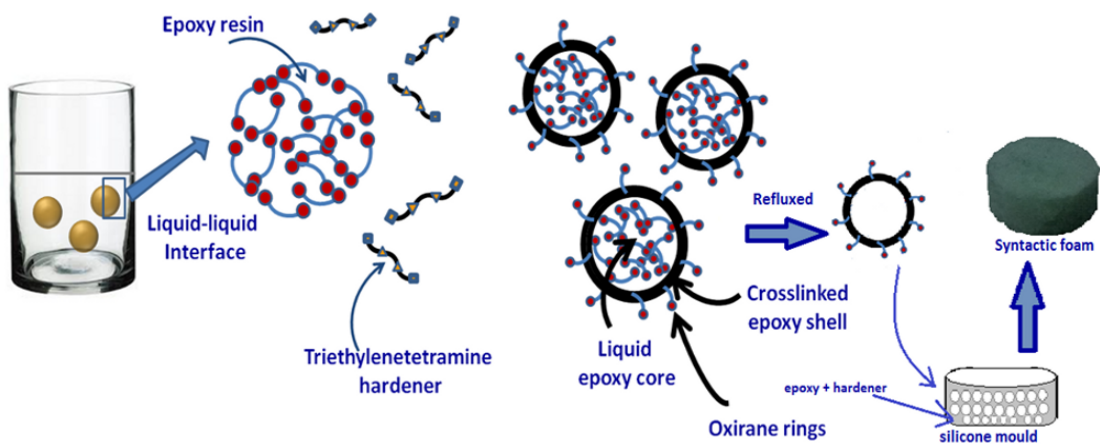
6.1. Introduction

In the last few years, polymeric microspheres have carved out their own niche application depending on their internal morphology i.e. hollow, encapsulating or solid. The former two find extensive usage in the field of buoyant syntactic foams [27] and self healing coatings [191, 192], while the latter hold potential in biomedical sciences [193], particularly targeted drug delivery [194]. In view of this, several polymeric microcapsules [31, 195, 196] based systems have been reported such as those based on epoxy [197, 198], PDMS [88], polystyrene [199], poly(urea-formaldehyde) [200], melamine formaldehyde [201], polyurethanes [202] and PMMA [23]. Some of the common techniques to prepare such microcapsules include self assembly, templating, etc. [203]. In-situ emulsion polymerisation and physical encapsulation are alternative techniques to prepare filled microcapsules [204-206]. The microsphere dimensions and core content can be tailored by altering the operating parameters, particularly stirring speed and solution concentration [204, 207].

The constituent hollow microbubbles used for the preparation of syntactic foams are either of polymer, metal or glass. Glass microbubbles are a common choice for preparing such foams due to the fact that they are available in varying densities which can give rise to a multitude of foams varying widely in their mechanical properties. However, such microbubbles are found to have a poor interfacial interaction with most of the polymer matrices. Besides it has been mentioned in the literature that inclusion of glass microbubbles restricts their usage to not more that ~ 64 % [208] in case of random close packing of spheres which inhibit the manufacturing of low density foams.

To overcome such limitations; polymer microbubbles are currently being explored. Thermoplastic polymers are commonly used for preparing such microbubbles. These microbubbles are malleable and expand upon heating due to the expansion of the blowing

agent incorporated within them. This allows high level of microbubble loading, leading to considerably low density and high compressive strength. Recent work on thermoplastic microbubbles in epoxy matrix syntactic foams achieved a volume fraction of 95 % at low density of 0.067 g cm^{-3} [31]. In principal, there are three methods of obtaining hollow polymer microbubbles:

- Drop or spray tower method

- Microencapsulation technique

- Interfacial engineering technique

6.1.1. Drop or Spray Tower Method

In the drop or spray tower method, a liquid-phase bubble is generated at the top of a vertical column, which is subsequently passed through a heated zone to eliminate the solvent. The resulting solid polymer shell is obtained at the bottom of the tower in a water bath [209].

6.1.2. Microencapsulation Technique

In the microencapsulation process, liquid is first encapsulated in a polymer solution, and the solvent is subsequently driven off to result in a polymeric shell. A schematic of the process is depicted in **Figure 6.1**. The shell wall polymer is first dissolved in a low boiling-point, high-vapour-pressure solvent that is immiscible in water. Under continuous stirring, an aqueous phase containing approximately required amount of surfactant is emulsified in the polymer solution. The resulting emulsion is a continuous polymer (oil) phase with water droplets uniformly distributed throughout. After requisite agitation, the droplet size is relatively uniform with an average diameter that is a function of the speed of agitation. The emulsion is then poured into the other aqueous phase containing surfactant. The result is a suspension in the second water phase of small polymer "bubbles" containing the first water phase. This solution is heated to drive off the

132

solvent, leaving polymer shells containing the first water phase. Finally, the shells are collected by sieving and gently heated to remove the water trapped within. Controlled removal of the entrapped water is very important if the microbubbles are to survive, as rapid drying tends to cause stress in the bubbles and produces small surface cracks. This effect has been observed in microbubbles with wall thicknesses less than 10 pm for removal temperatures greater than 50 °C.
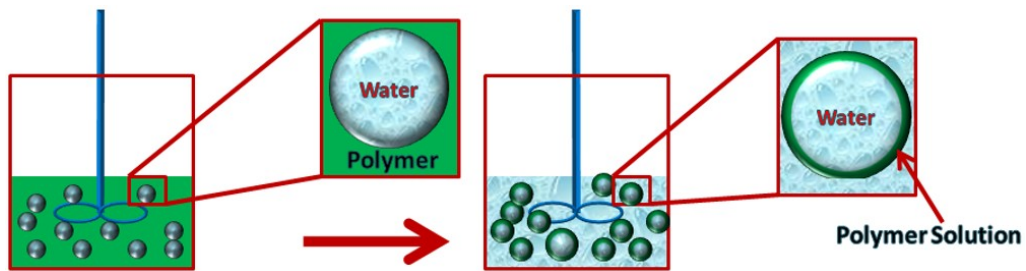
Fig.6.1: *Microencapsulation process for preparing polymer microbubbles*

6.1.3. Interfacial Engineering

The potential of interfacial reactions, which occur at or near the interfacial boundary of two immiscible solutions, towards the preparation of nano-crystals, thin films and polymers has been extensively studied in the past [210-212]. We hypothesize that this concept can be extended to prepare epoxy microcapsules by manipulating the reaction between the resin and hardener to take place preferentially at an interface, which in turn can be achieved by ordering the sequence of the reactants. Furthermore, by adjusting the resin : hardener ratio it should be possible to alter the thickness of microbubble shell wall. The encapsulated epoxy can be extracted in a suitable solvent to prepare hollow microbubbles with crosslinked epoxy as the shell wall. The same is achieved by suspending epoxy droplets in a suitable medium, followed by sequential addition of the hardener in non-stoichiometric amounts. Polydimethylsilicone (PDMS) was chosen as the reaction medium in view of its exceptional thermal stability and solubility differences [213]. The effect of operating parameters, particularly rate of stirring and resin: hardener

ratio on the microcapsule dimensions was also be studied. By varying, the resin: hardener ratio, it is possible to tune the core content of the microcapsules. Interfacial polymerization belongs to a sub-class of step-growth polymerization in which the reaction occurs at the water-oil interface, i.e. between an aqueous solution containing one of the reactants and another organic solution containing the second monomer. The primary advantage of this technique in the context of preparation of syntactic foams is the tailorability of obtaining varied radius ratio and particle dimensions by tuning the experimental parameters i.e. resin-hardener ratio and stirring speed respectively. Further refluxing of the microcapsules leads to the formation of hollow crosslinked epoxy shell microbubbles (**Figure 6.2**).
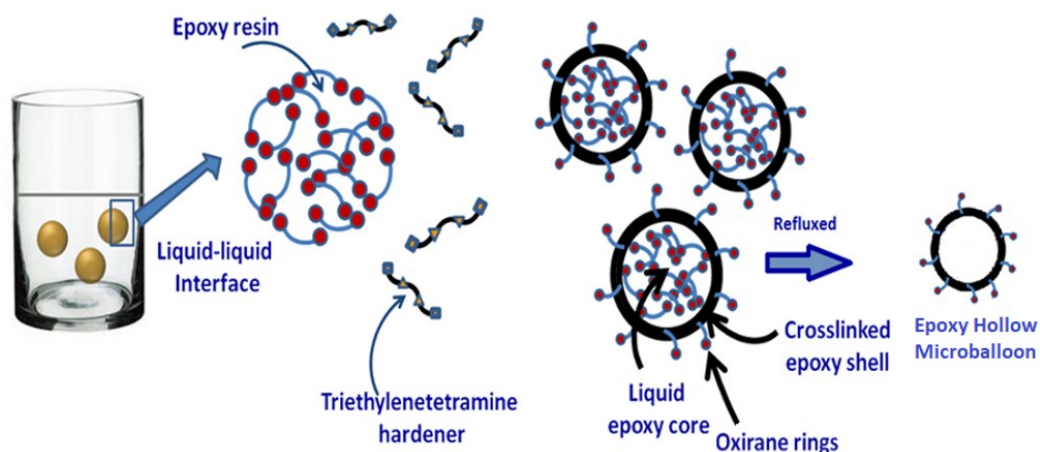
Fig.6.2: Preparation of epoxy microbubbles by interfacial engineering

In this chapter, we attempt to combine the concepts of suspension curing and interfacial engineering towards preparation of crosslinked epoxy microcapsules encapsulating liquid epoxy resin in the core. The potential of these preformed microbubbles, as hollow fillers, has also been studied for preparing epoxy based syntactic foams at various loadings (40-60 % v/v) of the filler. The same has been reported in different sub-sections of this chapter.

6.2. Experimental

6.2.1. Materials

Epoxy resin (Ciba Geigy, Araldite CY 230; epoxy equivalent 200 eq g^{-1}) and hardener (HY 951; amine content 24 eq kg^{-1}) was used as received. Double distilled water was used throughout the course of study. Polydimethyl silicone oil (CDH, kinematic viscosity 300 cS) was used without any further purification.

6.2.2. Characterization

Structural (FTIR) thermal (TGA and DSC) and morphological (SEM) characterization was performed as per the procedure reported in previous chapters. Average microcapsule dimensions and standard deviations were determined by measuring the diameters of about 100 microcapsules using ImageJ software. Mechanical testing of the samples was carried out by universal testing machine as per the procedures discussed earlier.

6.2.3. Interfacial Polymerization

The immiscibility of triethylenetetramine in silicone oil was substantiated by capturing the optical images of the suspensions prepared by stirring vigorously for 5 min (1000 rpm) using a computer interfaced microscope (Magnification 40 ×). Subsequently, crosslinked epoxy microcapsules filled with epoxy were prepared by interfacial polymerization of TETA hardener with epoxy resin with the former being added in less amounts, while keeping them suspended in silicone oil. The reaction was carried out under varying temperatures (50-75 °C), stirring speeds (400- 600 rpm) and varying resin: hardener ratio (100:1-100:13).

6.2.4. Microencapsulation of Epoxy

Crosslinked epoxy microcapsules were prepared by the interfacial reaction of silicone suspended epoxy resin with amine hardener under varying stirring speeds (400-

600 rpm) and varying resin: hardener ratio (100:1 -100:13). Liquid epoxy resin (10 g) was initially suspended in 200 ml PDMS. The temperature was slowly increased to 70 °C, followed by introduction of hardener through a hypodermic syringe (1 – 13 %). The reaction was allowed to proceed for 24h, following which the reaction medium was cooled and the resultant solid microcapsules were filtered, washed extensively and dried. The encapsulated epoxy within the free flowing microcapsules could be extracted by refluxing in toluene. The difference in the mass resulting due to extraction, as estimated gravimetrically, was used as an index for quantification of core content. Epoxy content of the neat resin and microspheres was quantified as per the standard procedure. In brief, a known amount of sample (~ 0.5 g) was refluxed with 25 ml of pyridine hydrochloride solution and the contents, post-cooling, were titrated against standard potassium hydroxide solution [214]. The microcapsules were refluxed in toluene and dried to obtain hollow microcapsules. The microcapsules were sieved to obtain a particle size range of 90-100 μm for inclusion in epoxy syntactic foams. A schematic of the entire procedure is presented in **Figure 6.3**.
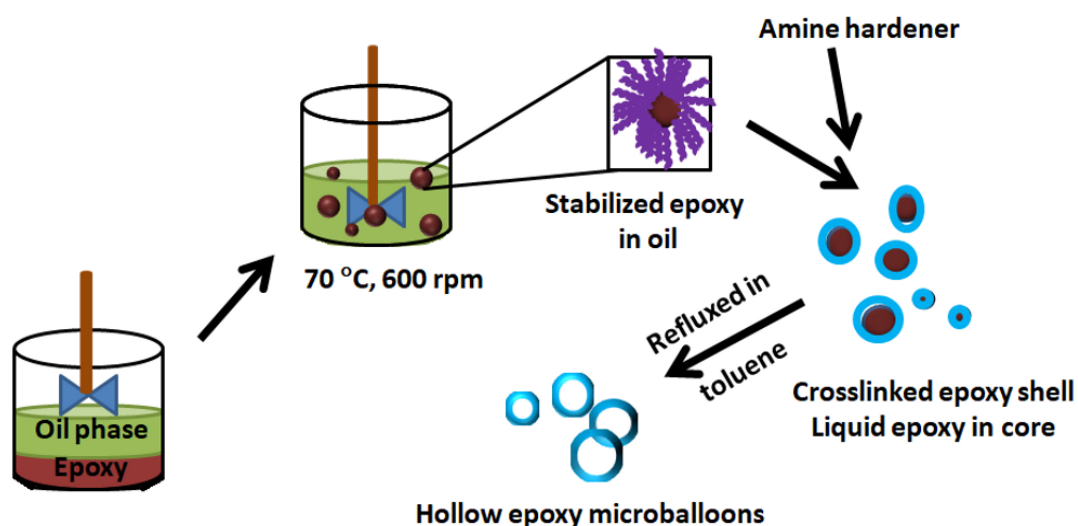
Fig. 6.3: Representative schematic of the encapsulation process

6.2.5. Preparation of Epoxy Syntactic Foams containing Epoxy Microbubbles

Requisite amount of epoxy microcapsules (40-60 % v/v) was added in the epoxy matrix and the contents were manually mixed and degassed followed by introduction of calculated amounts of amine based hardener. The slurry hence obtained was transferred to silicone moulds and cured for 48 hours at room temperature to prepare specimens for compressive testing. The amount of filler, i.e. epoxy microspheres was calculated as per the formula (**Equation 6.1**):

$$\frac{Mass\ of\ microspheres}{Mass\ of\ composite} = \frac{\rho_{microsphere} \times \Phi_{microspheres}}{\rho_{microsphere} \times \Phi_{microspheres} + \rho_{matrix} \times \Phi_{matrix}} \ldots\ldots\ldots\ldots 6.1$$

Where, $\rho_{microsphere}$, ρ_{matrix} refer to the density of epoxy microspheres (850 kg m^{-3}) and epoxy resin (1170 kg m^{-3}) respectively and $\Phi_{microspheres}$ *and* Φ_{matrix} refer to the desired volume fraction of epoxy microspheres and epoxy resin. The details of formulations and sample designations are listed in **Table 6.1**:

Table 6.1: Different compositions and designations of syntactic foams

Sample Code	Matrix (% v/v)	Microbubbles (% v/v)
E-40	60	40
E-50	50	50
E-60	40	60

6.2.6. Density Determination

Theoretical density of syntactic foam (ρ_{th}) was calculated according to the standard rule of mixtures (**Equation 6.2**):

$$\rho_{th} = \rho_{microsphere} * \Phi_{microspheres} + \rho_{matrix} * \Phi_{matrix} \ldots\ldots 6.2$$

The density of the foam was experimentally determined by averaging the mass: volume ratio of five specimens as per ASTM D1622–98. The ratio of theoretical and experimental densities was used to quantify the air void porosity trapped in the matrix during fabrication according to the following equation (**Equation 6.3**):

$$Void \ volume \ \% = \frac{\rho_{th} - \rho_{ex}}{\rho_{th}} \times 100 \ \ldots\ldots\ldots\ldots 6.3$$

6.3. Results and Discussion

6.3.1. Preparation of Epoxy Microcapsules
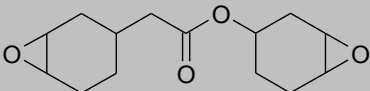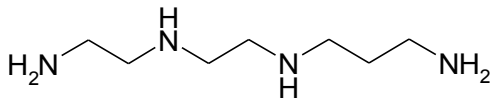
Epoxy microspheres were prepared by the reaction of a cycloaliphatic epoxy with triethylenetetramine in polydimethylsilicone medium using the underlying principles of interfacial engineering. The so formed microcapsules were refluxed in toluene to obtain hollow free flowing microcapsules. The effect of operating parameters, particularly stirring speed, temperature and hardener concentration on the microcapsule dimensions and core content was investigated.

The Hoy's solubility parameter(δ) of epoxy, TETA have been calculated based on the group contribution models of Hoy[215]and the values are reported in **Table 6.2**. As a first approximation and in the absence of strong interactions such as hydrogen bonding, solubility can be expected if $\delta 1 - \delta 2$ is less than 1.7-2.0 but not if appreciably larger. The easiest way to determine δ of a known structure is by the use of molar attraction constants E (**Equation 6.4**).

$$\delta = \frac{\rho \sum E}{M} \ \ldots\ldots\ldots\ldots\ldots 6.4$$

Where E values are summed over the structural configuration, with molecular weight, M and density ρ.

Table 6.2: *Density, Molar attraction constants and Solubility parameter*

Reactant	Density (g ml^{-1})	Molar attraction constant, (E, (calcm^3)$^{1/2}$ mole$^{-1)}$)	Solubility parameter(δ) cal$^{1/2}$cm$^{3/2}$ mL^{-1}
Cycloaliphatic epoxy	1.1	2068	9.0
Triethylenetetramine	0.9	1602	10.8

It can be seen that the solubility parameter of cycloaliphatic epoxy and TETA are in the same range, i.e. 9.0 and 10.8 cal$^{1/2}$ cm$^{3/2}$ mL^{-1} respectively. It was not possible to ascertain the Hoys parameter for polydimethylsiloxane in view of its inorganic-organic hybrid nature, however the Hansen solubility parameter (HSP) of epoxy, triethylenetetramine (TETA) and PDMS has been reported to be 20 MPa$^{1/2}$ [216], 22.7 MPa$^{1/2}$ [217] and 14.9 MPa$^{1/2}$ [218, 219] respectively, the large difference in the HSP (5.1-7.8) being clearly indicative of the immiscibility of PDMS with both epoxy as well as hardener. This difference in miscibility results in their existence as phase separated droplets under agitation. To verify the same the optical images of epoxy-PDMS and TETA-PDMS mixtures were captured, where the presence of droplets in the medium is clearly indicative of its immiscibility (**Figure 6.4**).
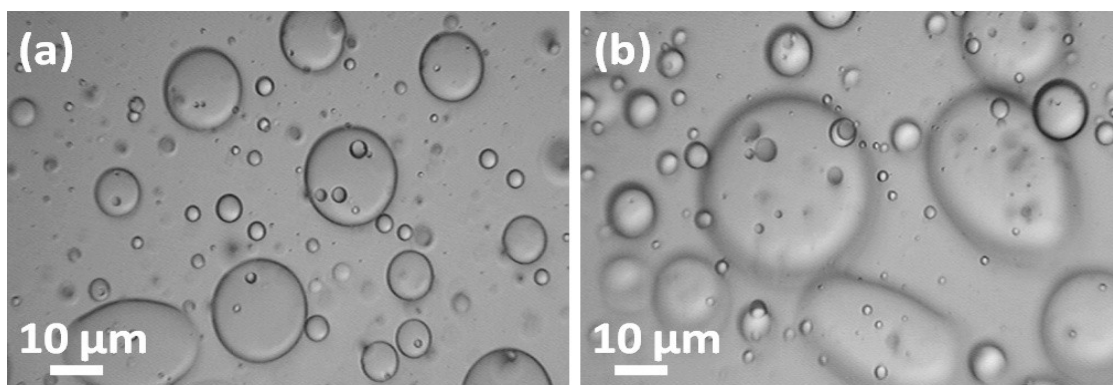
Fig.6.4: Optical images of a) epoxy-PDMS b) TETA –PDMS

6.3.2. Curing behaviour of Epoxy

Curing behaviour of the cycloaliphatic epoxy resin in the presence of TETA was investigated using non-isothermal calorimetric studies to arrive at the optimal reaction conditions, especially reaction time and temperature. The effect of increasing heating rate viz. 2.5, 5, 10 and 15 °C min^{-1} on the differential scanning calorimetric curves of neat epoxy are presented in **Figure 6.5**. The characteristic thermal parameters i.e. ΔH_{cure}, T_{onset} and T_{peak} are summarised in **Table 6.3**. As expected, increasing the heating rate (β) leads to a systematic shift in the trace towards higher temperatures. The curing reaction is primarily a kinetic event, which is a function of both time and temperature. On being subjected to a higher heating rate, the reactants get lesser time to react at any specific temperature, leading to the observed phenomenon. On the basis of the curing profile, preliminary studies on encapsulation were performed at temperatures starting from 60 °C to 90 °C. However, when the reaction medium was maintained at lower temperatures T < 65 °C, complete curing required prolonged periods (~ 36 h), which was too long to be of any industrial significance. As expected, the rate of the curing increased significantly with increasing temperature and free flowing microcapsules could be obtained within 10 h at 70 °C. Further increase in temperature was impractical in view of the strong vapour pressure- temperature dependence of TETA [220], which led to significant vaporization

of the amine. Therefore, detailed studies on the effect of other operating parameters were performed while maintaining the reaction medium at 70 °C.
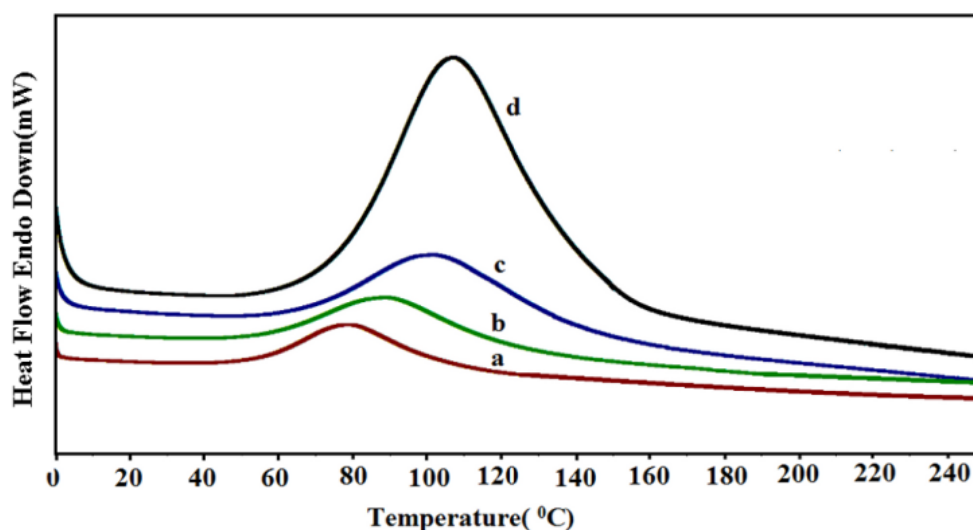
Fig.6.5: *Effect of heating rate on the DSC traces of epoxy a) 2.5,b) 5, c) 10 and d) 15 °C /min*

Table 6.3: *Characteristic curing parameters of epoxy*

Heating rate (β)/° C min^{-1}	T_{onset}/° C	T_{peak}/° C	ΔH_{cure}/J g^{-1}
2.5	54	79	320
5	56	89	323
10	65	102	343
15	75	107	322

6.3.3. Effect of Stirring Speed on Particle Size Distribution and Morphology

Operating parameters play a vital role in affecting the microcapsule dimensions, most influential being the rate of agitation, reaction temperature, concentration and nature of surfactant and interfacial tension of the media to name a few. Particularly, the extent of agitation decides the equilibrium between shear forces and interfacial tension between separate phases [221]. The effect of stirring speed on the microsphere size distribution is presented in **Figure 6.6**. In accordance with our expectations, increasing the rate of

stirring led to a shift in the particle size distribution towards lower dimensions, which could be attributed to the shearing of the large oily droplets into smaller microspheres. At lower stirring speeds (400 rpm), the particle size distribution profile exhibited maxima at ~ 130-150 μ, the position of which progressively shifted to 90-100 μ as the stirring speed was increased to 600 rpm.
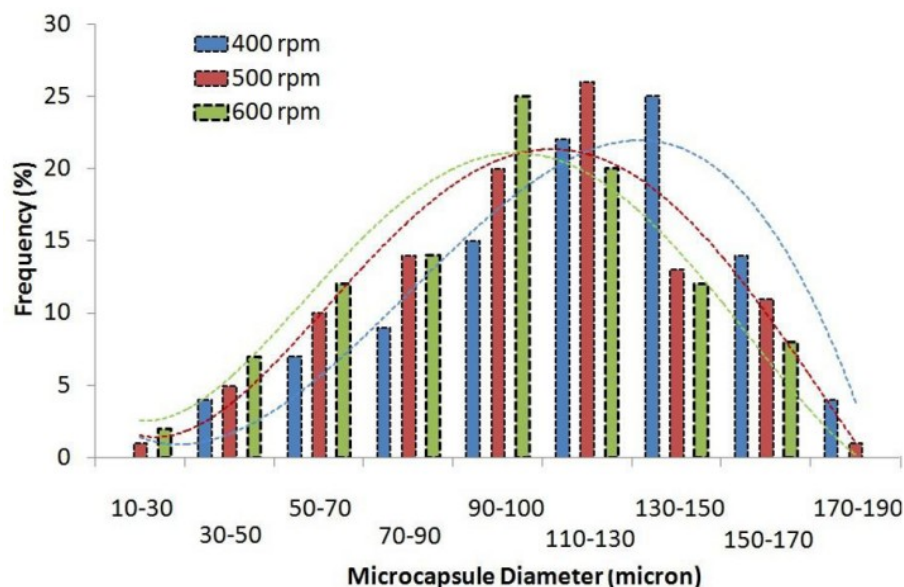
Fig.6.6: *Effect of stirring speed on the particle size distribution of microcapsules*

Representative SEM images depicting the morphology of the microcapsules are presented in **Figure 6.7**. It is evident that the extent of agglomeration of the microcapsules increased as the stirring speed is lowered. Under optimal reactions conditions, i.e. stirring speed of 600 rpm, reaction temperature of 70 °C and resin:hardener::100:2, perfectly spherical microcapsules were obtained with a core content of 25 %. Presumably, under the reaction conditions employed, the amine hardener is the limiting reagent, which reacts with excess epoxy at the silicone-epoxy interface. With the progress of reaction, the liquid amine diffuses into the reactive interface till complete exhaustion of the excess epoxy leaving behind the unreacted epoxy encapsulated in the crosslinked epoxy shell.
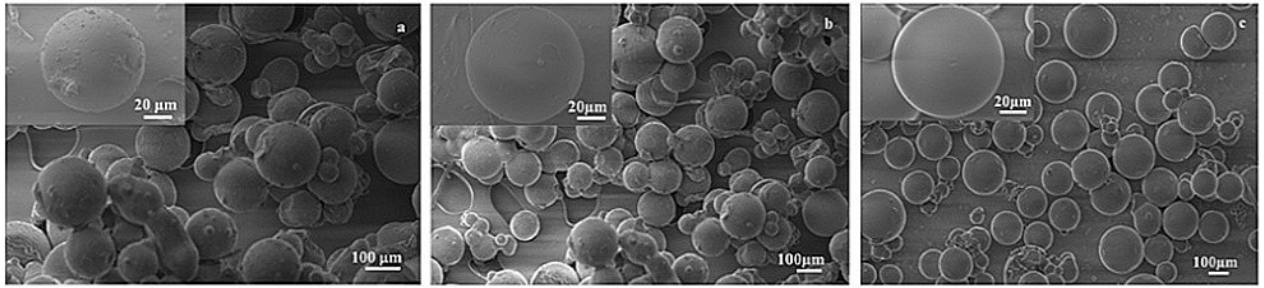
Fig.6.7: SEM images of representative microcapsules obtained by varying the rate of stirring a) 400, b) 500 and c) 600 rpm

6.3.4. Core Content of Epoxy Microbubble

Epoxy microcapsules, prepared by interfacial engineering were refluxed to transform them into hollow fillers for epoxy syntactic foams. For this purpose, pre-weighed dry epoxy microcapsules (10 g) were stirred in a round bottom flask, which was connected to a reflux condenser. Refluxing was performed for extended periods (4h), following which the mixture was allowed to cool. Finally the microcapsules were washed, dried and weighed. The core content was estimated gravimetrically as the ratio of the loss in mass to the initial amount of epoxy microcapsules. The same in presented in **Table 6.4**.

Table 6.4: Core content of epoxy microbubbles

Epoxy :TETA	$M_{microbubble}$post-refluxing (g)*	Core content (%)
100:13	9.90± 0.01	1
100:10	8.81± 0.03	12
100:5	7.81± 0.02	22
100:3	7.62± 0.01	24
100:2	7.51± 0.02	25

* Total mass of reactants : 10g

The variation in microcapsule core content and yield with increasing TETA concentration is presented in **Figure 6.8**. As expected, microcapsule yield increases with increasing hardener concentration, however this is associated with a concomitant decrease in the core content. It is to be noted that microcapsules could not be obtained as the concentration of the hardener was reduced further i.e. < 2 % w/w.
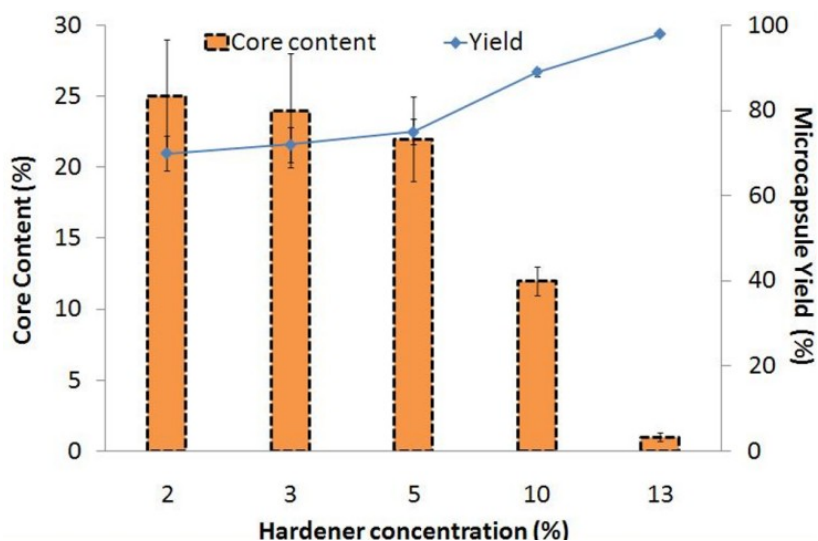
Fig. 6.8: *Effect of resin: hardener ratio on core content and yield*

6.3.5. Thermal Degradation

The TG-DTG traces of the epoxy resin before and after encapsulation is presented in **Figure 6.9**. As can be seen, liquid epoxy resin volatilizes and undergoes oxidative degradation at T ~ 210 °C. Encapsulation of the resin in crosslinked epoxy shell (TETA = 2 % w/w) shifts the degradation temperature towards higher temperature (T_{onset} = 350 °C). The thermo-oxidative degradation of epoxy resins has been extensively studied by several researchers, where a dual step degradation profile is reported. The oxidation of the main chain results in formation of condensables like acetone, carbon dioxide, hydrogen cyanide, aliphatic hydrocarbons etc [222].
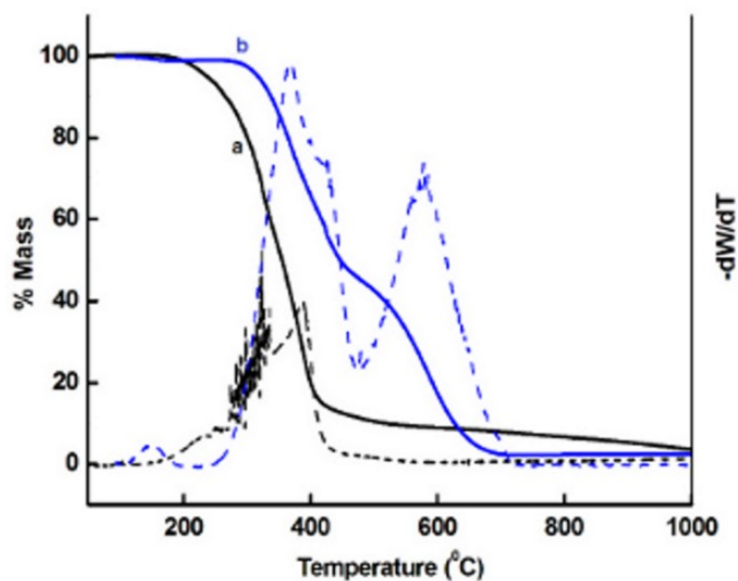
Fig.6.9: *TG-DTG traces of a) liquid epoxy b) microcapsules prepared using TETA (2 %).*

Dashed lines represent DTG traces.

The FTIR spectra of liquid epoxy resin and microcapsules are presented in **Figure 6.10**. It can be seen that the intensity of the absorption band due to –C-O-C (oxirane ring : 917 cm^{-1}) [223] reduces as a result of reaction with amine, however trace absorption still exists. The epoxy content of the microcapsules, as estimated using titrimetry, was found to decrease with increasing amount of hardener used for its preparation. Microcapsules prepared using 2 % hardener were found to exhibit an epoxy content of 45 meq g^{-1}, which is substantially large to permit further functionalization. We would like to highlight that epoxy functionalized polymeric microspheres possess immense potential in varied fields, particularly catalysis [205] and enzyme immobilization [224, 225]. The simplicity of our technique opens up vistas for preparation of epoxy functionalized microspheres with potential application in varied fields.
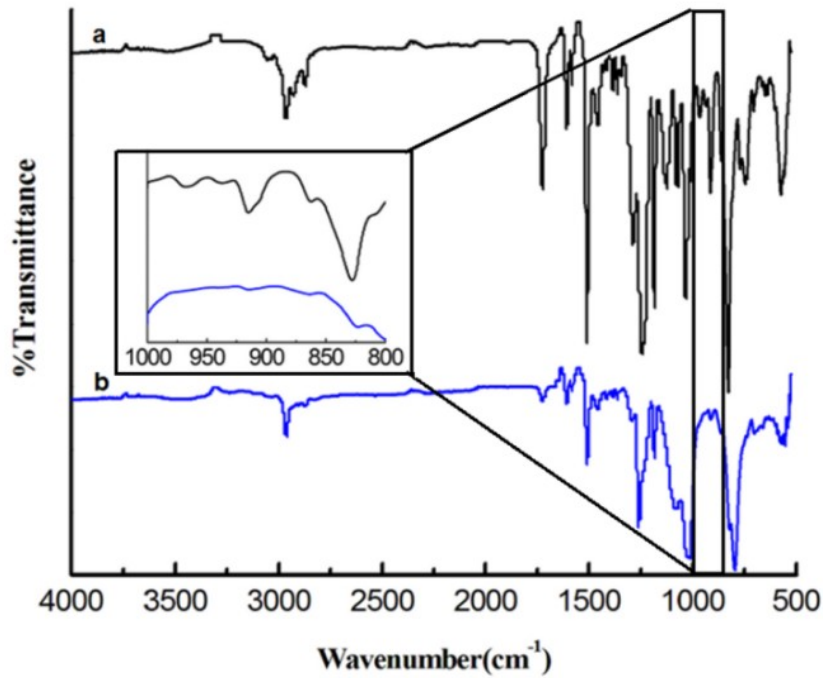
Fig. 6.10: *FTIR spectra of a) liquid epoxy b) microcapsules prepared using epoxy:*

hardener ::100:2

6.3.6. Syntactic Foams

Refluxed epoxy microcapsules were employed as hollow fillers (40-60 % v/v) in epoxy syntactic foam. The density of epoxy microbubbles was 850 kg m^{-3} which was significantly higher than commercially used glass microbubbles (150-600 kg m^{-3}). Theoretical and experimental densities of the foams and their influence on the mechanical properties of epoxy syntactic foams have been outlined in the sections to follow. Theoretical and experimental densities, along with the voidage associated with each of the sample configuration are presented in **Figure 6.11**. As expected, increasing microbubble loading led to a substantial decrease in the densities.
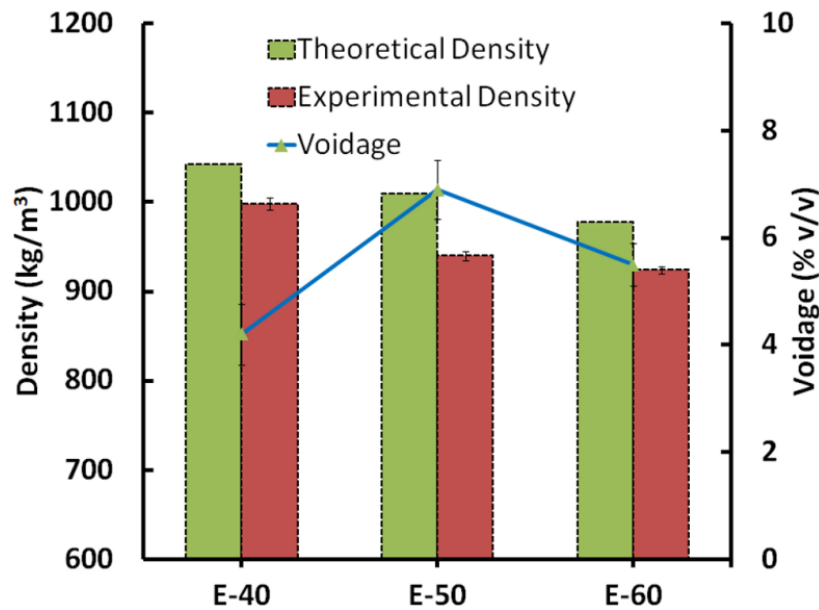
Fig.6.11: *Theoretical and experimental densities of syntactic foam*

6.3.6.1. Mechanical Properties of Syntactic Foams

The effect of increasing microbubble content (40-60 % v/v) on the mechanical properties of syntactic foams is discussed. The mechanical properties decreased on increasing the volume percentage of epoxy microcapsules. The presence of good interfacial adhesion between the microbubbles and matrix undoubtedly enhanced the mechanical properties nevertheless the properties deteriorated as loadings of epoxy microbubbles increased. Except for the differences in the compressive yield strength, compressive stress-strain curves of epoxy syntactic foams containing epoxy microbubbles are similar to their foamed counterpart having glass microbubbles. Representative stress-strain curves of syntactic foams are presented in **Figure 6.12**. Initial rise in stress in the stress-strain curve is accompanied by an increasing strain till the elastic limit in which the curve obeys Hooke's law. A slump at the end of the elastic region and preceding a plateau region marks the onset of cell wall buckling of microbubbles. The plateau region signals the breaking or crushing of the microbubbles. Increase in strain is observed at constant stress in this region. Densification of foams is a common phenomenon which accounts for

the complete crushing of microbubbles causing an increase in strain at low values of stress.
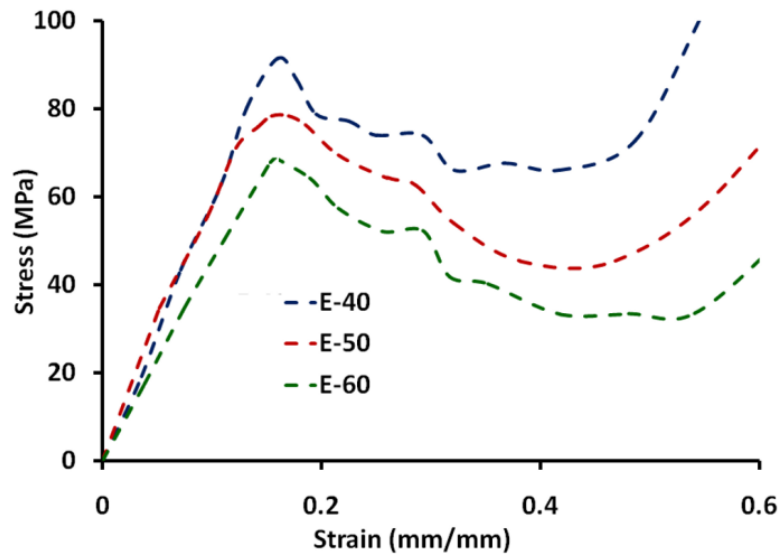
Fig.6.12: Compressive stress-strain curves of syntactic foam

Under compression, epoxy microbubbles get crushed and are solely responsible for the failure of the foam. The compressive strength values are found to deteriorate as volume fraction of epoxy microbubbles increase. The failure of the foams under compression is primarily due to shear cracking of microbubbles present in the matrix. At high loadings, these microbubbles tend to aggregate and thus shear at the local scale. Specific compressive strengths, calculated by dividing the compressive strength with the density of the foams exhibit a similar pattern as observed for the compressive strength. Area under the compressive stress-strain curve in compression, till the plateau region, is indicative of the energy absorbed by the foams hence toughness. The area under curve is influenced by two factors, namely the compressive strength of microbubbles and the length of the plateau region. Epoxy microbubbles provide both good compressive strength and an enhanced plateau region which accounts for their high area under the curve compared to neat epoxy. However increase in volume fraction of microbubbles is brought about by a simultaneous decrease in the area under the curve due to decreasing

compressive strengths at higher loadings of microbubbles. Addition of 40 % (v/v) epoxy microbubbles provides ~ 127 % and ~ 155 % improvements in compressive toughness and specific compressive toughness values compared to neat epoxy. The compressive properties of syntactic foams are presented in **Figure 6.13**.
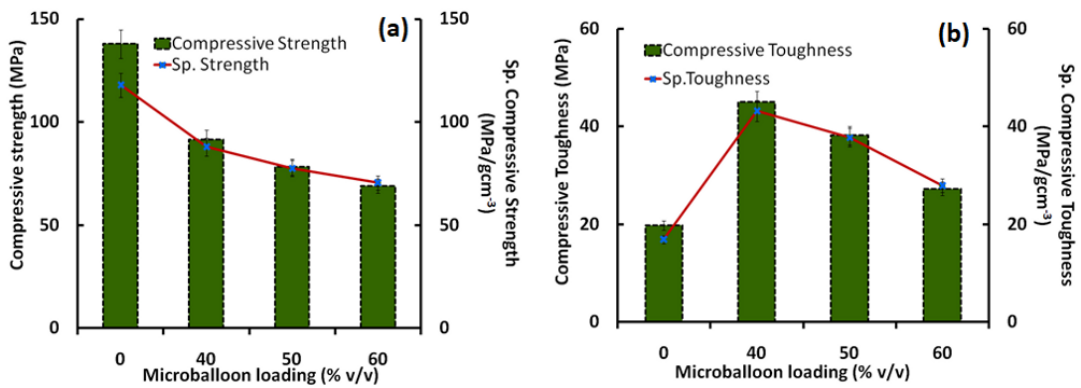
Fig.6.13: Compressive properties of epoxy syntactic foams

Tensile failure of syntactic foams is dominated by matrix failure. Unlike the failure of the foams in compression, failure under tensile loading is attributed to matrix cracking and debonding of microbubbles without being crushed. Nonetheless the tensile strength and specific tensile strength are found to decrease as the volume fraction of microbubbles increases. Tensile properties of syntactic foams are presented in **Figure 6.14**.
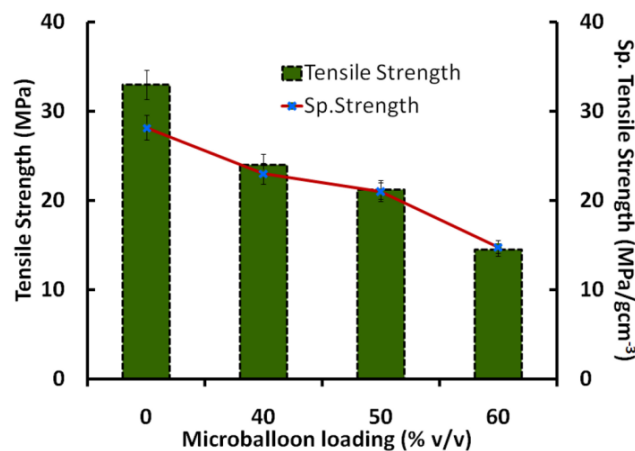
Fig.6.14: Tensile properties of epoxy syntactic foams at varied loadings of epoxy

microbubbles (40-60 % v/v)

Flexural failure is a combination of tensile and compressive failure modes wherein, the side facing the load cell experiences tensile forces and compressive forces operate on the other side. Flexural strength of syntactic foams containing epoxy microbubbles decreases as the volume fraction of microbubbles increases. The effect of decreasing densities of foams at high loadings of microbubbles is suppressed by a concurrent decrease in the flexural strength values the additive effect of which leads to lower values of specific flexural strengths at high loadings of epoxy microbubbles. Flexural properties of syntactic foams at varying loadings of epoxy microbubbles are presented in **Figure 6.15**.
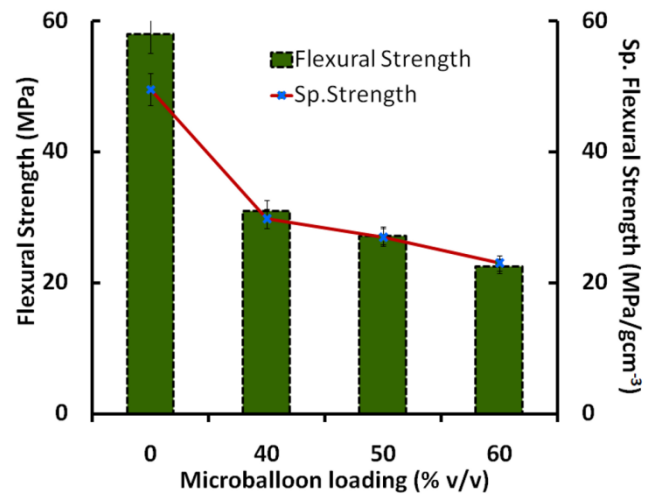
Fig.6.15: *Flexural properties of epoxy syntactic foams at varied loadings of epoxy*

microbubbles (40-60 % v/v)

Chapter VII

Polybenzoxazine-Glass Microbubble Syntactic Foams
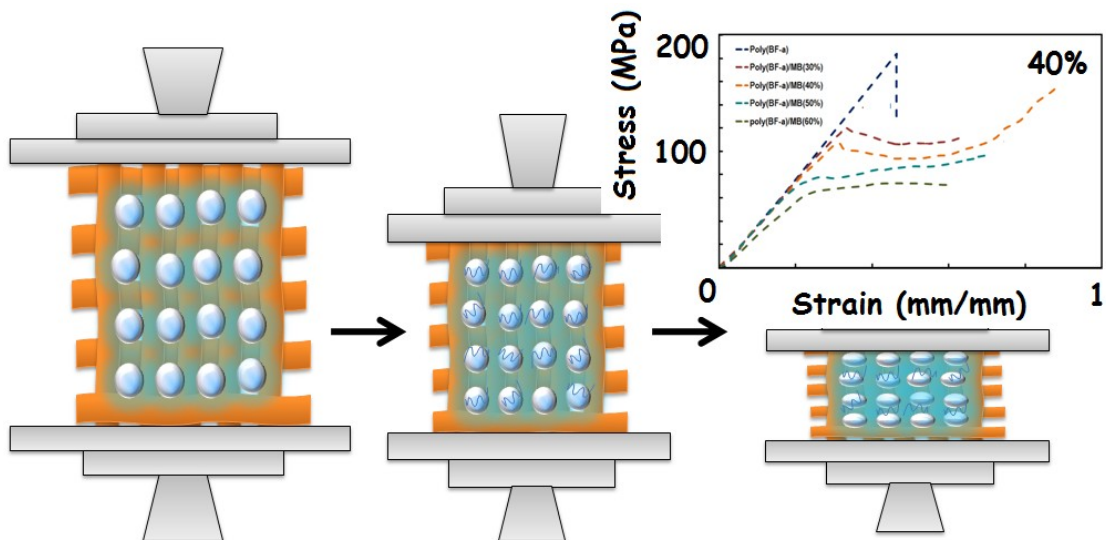
7.1. Introduction

The high-tech aerospace industry is in a continual search of materials with high thermal stability, robust mechanical response and most importantly low density, which directly translates to benefits in the form of low fuel consumption [47]. In this context, syntactic foams offer their excellent candidature and are hence trending as light-weight construction materials with high specific structural properties, especially as "core component" in sandwich structures [226, 227]. In general, polymeric syntactic foams are prepared by dispersing hollow fillers in a suitable polymeric resin. What is interesting in the context of syntactic foam is that it is possible to obtain a wide range of mechanical properties by judicious choosing the constituents, i.e. the polymeric resin, filler type and its volume fraction [58, 228, 229].

Among all hollow fillers, glass microbubbles (HGM) are most extensively used, in view of their economic viability, low coefficient of thermal expansion and chemical inertness [46]. Polymeric resins such as epoxies [95, 230-232], polyurethanes [233], silicones [234], phenolic resins [235] have been used in the past as matrix material for syntactic foams. Surprisingly, the potential of benzoxazines for this purpose has not yet been duly explored [236, 237]. Polybenzoxazines are well-known for their excellent thermal stability, and are particularly suitable for preparation of highly filled composites in view of their low melt viscosity and excellent wettability [238-240]. In addition, polybenzoxazines exhibit interesting properties such as negligible curing shrinkage [241], low water absorption [242], high glass transition temperature [243] and high char yield [244, 245]. Benzoxazines polymerize via thermally accelerated ring opening reaction and generate no volatile by product, a major processing benefit for the production of void free composites [242]. In the last few years, polybenzoxazines are emerging as strong contenders, even for engineering polymers like imides and epoxies [246, 247]. Attempts

towards preparation of benzoxazine based cellular foams are rather limited [236, 237], and mostly deal with conventional bisphenol-A based polybenzoxazines. One of the most interesting features associated with benzoxazines is the possibility of molecular designing flexibility [248-250], which greatly increase the scope of these materials [251, 252]. A wide range of mechanical properties can be obtained by varying the reactants used for preparation of benzoxazine i.e. amine and phenol [253, 254]. The properties of benzoxazine based syntactic foams can be significantly improved by changing the type of resin. Bisphenol-F based benzoxazines exhibit substantially better properties than Bisphenol A based resin in terms of flame retardance, dimensional and chemical resistance and most importantly mechanical response. Therefore it was considered of interest to prepare syntactic foams based on Bisphenol-F based benzoxazine resins.

Conventional processing techniques for syntactic foams include casting, extrusion and rotational moulding or buoyancy methods, where the procedure adopted is dependent upon the microbubble loading and the type of polymeric material [46, 115, 116]. In most cases, the viscosity of the resin-filler formulation increases tremendously with increasing microbubble loading. High microbubble content presents difficulty during stir-casting of the formulation. Therefore systematic understanding of the flow behaviour of resin-microbubble formulation becomes an essential aspect for smooth processing of specimens. Literature reports the use of diluents for improving the flow behaviour, to ease the processability issues associated with highly filled formulations [255]. Unfortunately, the subsequent removal of the diluent results in void formation, which adversely affects the mechanical performance and higher production costs. It is therefore essential to establish the processing window of the formulations to ascertain optimal conditions required for processing of syntactic foams. In this context, rheological studies can generate invaluable data. Unfortunately, systematic rheological studies on syntactic foam

formulations are rather scarce, with most of the studies dealing with thermoplastic-HGM formulations [117-119].

Here, in this chapter, we attempt the preparation of bisphenol-F benzoxazine based syntactic foam containing increasing loadings of hollow glass microbubbles (HGMs). The rheological behaviour of benzoxazine-HGM formulations has been systematically studied to gain an insight into the optimal conditions required for processing of these syntactic foams. The compressive properties of bisphenol-F based benzoxazine syntactic foams have been compared with existing literature. An appreciable enhancement in the compressive performance of the foams advocates a strong need to develop polybenzoxazines syntactic foams.

7.2. Experimental

7.2.1. Materials

Bisphenol-F-Aniline (BF-a) based benzoxazine resin with density of 1.24 g cm^{-3} was obtained from Anabond (Chennai, India). Hollow glass microbubbles (HGM K46, 3M) were used as hollow fillers for the preparation of syntactic foams. The physical properties of glass microbubbles are presented in Chapter 2 (**Table 2.1**).

7.2.2. Rheological Studies

Anton Paar Rheometer MCR-102 was used to study the rheological behaviour of the PBz/HGM formulations using parallel plate geometry (diameter 25 mm and gap thickness was maintained at 1 mm). A constant strain of 0.5 % and an angular frequency of 10 rad/s were maintained throughout the rheological experiments. Temperature-sweep experiments were performed over a range of temperature in three intervals : 30-150 °C at 5 °C min^{-1}, 150-280 °C at 3 °C min^{-1}, and finally at 280 °C for 1h. Subsequently, isothermal experiments were performed in oscillatory mode at 200 °C. The viscoelasticity

of the formulations in terms of complex viscosity (η*), shear storage modulus (G'), and shear loss modulus (G") w.r.t temperature were monitored.

7.2.3. Processing of Polybenzoxazine Syntactic Foams

Finely powdered bisphenol-F benzoxazine resin was mixed with HGMs at different volume fractions (30-60 % v/v). The procedure adopted for the processing syntactic foams involved introduction of pre-calculated amounts of finely powdered BF-a resin and microbubbles in a teflon mould. The contents were subjected to a compressive force of ~ 10 MPa and the formed pellet was subsequently subjected to a controlled curing program (150 °C for 15 mins, 180 °C for 15 mins and 200 °C for 60 mins). The details of the specimens prepared along with their sample designations have been presented in **Table 7.1**. Neat polybenzoxazine specimens has been referred to as PBF-a and the compositions containing glass microbubbles have been referred to as PBF-a/MB(X) where X indicates the volume fraction of HGM present in the specimen. For e.g. poly(BF-a) containing 40 % v/v of glass microbubbles has been designated as PBF-a/MB(40).

Table 7.1: Sample designations of PBF-a/HGM foams

Sample Designation	Matrix (% v/v)	Hollow glass microbubble (% v/v)
PBF-a	100	0
PBF-a/MB(30)	70	30
PBF-a/MB(40)	60	40
PBF-a/MB(50)	50	50
PBF-a/MB(60)	40	60

7.2.4. Density of Syntactic Foams

The amount of HGM and benzoxazines microspheres was calculated as per the **Equation 7.1**.

$$\frac{Mass\,of\,HGM}{Mass\,of\,syntactic\,foam} = \frac{\rho_{HGM} \times \Phi_{HGM}}{\rho_{HGM} \times \Phi_{HGM} + \rho_{matrix} \times \Phi_{matrix}} \dots\dots\dots\dots7.1$$

Where, ρ_{HGM}, ρ_{matrix} refer to the density of HGM (460 kg m^{-3}) and benzoxazine resin (1240 kg m^{-3}) respectively and Φ_{HGM} and Φ_{matrix} refer to the desired volume fractions of HGM and resin. Theoretical density of syntactic foam (ρ_{th}) was calculated according to the standard rule of mixtures (**Equation 7.2**).

$$\rho_{th} = \rho_{HGM} * \Phi_{HGM} + \rho_{matrix} * \Phi_{matrix} \dots\dots\dots7.2$$

The density of the foam was experimentally determined by averaging the mass: volume ratio of five specimens as per ASTM D1622–98. The ratio of theoretical and experimental densities was used to quantify the air void porosity trapped in the matrix during fabrication according to the **Equation 7.3**.

$$Void\ volume\ \% = \frac{\rho_{th} - \rho_{ex}}{\rho_{th}} \times 100 \dots\dots\dots\dots 7.3$$

7.2.5. Quasi-static Testing

Mechanical testing under compression mode was carried out using Universal Testing Machine (International Equipments). The detailed procedure is mentioned in Chapter 2 (**Section 2.2.7**). The techniques used for thermal and structural characterisation of samples have been presented in section. For dynamic DSC scans, the sample (5 ± 1 mg) was sealed in aluminium pans, and heated from 30 to 350 °C at 10 °C/min. N$_2$ was purged at rate of 50 ml/min to minimize oxidation of the sample during the curing process.

7.3. Results and Discussion

Rheokinetic studies were performed to arrive at the optimal conditions for processing of the PBF-a/HGM syntactic foams. The mechanical response of cured syntactic foams was evaluated under quasi-static regime.

7.3.1. Curing of Benzoxazine Resin

Benzoxazine monomers (Bz) reportedly undergo polymerization reaction via thermally accelerated cationic ring opening which results in the formation of a stable crosslinked polybenzoxazine network [256]. The ring strain associated with the heterocyclic oxazine ring drives the polymerisation reaction forward [249]. The reaction has been reported to be autocatalytic in nature in view of catalytic activity of the reactive species generated in-situ [257, 258]. The proposed mechanism for the polymerisation of the 1,3-benzoxazine monomer is presented is **Figure 7.1**. At elevated temperatures, the oxonium cation undergoes ring opening to form a reactive iminium species, which further undergo monomer insertion steps. The repetitive addition of monomer leads to the formation of cross linked polybenzoxazine system.
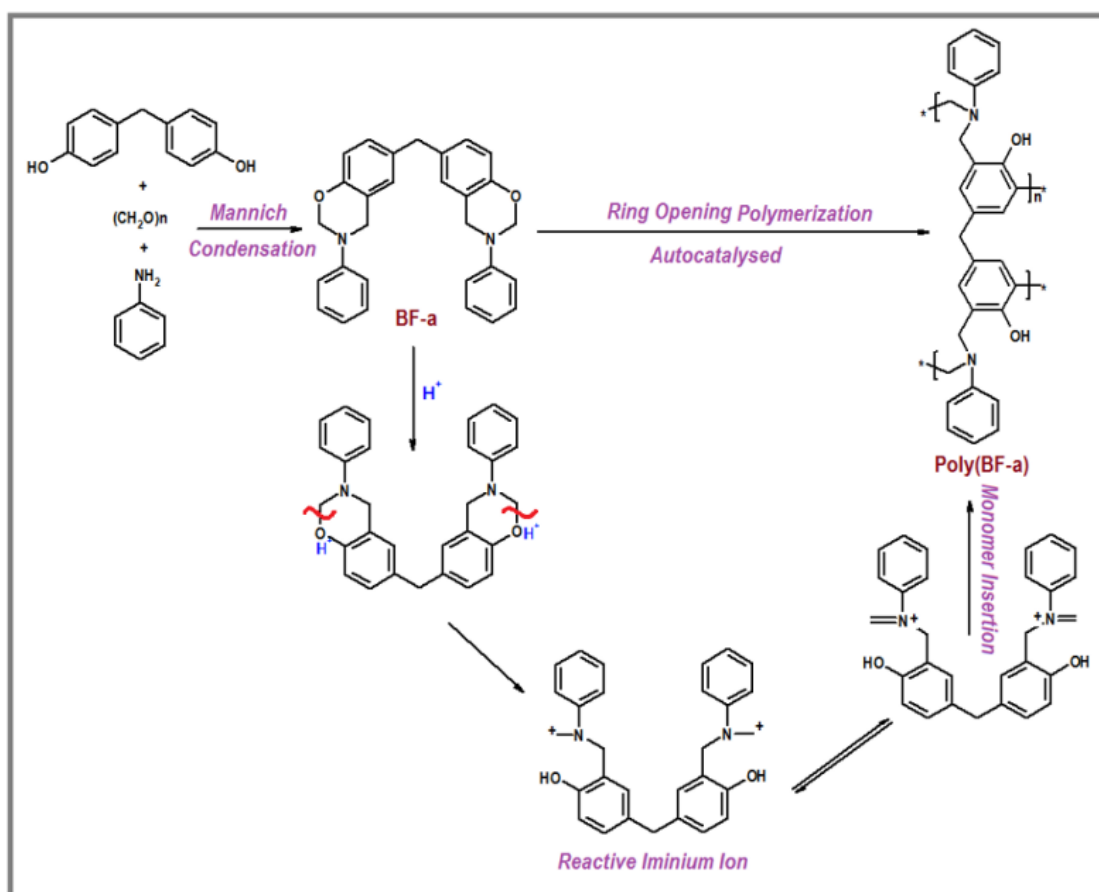
Scheme 7.1: *Scheme showing polymerization of bisphenol-F aniline (BF-a) benzoxazine*

Non-isothermal differential scanning calorimetry (DSC) traces (**Figure 7.1)** reveal that ring opening polymerization in bisphenol-F aniline benzoxazine (BF-a) initiates at 216 °C and reaches its peak at 231 °C. The curing profile remains practically unaffected by the addition of HGMs into the resin, even at higher loading. The onset and peak temperature associated with the curing of all the formulations are presented in **Table 7.2**. The enthalpy associated with the polymerisation reaction was also found to decrease with increasing concentration of HGMs, attributable to the reduced amount of monomer in the formulation.

Table 7.2: *Curing parameters of bisphenol-F aniline benzoxazine/HGM formulations*

Formulations	Matrix (% v/v)	Hollow glass microbubble (% v/v)	Curing parameters		
			T_{onset}(°C)	T_{peak} (°C)	Molar enthalpy of polymerization (J/g)
BF-a	100	0	217	231	321
BF-a/MB(30)	70	30	217	231	238
BF-a/MB(40)	60	40	219	232	188
BF-a/MB(50)	50	50	224	233	128
BF-a/MB(60)	40	60	226	234	102
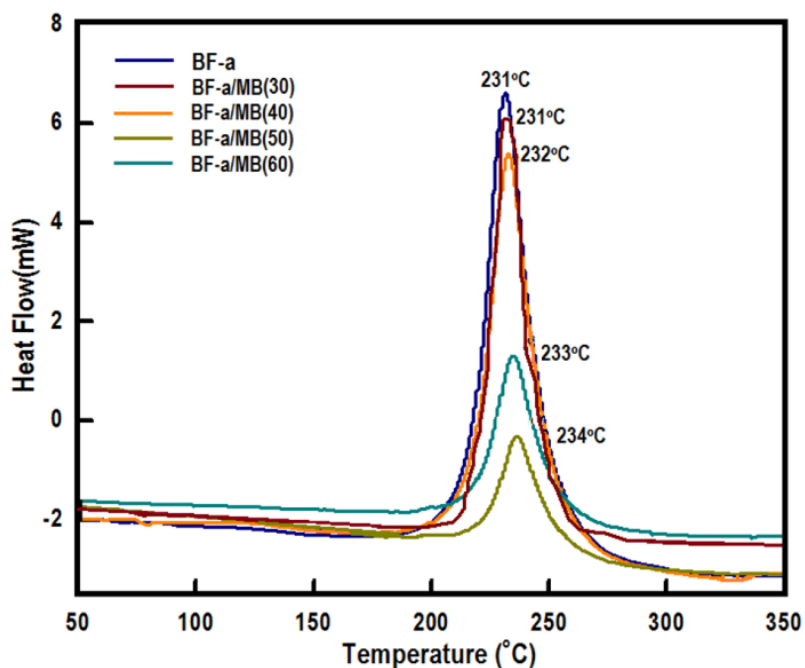
Fig.7.1: *Curing profile of BF-a/glass microbubbles formulation*

7.3.2. Rheokinetics of BF-a/HGM formulations

The processing conditions employed for the preparation of syntactic foam define the end properties of the material. In this context, the most crucial parameter is the viscosity of the formulation, which build-up continuously during the curing reaction. The dependence of the complex viscosity on temperature is presented in **Figure 7.2**. The BF-a resin undergoes liquefaction at ~ 65 °C, and the viscosity of the resin remains sufficiently low till 210 °C, to permit solventless processing of the formulations. Further increase in temperature resulted in ring opening of the oxazine moieties, thereby forming Mannich bases. Subsequently, a gel-type structure is formed, following which an exponential rise in viscosity is observed, due to cross linking within the linear chains. The rheological behaviour of the BF-a/HGM formulations is also included in **Figure 7.2**. In line with previous studies [259], introduction of HGMs result in an increase in the viscosity of the resin with the extent of increase being proportional to the amount of HGM loading (**Figure 7.2,** inset).
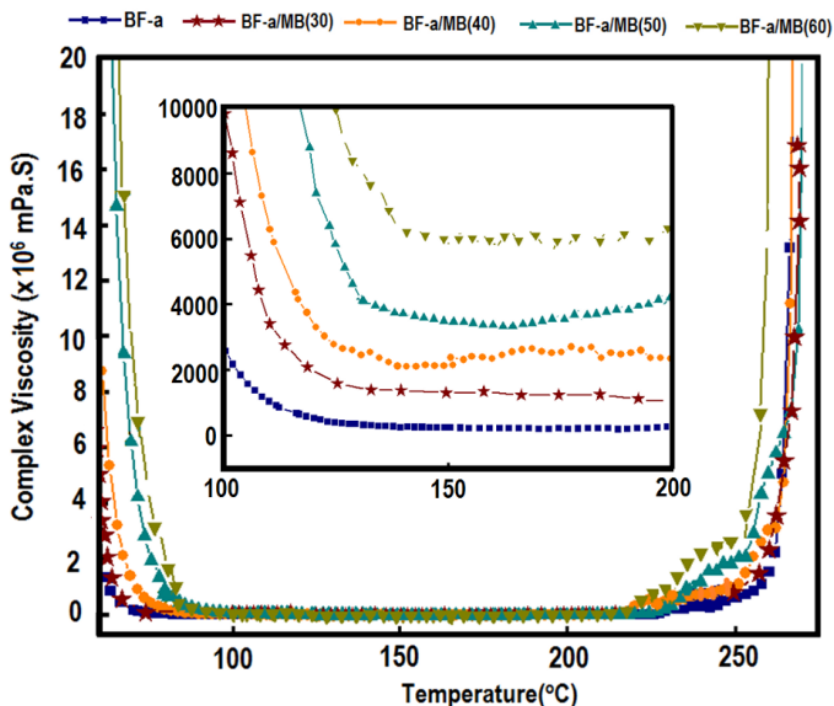
Fig.7.2: *Viscosity-temperature curve of BF-a/HGM formulations*

The variation in the storage and loss modulus due to curing is presented in **Figure 7.3**. The cross-over of the storage and loss moduli indicates the 'gel' point, where the free flow of the medium is restricted due to increased entanglement between the growing polymeric chains [260].
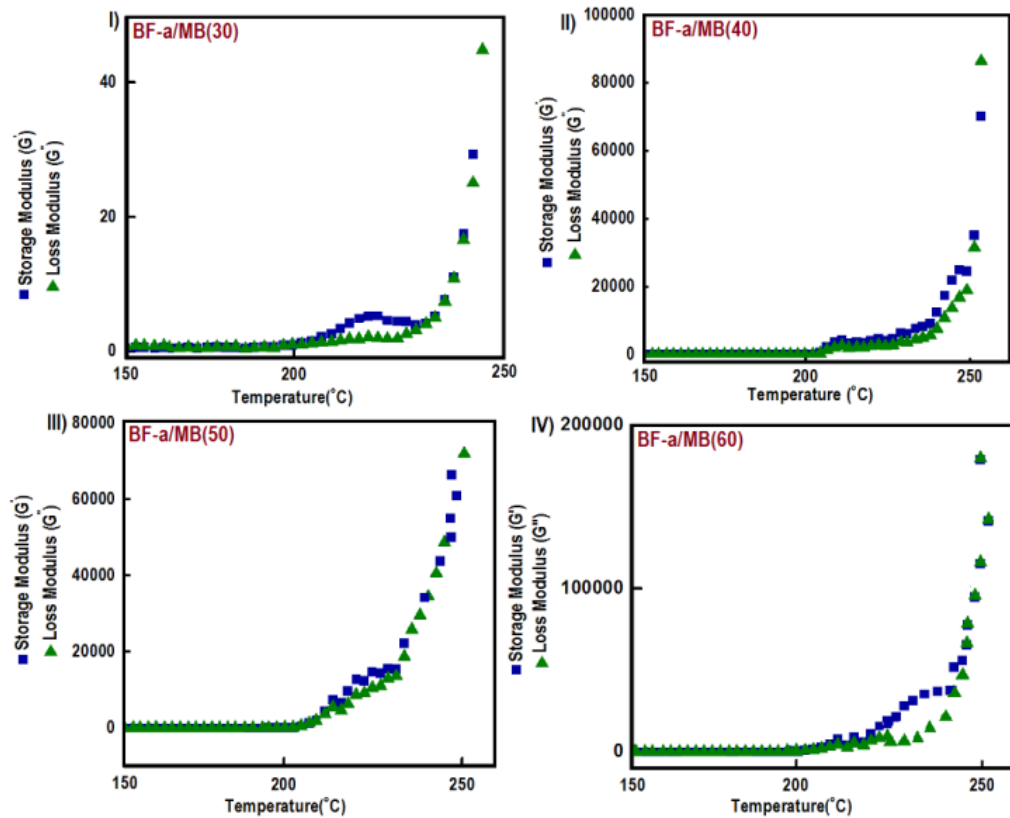
Fig. 7.3: Storage-Loss modulus curve of BF-a formulations with glass microbubbles

The 'gel' point for the BF-a was evidenced at ~ 205 °C (**Figure 7.4**), which remained unaffected due to introduction of the glass balloons.
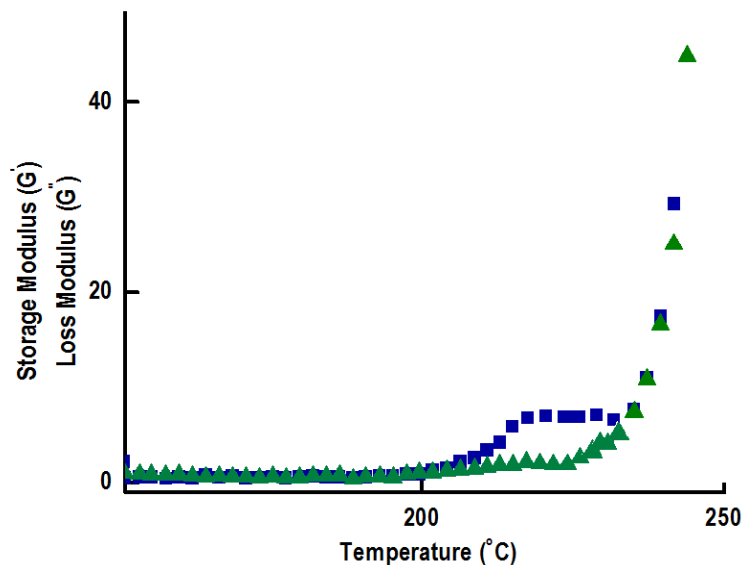
Fig.7.4: *Storage-Loss modulus curve of BF-a*

Rheological studies on benzoxazine/HGM formulations were performed under isothermal conditions also (T= 200 °C), and the results are presented in **Figure 7.5**. A slight increase in the gel time (cross-over point of storage and loss modulus) was evidenced, especially in formulations containing higher loadings of the microbubbles, which can be attributed to the increased restriction offered by HGMs to the reactive oxazine terminals.
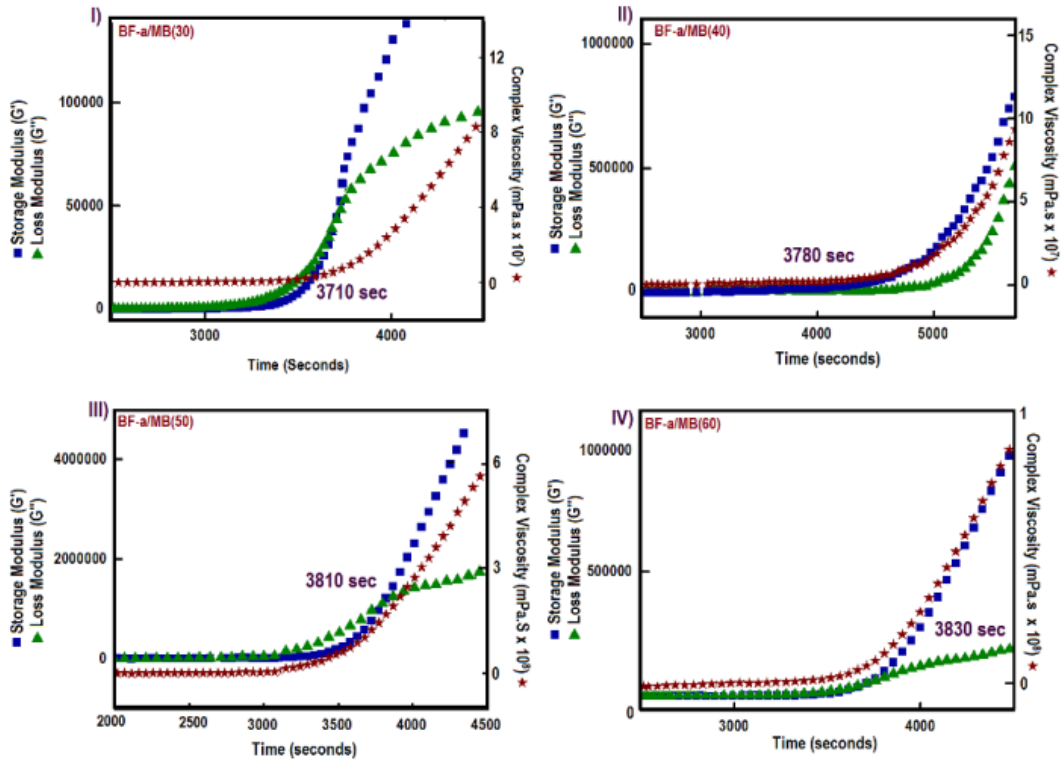
Fig.7.5: *Increase in complex viscosity, storage and loss modulus due to curing of the BF-a/HGM formulations under isothermal conditions (T=200 °C)*

The BF-a resin was observed to undergo gelation at ~ 3690 seconds (**Figure 7.6**), which increase to ~ 3800 seconds upon addition of HGMs (60 % v/v).
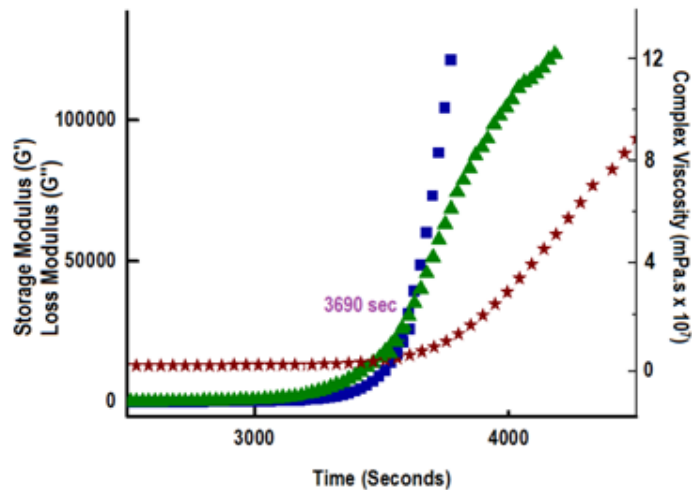
Fig.7.6: *Increase in complex viscosity, storage and loss modulus due to curing of the BF-a under isothermal conditions (T=200 °C)*

161

7.3.3. Mechanical Properties of Syntactic Foams

Syntactic foams were fabricated as per the processing parameters obtained from the rheological experiments. Complete curing of BF-a/HGM specimen can be evidenced by FT-IR studies (**Figure 7.7**). The presence of characteristic absorption associated with –OH is absent in the FT-IR spectra of BF-a resin.
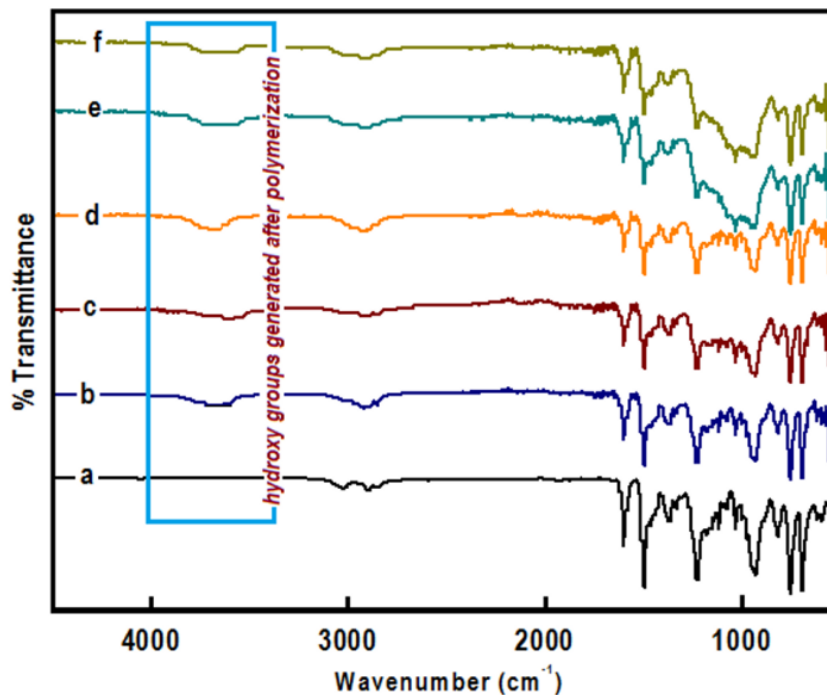
Fig.7.7: FTIR spectra a) BF-a b) PBF-a c) PBF-a/MB (30) d) PBF-a/MB (40)

e) PBF-a/MB (50) f) PBF-a/MB (60)

Monomer undergoes polymerization and generates hydroxyl groups, which participate in intramolecular six-membered hydrogen bonding [249, 261]. The presence of these hydroxyl groups is expected to result in enhanced interaction with surface of the glass microbubbles (**Figure 7.8**).
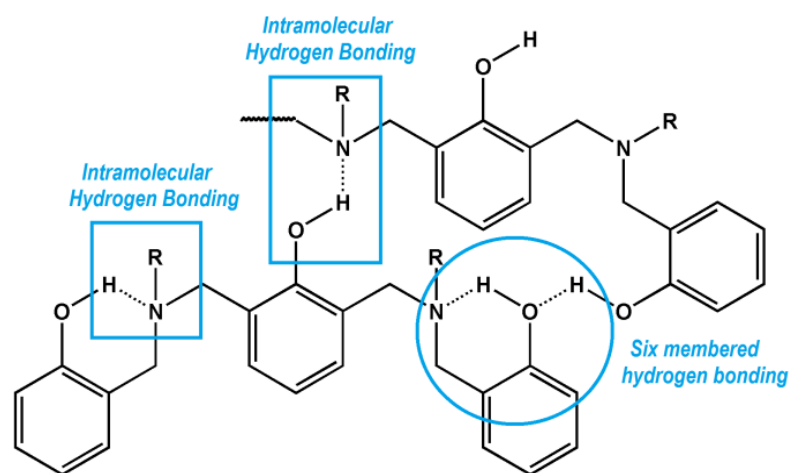
Fig.7.8: *Intramolecular hydrogen bonding in polybenzoxazine network*

Syntactic foams primarily comprise of three distinct phases i.e, matrix, microbubbles and voids [262]. Porosity in matrix is indicative of the amount of air which tends to get entrapped within the matrix during the processing stages. Also, the possibility of microbubble rupture cannot be ruled out completely. The processing of syntactic foams should be performed such that damage of the microbubbles is minimised, as their rupture will lead to an increase the density of the specimen. The designation of the specimens, with their respective theoretical as well as experimental densities and void content are presented in **Table 7.3**.

Table 7.3: *Sample designations, Densities and void content of the PBz/HGM syntactic foams*

Specimen designation	Theoretical density (g cm^{-3})	Experimental density (g m^{-3})	Void content (% v/v)
PBF-a	1.24	1.19 ± 5	4.0
PBF-a/MB(30)	1.00	0.97 ± 3	3.0
PBF-a/MB(40)	0.93	0.88 ± 4	5.3
PBF-a/MB(50)	0.85	0.80 ± 6	5.8
PBF-a/MB(60)	0.77	0.72 ± 7	6.0

As expected, cellular samples containing glass microbubbles exhibit relatively lower densities than neat PBF-a specimens. However, the experimental density of PBF-

a/HGM specimens was much lower than the theoretically predicted values. The difference in the densities was used to estimate the void percentage, which are also included in **Table 7.3**. It is particularly interesting to notice the large voidage in specimens containing high microbubble loading which indicates that the resin is unable to penetrate into the interstitial positions available within the microbubbles.

It is appropriate to compare the mechanical performance of cellular structures in terms of specific mechanical properties, where the density of the material is kept in consideration. The quasi-static properties of the syntactic foams under compressive loading containing varying loading of microbubbles (30-60 % v/v) are presented in **Figure 7.9**. Compressive strength of the specimens was found to decrease with increasing microbubble loading. Microbubble crushing is the primary mechanism responsible for the energy absorption of the foams in compressive mode [51], which is usually quantified in terms of the area under the stress-strain curve till the end of plateau region. It is clear that the specific properties reach maxima at 40 % glass microbubble loading. Our previous study revealed that epoxy syntactic foams containing varying loading of microbubbles (0-60 % v/v) show a compressive strength ranging from 140 to 60 MPa [229].
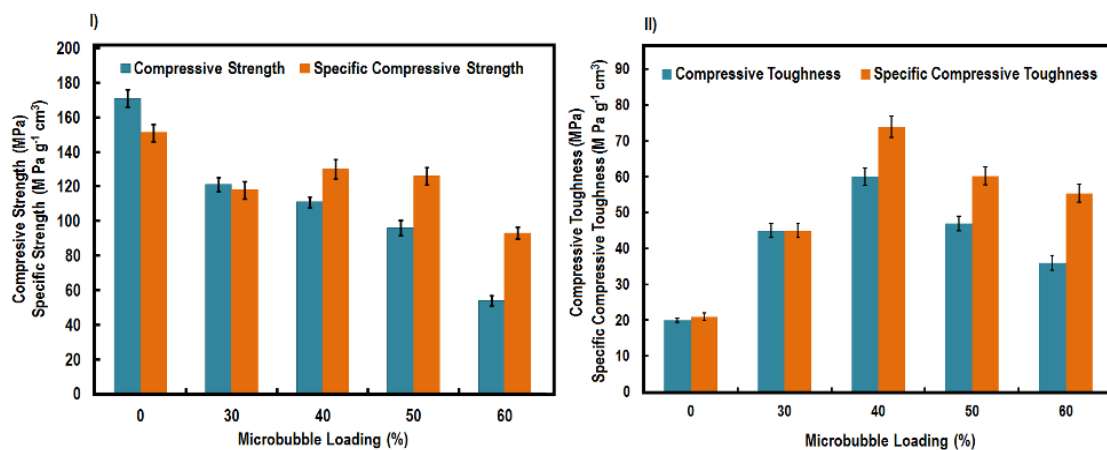
Fig 7.9: *I) Compression and specific compressive strength and II) Toughness and specific*

toughness of PBF-a/HGM specimens at different microbubble loading (0-60 %)

Representative compressive stress-strain curves of PBF-a/HGM syntactic foams at

different microbubble volume fraction are presented in **Figure 7.10**. The stress-strain curves reveal an initial linear elastic (Hookean) region, followed by an energy absorbing plateau region. The peak stress value is the compressive strength of the sample and the plateau region is visualized by an increase in strain without an appreciable increase in stress. In this plateau region, the microbubbles are subjected to extensive compressive loads, which results in their crushing. Beyond this, there is an exponential increase in stress without any appreciable increase in strain: a region signalling the onset of densification [70].
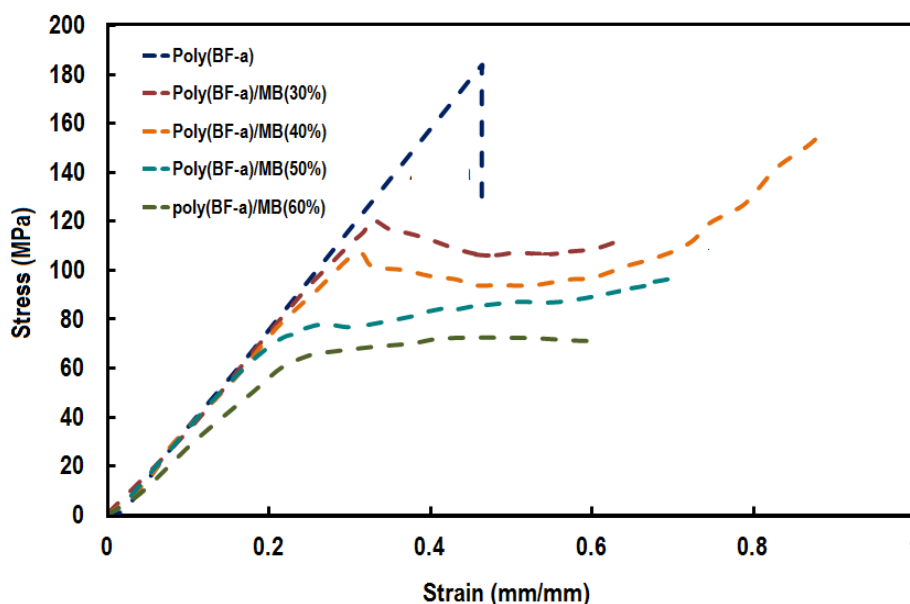
Fig 7.10: *Stress-strain curves of PBF-a/HGM specimens with different microbubble loading (0-60 % v/v)*

7.3.4. Thermal Characterization

TG-DTG traces of PBF-a/HGM syntactic foams containing hollow glass microbubbles in nitrogen atmosphere are presented in **Figure 7.11**. PBF–a began to lose weight at 280 °C and shows three stage degradation centered approximately at 310, 430, and 520 °C, with the middle peak exhibiting the maximum rate of weight loss. Ishida et al. has performed a detailed analysis on the thermal decomposition of aromatic amine

165

based polybenzoxazines [263]. The degradation mechanism involves cleavage of C–C, C–O and C–N bonds or chain scissions in the polybenzoxazine network which generated benzene derivatives, amines, phenolic compounds and Mannich base compounds as primary decomposition products. Primary decomposition products further recombine or undergoes degradation to generate the secondary decomposition products such as 2,3-benzofuran derivatives, iso-quinoline derivatives, biphenyl compounds and phenanthridine and are crucial for char formation. These products after successive dehydrogenation, cross-linking, and aromatization finally leads to the formation of highly cross-linked molecules, i.e. char [263]. The profile associated with the thermal degradation of PBF-a was found to remain unaltered, except for the substantial increase in the char content, from 48 % to 83 % (at 600 °C) as the microbubble loading increased to 60 %.
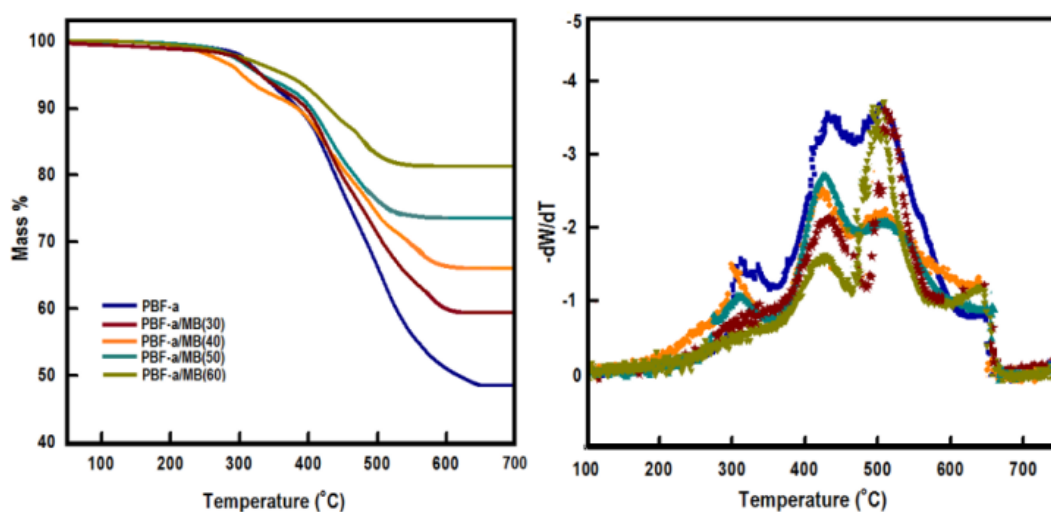
Fig 7.11: *TG-DTG traces of PBF-a and PBF-a/HGM syntactic foams*

Chapter VIII

Summary and Conclusions
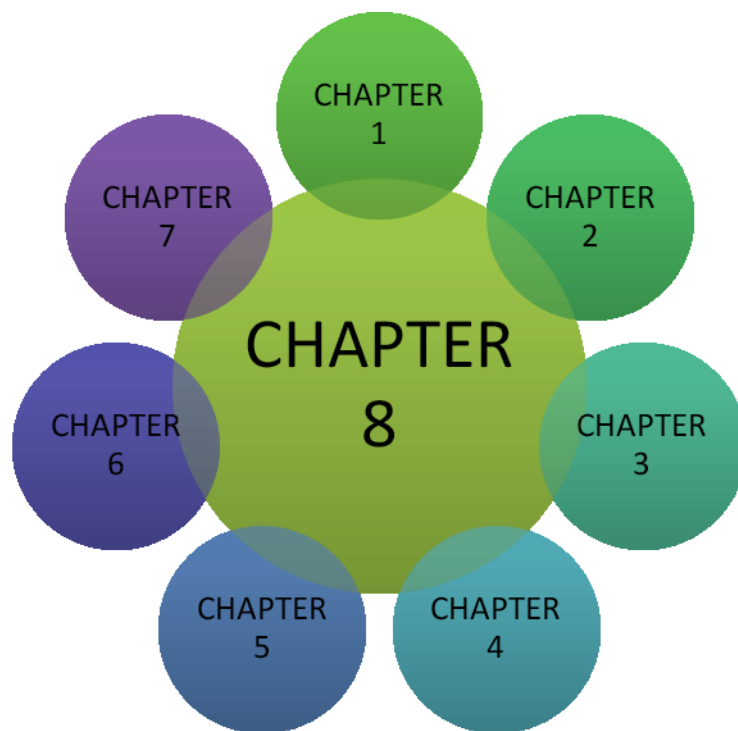
8.1. Summary

Syntactic foams belong to a sub-category of foams, which are formed by inclusion of hollow microbubbles in a resin matrix. Strictly speaking, they are biphasic systems consisting of matrix and microbubbles, however, owing to the presence of entrapped air (not within the microbubble), these are truly three phase systems. They are also referred to as physical foams because they are a result of incorporation of hollow fillers and their formation does not depend on any chemical reaction, which release the blowing gas. Since the hollow spheres can be regarded as reinforcements in a matrix, syntactic foams are also known as foamed composites. They are closed cell rigid foams, exhibiting relatively higher densities compared to their conventional blown or self expanding foams and higher specific mechanical properties. What renders this class of foam even more interesting is their tailorability, which can be done by altering the type of microbubbles and/ or its volume fraction. Their lightweight features coupled with excellent specific mechanical properties, low moisture absorption and low thermal conductivity have enabled the usage of syntactic foams in demanding applications, especially navy and aerospace. Syntactic foams are also gaining popularity as 'core' materials in sandwiched structures for protection against primary and secondary blasts e.g. underbelly of tanks. The use of syntactic foams in these explosion-prone areas could reduce the severity by absorbing the blast energy either completelyor partially. This energy absorption ability of syntactic foams is attributed to the presence of brittle microbubbles, which undergorupertureupon encountering a dynamic mechanical load and in the process absorb substantial amount of energy.

The thesis acquaints the preparation, characterization and results of polymeric syntactic foams containing appropriate fillers for potential as blast mitigating material. In

this context, quasi-static and dynamic mechanical properties of syntactic foams have been evaluated. The flow behaviour of the foam formulations has also been investigated.

8.1.1. Chemorheology and Mechanical Properties of Epoxy Syntactic Foams

- For maximum energy absorption, syntactic foams with high microbubble loadings are desirable. However, the processing of such formulations is impractical in view of their high viscosity. In this context, the rheological behaviour of epoxy resin–hollow glass microbubble formulations with varying microbubble loadings (0-70) % v/v has been studied. The introduction of either kind of glass microbubbles (K15, density = 150 kg/m^3 and K46, density = 460 kg/m^3) led to a significant increase in the viscosity, rendering formulations with high microbubble loadings (≥ 60 % v/v) practically impossible to process without due dilution. Interestingly, there is an upper limit of microbubble loading (hexagonal closed packing), restricting the packing to a maximum of ~ 74 % (v/v). Our studies reveal that processing by stir casting techniques permits a maxima of ~ 64 % (v/v) microbubbles; which lead to formation of a 'Jammed' state, essentially ending up in a random close packed structure.

- Rheological studies revealed that the mechanism of epoxy and aminereaction remained unaltered due to inclusion of microbubbles. Activation energies associated with the curing of neat epoxy as well as epoxy-glass microbubble syntactic foam formulations (SF46-40 and SF15-40) were found to be of the same order.

- Mechanical properties of all the syntactic foams were determined in the quasi-static mode. A concomitant decrease in quasi-static mechanical properties withincreasing loadings of either type of glass microbubbles was observed. However, specific mechanical properties improved substantially and optimal

168

improvements were observed in formulations containing 40 % microbubble loading.An increase of ~ 72 % and ~ 192 % was observed in the quasi-static specific toughness values of SF15-40 and SF46-40 syntactic foams respectively.

- High-strain-rate studies using a split hopkinson bar were performed to establish the strain-rate sensitivity of polymer syntactic foams. In line with quasi-static tests, the flow stress (maxima in the stress-strain curve) for compositions containing 40 % loading was substantially higher 151 MPa as compared to 38 MPa (60 % loadings).

- Syntactic foams were subjected to controlled transient blast loadings on an experimental shock tube facility. Sandwich type specimens with a core of epoxy-HGM 40 % (v/v) microbubble loadings were found to withstand dynamic blast loads ~ 90 psi, while control samples (without foam core) underwent extensive deformation (microstrain: 1701 $\mu\varepsilon$) at ~ 36 psi, thereby highlighting the potential of syntactic foam as a energy absorbingmaterialsfor blast mitigating applications.

8.1.2. Two-dimensional (2D) Layered Filler Reinforced Epoxy Syntactic Foams

- Three different types of 2D layered fillers were studied to explore their potential towards improving the mechanical properties of epoxy-HGM syntactic foams, namely molybdenum disulfide (0.01-0.04 % v/v), reduced graphene oxide (0.1-1 % v/v) and organically modified nanoclay (0.1-1 % v/v).

- Homogeneous dispersion of these fillers could be achieved by ultrasonication for extended time periods (~ 12 h).The ultrasonication step also led to a reduction in the void content of the syntactic foam specimens.

- Rheological studies revealed that the incorporation of nanofillers did not affect the processability of these formulations. Negligible change in the viscosity of the formulations was observed,probably due to the low loadings of the filler.

- Isothermal gelation profiles at 60 °C of neat syntactic foams and those containing 2D fillers were similar and depicted an initial dominance of loss modulus over storage modulus, appearance of a cross-over region indicating the gel point of formulation and storage modulus becoming comparable to the loss modulus and complete crosslinking of the sample.

- Quasi-static mechanical properties demonstrated a ~ 27 % increase in tensile strength, ~ 33 % increase in flexural strength and ~ 21 % increase in compressive toughness and specific compressive toughness for MoS_2 (0.02 % v/v) reinforced syntactic foams.

- For reduced graphene oxide (0.5 % v/v), ~ 15 % increase in the tensile strength, ~ 9 % in compressive strength, ~ 28 % increase in the flexural strength and ~ 20 % increase in compressive and specific compressive toughness was observed ascompared to neat syntactic foam (S40).

- Improvements in the property ofnanoclay reinforced syntactic foams (S40C5) as comparable to neat foams were of the order of ~ 10 %, ~ 2 %, ~ 17 %, ~ 13 % and ~ 13 % in tensile strength, compressive strength, flexural strength, compressive toughness and specific compressive toughness respectively.

- Introduction of layered fillers led to an increase in the flow stress values at high strain rates indicating their potential as a reinforcing filler under high strain rates.

8.1.3. Poly(dimethylsiloxane) Toughened Epoxy Syntactic Foams

- Elastomeric poly (dimethylsiloxane) microspheres were prepared by the reaction of vinyl terminated silicone macromonomer with a platinum based curing agent using a suspension polymerisationroute.

- By varying the operating parameters(solution concentration and stirring speed) PDMS microspheres ranging from 58-255 μm could be obtained.

- Thermogravimetric analysis of the preformed elastomeric microspheres depicted exceptional thermal stability ($T_{5\%}$ > 400 °C) and a high char content (68 % at 600 °C).

- Introduction of PDMS microspheres (3-7 % v/v) did not alter the rheological profile of epoxy-HGM formulation significantly, however led to substantial enhancement in the quasi-static flexural properties of syntactic foams, while the compressive properties remained unaffected.

- Improvements in SF46-40 were of the order of ~ 18 %, ~ 24 % and ~ 37 % in flexural strength, flexural strain and flexural toughness respectively. For SF15-40, improvementof the order of ~ 66 %, ~ 78 % and ~ 184 % in flexural strength, flexural strain and flexural toughness respectively was observed.

8.1.4. Electrospun Nanofiber Reinforced Epoxy Syntactic Foams

- Syntactic foams of epoxy-hollow glass microbubbles were reinforced with electrospun polyamide nanofibers (0.25-4 % v/v).

- The operating conditions favourable for preparing smooth electrospun nanofibers were first optimised. At lower solution concentrations, electrospraying was observed. As the solution concentraion increased, fibers with beaded morphology

171

were formed and at concetration > 15 % w/v, sufficient entanglements between the macromolecules led to formation of smooth beadless fibers.

- A reduction in the void content was observed for nylon 6 reinforced syntactic foams. The voids content reduced from 5.2 % to 2.4 % for SF40 and SF40N25 specimens respectively, i.e. a reduction of ~ 53 % was observed.

- Introduction of nylon 6 nanofibers resulted in only marginal improvements in compressive properties when the fibers were dispersed randomly at low concentrations (< 1 % v/v).

- Proper orientation of the nylon 6 nanofibers (0.25 % v/v) normal to the load axis resulted in ~ 7 % improvements in compressive properties. However, the flexural strength and flexural strain enhanced significantly by 75 % and 62 %.

8.1.5. Epoxy-Epoxy Microbubble Syntactic Foams

- Epoxy microspheres were prepared by interfacial engineering reaction of silicone suspended epoxy with triethylene tetramine. The microsphere dimensions and core contentcould be tuned by varying the stirring speed (400-600 rpm)and epoxy-hardener ratio (100:13- 100:2).

- A stirring speed of 600 rpm and epoxy amine ratio of 100:2 favoured the formation of epoxy microcapsules in the size range of 90-100 μm with a core content of 25 %.

- Refluxed epoxy microbubbles were employed as fillers (40-60 % v/v) in epoxy syntactic foams. The density of hollow epoxy microbubbles was 850 kg m^{-3}.

- A concomitant decrease in the quasi-static mechanical properties was observed as the volume fraction of epoxy microbubbles was increased.

- Substantial increase in compressive toughness (~ 127 %) was observed for E-40 compared to neat syntactic foam.

- Epoxy microbubbles offer a good candidature to prepare epoxy syntactic foams. It is however, possible to obtain larger improvement in properties with further increase in the core content.

8.1.6. Polybenzoxazine-Glass Microbubble Syntactic Foams

- Polybenzoxazine syntactic foams were prepared by incorporation of hollow glass microbubbles (K46, 30-60 % v/v) into a bisphenol F aniline based benzoxazine resin.

- Non-isothermal calorimetric studies on neat resin revealed that the initiation of polymerization occurred ~ 216 °C and reached its maxima at 231 °C. The same remained unaffected upon addition of hollow glass microbubbles.

- Substantial increase in complex viscosity of the formulations, compared to the neat resin, was evident with increasing loading of glass microbubbles.

- Rheological studies including temperature sweep experiment indicated gelling at ~ 205 °C, which remained unchanged upon inclusion of glass microbubbles. However, a slight increase in the gel time (isothermal study, T = 200 °C) was observed for microbubbles filled formulations due to the physical restraint offered by microbubbles to the reactive oxazine terminals.

- Neat polybenzoxazines exhibited a compressive strength of ~ 171 MPa. The inclusion of glass microbubbles (40-60 % v/v) led to a decrease in the compressive strengths however, the properties were comparatively superior to those of epoxy syntactic foams at comparable loadings. An enhancement of ~ 200 % in compressive toughness was observed as compared to neat polybenzoxazine.

- The high thermal stability combined with exceptional compressive properties of polybenzoxazine syntactic foams open up new vistas in high tech applications.

8.2. Recommendations for future work

- Endowing self-healing capabilities in syntactic foams would render highly diversified and advanced applications of these foams in the future.

- Development of elastomeric especially polyurea based syntactic foams in the near future would enhance the applications of these foams in defence and allied areas.

References

1.   Kelly, M., H. Arora, and J.P. Dear, *The Comparison of Various Foam Polymer Types in Composite Sandwich Panels Subjected to Full Scale Air Blast Loading.* Procedia Engineering, 2014. **88**(0): p. 48-53.

2.   Daniel, I.M., J.-M. Cho, and B.T. Werner, *Characterization and modeling of stain-rate-dependent behavior of polymeric foams.* Composites Part A: Applied Science and Manufacturing, 2013. **45**(0): p. 70-78.

3.   Gardner, N., et al., *Blast Mitigation in a Sandwich Composite Using Graded Core and Polyurea Interlayer.* Experimental Mechanics, 2012. **52**(2): p. 119-133.

4.   Chakravarty, U.K., *An investigation on the dynamic response of polymeric, metallic, and biomaterial foams.* Composite Structures, 2010. **92**(10): p. 2339-2344.

5.   Langdon, G.S., et al., *The response of sandwich structures with composite face sheets and polymer foam cores to air-blast loading: Preliminary experiments.* Engineering Structures, 2012. **36**(0): p. 104-112.

6.   Yang, S. and C. Qi, *Blast-Resistant Improvement of Sandwich Armor Structure with Aluminum Foam Composite.* Advances in Materials Science and Engineering, 2013. **2013**: p. 8.

7.   Sadler, R.L., et al., *Water immersion effect on swelling and compression properties of Eco-Core, PVC foam and balsa wood.* Composite Structures, 2009. **90**(3): p. 330-336.

8.   Gupta, N. and E. Woldesenbet, *Hygrothermal studies on syntactic foams and compressive strength determination.* Composite Structures, 2003. **61**(4): p. 311-320.

9.   Lee, S.T., et al., *Polymeric Foams*, in *Science and Technology*. 2006, CRC Press: Boca Raton.

10. Lee, L.J., et al., *Polymer nanocomposite foams.* Composites Science and Technology, 2005. **65**(15): p. 2344-2363.

11. Landrock, A.H., *5 - Miscellaneous and specialty foams: Epoxy Foams, Polyester Foams, Silicone Foams, Urea-Formaldehyde Foams, Polybenzimidazole, Foams, Polyimide Foams, Polyphosphazene Foams, and Syntactic Foams*, in *Handbook of Plastic Foams*, A.H. Landrock, Editor. 1995, William Andrew Publishing: Park Ridge, NJ. p. 253-266.

12. Ferguson, J.B., et al., *Al–Al2O3 syntactic foams—Part II: Predicting mechanical properties of metal matrix syntactic foams reinforced with ceramic spheres.* Materials Science and Engineering: A, 2013. **582**(0): p. 423-432.

13. Song, B., et al., *Confinement effects on the dynamic compressive properties of an epoxy syntactic foam.* Composite Structures, 2005. **67**(3): p. 279-287.

14. Zhang, L. and J. Ma, *Effect of coupling agent on mechanical properties of hollow carbon microsphere/phenolic resin syntactic foam.* Composites Science and Technology, 2010. **70**(8): p. 1265-1271.

15. Labella, M., et al., *Mechanical and thermal properties of fly ash/vinyl ester syntactic foams.* Fuel, 2014. **121**(0): p. 240-249.

16. Pellegrino, A., et al., *The mechanical response of a syntactic polyurethane foam at low and high rates of strain.* International Journal of Impact Engineering, 2015. **75**(0): p. 214-221.

17. Kumar, B.R.B., et al., *Data characterizing tensile behavior of cenosphere/HDPE syntactic foam.* Data in Brief, 2016. **6**(Supplement C): p. 933-941.

18. Jayavardhan, M.L., et al., *Development of glass microballoon/HDPE syntactic foams by compression molding.* Composites Part B: Engineering, 2017. **130**(Supplement C): p. 119-131.

19. Sharma, J., N. Chand, and M.N. Bapat, *Effect of cenosphere on dielectric properties of low density polyethylene.* Results in Physics, 2012. **2**(Supplement C): p. 26-33.

20. Bharath Kumar, B.R., et al., *Effect of particle surface treatment and blending method on flexural properties of injection-molded cenosphere/HDPE syntactic foams.* Journal of Materials Science, 2016. **51**(8): p. 3793-3805.

21. Bharath Kumar, B.R., et al., *Processing of cenosphere/HDPE syntactic foams using an industrial scale polymer injection molding machine.* Materials & Design, 2016. **92**: p. 414-423.

22. Bharath Kumar, B.R., et al., *Quasi-Static and High Strain Rate Compressive Response of Injection-Molded Cenosphere/HDPE Syntactic Foam.* JOM, 2016. **68**(7): p. 1861-1871.

23. Mae, H., M. Omiya, and K. Kishimoto, *Effects of strain rate and density on tensile behavior of polypropylene syntactic foam with polymer microballoons.* Materials Science and Engineering: A, 2008. **477**(1): p. 168-178.

24. Lehmhus, D., et al., *Quasi-static and Dynamic Mechanical Performance of Glass Microsphere- and Cenosphere-based 316L Syntactic Foams.* Procedia Materials Science, 2014. **4**(0): p. 383-387.

25. Swetha, C. and R. Kumar, *Quasi-static uni-axial compression behaviour of hollow glass microspheres/epoxy based syntactic foams.* Materials & Design, 2011. **32**(8-9): p. 4152-4163.

26. Li, P., et al., *Strain rate dependent compressive properties of glass microballoon epoxy syntactic foams.* Materials Science and Engineering: A, 2009. **515**(1–2): p. 19-25.

27.   Gupta, N. and R. Nagorny, *Tensile properties of glass microballoon-epoxy resin syntactic foams.* Journal of Applied Polymer Science, 2006. **102**(2): p. 1254-1261.

28.   Zhu, B., et al., *Thermal, dielectric and compressive properties of hollow glass microsphere filled epoxy-matrix composites.* Journal of Reinforced Plastics and Composites, 2012. **31**(19): p. 1311-1326.

29.   Lin, T.C., N. Gupta, and A. Talalayev, *Thermoanalytical characterization of epoxy matrix-glass microballoon syntactic foams.* Journal of Materials Science, 2009. **44**(6): p. 1520-1527.

30.   Deepthi, M.V., et al., *Mechanical and thermal characteristics of high density polyethylene–fly ash Cenospheres composites.* Materials & Design, 2010. **31**(4): p. 2051-2060.

31.   Dando, K.R., et al., *Production and characterization of epoxy syntactic foams highly loaded with thermoplastic microballoons.* Journal of Cellular Plastics. **0**(0): p. 0021955X17700093.

32.   Goel, M.D., et al., *Dynamic compression behavior of cenosphere aluminum alloy syntactic foam.* Materials & Design, 2012. **42**: p. 418-423.

33.   Goel, M.D., et al., *Effect of strain rate and relative density on compressive deformation behavior of aluminum cenosphere syntactic foam.* Materials Science and Engineering: A, 2014. **590**(0): p. 406-415.

34.   Shah, D.U., F. Vollrath, and D. Porter, *Silk cocoons as natural macro-balloon fillers in novel polyurethane-based syntactic foams.* Polymer, 2015. **56**(0): p. 93-101.

35.   Fine, T., H. Sautereau, and V. Sauvant-Moynot, *Innovative processing and mechanical properties of high temperature syntactic foams based on a*

thermoplastic/thermoset matrix. Journal of Materials Science, 2003. **38**(12): p. 2709-2716.

36.   Bharath Kumar, B.R., et al., *Effect of cenosphere surface treatment and blending method on the tensile properties of thermoplastic matrix syntactic foams.* Journal of Applied Polymer Science, 2016. **133**(35): p. n/a-n/a.

37.   Higuchi, M., et al., *Controlling of Distribution of Mechanical Properties in Functionally-Graded Syntactic Foams for Impact Energy Absorption.* Materials Science Forum, 2012. **706-709**: p. 729-734.

38.   Gupta, N. and W. Ricci, *Comparison of compressive properties of layered syntactic foams having gradient in microballoon volume fraction and wall thickness.* Materials Science and Engineering: A, 2006. **427**(1): p. 331-342.

39.   Caeti, R., N. Gupta, and M. Porfiri, *Processing and compressive response of functionally graded composites.* Materials Letters, 2009. **63**(22): p. 1964-1967.

40.   Tagliavia, G., M. Porfiri, and N. Gupta, *Influence of moisture absorption on flexural properties of syntactic foams.* Composites Part B: Engineering, 2012. **43**(2): p. 115-123.

41.   S., K.C., et al., *Processing and compressive strengths of syntactic foams with and without fibrous reinforcements.* Journal of Applied Polymer Science, 2001. **81**(2): p. 405-411.

42.   Palumbo, M. and E. Tempesti, *Fiber-Reinforced Syntactic Foams as a New Lightweight Structural Three-Phase Composite.* Applied Composite Materials, 2001. **8**(5): p. 343-359.

43.   Bardella, L., et al., *A critical evaluation of micromechanical models for syntactic foams.* Mechanics of Materials, 2012. **50**: p. 53-69.

44. Shunmugasamy, V.C., D. Pinisetty, and N. Gupta, *Electrical properties of hollow glass particle filled vinyl ester matrix syntactic foams.* Journal of Materials Science, 2014. **49**(1): p. 180-190.

45. Yung, K.C., et al., *Preparation and properties of hollow glass microsphere-filled epoxy-matrix composites.* Composites Science and Technology, 2009. **69**(2): p. 260-264.

46. Shutov, F.A., *Syntactic polymer foams*, in *Chromatography/Foams/Copolymers*. 1986, Springer Berlin Heidelberg: Berlin, Heidelberg. p. 63-123.

47. Gupta, N., et al., *Applications of Polymer Matrix Syntactic Foams.* JOM, 2014. **66**(2): p. 245-254.

48. Frollini, E., C.G. Silva, and E.C. Ramires, *2 - Phenolic resins as a matrix material in advanced fiber-reinforced polymer (FRP) composites*, in *Advanced Fibre-Reinforced Polymer (FRP) Composites for Structural Applications*, J. Bai, Editor. 2013, Woodhead Publishing. p. 7-43.

49. Rohatgi, P., N. Gupta, and S. Alaraj, *Thermal expansion of aluminum–fly ash cenosphere composites synthesized by pressure infiltration technique.* Journal of Composite materials, 2006. **40**(13): p. 1163-1174.

50. Porfiri, M., N. Nguyen, and N. Gupta, *Thermal conductivity of multiphase particulate composite materials.* Journal of materials science, 2009. **44**(6): p. 1540-1550.

51. Dimchev, M., R. Caeti, and N. Gupta, *Effect of carbon nanofibers on tensile and compressive characteristics of hollow particle filled composites.* Materials & Design, 2010. **31**(3): p. 1332-1337.

52.   Gupta, N. and V.C. Shunmugasamy, *High strain rate compressive response of syntactic foams: Trends in mechanical properties and failure mechanisms.* Materials Science and Engineering: A, 2011. **528**(25–26): p. 7596-7605.

53.   Santhosh Kumar, K.S., C.P. Reghunadhan Nair, and K.N. Ninan, *Mechanical properties of polybenzoxazine syntactic foams.* Journal of Applied Polymer Science, 2008. **108**(2): p. 1021-1028.

54.   Gupta, N. and E. Woldesenbet, *Microballoon wall thickness effects on properties of syntactic foams.* Journal of Cellular Plastics, 2004. **40**(6): p. 461-480.

55.   Shunmugasamy, V.C., D. Pinisetty, and N. Gupta, *Thermal expansion behavior of hollow glass particle/vinyl ester composites.* Journal of Materials Science, 2012. **47**(14): p. 5596-5604.

56.   Gupta, N., et al., *Characterization of Mechanical and Electrical Properties of Epoxy-Glass Microballoon Syntactic Composites.* Ferroelectrics, 2006. **345**(1): p. 1-12.

57.   Rizzi, E., E. Papa, and A. Corigliano, *Mechanical behavior of a syntactic foam: experiments and modeling.* International Journal of Solids and Structures, 2000. **37**(40): p. 5773-5794.

58.   Gupta, N., E. Woldesenbet, and P. Mensah, *Compression properties of syntactic foams: effect of cenosphere radius ratio and specimen aspect ratio.* Composites Part A: Applied Science and Manufacturing, 2004. **35**(1): p. 103-111.

59.   Gupta, N., R. Ye, and M. Porfiri, *Comparison of tensile and compressive characteristics of vinyl ester/glass microballoon syntactic foams.* Composites Part B: Engineering, 2010. **41**(3): p. 236-245.

60.   Andrews, E., W. Sanders, and L.J. Gibson, *Compressive and tensile behaviour of aluminum foams.* Materials Science and Engineering: A, 1999. **270**(2): p. 113-124.

61. Roberts, A.P. and E.J. Garboczi, *Elastic moduli of model random three-dimensional closed-cell cellular solids.* Acta Materialia, 2001. **49**(2): p. 189-197.

62. Gibson, L.J., *Biomechanics of cellular solids.* Journal of biomechanics, 2005. **38**(3): p. 377-399.

63. Raghu, P., S. Kunigal, and R. Larry, *Energy Absorption Performance of a Eco-Core - A Syntactic Foam*, in *48th AIAA/ASME/ASCE/AHS/ASC Structures, Structural Dynamics, and Materials Conference*. 2007, American Institute of Aeronautics and Astronautics.

64. Irshidat, M., *Physics-Based Simulation and Experiment on Blast Protection of Infill Walls and Sandwich Composites Using New Generation of Nano Particle Reinforced Materials*, in *Engineering Science*. 2010, The University of Mississippi.

65. Nguyen, N.Q. and N. Gupta, *Analyzing the effect of fiber reinforcement on properties of syntactic foams.* Materials Science and Engineering: A, 2010. **527**(23): p. 6422-6428.

66. Zhang, L. and J. Ma, *Effect of carbon nanofiber reinforcement on mechanical properties of syntactic foam.* Materials Science and Engineering: A, 2013. **574**(0): p. 191-196.

67. Ullas, A.V., et al., *Electrospun Polyamide Nanofiber-Reinforced Hybrid Syntactic Foams.* Polymer-Plastics Technology and Engineering, 2016. **55**(17): p. 1797-1806.

68. Maharsia, R.R. and H.D. Jerro, *Enhancing tensile strength and toughness in syntactic foams through nanoclay reinforcement.* Materials Science and Engineering: A, 2007. **454-455**: p. 416-422.

69. Wouterson, E.M., et al., *Nano-toughening versus micro-toughening of polymer syntactic foams.* Composites Science and Technology, 2007. **67**(14): p. 2924-2933.

70. Gupta, N., et al., *Studies on compressive failure features in syntactic foam material.* Journal of Materials Science, 2001. **36**(18): p. 4485-4491.

71. Samsudin, S.S., et al., *Development and characterization of epoxy syntactic foam filled with epoxy hollow spheres.* Express Polymer Letters, 2011. **5**(7).

72. Wang, L., et al., *Flexural properties of epoxy syntactic foams reinforced by fiberglass mesh and/or short glass fiber.* Materials & Design, 2014. **55**(0): p. 929-936.

73. Colloca, M., N. Gupta, and M. Porfiri, *Tensile properties of carbon nanofiber reinforced multiscale syntactic foams.* Composites Part B: Engineering, 2013. **44**(1): p. 584-591.

74. Asif, A., V.L. Rao, and K.N. Ninan, *Nanoclay reinforced thermoplastic toughened epoxy hybrid syntactic foam: Surface morphology, mechanical and thermo mechanical properties.* Materials Science and Engineering: A, 2010. **527**(23): p. 6184-6192.

75. Saha, M.C. and S. Nilufar, *Nanoclay-reinforced syntactic foams: Flexure and thermal behavior.* Polymer Composites, 2010. **31**(8): p. 1332-1342.

76. Zegeye, E., A.K. Ghamsari, and E. Woldesenbet, *Mechanical properties of graphene platelets reinforced syntactic foams.* Composites Part B: Engineering, 2014. **60**(0): p. 268-273.

77. Maharsia, R., N. Gupta, and H.D. Jerro, *Investigation of flexural strength properties of rubber and nanoclay reinforced hybrid syntactic foams.* Materials Science and Engineering: A, 2006. **417**(1–2): p. 249-258.

78. Gupta, N., R. Maharsia, and H. Dwayne Jerro, *Enhancement of energy absorption characteristics of hollow glass particle filled composites by rubber addition.* Materials Science and Engineering: A, 2005. **395**(1): p. 233-240.

79. Huang, Y.-J., L. Vaikhanski, and S.R. Nutt, *3D long fiber-reinforced syntactic foam based on hollow polymeric microspheres.* Composites Part A: Applied Science and Manufacturing, 2006. **37**(3): p. 488-496.

80. S., S.K.K., R.N.C. P., and N.K. N., *Silica fiber–polybenzoxazine–syntactic foams; Processing and properties.* Journal of Applied Polymer Science, 2008. **107**(2): p. 1091-1099.

81. Ouellet, S., D. Cronin, and M. Worswick, *Compressive response of polymeric foams under quasi-static, medium and high strain rate conditions.* Polymer Testing, 2006. **25**(6): p. 731-743.

82. Saurabh, C., et al., *Microwave assisted glycolysis of poly(ethylene terepthalate) for preparation of polyester polyols.* Journal of Applied Polymer Science, 2013. **129**(5): p. 2779-2788.

83. Roy, P.K., et al., *Tertiary recycling of poly(ethylene terephthalate) wastes for production of polyurethane–polyisocyanurate foams.* Journal of Environmental Chemical Engineering, 2013. **1**(4): p. 1062-1069.

84. Luong, D.D., et al., *High Strain Rate Compressive Behavior of Polyurethane Resin and Polyurethane/Al2O3 Hollow Sphere Syntactic Foams.* Journal of Composites, 2014. **2014**: p. 10.

85. Corp., S.D.L.M.U.S.M., *The USS Cole is towed away from the port city of Aden, Yemen. 001029-M-0557M-011.* 2000.

86. D.I.D.s.member., *Force Protection's MRAPS to Stalk Mines on Battlefiled.* 2011.

87. Pinisetty, D., V.C. Shunmugasamy, and N. Gupta, *6 - Hollow Glass Microspheres in Thermosets—Epoxy Syntactic Foams*, in *Hollow Glass Microspheres for Plastics, Elastomers, and Adhesives Compounds*, S.E. Amos and B. Yalcin, Editors. 2015, William Andrew Publishing: Oxford. p. 147-174.

88. Ullas, A.V., D. Kumar, and P.K. Roy, *Poly(dimethylsiloxane)-toughened syntactic foams.* Journal of Applied Polymer Science, 2018. **135**(8): p. 45882.

89. Jha, N., et al., *Titanium cenosphere syntactic foam with coarser cenosphere fabricated by powder metallurgy at lower compaction load.* Transactions of Nonferrous Metals Society of China, 2014. **24**(1): p. 89-99.

90. Poveda, R.L. and N. Gupta, *Carbon-Nanofiber-Reinforced Syntactic Foams: Compressive Properties and Strain Rate Sensitivity.* JOM, 2013. **66**(1): p. 66-77.

91. Benderly, D., et al., *Effect of composition on the fracture toughness and flexural strength of syntactic foams.* Polymer Composites, 2004. **25**(2): p. 229-236.

92. Ullas, A.V., et al., *Epoxy-glass Microballoon Syntactic Foams for Blast Mitigating Applications.* Defence Science Journal, 2018. **68**(2): p. 8.

93. Vitali, N.F., *Shock (Blast) Mitigation by "Soft" Condensed Matter.* MRS Symp. Proc, 2003. **759**: p. 4.3.1- 4.3.12.

94. Tan, P.J., S.R. Reid, and J.J. Harrigan, *On the dynamic mechanical properties of open-cell metal foams – A re-assessment of the 'simple-shock theory'.* International Journal of Solids and Structures, 2012. **49**(19): p. 2744-2753.

95. Ullas, A., et al., *Epoxy-Filled Microcapsules by Interfacial Engineering.* Polymer-Plastics Technology and Engineering, 2016. **55**(9): p. 937-942.

96. Bardella, L., et al., *A micromechanical model for quasi-brittle compressive failure of glass-microballoons/thermoset-matrix syntactic foams.* Journal of the European Ceramic Society, 2014. **34**(11): p. 2605-2616.

97.   Panteghini, A. and L. Bardella, *On the compressive strength of glass microballoons-based syntactic foams.* Mechanics of Materials, 2015. **82**(0): p. 63-77.

98.   Ambika Devi, K., et al., *Syntactic foam composites of epoxy-allyl phenol-bismaleimide ternary blend—Processing and properties.* Journal of Applied Polymer Science, 2007. **105**(6): p. 3715-3722.

99.   Abrate, S., *Impulsive Response of Sandwich Structures.* Procedia Engineering, 2014. **88**(0): p. 62-68.

100.   Atas, C. and C. Sevim, *On the impact response of sandwich composites with cores of balsa wood and PVC foam.* Composite Structures, 2010. **93**(1): p. 40-48.

101.   d'Almeida, J.R.M., *An analysis of the effect of the diameters of glass microspheres on the mechanical behavior of glass-microsphere/epoxy-matrix composites.* Composites Science and Technology, 1999. **59**(14): p. 2087-2091.

102.   Huang, R. and P. Li, *Elastic behaviour and failure mechanism in epoxy syntactic foams: The effect of glass microballoon volume fractions.* Composites Part B: Engineering, 2015. **78**(0): p. 401-408.

103.   Karthikeyan, C.S., S. Sankaran, and Kishore, *Elastic behaviour of plain and fibre-reinforced syntactic foams under compression.* Materials Letters, 2004. **58**(6): p. 995-999.

104.   Alonso, M.V., M.L. Auad, and S. Nutt, *Short-fiber-reinforced epoxy foams.* Composites Part A: Applied Science and Manufacturing, 2006. **37**(11): p. 1952-1960.

105.   Kang, S., et al., *Preparation and characterization of epoxy composites filled with functionalized nanosilica particles obtained via sol–gel process.* Polymer, 2001. **42**(3): p. 879-887.

106. Gassan, J. and A.K. Bledzki, *Possibilities for improving the mechanical properties of jute/epoxy composites by alkali treatment of fibres.* Composites Science and Technology, 1999. **59**(9): p. 1303-1309.

107. Mostafa, H.E., W.W. El-Dakhakhni, and W.F. Mekky, *Use of reinforced rigid polyurethane foam for blast hazard mitigation.* Journal of Reinforced Plastics and Composites, 2010. **29**(20): p. 3048-3057.

108. Verdejo, R., et al., *Fluid dynamics of evolving foams.* Physical Chemistry Chemical Physics, 2009. **11**(46): p. 10860-10866.

109. Kalpathy, S. and A. Ravi Shreyes, *Thermodiffusion as a means to manipulate liquid film dynamics on chemically patterned surfaces*. Vol. 146. 2017. 214706.

110. Jahsman, W.E., *Static and Dynamic Material Behavior of Syntactic Foam*, in *Mechanical Behavior of Materials under Dynamic Loads: Symposium Held in San Antonio, Texas, September 6-8, 1967*, U.S. Lindholm, Editor. 1968, Springer Berlin Heidelberg: Berlin, Heidelberg. p. 365-387.

111. Jodrey, W.S. and E.M. Tory, *Computer simulation of close random packing of equal spheres.* Physical Review A, 1985. **32**(4): p. 2347-2351.

112. Visscher, W.M. and M. Bolsterli, *Random Packing of Equal and Unequal Spheres in Two and Three Dimensions.* Nature, 1972. **239**: p. 504.

113. Torquato, S., T.M. Truskett, and P.G. Debenedetti, *Is Random Close Packing of Spheres Well Defined?* Physical Review Letters, 2000. **84**(10): p. 2064-2067.

114. Saha, M.C., et al., *Processing and performance evaluation of hollow microspheres filled epoxy composites.* Polymer Composites, 2008. **29**(3): p. 293-301.

115. Bunn, P. and J.T. Mottram, *Manufacture and compression properties of syntactic foams.* Composites, 1993. **24**(7): p. 565-571.

116. Islam, M.M. and H.S. Kim, *Manufacture of Syntactic Foams: Pre-Mold Processing.* Materials and Manufacturing Processes, 2007. **22**(1): p. 28-36.

117. Pötschke, P., T.D. Fornes, and D.R. Paul, *Rheological behavior of multiwalled carbon nanotube/polycarbonate composites.* Polymer, 2002. **43**(11): p. 3247-3255.

118. Xiao, H.-W., S.-Q. Huang, and T. Jiang, *Morphology, rheology, and mechanical properties of dynamically cured EPDM/PP blend: Effect of curing agent dose variation.* Journal of Applied Polymer Science, 2004. **92**(1): p. 357-362.

119. Jain, A.K., N.K. Gupta, and A.K. Nagpal, *Effect of dynamic cross-linking on melt rheological properties of polypropylene/ethylene-propylene-diene rubber blends.* Journal of Applied Polymer Science, 2000. **77**(7): p. 1488-1505.

120. Devi, A.K., et al., *Syntactic Foam Composites of Epoxy-Allyl Phenol-Bismaleimide Ternary Blend—Processing and Properties.* Journal of Applied Polymer Science, 2007. **105**: p. 3715-3722.

121. Halley, P.J. and M.E. Mackay, *Chemorheology of thermosets—an overview.* Polymer Engineering & Science, 1996. **36**(5): p. 593-609.

122. Roller, M.B., *Rheology of curing thermosets: A review.* Polymer Engineering & Science, 1986. **26**(6): p. 432-440.

123. Grenier-Loustalot, M.-F. and P. Grenier, *The mechanism of epoxy-resin curing in the presence of glass and carbon fibres.* Polymer, 1992. **33**(6): p. 1187-1199.

124. Karbhari, V.M. and R. Lee, *On the Effect of E-Glass Fiber on the Cure Behavior of Vinylester Composites.* Journal of Reinforced Plastics and Composites, 2002. **21**(10): p. 901-918.

125. Roy, P.K., et al., *Effect of SBA-15 on the energy absorption characteristics of epoxy resin for blast mitigation applications.* Iranian Polymer Journal, 2013. **22**(9): p. 709-719.

126. Chaudhary, S., et al., *Toughening of Epoxy with Preformed Polyethylene Thermoplastic Filler.* Polymer-Plastics Technology and Engineering, 2015. **54**(9): p. 907-915.

127. Li, H., et al., *Preparation of high performance adhesives matrix based on epoxy resin modified by bis-hydroxy terminated polyphenylene oxide.* Journal of Adhesion Science and Technology, 2018. **32**(11): p. 1224-1238.

128. Kinloch, A.J., *Toughening Epoxy Adhesives to Meet Today's Challenges.* MRS Bulletin, 2003. **28**(6): p. 445-448.

129. Sprenger, S., *Epoxy resins modified with elastomers and surface-modified silica nanoparticles.* Polymer, 2013. **54**(18): p. 4790-4797.

130. Marimuthu, S., L.M. Suguna, and R.B.S. R., *Chemistry of Siloxane Amide as a New Curing Agent for Epoxy Resins: Material Characterization and Properties.* Macromolecular Chemistry and Physics, 2005. **206**(24): p. 2501-2511.

131. H., B. and Z.S. A., *Studies in the molecular weight distribution of epoxide resins. IV. Molecular weight distributions of epoxide resins made from bisphenol a and epichlorohydrin.* Journal of Applied Polymer Science, 1977. **21**(7): p. 1843-1857.

132. S., E.N., et al., *Kinetics of epoxide resins formation from epichlorohydrin and bisphenol-A.* Journal of Polymer Science: Polymer Chemistry Edition, 1982. **20**(5): p. 1231-1245.

133. Brian, D. and J.J.L. P., *Chain transfer agents in cationic photopolymerization of a bis-cycloaliphatic epoxide monomer: Kinetic and physical property effects.*

Journal of Polymer Science Part A: Polymer Chemistry, 2013. **51**(9): p. 2058-2067.

134. Ehlers, J.-E., et al., *Theoretical Study on Mechanisms of the Epoxy−Amine Curing Reaction.* Macromolecules, 2007. **40**(12): p. 4370-4377.

135. Narkis, M., S. Kenig, and M. Puterman, *Three-phase syntactic foams.* Polymer Composites, 1984. **5**(2): p. 159-165.

136. Ivankovic, M., et al., *Curing kinetics and chemorheology of epoxy/anhydride system.* Journal of Applied Polymer Science, 2003. **90**(11): p. 3012-3019.

137. Zeltmann, S.E., et al., *Prediction of modulus at various strain rates from dynamic mechanical analysis data for polymer matrix composites.* Composites Part B: Engineering, 2017. **120**: p. 27-34.

138. Zeltmann, S.E., et al., *Prediction of strain rate sensitivity of high density polyethylene using integral transform of dynamic mechanical analysis data.* Polymer, 2016. **101**(Supplement C): p. 1-6.

139. Park, S.-J., F.-L. Jin, and C. Lee, *Preparation and physical properties of hollow glass microspheres-reinforced epoxy matrix resins.* Materials Science and Engineering: A, 2005. **402**(1): p. 335-340.

140. Chaudhary, S., et al., *Strain rate sensitivity of toughened epoxy.* Iranian Polymer Journal, 2015. **24**(10): p. 871-881.

141. Colloca, M., N. Gupta, and M. Porfiri, *Tensile properties of carbon nanofiber reinforced multiscale syntactic foams.* Composites: Part B 2013. **44**: p. 584-591.

142. Ku-Herrera, J.J., et al., *Interactions between the glass fiber coating and oxidized carbon nanotubes.* Applied Surface Science, 2015. **330**: p. 383-392.

143. Naik, N.K., et al., *High strain rate mechanical behavior of epoxy under compressive loading: Experimental and modeling studies.* Materials Science and Engineering: A, 2011. **528**(3): p. 846-854.

144. Shim, J. and D. Mohr, *Using split Hopkinson pressure bars to perform large strain compression tests on polyurea at low, intermediate and high strain rates.* International Journal of Impact Engineering, 2009. **36**(9): p. 1116-1127.

145. Matusinovic, Z., et al., *Polystyrene/molybdenum disulfide and poly(methyl methacrylate)/molybdenum disulfide nanocomposites with enhanced thermal stability.* Polymer Degradation and Stability, 2012. **97**(12): p. 2481-2486.

146. Wan, S., et al., *Synergistic Toughening of Graphene Oxide–Molybdenum Disulfide–Thermoplastic Polyurethane Ternary Artificial Nacre.* ACS Nano, 2015. **9**(1): p. 708-714.

147. Bertolazzi, S., J. Brivio, and A. Kis, *Stretching and Breaking of Ultrathin MoS2.* ACS Nano, 2011. **5**(12): p. 9703-9709.

148. Eksik, O., et al., *Epoxy Nanocomposites with Two-Dimensional Transition Metal Dichalcogenide Additives.* ACS Nano, 2014. **8**(5): p. 5282-5289.

149. Geim, A.K. and K.S. Novoselov, *The rise of graphene.* Nature Materials, 2007. **6**: p. 183.

150. Mehrpouya, F., et al., *Nanostructured Electrospun Hybrid Graphene/Polyacrylonitrile Yarns.* Nanomaterials, 2017. **7**(10): p. 293.

151. Monteserín, C., et al., *Effects of Graphene Oxide and Chemically-Reduced Graphene Oxide on the Dynamic Mechanical Properties of Epoxy Amine Composites.* Polymers, 2017. **9**(9): p. 449.

152. Bharti, et al., *Removal of Trinitrotoluene with Nano Zerovalent Iron Impregnated Graphene Oxide.* Water, Air, & Soil Pollution, 2017. **229**(1): p. 17.

153. Aradhana, R., S. Mohanty, and S.K. Nayak, *Comparison of mechanical, electrical and thermal properties in graphene oxide and reduced graphene oxide filled epoxy nanocomposite adhesives.* Polymer, 2018. **141**: p. 109-123.

154. Assaedi, H., F.U.A. Shaikh, and I.M. Low, *Effect of nano-clay on mechanical and thermal properties of geopolymer.* Journal of Asian Ceramic Societies, 2016. **4**(1): p. 19-28.

155. Melanie, B., et al., *Barrier properties of poly(lactic acid)/cloisite 30B composites and their relation between oxygen permeability and relative humidity.* Journal of Applied Polymer Science, 2017. **134**(5).

156. Hadj-Hamou, A.S., et al., *Effect of cloisite 30B on the thermal and tensile behavior of poly(butylene adipate-co-terephthalate)/poly(vinyl chloride) nanoblends.* Polymer Bulletin, 2014. **71**(6): p. 1483-1503.

157. Sharma, S., M. Kumar Poddar, and V.S. Moholkar, *Enhancement of thermal and mechanical properties of poly(MMA-co-BA)/Cloisite 30B nanocomposites by ultrasound-assisted in-situ emulsion polymerization.* Ultrasonics Sonochemistry, 2017. **36**: p. 212-225.

158. Lynda, Z., et al., *Relationship between structure and rheological, mechanical and thermal properties of polylactide/Cloisite 30B nanocomposites.* Journal of Applied Polymer Science, 2010. **116**(3): p. 1357-1365.

159. Yalcin, B., S.E. Amos, and J. Tangeman, *2 - Characterization*, in *Hollow Glass Microspheres for Plastics, Elastomers, and Adhesives Compounds*. 2015, William Andrew Publishing: Oxford. p. 7-34.

160. Gladysz, G.M. and K.K. Chawla, *Chapter 6 - Cellular Materials*, in *Voids in Materials*. 2015, Elsevier: Amsterdam. p. 103-130.

161. He, Z. and W. Que, *Molybdenum disulfide nanomaterials: Structures, properties, synthesis and recent progress on hydrogen evolution reaction.* Applied Materials Today, 2016. **3**: p. 23-56.

162. Guardia, L., et al., *Production of aqueous dispersions of inorganic graphene analogues by exfoliation and stabilization with non-ionic surfactants.* RSC Advances, 2014. **4**(27): p. 14115-14127.

163. Shadlou, S., B. Ahmadi-Moghadam, and F. Taheri, *The effect of strain-rate on the tensile and compressive behavior of graphene reinforced epoxy/nanocomposites.* Materials & Design, 2014. **59**: p. 439-447.

164. Peter, S. and E. Woldesenbet, *Nanoclay syntactic foam composites—High strain rate properties.* Materials Science and Engineering: A, 2008. **494**(1): p. 179-187.

165. Jiang, J.-W., *Graphene versus MoS2: A short review.* Frontiers of Physics, 2015. **10**(3): p. 287-302.

166. Zegeye, E.F. and E. Woldesenbet, *Processing and mechanical characterization of carbon nanotube reinforced syntactic foams.* Journal of Reinforced Plastics and Composites, 2012. **31**(15): p. 1045-1052.

167. Poveda, R.L., G. Dorogokupets, and N. Gupta, *Carbon nanofiber reinforced syntactic foams: Degradation mechanism for long term moisture exposure and residual compressive properties.* Polymer Degradation and Stability, 2013. **98**(10): p. 2041-2053.

168. John, B., C.P.R. Nair, and K.N. Ninan, *Effect of nanoclay on the mechanical, dynamic mechanical and thermal properties of cyanate ester syntactic foams.* Materials Science and Engineering: A, 2010. **527**(21–22): p. 5435-5443.

169. Kinloch, A.J., et al., *Deformation and fracture behaviour of a rubber-toughened epoxy: 1. Microstructure and fracture studies.* Polymer, 1983. **24**(10): p. 1341-1354.

170. Chikhi, N., S. Fellahi, and M. Bakar, *Modification of epoxy resin using reactive liquid (ATBN) rubber.* European Polymer Journal, 2002. **38**(2): p. 251-264.

171. Ratna, D. and A.K. Banthia, *Rubber toughened epoxy.* Macromolecular Research, 2004. **12**(1): p. 11-21.

172. Pearson, R.A. and A.F. Yee, *Toughening mechanisms in elastomer-modified epoxies.* Journal of Materials Science, 1986. **21**(7): p. 2475-2488.

173. Pearson, R.A. and A.F. Yee, *Influence of particle size and particle size distribution on toughening mechanisms in rubber-modified epoxies.* Journal of Materials Science, 1991. **26**(14): p. 3828-3844.

174. Roy, P.K., et al., *Polysiloxane-based core-shell microspheres for toughening of epoxy resins.* Journal of Polymer Research, 2014. **21**(1): p. 348.

175. Jiao, L., et al., *Bubble removal in viscoelastic solution by ultrasonic vibration.* AIP Conference Proceedings, 2013. **1547**(1): p. 294-302.

176. Horikawa, H., *System for ultrasonic wave type bubble removal.* The Journal of the Acoustical Society of America, 1980. **68**(6): p. 1910-1910.

177. Frigione, M., C. Naddeo, and D. Acierno, *Cold-Curing Epoxy Resins: Aging and Environmental Effects. I - Thermal Properties*, in *Journal of Polymer Engineering*. 2001. p. 23.

178. Andrae, A.S.G., et al., *Life Cycle Assessment of Japanese High-Temperature Conductive Adhesives.* Environmental Science & Technology, 2008. **42**(8): p. 3084-3089.

179. Lee, J.N., C. Park, and G.M. Whitesides, *Solvent Compatibility of Poly(dimethylsiloxane)-Based Microfluidic Devices.* Analytical Chemistry, 2003. **75**(23): p. 6544-6554.

180. Skourlis, T., D. T., and P. CD., *The role of a polyamide interphase on carbon fibres reinforcing an epoxy matrix.* Composites Science and Technology, 1993. **48**: p. 119-125.

181. Jayalatha, G. and S.K.N. Kutty, *Effect of short nylon-6 fibres on natural rubber-toughened polystyrene.* Materials & Design, 2013. **43**: p. 291-298.

182. Liu, Y., et al., *Crystalline Morphology and Polymorphic Phase Transitions in Electrospun Nylon 6 Nanofibers.* Macromolecules, 2007. **40**(17): p. 6283-6290.

183. Unal, H., F. Fındık, and A. Mimaroglu, *Mechanical behavior of nylon composites containing talc and kaolin.* Journal of Applied Polymer Science, 2003. **88**(7): p. 1694-1697.

184. Yu Aiping, et al., *Enhanced Thermal Conductivity in a Hybrid Graphite Nanoplatelet – Carbon Nanotube Filler for Epoxy Composites.* Advanced Materials, 2008. **20**: p. 4740–4744.

185. Huanga, Z.-M., et al., *A review on polymer nanofibers by electrospinning and their applications in nanocomposites.* Composites Science and Technology, 2003. **63**: p. 2223-2253.

186. Nugroho, R.W.N., et al., *Crosslinked PVAL nanofibers with enhanced long-term stability prepared by single-step electrospinning.* Polymers for Advanced Technologies, 2013. **24**(4): p. 421-429.

187. Gupta, P., et al., *Electrospinning of linear homopolymers of poly(methyl methacrylate): exploring relationships between fiber formation, viscosity,*

molecular weight and concentration in a good solvent. Polymer, 2005. **46**(13): p. 4799-4810.

188.   Manju, P.K. Roy, and A. Ramanan, *Toughening of epoxy resin using Zn4O (1,4-benzenedicarboxylate)3 metal-organic frameworks.* RSC Advances, 2014. **4**(94): p. 52338-52345.

189.   Puterman, M., M. Narkis, and S. Kenig, *Syntactic Foams I. Preparation, Structure and Properties.* Journal of Cellular Plastics, 1980. **16**(4): p. 223-229.

190.   Gupta, N., D. Pinisetty, and V. Shunmugasamy, Chakravarthy,, *Reinforced Polymer Matrix Syntactic Foams*, in *Effect of Nano and MIcro- Scale Reinforcement*. 2013, Springrer International Publishing: New York.

191.   Wu, D.Y., S. Meure, and D. Solomon, *Self-healing polymeric materials: A review of recent developments.* Progress in Polymer Science, 2008. **33**(5): p. 479-522.

192.   Tripathi, M., et al., *Influence of microcapsule shell material on the mechanical behavior of epoxy composites for self-healing applications.* Journal of Applied Polymer Science, 2014. **131**(15): p. 40572.

193.   Zhenqiu, Y., et al., *Preparation of microspheres with microballoons inside for floating drug-delivery systems.* Journal of Applied Polymer Science, 2004. **94**(1): p. 197-202.

194.   Freiberg, S. and X.X. Zhu, *Polymer microspheres for controlled drug release.* International Journal of Pharmaceutics, 2004. **282**(1–2): p. 1-18.

195.   Cavalieri, F., et al., *Stable Polymeric Microballoons as Multifunctional Device for Biomedical Uses: Synthesis and Characterization.* Langmuir, 2005. **21**(19): p. 8758-8764.

196.   Wu, A.S., et al., *3D Printed Silicones with Shape Memory.* Scientific Reports, 2017. **7**(1): p. 4664.

197.   Pratibha, S., et al., *Interfacial encapsulation of bio-based benzoxazines in epoxy shells for temperature triggered healing.* Journal of Applied Polymer Science, 2015. **132**(47).

198.   Tripathi, M., D. Kumar, and P.K. Roy, *Microencapsulation of reactive amine by interfacially engineered epoxy microcapsules for smart applications.* Iranian Polymer Journal, 2017. **26**(7): p. 489-497.

199.   Sharma, P., et al., *Microencapsulated cardanol derived benzoxazines for self-healing applications.* Materials Letters, 2014. **133**: p. 266-268.

200.   Tripathi, M., et al., *Application of microencapsulated unsaturated polyester toward temperature-triggered healing in epoxy composites.* Journal of Intelligent Material Systems and Structures, 2016. **27**(12): p. 1650-1657.

201.   Manorama, T., et al., *Influence of microcapsule shell material on the mechanical behavior of epoxy composites for self-healing applications.* Journal of Applied Polymer Science, 2014. **131**(15).

202.   Kardar, P., *Preparation of polyurethane microcapsules with different polyols component for encapsulation of isophorone diisocyanate healing agent.* Progress in Organic Coatings, 2015. **89**: p. 271-276.

203.   Dennis, L., V.D. M., and v.H.J.C. M., *Polymeric Microcapsules for Synthetic Applications.* Macromolecular Bioscience, 2008. **8**(11): p. 991-1005.

204.   Roy, P., et al., *Polysiloxane-based core-shell microspheres for toughening of epoxy resins.* Journal of Polymer Research, 2014. **21**(1): p. 1-9.

205.   Yu, X., et al., *Crosslinked epoxy microspheres: Preparation, surface-initiated polymerization, and use as macroporous silica porogen.* Journal of Applied Polymer Science, 2013. **128**(5): p. 2829-2839.

206.   Sharma, P., et al., *Microencapsulated cardanol derived benzoxazines for self-healing applications.* Materials Letters, 2014. **133**(0): p. 266-268.

207.   Manju, et al., *Core-shell polysiloxane-MOF 5 microspheres as a stationary phase for gas-solid chromatographic separation.* RSC Advances, 2014. **4**(34): p. 17429-17433.

208.   Song, C., P. Wang, and H.A. Makse, *A phase diagram for jammed matter.* Nature, 2008. **453**: p. 629.

209.   Casanova, F. and L. Santos, *Encapsulation of cosmetic active ingredients for topical application – a review.* Journal of Microencapsulation, 2016. **33**(1): p. 1-17.

210.   Scott, C., et al., *Liquid-Core Capsules via Interfacial Polymerization: A Free-Radical Analogy of the Nylon Rope Trick.* Journal of the American Chemical Society, 2005. **127**(12): p. 4160-4161.

211.   Detsri, E. and S.T. Dubas, *Interfacial polymerization of polyaniline and its layer-by-layer assembly into polyelectrolytes multilayer thin-films.* Journal of Applied Polymer Science, 2013. **128**(1): p. 558-565.

212.   Rao, C.N.R., et al., *Use of the liquid–liquid interface for generating ultrathin nanocrystalline films of metals, chalcogenides, and oxides.* Journal of Colloid and Interface Science, 2005. **289**(2): p. 305-318.

213.   Wang, X., et al., *Magnetic molecularly imprinted polymer particles synthesized by suspension polymerization in silicone oil.* Macromolecular Rapid Communications, 2006. **27**(14): p. 1180-1184.

214.   Siggia, S., ed. *Quantitative Organic Analysis.* 3rd ed. Vol. p 242. 1967, Wiley: New York.

215. Hoy, K.L., *New Values of the Solubility Parameters from Vapor Pressure Data.* Journal of paint technology, 1970. **42**: p. 76-118.

216. Launay, H., C.M. Hansen, and K. Almdal, *Hansen solubility parameters for a carbon fiber/epoxy composite.* Carbon, 2007. **45**(15): p. 2859-2865.

217. Wright, D.C., *Environmental Stress Cracking of Plastics.* 1996, Shrawbery, Shrewsbery, Shropshire, United Kingdom: iSmithers Rapra Publishing.

218. Yoo, J.S., S.J. Kim, and J.S. Choi, *Swelling equilibria of mixed solvent/poly(dimethylsiloxane) systems* Journal of Chemical and Engineering Data, 1999. **44**(1): p. 16-22.

219. Du, Y., Y. Xue, and H.L. Frisch, *Physical Properties of Polymers Handbook.* 1996, Woodbury, NY: AIP Press

220. Efimova, A.A., et al., *Vapour pressure and enthalpy of vaporization of aliphatic poly-amines.* The Journal of Chemical Thermodynamics, 2010. **42**(3): p. 330-336.

221. Rallison, J.M., *The Deformation of Small Viscous Drops and Bubbles in Shear Flows.* Annual Review of Fluid Mechanics, 1984. **16**(1): p. 45-66.

222. Vogt, J., *Thermal analysis of epoxy-resins: Identification of decomposition products.* Thermochimica Acta, 1985. **85**(0): p. 411-414.

223. Ramírez, C., et al., *Epoxy/POSS organic–inorganic hybrids: ATR-FTIR and DSC studies.* European Polymer Journal, 2008. **44**(10): p. 3035-3045.

224. Luo, X. and L. Zhang, *Immobilization of Penicillin G Acylase in Epoxy-Activated Magnetic Cellulose Microspheres for Improvement of Biocatalytic Stability and Activities.* Biomacromolecules, 2010. **11**(11): p. 2896-2903.

225. Bicak, N., et al., *Polystyrene microspheres having epoxy functional dangling chains linked by hydrolytically stable bonds via ATRP.* Journal of Polymer Science Part A: Polymer Chemistry, 2006. **44**(23): p. 6708-6716.

226. John, M. and G. Li, *Self-healing of sandwich structures with a grid stiffened shape memory polymer syntactic foam core.* Smart Materials and Structures, 2010. **19**(7): p. 075013.

227. Hiel, C., D. Dittman, and O. Ishai, *Composite sandwich construction with syntactic foam core-A practical assessment of post-impact damage and residual strength.* Composites, 1993. **24**: p. 447-450.

228. Bardella, L. and F. Genna, *On the elastic behavior of syntactic foams.* International Journal of Solids and Structures, 2001. **38**(40-41): p. 7235-7260.

229. Ullas, A., D. Kumar, and P. Roy, *Poly (dimethylsiloxane)-toughened syntactic foams.* Journal of Applied Polymer Science, 2018. **135**(8).

230. Gupta, N. and R. Nagorny, *Tensile properties of glass microballoon-epoxy resin syntactic foams.* Journal of Applied Polymer Science, 2006. **102**(2): p. 1254-1261.

231. Ullas, A., et al., *Electrospun Polyamide Nanofiber-Reinforced Hybrid Syntactic Foams.* Polymer-Plastics Technology and Engineering, 2016. **55**(17): p. 1797-1806.

232. Ullas, A., et al., *Epoxy-glass Microballoon Syntactic Foams for Blast Mitigating Applications.* Defence Science Journal, 2018. **68**(2): p. 210.

233. Shah, D.U., F. Vollrath, and D. Porter, *Silk cocoons as natural macro-balloon fillers in novel polyurethane-based syntactic foams.* Polymer, 2015. **56**: p. 93-101.

234. Kenig, S., I. Raiter, and M. Narkis, *Three-phase silicone based syntactic foams.* Journal of cellular plastics, 1984. **20**(6): p. 423-429.

235. McIlroy, H., *Phenolic resin syntactic foams.* 1980, Bendix Corp., Kansas City, MO (USA).

236. Santhosh Kumar, K., C. Reghunadhan Nair, and K. Ninan, *Mechanical properties of polybenzoxazine syntactic foams.* Journal of Applied Polymer Science, 2008. **108**(2): p. 1021-1028.

237. Santhosh Kumar, K., C. Reghunadhan Nair, and K. Ninan, *Silica fiber–polybenzoxazine–syntactic foams; Processing and properties.* Journal of Applied Polymer Science, 2008. **107**(2): p. 1091-1099.

238. Ishida, H. and S. Rimdusit, *Very high thermal conductivity obtained by boron nitride-filled polybenzoxazine.* Thermochimica Acta, 1998. **320**(1-2): p. 177-186.

239. Rimdusit, S., W. Tanthapanichakoon, and C. Jubsilp, *High performance wood composites from highly filled polybenzoxazine.* Journal of Applied Polymer Science, 2006. **99**(3): p. 1240-1253.

240. Sharma, P., D. Kumar, and P.K. Roy, *Microwave-Assisted Sustainable Synthesis of Telechelic Poly (ethylene glycol) s with Benzoxazine End Groups.* ChemistrySelect, 2016. **1**(21): p. 6941-6947.

241. Ishida, H. and H.Y. Low, *A study on the volumetric expansion of benzoxazine-based phenolic resin.* Macromolecules, 1997. **30**(4): p. 1099-1106.

242. Ishida, H. and D.J. Allen, *Physical and mechanical characterization of near-zero shrinkage polybenzoxazines.* Journal of polymer science Part B: Polymer physics, 1996. **34**(6): p. 1019-1030.

243. Lin, C.H., et al., *Flexible polybenzoxazine thermosets with high glass transition temperatures and low surface free energies.* Polymer Chemistry, 2012. **3**(4): p. 935-945.

244. Kim, H., Z. Brunovska, and H. Ishida, *Synthesis and thermal characterization of polybenzoxazines based on acetylene-functional monomers.* Polymer, 1999. **40**(23): p. 6565-6573.

245.   Ghosh, N., B. Kiskan, and Y. Yagci, *Polybenzoxazines—new high performance thermosetting resins: synthesis and properties.* Progress in polymer Science, 2007. **32**(11): p. 1344-1391.

246.   Yagci, Y., B. Kiskan, and N.N. Ghosh, *Recent advancement on polybenzoxazine—a newly developed high performance thermoset.* Journal of Polymer Science Part A: Polymer Chemistry, 2009. **47**(21): p. 5565-5576.

247.   Shen, S.B. and H. Ishida, *Development and characterization of high-performance polybenzoxazine composites.* Polymer composites, 1996. **17**(5): p. 710-719.

248.   Chernykh, A., T. Agag, and H. Ishida, *Synthesis of linear polymers containing benzoxazine moieties in the main chain with high molecular design versatility via click reaction.* Polymer, 2009. **50**(2): p. 382-390.

249.   Ishida, H., *Overview and historical background of polybenzoxazine research*, in *Handbook of benzoxazine resins*. 2011, Elsevier. p. 3-81.

250.   Sharma, P., et al., *Sustainable Bis-benzoxazines from Cardanol and PET-Derived Terephthalamides.* ACS Sustainable Chemistry & Engineering, 2015. **4**(3): p. 1085-1093.

251.   Sharma, P., et al., *Microencapsulated cardanol derived benzoxazines for self-healing applications.* Materials Letters, 2014. **133**: p. 266-268.

252.   Sharma, P., et al., *Interfacial encapsulation of bio-based benzoxazines in epoxy shells for temperature triggered healing.* Journal of Applied Polymer Science, 2015. **132**(47).

253.   Allen, D.J. and H. Ishida, *Physical and mechanical properties of flexible polybenzoxazine resins: Effect of aliphatic diamine chain length.* Journal of Applied Polymer Science, 2006. **101**(5): p. 2798-2809.

254. Shukla, S., et al., *Cardanol benzoxazines–interplay of oxazine functionality (mono to tetra) and properties.* RSC Advances, 2015. **5**(95): p. 78071-78080.

255. Ambika Devi, K., et al., *Syntactic foam composites of epoxy-allyl phenol-bismaleimide ternary blend—Processing and properties.* Journal of Applied Polymer Science, 2007. **105**(6): p. 3715-3722.

256. Wang, Y.-X. and H. Ishida, *Cationic ring-opening polymerization of benzoxazines.* Polymer, 1999. **40**(16): p. 4563-4570.

257. Shi, Z., et al., *Investigation of isothermal curing behaviour during the synthesis of polybenzoxazine-layered silicate nanocomposites via cyclic monomer.* European polymer journal, 2002. **38**(4): p. 727-733.

258. Jang, J. and S. Shin, *Cure studies of a benzoxazine-based phenolic resin by isothermal experiment.* Polymer journal, 1995. **27**(6): p. 601.

259. Sharma, P., D. Kumar, and P.K. Roy, *Enhancing the processibility of high temperature polymerizing cardanol derived benzoxazines using eco-friendly curing accelerators.* Polymer, 2018. **138**: p. 343-351.

260. Pratibha, S., K. Devendra, and R.P. K., *Poly(benzoxazine–co–urea): A Solventless Approach Towards The Introduction of Alternating Urea Linkages In Polybenzoxazine.* ChemistrySelect, 2017. **2**(19): p. 5372-5377.

261. Ishida, H. and Y.H. Lee, *Study of hydrogen bonding and thermal properties of polybenzoxazine and poly-(ε-caprolactone) blends.* Journal of polymer science Part B: Polymer physics, 2001. **39**(7): p. 736-749.

262. Gupta, N., E. Woldesenbet, and S. Sankaran, *Studies on compressive failure features in syntactic foam material.* Journal of Materials Science, 2001. **36**(18): p. 4485-4491.

263. Hemvichian, K. and H. Ishida, *Thermal decomposition processes in aromatic amine-based polybenzoxazines investigated by TGA and GC–MS*. Polymer, 2002. **43**(16): p. 4391-4402.

LIST OF PUBLICATIONS

PUBLISHED

1. **Epoxy Filled Microcapsules by Interfacial Engineering** in Journal of Polymer-Plastics Technology and Engineering **DOI:** 10.1080/03602559.2015.1132441
   A. V. Ullas, Rahamattulah, Devendra Kumar & Prasun K. Roy

2. **Electrospun Polyamide Nanofiber Reinforced Hybrid Syntactic Foams** in Journal of Polymer-Plastics Technology and Engineering **DOI:**10.1080/03602559.2016.1163590
   A. V. Ullas, Bariya Qayyum, Devendra Kumar & Prasun K. Roy

3. **Poly(dimethylsiloxane)-toughened Syntactic Foams** in Journal of Applied Polymer Science **DOI:** 10.1002/app.45882
   A.V. Ullas, D.Kumar & P.K.Roy

4. **Epoxy-glass Microballoon Syntactic Foams for Blast Mitigating Applications** in Defence Science Journal **DOI:** 10.14429/dsj.68.12048
   A.V.Ullas, P.K.Sharma, P.Chandel, P.Sharma, D.Kumar & P.K.Roy

5. **Rheokinetic Studies and Compressive Response of High Performance Polybenzoxazine Syntactic Foams** in Journal of Applied Polymer Science **DOI:** 10.1002/app.47234
   A.V.Ullas, Pratibha Sharma, Devendra Kumar, Prasun Roy

REVISIONS SUBMITTED

1. **Exfoliated 2D molybdenum disulfide reinforced epoxy syntactic foams** in Journal of Cellular Plastics
   A.V.Ullas, Devendra Kumar, Prasun Roy

COMMUNICATED

1. **Epoxy-glass microballoon syntactic foams: Rheological optimization of the processing window** in Advances in Polymer Technology
   A.V.Ullas, Devendra Kumar, Prasun Kumar Roy

CONFERENCE PROCEEDINGS

1. **MACRO-2015 Kolkata**
   "Compressive Behaviour of Epoxy Syntactic Foams containing Hollow Epoxy Microcapsules"
   A.V.Ullas, Rahamtullah, Prasun Kumar Roy, Devendra Kumar

2. **International Conference on Study of Nanomaterials and Scientific Development in 21st Century (ICSNSDC)- November 2017, Gwalior**
   "Compressive and Tensile Fracture Features of Syntactic Foam-Microscopic Visualization"
   A.V.Ullas, Devendra Kumar, Prasun Kumar Roy

3. **International Conference on Advances in Polymer Science & Technology (APA-2017)- November 2017, New Delhi**
   "Chemo-Rheology and Mechanical Properties of Epoxy-Glass Balloon Syntactic Foams"
   A.V.Ullas, Devendra Kumar, Prasun Kumar Roy

BIO-DATA

A.V.ULLAS
H.N-11/265, Near Dhania Mehri Pul, Rajajipuram, Lucknow-226017
Email ID: vishuullas@gmail.com

PERSONAL DETAILS	Male, Single Date of Birth: 03 May 1986 Languages Known: Hindi, English
EDUCATION	M.Tech (Polymer Technology), 2012 Department of Applied Chemistry and Polymer Technology Delhi Technological University, Delhi
HONOURS	GATE 2017 (ENGINEERING SCIENCES (XE)) Qualified